

Han-Xiong Li  
Chenkun Qi

Intelligent Systems, Control and  
Automation: Science and Engineering

# Spatio-Temporal Modeling of Nonlinear Distributed Parameter Systems

A Time/Space Separation Based Approach



Springer

# Spatio-Temporal Modeling of Nonlinear Distributed Parameter Systems

International Series on  
INTELLIGENT SYSTEMS, CONTROL, AND AUTOMATION:  
SCIENCE AND ENGINEERING

---

VOLUME 50

---

*Editor:*

Professor S.G. Tzafestas, National Technical University of Athens, Athens, Greece

*Editorial Advisory Board*

Professor P. Antsaklis, University of Notre Dame, Notre Dame, IN, USA

Professor P. Borne, Ecole Centrale de Lille, Lille, France

Professor D.G. Caldwell, University of Salford, Salford, UK

Professor C.S. Chen, University of Akron, Akron, Ohio, USA

Professor T. Fukuda, Nagoya University, Nagoya, Japan

Professor S. Monaco, University La Sapienza, Rome, Italy

Professor G. Schmidt, Technical University of Munich, Munich, Germany

Professor S.G. Tzafestas, National Technical University of Athens, Athens, Greece

Professor F. Harashima, University of Tokyo, Tokyo, Japan

Professor N.K. Sinha, McMaster University, Hamilton, Ontario, Canada

Professor D. Tabak, George Mason University, Fairfax, Virginia, USA

Professor K. Valavanis, University of Denver, Denver, USA

For other titles published in this series, go to  
[www.springer.com/series/6259](http://www.springer.com/series/6259)

Han-Xiong Li • Chenkun Qi

# Spatio-Temporal Modeling of Nonlinear Distributed Parameter Systems

A Time/Space Separation Based Approach

Han-Xiong Li  
City University of Hong Kong  
Dept of Manufacturing  
Engineering and  
Engineering Management  
Hong Kong  
China, People's Republic

Chenkun Qi  
Shanghai Jiao Tong University  
School of Mechanical Engineering  
Shanghai  
China, People's Republic  
E-mail: [chenkqi@sjtu.edu.cn](mailto:chenkqi@sjtu.edu.cn)

and

Central South University  
School of Mechanical and  
Electrical Engineering  
Changsha  
China, People's Republic  
E-mail: [mehxli@cityu.edu.hk](mailto:mehxli@cityu.edu.hk)

ISBN 978-94-007-0740-5

e-ISBN 978-94-007-0741-2

DOI 10.1007/978-94-007-0741-2

Springer Dordrecht Heidelberg London New York

© Springer Science+Business Media B.V. 2011

No part of this work may be reproduced, stored in a retrieval system, or transmitted in any form or by any means, electronic, mechanical, photocopying, microfilming, recording or otherwise, without written permission from the Publisher, with the exception of any material supplied specifically for the purpose of being entered and executed on a computer system, for exclusive use by the purchaser of the work.

*Typesetting & Cover design:* Scientific Publishing Services Pvt. Ltd., Chennai, India

Printed on acid-free paper

Springer is part of Springer Science+Business Media ([www.springer.com](http://www.springer.com))

# Preface

Distributed parameter systems (DPS) widely exist in many industrial processes, e.g., thermal process, fluid process and transport-reaction process. These processes are described in partial differential equations (PDE), and possess complex spatio-temporal coupled, infinite-dimensional and nonlinear dynamics. Modeling of DPS is essential for process control, prediction and analysis. Due to its infinite-dimensionality, the model of PDE can not be directly used for implementations. In fact, the approximate models in finite-dimension are often required for applications. When the PDEs are known, the modeling actually becomes a *model reduction* problem. However, there are often some unknown uncertainties (e.g., unknown parameters, nonlinearity and model structures) due to incomplete process knowledge. Thus the *data-based modeling* (i.e. *system identification*) is necessary to estimate the models from the process data. The model identification of DPS is an important area in the field of system identification. However, compared with traditional lumped parameter systems (LPS), the system identification of DPS is more complicated and difficult. In the last few decades, there are many studies on the system identification of DPS. The purpose of this book is to provide a brief review of the previous work on model reduction and identification of DPS, and develop new spatio-temporal models and their relevant identification approaches. All these work will be presented in a unified view from time/space separation. The book also illustrates their applications to thermal processes in the electronics packaging and chemical industry.

In the book, a systematic overview and classification on the modeling of DPS is presented first, which includes model reduction, parameter estimation and system identification. Next, a class of block-oriented nonlinear systems in traditional LPS is extended to DPS, which results in the spatio-temporal Wiener and Hammerstein systems and their identification methods. Then, the traditional Volterra model is extended to DPS, which results in the spatio-temporal Volterra model and its identification algorithm. All these methods are based on linear time/space separation. Sometimes, the nonlinear time/space separation can play a better role in modeling of very complex process. Thus, a nonlinear time/space separation based neural modeling is also presented for a class of DPS with more complicated dynamics. Finally, all these modeling approaches are successfully applied to industrial thermal processes, including a catalytic rod, a packed-bed reactor and a snap curing oven.

The book assumes a basic knowledge about distributed parameter systems, system modeling and identification. It is intended for researchers, graduate students and engineers interested in distributed parameter systems, nonlinear systems, and process modeling and control.

Authors are grateful to students, colleagues and visitors in our research group for their support and contributions, and also would like to thank the Research Grant Council of Hong Kong and National Natural Science Foundation of China for their financial support to our research. Last, but not least, we would like to express our deepest gratitude to our wives, children and parents for their love, understanding and support.

Han-Xiong Li  
City University of Hong Kong  
Central South University  
Chenkun Qi  
Shanghai Jiao Tong University

# Contents

<b>Preface</b> .....	<b>V</b>
<b>List of Figures</b> .....	<b>XI</b>
<b>List of Tables</b> .....	<b>XV</b>
<b>Abbreviations</b> .....	<b>XVII</b>
<b>1 Introduction</b> .....	<b>1</b>
1.1 Background .....	1
1.1.1 Examples of Distributed Parameter Processes .....	1
1.1.2 Motivation .....	5
1.2 Contributions and Organization of the Book .....	7
References .....	10
<b>2 Modeling of Distributed Parameter Systems: Overview and Classification</b> .....	<b>13</b>
2.1 Introduction .....	13
2.2 White-Box Modeling: Model Reduction for Known DPS .....	16
2.2.1 Eigenfunction Method .....	16
2.2.2 Green's Function Method .....	17
2.2.3 Finite Difference Method .....	17
2.2.4 Weighted Residual Method .....	18
2.2.4.1 Classification Based on Weighting Functions .....	21
2.2.4.2 Classification Based on Basis Functions .....	23
2.2.5 Comparison Studies of Spectral and KL Method .....	29
2.3 Grey-Box Modeling: Parameter Estimation for Partly Known DPS .....	31
2.3.1 FDM Based Estimation .....	31
2.3.2 FEM Based Estimation .....	32
2.3.3 Spectral Based Estimation .....	33
2.3.4 KL Based Estimation .....	33
2.4 Black-Box Modeling: System Identification for Unknown DPS .....	33
2.4.1 Green's Function Based Identification .....	34
2.4.2 FDM Based Identification .....	34
2.4.3 FEM Based Identification .....	35
2.4.4 Spectral Based Identification .....	36
2.4.5 KL Based Identification .....	38



2.4.6	Comparison Studies of Neural Spectral and Neural KL Method .....	38
2.5	Concluding Remarks .....	41
	References .....	42
<b>3</b>	<b>Spatio-Temporal Modeling for Wiener Distributed Parameter Systems.....</b>	<b>51</b>
3.1	Introduction .....	51
3.2	Wiener Distributed Parameter System.....	52
3.3	Spatio-Temporal Wiener Modeling Methodology .....	54
3.4	Karhunen-Loève Decomposition .....	54
3.5	Wiener Model Identification.....	57
3.5.1	Model Parameterization .....	58
3.5.2	Parameter Estimation .....	59
3.6	Simulation and Experiment .....	61
3.6.1	Catalytic Rod.....	62
3.6.2	Snap Curing Oven .....	65
3.7	Summary.....	70
	References .....	70
<b>4</b>	<b>Spatio-Temporal Modeling for Hammerstein Distributed Parameter Systems.....</b>	<b>73</b>
4.1	Introduction .....	73
4.2	Hammerstein Distributed Parameter System .....	75
4.3	Spatio-Temporal Hammerstein Modeling Methodology .....	76
4.4	Karhunen-Loève Decomposition .....	76
4.5	Hammerstein Model Identification .....	77
4.5.1	Model Parameterization .....	78
4.5.2	Structure Selection .....	79
4.5.3	Parameter Estimation .....	83
4.6	Simulation and Experiment .....	85
4.6.1	Catalytic Rod.....	86
4.6.2	Snap Curing Oven .....	89
4.7	Summary.....	93
	References .....	93
<b>5</b>	<b>Multi-channel Spatio-Temporal Modeling for Hammerstein Distributed Parameter Systems.....</b>	<b>95</b>
5.1	Introduction .....	95
5.2	Hammerstein Distributed Parameter System .....	97
5.3	Basic Identification Approach .....	97
5.3.1	Basis Function Expansion .....	97
5.3.2	Temporal Modeling Problem .....	100
5.3.3	Least-Squares Estimation .....	101
5.3.4	Singular Value Decomposition .....	101
5.4	Multi-channel Identification Approach.....	103

5.4.1	Motivation .....	103
5.4.2	Multi-channel Identification.....	103
5.4.3	Convergence Analysis.....	106
5.5	Simulation and Experiment .....	112
5.5.1	Packed-Bed Reactor .....	113
5.5.2	Snap Curing Oven .....	116
5.6	Summary.....	119
	References .....	119
<b>6</b>	<b>Spatio-Temporal Volterra Modeling for a Class of Nonlinear DPS.....</b>	<b>123</b>
6.1	Introduction .....	123
6.2	Spatio-Temporal Volterra Model.....	124
6.3	Spatio-Temporal Modeling Approach .....	126
6.3.1	Time/Space Separation.....	127
6.3.2	Temporal Modeling Problem .....	129
6.3.3	Parameter Estimation .....	130
6.4	State Space Realization.....	131
6.5	Convergence Analysis .....	133
6.6	Simulation and Experiment .....	138
6.6.1	Catalytic Rod.....	138
6.6.2	Snap Curing Oven .....	141
6.7	Summary.....	145
	References .....	145
<b>7</b>	<b>Nonlinear Dimension Reduction Based Neural Modeling for Nonlinear Complex DPS.....</b>	<b>149</b>
7.1	Introduction .....	149
7.2	Nonlinear PCA Based Spatio-Temporal Modeling Framework .....	150
7.2.1	Modeling Methodology.....	150
7.2.2	Principal Component Analysis.....	151
7.2.3	Nonlinear PCA for Projection and Reconstruction .....	153
7.2.4	Dynamic Modeling.....	153
7.3	Nonlinear PCA Based Spatio-Temporal Modeling in Neural System ...	154
7.3.1	Neural Network for Nonlinear PCA.....	154
7.3.2	Neural Network for Dynamic Modeling .....	156
7.4	Simulation and Experiment .....	157
7.4.1	Catalytic Rod.....	157
7.4.2	Snap Curing Oven .....	160
7.5	Summary.....	163
	References .....	164
<b>8</b>	<b>Conclusions.....</b>	<b>167</b>
8.1	Conclusions .....	167
	References .....	170
<b>Index .....</b>		<b>173</b>

# List of Figures

<b>Fig.1.1</b> Snap curing oven system.....	2
<b>Fig.1.2</b> A catalytic rod.....	3
<b>Fig.1.3</b> A catalytic packed-bed reactor.....	4
<b>Fig.1.4</b> Spatio-temporal models for nonlinear DPS.....	7
<b>Fig.1.5</b> Spatial information processing for DPS modeling.....	8
<b>Fig.2.1</b> Geometric interpretations of finite difference and method of lines.....	18
<b>Fig.2.2</b> Geometric interpretation of time-space separation for $n=3$ .....	19
<b>Fig.2.3</b> Framework of weighted residual method.....	20
<b>Fig.2.4</b> Geometric interpretation of weighted residual method.....	20
<b>Fig.2.5</b> Piecewise linear polynomials in one dimension.....	24
<b>Fig.2.6</b> Eigenfunctions of Case 1.....	26
<b>Fig.2.7</b> Separation of eigenspectrum.....	26
<b>Fig.2.8</b> Empirical eigenfunctions of Case 1.....	28
<b>Fig.2.9</b> KL and spectral method for Case 1.....	30
<b>Fig.2.10</b> KL and spectral method for Case 2.....	30
<b>Fig.2.11</b> Output error approach.....	32
<b>Fig.2.12</b> Geometric interpretation of FDM based identification.....	35
<b>Fig.2.13</b> Neural spectral method.....	37
<b>Fig.2.14</b> Neural observer spectral method.....	37
<b>Fig.2.15</b> Neural KL method.....	38
<b>Fig.2.16</b> Neural spectral and neural KL methods for Case 1.....	39
<b>Fig.2.17</b> Neural spectral and neural observer spectral methods for Case 1.....	39
<b>Fig.2.18</b> Neural spectral method for Case 2.....	40
<b>Fig.2.19</b> Neural KL method for Case 2.....	40
<b>Fig.3.1</b> Wiener distributed parameter system.....	53
<b>Fig.3.2</b> Time/space separation of Wiener distributed parameter system.....	53
<b>Fig.3.3</b> KL based modeling methodology for Wiener distributed parameter system.....	54
<b>Fig.3.4</b> Wiener model.....	57
<b>Fig.3.5</b> Catalytic rod: Measured output for Wiener modeling.....	63
<b>Fig.3.6</b> Catalytic rod: KL basis functions for KL-Wiener modeling.....	64
<b>Fig.3.7</b> Catalytic rod: KL-Wiener model output.....	64
<b>Fig.3.8</b> Catalytic rod: Prediction error of KL-Wiener model.....	64
<b>Fig.3.9</b> Catalytic rod: Spline basis functions for SP-Wiener modeling.....	65
<b>Fig.3.10</b> Catalytic rod: $SNAE(t)$ of SP-Wiener and KL-Wiener models.....	65
<b>Fig.3.11</b> Sensors placement for modeling of snap curing oven.....	66

<b>Fig.3.12</b> Snap curing oven: Input signals of heater 1 in the experiment.....	67
<b>Fig.3.13</b> Snap curing oven: KL basis functions ( $i=1$ ) for KL-Wiener modeling..	67
<b>Fig.3.14</b> Snap curing oven: KL basis functions ( $i=2$ ) for KL-Wiener modeling..	67
<b>Fig.3.15</b> Snap curing oven: Performance of KL-Wiener model at sensor s1 .....	68
<b>Fig.3.16</b> Snap curing oven: Performance of KL-Wiener model at sensor s6 .....	68
<b>Fig.3.17</b> Snap curing oven: Predicted temperature distribution of KL-Wiener model at $t=10000s$ .....	68
<b>Fig.3.18</b> Snap curing oven: Spline basis functions ( $i=1$ ) for SP-Wiener modeling .....	69
<b>Fig.3.19</b> Snap curing oven: Spline basis functions ( $i=2$ ) for SP-Wiener modeling .....	69
<b>Fig.3.20</b> Snap curing oven: Predicted temperature distribution of SP-Wiener model at $t=10000s$ .....	69
<b>Fig.4.1</b> Hammerstein distributed parameter system .....	75
<b>Fig.4.2</b> Time/space separation of Hammerstein distributed parameter system ....	75
<b>Fig.4.3</b> KL based modeling methodology for Hammerstein distributed parameter system .....	76
<b>Fig.4.4</b> Hammerstein model .....	78
<b>Fig.4.5</b> Structure design of Hammerstein model .....	82
<b>Fig.4.6</b> Catalytic rod: Measured output for Hammerstein modeling .....	87
<b>Fig.4.7</b> Catalytic rod: KL basis functions for KL-Hammerstein modeling .....	87
<b>Fig.4.8</b> Catalytic rod: KL-Hammerstein model output .....	88
<b>Fig.4.9</b> Catalytic rod: Prediction error of KL-Hammerstein model.....	88
<b>Fig.4.10</b> Catalytic rod: Spline basis functions for SP-Hammerstein modeling ....	88
<b>Fig.4.11</b> Catalytic rod: Comparison of SP- and KL-Hammerstein models .....	89
<b>Fig.4.12</b> Catalytic rod: Comparison of OFR-LSE-SVD and LSE-SVD for algorithms KL-Hammerstein model .....	89
<b>Fig.4.13</b> Snap curing oven: KL basis functions ( $i=1$ ) for KL-Hammerstein modeling .....	90
<b>Fig.4.14</b> Snap curing oven: KL basis functions ( $i=2$ ) for KL-Hammerstein modeling .....	90
<b>Fig.4.15</b> Snap curing oven: Performance of KL-Hammerstein model at sensor s1 .....	91
<b>Fig.4.16</b> Snap curing oven: Performance of KL-Hammerstein model at sensor s6 .....	91
<b>Fig.4.17</b> Snap curing oven: Predicted temperature distribution of KL-Hammerstein model at $t=10000s$ .....	91
<b>Fig.4.18</b> Snap curing oven: Spline basis functions ( $i=1$ ) for SP-Hammerstein modeling .....	92
<b>Fig.4.19</b> Snap curing oven: Spline basis functions ( $i=2$ ) for SP-Hammerstein modeling .....	92
<b>Fig.5.1</b> Hammerstein distributed parameter system .....	97
<b>Fig.5.2</b> Multi-channel identification of spatio-temporal Hammerstein model ...	104
<b>Fig.5.3</b> Multi-channel spatio-temporal Hammerstein model.....	105

<b>Fig.5.4</b> Spatio-temporal Laguerre model of the $c^{\text{th}}$ channel.....	106
<b>Fig.5.5</b> Packed-bed reactor: Process output for multi-channel Hammerstein modeling .....	114
<b>Fig.5.6</b> Packed-bed reactor: KL basis functions for multi-channel Hammerstein modeling.....	114
<b>Fig.5.7</b> Packed-bed reactor: Prediction output of 3-channel Hammerstein model.....	115
<b>Fig.5.8</b> Packed-bed reactor: Prediction error of 3-channel Hammerstein model .....	115
<b>Fig.5.9</b> Packed-bed reactor: $TNAE(x)$ of Hammerstein models.....	115
<b>Fig.5.10</b> Packed-bed reactor: $SNAE(t)$ of Hammerstein models.....	116
<b>Fig.5.11</b> Packed-bed reactor: $RMSE$ of 3-channel Hammerstein model.....	116
<b>Fig.5.12</b> Snap curing oven: KL basis functions ( $i=1$ ) for multi-channel Hammerstein modeling.....	117
<b>Fig.5.13</b> Snap curing oven: KL basis functions ( $i=2$ ) for multi-channel Hammerstein modeling.....	117
<b>Fig.5.14</b> Snap curing oven: Performance of 3-channel Hammerstein model at sensor s1 .....	118
<b>Fig.5.15</b> Snap curing oven: Performance of 3-channel Hammerstein model at sensor s6 .....	118
<b>Fig.5.16</b> Snap curing oven: Predicted temperature distribution of 3-channel Hammerstein model at $t=10000s$ .....	118
<b>Fig.6.1</b> Spatio-temporal Volterra modeling approach .....	126
<b>Fig.6.2</b> Laguerre network for state space realization of Volterra model .....	132
<b>Fig.6.3</b> Catalytic rod: Measured output for Volterra modeling .....	139
<b>Fig.6.4</b> Catalytic rod: KL basis functions for Volterra modeling.....	139
<b>Fig.6.5</b> Catalytic rod: Predicted output of 2 <sup>nd</sup> -order Volterra model .....	140
<b>Fig.6.6</b> Catalytic rod: Prediction error of 2 <sup>nd</sup> -order Volterra model .....	140
<b>Fig.6.7</b> Catalytic rod: $SNAE(t)$ of 1 <sup>st</sup> and 2 <sup>nd</sup> -order Volterra models .....	140
<b>Fig.6.8</b> Catalytic rod: $TNAE(x)$ of 1 <sup>st</sup> and 2 <sup>nd</sup> -order Volterra models .....	141
<b>Fig.6.9</b> Catalytic rod: $RMSE$ of 2 <sup>nd</sup> -order Volterra model .....	141
<b>Fig.6.10</b> Snap curing oven: KL basis functions ( $i=1$ ) for Volterra modeling .....	142
<b>Fig.6.11</b> Snap curing oven: KL basis functions ( $i=2$ ) for Volterra modeling .....	142
<b>Fig.6.12</b> Snap curing oven: Performance of 2 <sup>nd</sup> -order Volterra model at sensor s1 .....	143
<b>Fig.6.13</b> Snap curing oven: Performance of 2 <sup>nd</sup> -order Volterra model at sensor s6 .....	143
<b>Fig.6.14</b> Snap curing oven: Predicted temperature distribution of 2 <sup>nd</sup> -order Volterra model at $t=10000s$ .....	143
<b>Fig.6.15</b> Snap curing oven: $SNAE(t)$ of 1 <sup>st</sup> -order Volterra model.....	144
<b>Fig.6.16</b> Snap curing oven: $SNAE(t)$ of 2 <sup>nd</sup> -order Volterra model.....	144
<b>Fig.6.17</b> Snap curing oven: $RMSE$ of 2 <sup>nd</sup> -order Volterra model.....	145

<b>Fig.7.1</b> NL-PCA based spatio-temporal modeling methodology .....	151
<b>Fig.7.2</b> NL-PCA network .....	155
<b>Fig.7.3</b> Catalytic rod: Measured output for neural modeling.....	158
<b>Fig.7.4</b> Catalytic rod: NL-PCA reconstruction error .....	159
<b>Fig.7.5</b> Catalytic rod: NL-PCA-RBF model prediction - $\hat{y}_1(t)$ .....	159
<b>Fig.7.6</b> Catalytic rod: NL-PCA-RBF model prediction - $\hat{y}_2(t)$ .....	159
<b>Fig.7.7</b> Catalytic rod: NL-PCA-RBF model prediction error.....	160
<b>Fig.7.8</b> Catalytic rod: $SNAE(t)$ of NL-PCA-RBF and PCA-RBF models .....	160
<b>Fig.7.9</b> Snap curing oven: Performance of NL-PCA-RBF model at sensor s1...	161
<b>Fig.7.10</b> Snap curing oven: Performance of NL-PCA-RBF model at sensor s2 .....	161
<b>Fig.7.11</b> Snap curing oven: Predicted temperature distribution of NL-PCA-RBF model at $t=10000s$ .....	162

# List of Tables

<b>Table 2.1</b> Dimensionless parameters for Case 1 .....	15
<b>Table 2.2</b> Dimensionless parameters for Case 2 .....	16
<b>Table 2.3</b> Classification of spatial basis functions .....	23
<b>Table 3.1</b> Snap curing oven: $TNAE(x)$ of KL-Wiener and SP-Wiener models ....	70
<b>Table 4.1</b> Snap curing oven: $TNAE(x)$ of KL-Hammerstein and SP-Hammerstein models.....	93
<b>Table 4.2</b> Snap curing oven: $TNAE(x)$ of OFR-LSE-SVD and LSE-SVD algorithms for KL-Hammerstein model.....	93
<b>Table 5.1</b> Snap curing oven: $TNAE(x)$ of Hammerstein models .....	119
<b>Table 6.1</b> Snap curing oven: $TNAE(x)$ of 1st and 2nd-order Volterra models ...	144
<b>Table 7.1</b> Catalytic rod: Comparison of PCA and NL-PCA for modeling.....	160
<b>Table 7.2</b> Snap curing oven: $TNAE(x)$ of PCA-RBF and NL-PCA-RBF models.....	162
<b>Table 7.3</b> Snap curing oven: accuracy comparison for all models.....	162
<b>Table 7.4</b> Snap curing oven: computation comparison for all modeling approaches (seconds) .....	163

# Abbreviations

AE	Algebraic Equation
AIM	Approximated Inertial Manifold
BF	Basis Function
DE	Difference Equation
DPS	Distributed Parameter System
EEF	Empirical Eigenfunction
EF	Eigenfunction
ERR	Error Reduction Ratio
FDM	Finite Difference Method
FEM	Finite Element Method
FMNS	Fading Memory Nonlinear System
IC	Integrated Circuit
IM	Inertial Manifold
IV	Instrumental Variables Method
KL	Karhunen-Loève Decomposition
KL-Hammerstein	Karhunen-Loève based Hammerstein Model
KL-Wiener	Karhunen-Loève based Wiener Model
LDS	Lattice Dynamical System
LPS	Lumped Parameter System
LSE	Least-Squares Estimation
LTI	Linear Time Invariant
MARE	Mean of Absolute Relative Error
MIMO	Multi-Input-Multi-Output
MO	Multi-Output
MOL	Method of Lines



NARX	Nonlinear Autoregressive with Exogenous Input
NL-PCA	Nonlinear PCA
NL-PCA-RBF	NL-PCA based RBF model
ODE	Ordinary Differential Equation
OFR	Orthogonal Forward Regression
PCA	Principal Component Analysis
PCA-RBF	PCA based RBF model
PDE	Partial Differential Equation
POD	Proper Orthogonal Decomposition
RBF	Radial Basis Function
RMSE	Root of Mean Squared Error
SISO	Single-Input-Single-Output
SNAE	Spatial Normalized Absolute Error
SNR	Signal-to-Noise Ratio
SO	Single-Output
SP-Hammerstein	Spline Functions based Hammerstein Model
SP-Wiener	Spline Functions based Wiener Model
SVD	Singular Value Decomposition
TNAE	Temporal Normalized Absolute Error
WRM	Weighted Residual Method

# 1 Introduction

**Abstract.** This chapter is an introduction of the book. Starting from typical examples of distributed parameter systems (DPS) encountered in the real-world, it briefly introduces the background and the motivation of the research, and finally the contributions and organization of the book.

## 1.1 Background

Advanced technological needs, such as, semiconductor manufacturing, nanotechnology, biotechnology, material engineering and chemical engineering, have motivated control of material microstructure, fluid flows, spatial profiles (e.g., temperature field) and product size distributions (Christofides, 2001a). These physical, chemical or biological processes all lead to so called distributed parameter systems (DPS) because their inputs and outputs vary both temporally and spatially. As the significant progress in the sensor, actuator and computing technology, the studies of distributed parameter processes become more and more active and practical in science and engineering. Recently several special issues for control of DPS have been organized by Dochain *et al.* (2003), Christofides (2002, 2004), Christofides & Armaou (2005), and Christofides & Wang (2008). Modeling is the first step for many applications such as prediction, control and optimization. This book will focus on the modeling problem of nonlinear DPS with application examples chosen as industrial thermal processes. In general, the modeling approaches presented are applicable to a wide range of distributed parameter processes.

Next, we will introduce some typical thermal process in integrated circuit (IC) packaging and chemical industry, which will be used as examples in the rest of chapters.

### 1.1.1 Examples of Distributed Parameter Processes

#### a) Thermal Process in IC Packaging Industry

One important thermal process in the semiconductor back-end packaging industry considered in this book is the curing process (Deng, Li & Chen, 2005). After the required amount of epoxy is dispensed on the leadframe from the dispenser, and a die is moved from the wafer to attach on the leadframe by the bond arm, then the bonded leadframe is moved into the snap curing oven to cure at a specified temperature. As shown in Figure 1.1, the snap curing oven is an important equipment to provide the required curing temperature distribution. The oven has four heaters for heating and four thermocouples for temperature sensing in the operation. The parts to be cured will be moved in and out from inlet and outlet, respectively.

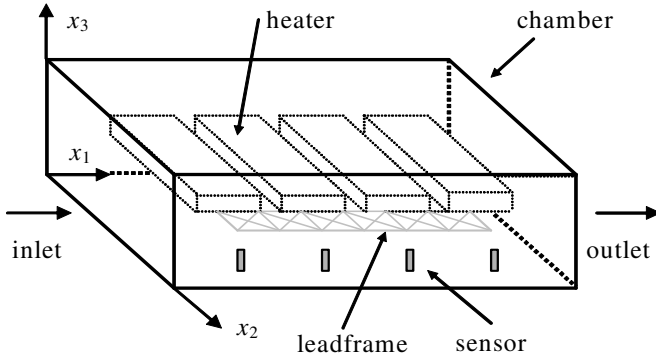


**Fig. 1.1** Snap curing oven system

The temperature distribution inside the chamber is often needed for a quality curing control as well as the fundamental analysis for oven design. In practice, it is difficult to place many sensors to measure the temperature distribution during the curing. Thus it motivates us to build a model of the oven and use it to estimate the temperature distribution of the curing process.

This thermal process can be simplified for the easy modeling. The volume of the epoxy between a die and the leadframe is much smaller as compared to the volume of the leadframe and the volume of the oven chamber. Also, the volume of the leadframe is much smaller as compared to the volume of the oven chamber. Thus, the effects of the epoxy and the leadframe on the temperature in the oven chamber are usually neglected in modeling of the curing process. These effects can be considered as disturbances and could be compensated in the later control process.

This thermal process will follow the basic principles of the heat transfer (conduction, radiation and convection). The fundamental heat transfer equation of the oven can be expressed as a nonlinear parabolic **partial differential equation (PDE)** with some unknown parameters, unknown nonlinearities and unknown boundary conditions:

$$\rho(T)c \frac{\partial T}{\partial t} = \frac{\partial}{\partial x_1} \left( k(T) \frac{\partial T}{\partial x_1} \right) + \frac{\partial}{\partial x_2} \left( k(T) \frac{\partial T}{\partial x_2} \right) + \frac{\partial}{\partial x_3} \left( k(T) \frac{\partial T}{\partial x_3} \right) + f_c(T) + f_r(T) + bu(t), \quad (1.1)$$

where

$T = T(x_1, x_2, x_3, t)$  is the temperature at time  $t$  and location  $(x_1, x_2, x_3)$ ,

$x_1 \in [0, x_{10}]$ ,  $x_2 \in [0, x_{20}]$  and  $x_3 \in [0, x_{30}]$  are spatial coordinates,

$k(T)$  is the thermal conductivity, which is usually inaccurately given,

$\rho(T)$  is the density, which is usually inaccurately given,

$c$  is the specific heat,

$f_c(T)$  and  $f_r(T)$  are the effects of convection and radiation respectively, which are usually inaccurately given,

$u(t) = [u_1(t), u_2(t), u_3(t), u_4(t)]^T$  denotes the vector of manipulated inputs with the spatial distribution  $b = [b_1(x_1, x_2, x_3), b_2(\cdot), b_3(\cdot), b_4(\cdot)]$ ,

$T_0 = T(x_1, x_2, x_3, 0)$  is the initial condition.

The boundary conditions are nonlinear functions of the boundary temperature, the space coordinates of the oven  $(x_1, x_2, x_3)$  and the ambient temperature  $T_a$  as follows:

$$k \frac{\partial T}{\partial x_i} \Big|_{x_i=0} = f_{i1}(x_1, x_2, x_3, T, T_a) \Big|_{x_i=0},$$

$$k \frac{\partial T}{\partial x_i} \Big|_{x_i=x_{i0}} = f_{i2}(x_1, x_2, x_3, T, T_a) \Big|_{x_i=x_{i0}}, i = 1, 2, 3,$$

However, it is difficult to obtain these nonlinear functions  $f_{i1} - f_{i2}$  using only physical insights.

## b) Thermal Process in Chemical Industry

### *Catalytic Rod*

Consider a long thin rod in a reactor as shown in [Figure 1.2](#), which is a typical thermal process in chemical industry ([Christofides, 2001b](#)). The reactor is fed with pure species  $A$  and a zero-th order exothermic catalytic reaction of the form  $A \rightarrow B$  takes place in the rod. Since the reaction is exothermic, a cooling medium that is in contact with the rod is used for cooling.

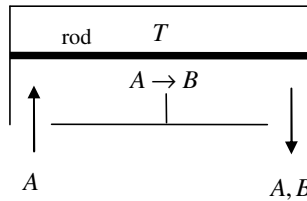


**Fig. 1.2** A catalytic rod

Under the assumptions of constant density and heat capacity, constant conductivity of the rod, constant temperature at both sides of the rod, and excess of species  $A$  in the furnace, the nominal mathematical model which describes the

spatio-temporal evolution of the rod temperature consists of the following **parabolic PDE** (Christofides, 2001b):

$$\frac{\partial T}{\partial t} = \frac{\partial^2 T}{\partial x^2} + f(T, \theta) + b(x)u(t), \quad (1.2)$$

subject to the Dirichlet boundary conditions:

$$T(0, t) = 0, \quad T(\pi, t) = 0,$$

and initial conditions:

$$T(x, 0) = 0,$$

where  $T$  denotes the temperature in the reactor,  $u(t)$  denotes the manipulated input (temperature of the cooling medium) with the actuator distribution  $b(x)$ .  $\theta$  denotes some unknown system parameters (e.g., heat of reaction, heat transfer coefficient and activation energy).  $f$  is an unknown nonlinear function.

### Packed-Bed Reactor

Consider the temperature distribution in a long, thin non-isothermal catalytic packed-bed reactor in chemical industry (Christofides, 1998). As shown in **Figure 1.3**, a reaction of the form  $A \rightarrow B$  takes place on the catalyst. The reaction is endothermic and a jacket is used to heat the reactor.

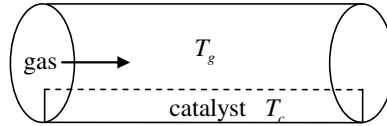


**Fig. 1.3** A catalytic packed-bed reactor

Under the assumptions of negligible diffusive phenomena for the gas phase, constant density and heat capacity of the catalyst and the gas, and excess of species  $A$  in the reactor, a nominal dimensionless model that describes the temperature dynamics of this nonlinear tubular chemical reactor is provided as follows (Christofides, 1998)

$$\frac{\partial T_g}{\partial t} = -\frac{\partial T_g}{\partial x} + f(T_g, T_c, \theta) + b(x)u(t), \quad (1.3)$$

$$\frac{\partial T_c}{\partial t} = \frac{\partial^2 T_c}{\partial x^2} + g(T_g, T_c, \theta) + b(x)u(t), \quad (1.4)$$

subject to the boundary conditions

$$x = 0, \frac{\partial T_c}{\partial x} = 0, T_g = 0,$$

$$x = 1, \frac{\partial T_c}{\partial x} = 0,$$

where  $T_g$  and  $T_c$  denote the temperature of the gas and the catalyst, respectively.  $u$  denotes the manipulated input (the temperature of the jacket) with the actuator distribution  $b(x)$ .  $\theta$  are unknown system parameters.  $f$  and  $g$  are unknown nonlinear functions.

### 1.1.2 Motivation

The industrial thermal processes mentioned are typical nonlinear distributed parameter systems that have following common features:

- These processes are usually described in partial differential equations (PDE) that show **time/space coupled** dynamics.
- The dynamics of these processes are strongly nonlinear.
- There exist uncertainties (e.g., unknown structure, unknown parameters, and external disturbances, etc.) in the process.

These features are also common to many other industrial distributed processes. Modeling is essential to process prediction, control and optimization. Though modeling of **lumped parameter systems (LPS)** has been widely studied, modeling of DPS, especially with the unknown uncertainties, achieves little progress. This motivates us to study the modeling of unknown nonlinear DPS in this book.

Since the DPS is described in PDE that is infinite-dimensional, even for the known DPS, the reduction to finite-dimensional **ordinary differential equations (ODE)** is needed because only finite number of actuators/sensors can be used in practice. The common model reduction methods include **finite difference method (FDM)** (Mitchell & Griffiths, 1980), **finite element method (FEM)** (Brenner & Ridgway Scott, 1994), **spectral method** (Canuto *et al.*, 1988; Boyd, 2000) and **Karhunen-Loève (KL) method** (Sirovich, 1987; Holmes *et al.*, 1996; Newman, 1996a). FDM and FEM may lead to very high-order models, which are not suitable for real-time control. Because the spectral method and KL method can result in low-order models, they are widely used for model reduction in control. However, the spectral method requires more knowledge of the process. Though, a hybrid spectral/intelligent modeling approach is proposed recently (Deng, Li & Chen, 2005) to explore a wider range of application under uncertainties, still it is limited to the parabolic type of processes. Compared with the spectral method, KL method can lead to lower-order models and is suitable for more complex and wider range of systems. However, it requires much more sensors to obtain the process data.

When there are strong uncertainties in the DPS, modeling with the input-output data seems the only solution. If the structure of the DPS is known and only some of its parameters are unknown, then many parameter estimation methods can be used (e.g., Banks & Kunisch, 1989; Coca & Billings, 2000; Demetriou & Rosen, 1994). Though the nonlinear DPS in unknown structure is common in the industry, its

modeling problem is extremely difficult and achieves little progress. With little knowledge of the process, a data-based modeling becomes necessary for DPS in unknown structure. These data-based approaches need little physical or chemical knowledge of the process, and thus are more feasible to use in the practice. Still, these kinds of methods have different limitations as follows.

- Green's function based identification (Gay & Ray, 1995; Zheng, Hoo & Piovoso, 2002) leads to a single spatio-temporal kernel model, which is suitable for control design because of its linear structure. However, it is only a linear approximation of the nonlinear DPS. It may not be applicable to a highly nonlinear DPS.
- FDM and FEM based identification (Gonzalez-Garcia, Rico-Martinez & Kevredidis, 1998; Guo & Billings, 2007; Coca & Billings, 2002) will lead to a high-order model, which may result in an impractical high-order controller.
- KL based identification (Zhou, Liu, Dai & Yuan, 1996; Smaoui & Al-Enezi, 2004; Sahan *et al.*, 1997; Romijn *et al.*, 2008; Aggelogiannaki & Sarimveis, 2008; Qi & Li, 2008a) may lead to a low-order model. Since most of KL based identification use neural network for modeling the dynamics, its nonlinear structure may result in a very complicated control design.

In general, it is still very necessary to develop some new unknown nonlinear DPS modeling approach to overcome these limitations.

In modeling of the traditional lumped parameter systems (LPS), the following models have been widely studied because of their significant properties.

- Traditional block-oriented nonlinear models have been often used because of their simple nonlinear structure, ability to approximate a large class of nonlinear processes and efficient control schemes (e.g., Narendra & Gallman, 1966; Stoica & Söderström, 1982; Bai, 1998; Zhu, 2000; Gómez & Baeyens, 2004; Westwick & Verhaegen, 1996; Hagenblad & Ljung, 2000). They consist of the interconnection of linear time invariant (LTI) systems and static nonlinearities. Two common model structures are: the Hammerstein model, which consists of the cascade connection of a static nonlinearity followed by a LTI system, the Wiener model, in which the order of the linear and the nonlinear blocks is reversed.
- Traditional Volterra model consists of a series of temporal kernel, which is a high-order and nonlinear extension of linear impulse response model (Boyd & Chua, 1985; Schetzen, 1980; Rugh, 1981; Doyle III *et al.*, 1995; Maner *et al.*, 1996; Parker *et al.*, 2001). It has been used for LPS modeling because of its simple nonlinear structure.
- In the field of machine learning, nonlinear principal component analysis (NL-PCA) has been widely studied for nonlinear dimension reduction of high-dimensional data (e.g., Dong & McAvoy, 1996; Kramer, 1991; Hsieh, 2001; Kirby & Miranda, 1994; Smaoui, 2004; Webb, 1996; Wilson, Irwin & Lightbody, 1999). They can achieve a lower-order or more accurate model than the KL method for a nonlinear problem because the KL method is only a linear dimension reduction.

However, all these methods are temporal models and can not model spatio-temporal dynamics directly. Whether these methods that are efficient in the traditional temporal dynamics can be applied to the spatio-temporal dynamics is an open question that needs to be answered in this book.

The book has two major objectives:

(1) to develop some useful spatio-temporal modeling approaches for unknown nonlinear DPS, based on the idea of the traditional Wiener, Hammerstein, Volterra and neural method;

(2) to apply the presented methods to thermal processes in IC packaging and chemical industry.

The work in this book mainly includes:

- To provide a systematic overview and classification on the DPS modeling;
- To develop spatio-temporal Wiener and Hammerstein models for the nonlinear DPS with the help of the KL method;
- To develop spatio-temporal Hammerstein and Volterra models for the nonlinear DPS using the idea of spatio-temporal kernels;
- To develop the spatio-temporal neural model for the nonlinear DPS;
- To apply and evaluate the presented models on modeling of typical thermal processes in IC packaging and chemical industry through simulation and experiment.

## 1.2 Contributions and Organization of the Book

In this book, we will present the spatio-temporal Wiener (Chapter 3), spatio-temporal Hammerstein (Chapters 4 & 5), spatio-temporal Volterra (Chapter 6) and spatio-temporal neural NARX (nonlinear autoregressive with exogenous input) (Chapter 7) modeling approaches for the unknown nonlinear DPS.

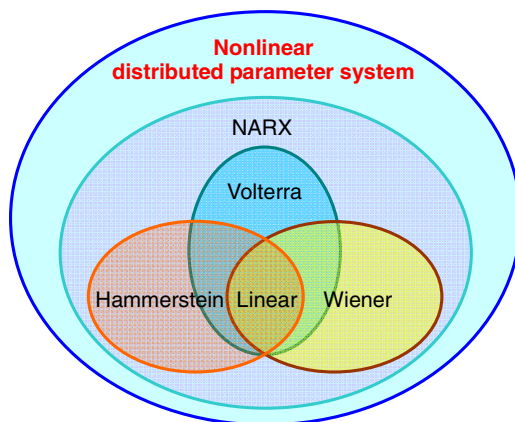


**Fig. 1.4** Spatio-temporal models for nonlinear DPS



The relationship of these models is shown in [Figure 1.4](#). The Wiener, Hammerstein and Volterra models are complexity restricted nonlinear models included in a general class of NARX models with the linear model as a special case. The Wiener, Hammerstein and Volterra models have special nonlinear structures, while the NARX model is useful for describing more complex nonlinear systems.

The way to process the spatial information is a crucial work in DPS modeling. In this book, three different approaches are classified in [Figure 1.5](#).

- *KL based approach.* The DPS is separated into a set of spatial basis functions and temporal dynamics using the KL method for time/space separation. Then the traditional modeling approach is used to model the temporal dynamics. With the time-space synthesis, the spatio-temporal dynamics can be reconstructed. The work will be described in details in [Chapters 3 and 4](#).
- *Kernel based approach.* The traditional model can be extended to DPS via the spatio-temporal kernel. After the time/space separation using the KL method, the model can be estimated in the temporal domain. The work will be described in details in [Chapters 5 and 6](#).
- *NL-PCA based approach.* The nonlinear time/space separation of DPS is performed using nonlinear PCA. Then traditional modeling approach can be used to model the temporal dynamics. With the nonlinear time/space synthesis, the spatio-temporal dynamics can be recovered. The work will be described in details in [Chapter 7](#).

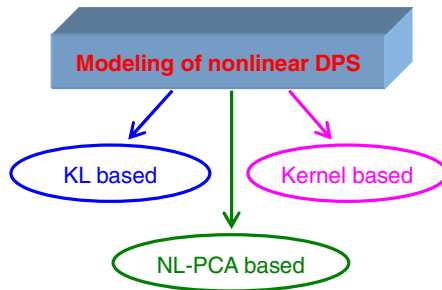


**Fig. 1.5** Spatial information processing for DPS modeling

This book provides several useful modeling frameworks for control of unknown nonlinear DPS. The developed modeling methodologies not only can be used in the thermal process, but also can be easily applied to other distributed industrial processes. The contents of each chapter will be summarized as below with emphases on the main contributions.

[Chapter 2](#) is a systematic overview and classification on the DPS modeling. Three DPS modeling problems, model reduction for known DPS, parameter estimation for DPS with unknown parameters, and system identification for DPS in

unknown structure, are discussed. Various approaches are classified with their limitations and advantages summarized as well. This overview motivates us to develop new DPS modeling methods.

In **Chapter 3**, a KL based Wiener modeling approach is presented (Qi & Li, 2008b). A **spatio-temporal Wiener model** (a linear DPS followed by a static nonlinearity) is established for modeling nonlinear DPS. After the time/space separation, it can be represented by traditional Wiener system with a set of spatial basis functions. To obtain a low-order model, the KL method is used for the time/space separation and dimension reduction. Then the Wiener model is obtained using the least-squares estimation and the instrumental variables method, which can achieve consistent estimates under process noise.

In **Chapter 4**, a KL based Hammerstein modeling approach is provided (Qi & Li, 2009a). A **spatio-temporal Hammerstein model** (a static nonlinearity followed by a linear DPS) is constructed for modeling the nonlinear DPS. After the time/space separation, it can be represented by the traditional Hammerstein system with a set of spatial basis functions. To achieve a low-order model, the KL method is used for the time/space separation and dimension reduction. To obtain a parsimonious Hammerstein model, the orthogonal forward regression algorithm is used to determine the compact or sparse model structure, and then the parameters are estimated using the least-squares method and the singular value decomposition. This method can obtain a low-order and parsimonious Hammerstein model.

In **Chapter 5**, a kernel based multi-channel spatio-temporal Hammerstein modeling approach is presented (Qi, Zhang & Li, 2009). For modeling nonlinear DPS, a **spatio-temporal Hammerstein model** (a static nonlinearity followed by a linear spatio-temporal kernel) is constructed. A basic identification approach with the least-squares estimation and singular value decomposition can work well if the model structure is matched with the system. When there are some unmodeled dynamics, a multi-channel modeling framework is presented to achieve a better performance, which can guarantee the convergence under noisy measurements.

In **Chapter 6**, a Volterra kernel based spatio-temporal modeling approach is presented (Li, Qi & Yu, 2009; Li & Qi, 2009). To reconstruct the spatio-temporal dynamics, a **spatio-temporal Volterra model** is constructed with a series of spatio-temporal kernel. To achieve a low-order model, the KL method is used for the time/space separation and dimension reduction. Then the model is estimated with a least-squares algorithm, which can guarantee the convergence under noisy measurements.

In **Chapter 7**, a NL-PCA based neural modeling approach is presented (Qi & Li, 2009b). One NL-PCA network is trained for nonlinear dimension reduction and nonlinear time/space reconstruction, and then the other neural model is to learn the system dynamics. With the powerful capability of dimension reduction and intelligent learning, this **spatio-temporal neural model** can describe more complex and strong nonlinear DPS.

**Chapter 8** provides conclusions and future challenges.

## References

- [1] Aggelogiannaki, E., Sarimveis, H.: Nonlinear model predictive control for distributed parameter systems using data driven artificial neural network models. *Computers and Chemical Engineering* 32(6), 1225–1237 (2008)
- [2] Bai, E.W.: An optimal two-stage identification algorithm for Hammerstein-Wiener nonlinear systems. *Automatica* 34(3), 333–338 (1998)
- [3] Banks, H.T., Kunisch, K.: Estimation techniques for distributed parameter systems. Birkhauser, Boston (1989)
- [4] Boyd, J.P.: Chebyshev and Fourier spectral methods, 2nd edn. Dover Publications, New York (2000)
- [5] Boyd, S., Chua, L.O.: Fading memory and the problem of approximating nonlinear operators with Volterra series. *IEEE Transactions on Circuits and Systems* 32(11), 1150–1161 (1985)
- [6] Brenner, S.C., Ridgway Scott, L.: The mathematical theory of finite element methods. Springer, New York (1994)
- [7] Canuto, C., et al.: Spectral methods in fluid dynamics. Springer, New York (1988)
- [8] Christofides, P.D.: Robust control of parabolic PDE systems. *Chemical Engineering Science* 53(16), 2949–2965 (1998)
- [9] Christofides, P.D.: Control of nonlinear distributed process systems: Recent developments and challenges. *AIChE Journal* 47(3), 514–518 (2001a)
- [10] Christofides, P.D.: Nonlinear and robust control of PDE systems: Methods and applications to transport-reaction processes. Birkhäuser, Boston (2001b)
- [11] Christofides, P.D., Armaou, A. (eds.): Control of multiscale and distributed process systems - Preface. *Computers and Chemical Engineering* 29(4), 687–688 (2005)
- [12] Christofides, P.D., Wang, X.Z. (eds.): Special issue on ‘control of particulate processes’. *Chemical Engineering Science* 63(5), 1155 (2008)
- [13] Christofides, P.D. (ed.): Special volume on ‘control of distributed parameter systems’. *Computers and Chemical Engineering* 26(7-8), 939–940 (2002)
- [14] Christofides, P.D. (ed.): Special issue on ‘control of complex process systems’. *International Journal of Robust and Nonlinear Control* 14(2), 87–88 (2004)
- [15] Coca, D., Billings, S.A.: Direct parameter identification of distributed parameter systems. *International Journal of Systems Science* 31(1), 11–17 (2000)
- [16] Coca, D., Billings, S.A.: Identification of finite dimensional models of infinite dimensional dynamical systems. *Automatica* 38(11), 1851–1865 (2002)
- [17] Demetriou, M.A., Rosen, I.G.: Adaptive identification of second-order distributed parameter systems. *Inverse Problems* 10(2), 261–294 (1994)
- [18] Deng, H., Li, H.-X., Chen, G.: Spectral-approximation-based intelligent modeling for distributed thermal processes. *IEEE Transactions on Control Systems Technology* 13(5), 686–700 (2005)
- [19] Dochain, D., Dumont, G., Gorinevsky, D., Ogunnaike, T. (eds.): Special issue on ‘control of industrial spatially distributed processes’. *IEEE Transactions on Control Systems Technology* 11(5), 609–611 (2003)
- [20] Dong, D., McAvoy, T.J.: Nonlinear principal component analysis-based on principal curves and neural networks. *Computers and Chemical Engineering* 20(1), 65–78 (1996)
- [21] Doyle III, F.J., Ogunnaike, B.A., Pearson, R.K.: Nonlinear model-based control using second-order Volterra Models. *Automatica* 31(5), 697–714 (1995)

- [22] Gay, D.H., Ray, W.H.: Identification and control of distributed parameter systems by means of the singular value decomposition. *Chemical Engineering Science* 50(10), 1519–1539 (1995)
- [23] Gómez, J.C., Jutan, A., Baeyens, E.: Wiener model identification and predictive control of a pH neutralisation process. *IEE Proceedings-Control Theory and Applications* 151(3), 329–338 (2004)
- [24] Gonzalez-Garcia, R., Rico-Martinez, R., Kevredidis, I.G.: Identification of distributed parameter systems: A neural net based approach. *Computers and Chemical Engineering* 22, S965–S968 (1998)
- [25] Guo, L.Z., Billings, S.A.: State-space reconstruction and spatio-temporal prediction of lattice dynamical systems. *IEEE Transactions on Automatic Control* 52(4), 622–632 (2007)
- [26] Hagenblad, A., Ljung, L.: Maximum likelihood estimation of Wiener models. Report no.: LiTH-ISY-R-2308, Linköping University, Sweden (2000)
- [27] Holmes, P., Lumley, J.L., Berkooz, G.: Turbulence, coherent structures, dynamical systems, and symmetry. Cambridge University Press, New York (1996)
- [28] Hsieh, W.W.: Nonlinear principal component analysis by neural networks. *Tellus Series A - Dynamic Meteorology and Oceanography* 53(5), 599–615 (2001)
- [29] Kirby, M., Miranda, R.: The nonlinear reduction of high-dimensional dynamical systems via neural networks. *Physical Review Letter* 72(12), 1822–1825 (1994)
- [30] Kramer, M.A.: Nonlinear principal component analysis using autoassociative neural networks. *AIChE Journal* 37(2), 233–243 (1991)
- [31] Li, H.-X., Qi, C.K.: Incremental modeling of nonlinear distributed parameter processes via spatio-temporal kernel series expansion. *Industrial & Engineering Chemistry Research* 48(6), 3052–3058 (2009)
- [32] Li, H.-X., Qi, C.K., Yu, Y.G.: A spatio-temporal Volterra modeling approach for a class of nonlinear distributed parameter processes. *Journal of Process Control* 19(7), 1126–1142 (2009)
- [33] Maner, B.R., Doyle III, F.J., Ogunnaike, B.A., Pearson, R.K.: Nonlinear model predictive control of a simulated multivariable polymerization reactor using second-order Volterra models. *Automatica* 32(9), 1285–1301 (1996)
- [34] Mitchell, A.R., Griffiths, D.F.: The finite difference method in partial differential equations. Wiley, Chichester (1980)
- [35] Narendra, K., Gallman, P.: An iterative method for the identification of nonlinear systems using a Hammerstein model. *IEEE Transactions on Automatic Control* 11(3), 546–550 (1966)
- [36] Newman, A.J.: Model reduction via the Karhunen-Loève expansion part I: An exposition. Technical Report T.R.96-32, University of Maryland, College Park, Maryland (1996a)
- [37] Parker, R.S., Heemstra, D., Doyle III, F.J., Pearson, R.K., Ogunnaike, B.A.: The identification of nonlinear models for process control using tailored “plant-friendly” input sequences. *Journal of Process Control* 11(2), 237–250 (2001)
- [38] Qi, C.K., Li, H.-X.: Hybrid Karhunen-Loève/neural modeling for a class of distributed parameter systems. *International Journal of Intelligent Systems Technologies and Applications* 4(1-2), 141–160 (2008a)
- [39] Qi, C.K., Li, H.-X.: A Karhunen-Loève decomposition based Wiener modeling approach for nonlinear distributed parameter processes. *Industrial & Engineering Chemistry Research* 47(12), 4184–4192 (2008b)

- [40] Qi, C.K., Li, H.-X.: A time/space separation based Hammerstein modeling approach for nonlinear distributed parameter. *Computers & Chemical Engineering* 33(7), 1247–1260 (2009a)
- [41] Qi, C.K., Li, H.-X.: Nonlinear dimension reduction based neural modeling for spatio-temporal processes. *Chemical Engineering Science* 64(19), 4164–4170 (2009b)
- [42] Qi, C.K., Zhang, H.-T., Li, H.-X.: A multi-channel spatio-temporal Hammerstein modeling approach for nonlinear distributed parameter processes. *Journal of Process Control* 19(1), 85–99 (2009)
- [43] Romijn, R., Özkan, L., Weiland, S., Ludlage, J., Marquardt, W.: A grey-box modeling approach for the reduction of nonlinear systems. *Journal of Process Control* 18(9), 906–914 (2008)
- [44] Rugh, W.: *Nonlinear system theory: The Volterra/Wiener approach*. Johns Hopkins University Press, Baltimore (1981)
- [45] Sahan, R.A., Koc-Sahan, N., Albin, D.C., Liakopoulos, A.: Artificial neural network-based modeling and intelligent control of transitional flows. In: *Proceeding of the 1997 IEEE International Conference on Control Applications*, Hartford, CT, pp. 359–364 (1997)
- [46] Schetzen, M.: *The Volterra and Wiener theories of nonlinear systems*. Wiley, New York (1980)
- [47] Sirovich, L.: Turbulence and the dynamics of coherent structures parts I-III. *Quarterly of Applied Mathematics* 45(3), 561–590 (1987)
- [48] Smaoui, N.: Linear versus nonlinear dimensionality reduction of high-dimensional dynamical systems. *SIAM Journal on Scientific Computing* 25(6), 2107–2125 (2004)
- [49] Smaoui, N., Al-Enezi, S.: Modelling the dynamics of nonlinear partial differential equations using neural networks. *Journal of Computational and Applied Mathematics* 170(1), 27–58 (2004)
- [50] Stoica, P., Söderström, T.: Instrumental-variable methods for identification of Hammerstein systems. *International Journal of Control* 35(3), 459–476 (1982)
- [51] Webb, A.R.: An approach to non-linear principal components analysis using radially symmetric kernel functions. *Journal Statistics and Computing* 6(2), 159–168 (1996)
- [52] Westwick, D., Verhaegen, M.: Identifying MIMO Wiener systems using subspace model identification methods. *Signal Processing* 52(2), 235–258 (1996)
- [53] Wilson, D.J.H., Irwin, G.W., Lightbody, G.: RBF principal manifolds for process monitoring. *IEEE Transactions on Neural Networks* 10(6), 1424–1434 (1999)
- [54] Zheng, D., Hoo, K.A., Piovoso, M.J.: Low-order model identification of distributed parameter systems by a combination of singular value decomposition and the Karhunen-Loève expansion. *Industrial & Engineering Chemistry Research* 41(6), 1545–1556 (2002)
- [55] Zhou, X.G., Liu, L.H., Dai, Y.C., Yuan, W.K., Hudson, J.L.: Modeling of a fixed-bed reactor using the KL expansion and neural networks. *Chemical Engineering Science* 51(10), 2179–2188 (1996)
- [56] Zhu, Y.C.: Identification of Hammerstein models for control using ASYM. *International Journal of Control* 73(18), 1692–1702 (2000)

## 2 Modeling of Distributed Parameter Systems: Overview and Classification

**Abstract.** This chapter provides a systematic overview of the distributed parameter system (DPS) modeling and its classification. Three different problems in DPS modeling are discussed, which includes model reduction for known DPS, parameter estimation for DPS, and system identification for unknown DPS. All approaches are classified into different categories with their limitations and advantages briefly discussed. This overview motivates us to develop new methods for DPS modeling.

### 2.1 Introduction

When the distributed parameter system (DPS) is known, partial differential equations (PDE), which are derived from the physical and chemical knowledge (i.e., *first-principle modeling*) under simplified assumptions, can provide a nominal model of the system. Though there are usually some uncertainties between the nominal model and the system, it can capture the dominant dynamics of the system. Because of limited computation capacity for numerical implementation and a finite number of actuators and sensors for sensing and control, such infinite-dimensional systems need to be reduced into finite-dimensional approximation systems, e.g., ordinary differential equations (ODE), and difference equations (DE), etc. This is so called *model reduction* of the DPS.

However, in many situations it is very difficult to get an accurate nominal PDE description via the first-principle modeling because of incomplete physical and chemical process knowledge (e.g., unknown system parameters, unknown model structure and disturbance). These uncertainties existing in the process make the modeling problem more difficult and challenging.

When the DPS is unknown, extra efforts are needed besides the previous model reduction. Two different situations may happen. One is *grey-box modeling*, where the PDE structure is available from a priori knowledge with only some parameters need to determine. These unknown parameters can be estimated from the input-output data, which is the so-called *parameter estimation* of the DPS. Another situation is *black-box modeling*, where the PDE structure is unknown. Then both model structure and parameters need to be determined or identified from the measurement, which is the so-called *system identification* of the DPS.

The aforementioned problems: *model reduction*, *parameter estimation* and *system identification* are fundamentals of the DPS modeling. In the last several decades, many researchers in the field of mathematics and engineering have made much effort on these problems. For each problem, though many different methods have been developed, most of these methods can be synthesized into several

categories. Moreover, different problems and their corresponding methods perhaps share some common properties. Though this book will focus on the system identification problem, for easy understanding, it will only provide an overview on selected problems rather than the whole area.

Since it is a very large and complex field, it is almost impossible to review every work in the area. We will focus on the applicable methods and their classifications. For simplicity, some of the complicated mathematical theories, such as, existence and uniqueness of the PDE solution, modeling error analysis, parameter identifiability, convergence of the estimation algorithm, etc., will not be included in this chapter. See the related references for more details on these problems.

This chapter is organized as follows: model reduction for known DPS in [Section 2.2](#), parameter estimation for known structure of DPS in [Section 2.3](#) and system identification for unknown structure of DPS in [Section 2.4](#). Conclusions will be given in [Section 2.5](#) together with new modeling ideas that will be studied in the rest of the book.

For simplicity, we consider a class of quasi-linear parabolic systems in one-dimensional spatial domain

$$\frac{\partial y(x,t)}{\partial t} = \alpha \frac{\partial^2 y}{\partial x^2} + \beta \frac{\partial y}{\partial x} + f(y) + wb(x)u(t), \quad (2.1)$$

subject to the boundary conditions

$$y(0,t) = 0, y(\pi,t) = 0, \quad (2.2)$$

and the initial condition

$$y(x,0) = y_0(x), \quad (2.3)$$

where  $y(x,t) \in \mathbb{R}$  denotes the output variable,  $[0,\pi] \subset \mathbb{R}$  is the spatial domain of definition of the system,  $x \in [0,\pi]$  is the spatial coordinate,  $t \in [0,\infty)$  is the time,  $u(t) = [u_1 \ u_2 \ \dots \ u_m]^T \in \mathbb{R}^m$  denotes the vector of manipulated inputs,  $f(y)$  is a nonlinear function,  $\alpha$ ,  $\beta$  and  $w$  are constants,  $b(x)$  is a vector function of  $x$  of the form  $b(x) = [b_1 \ b_2 \ \dots \ b_m]$ ,  $b_i(x)$  describes how the control action  $u_i(t)$  is distributed in the interval  $[0,\pi]$ . Define the spatial operator  $\mathcal{A}$  as

$$\mathcal{A}y = \alpha \frac{\partial^2 y}{\partial x^2} + \beta \frac{\partial y}{\partial x}. \quad (2.4)$$

Two industrial cases will be used to demonstrate and compare different modeling methods (e.g., spectral method and KL method). The first case is a quasi-linear parabolic process, and the second one is a nonlinear parabolic process.

### Case 1: Quasi-linear Parabolic Process

Consider the catalytic rod given in [Section 1.1.2](#), and assume that the dimensionless reaction rate  $\beta_T$  is spatially-varying, the spatio-temporal evolution of the

dimensionless rod temperature is described by the following quasi-linear parabolic PDE,

$$\frac{\partial y}{\partial t} = k \frac{\partial^2 y}{\partial x^2} + \beta_r(x)(e^{-\frac{\gamma}{1+y}} - e^{-\gamma}) + \beta_u(b(x)u(t) - y), \quad (2.5)$$

subject to the Dirichlet boundary conditions,

$$y(0, t) = 0, y(\pi, t) = 0, \quad (2.6)$$

and the initial condition,

$$y(x, 0) = y_0(x), \quad (2.7)$$

where the parameter values are given in [Table 2.1](#).

**Table 2.1** Dimensionless parameters for Case 1

Parameter	Real values	Nominal values	Definition
$k$	1	1	Diffusion coefficient
$\beta_r$	$12(\cos(x) + 1)$	---	Heat of reaction
$\beta_u$	20	20	Heat transfer coefficient
$\gamma$	2	---	Activation energy

### Case 2: Nonlinear Parabolic Process

Consider the catalytic rod given in [Section 1.1.2](#) again, and assume that the spatial differential operator is nonlinear (e.g., nonlinear dependence of the thermal conductivity on temperature) with the convection feature and that the dimensionless reaction rate  $\beta_r$  is spatially-varying. In this case, the process will be described in the following nonlinear parabolic PDE,

$$\frac{\partial y}{\partial t} = \frac{\partial}{\partial x}(k(y)\frac{\partial y}{\partial x}) - v\frac{\partial y}{\partial x} + \beta_r(x)(e^{-\frac{\gamma}{1+y}} - e^{-\gamma}) + \beta_u(b(x)u(t) - y), \quad (2.8)$$

subject to the boundary conditions,

$$y(0, t) = 0, y(\pi, t) = 0, \quad (2.9)$$

and the initial condition,

$$y(x, 0) = y_0(x), \quad (2.10)$$

where the parameter values can be found in [Table 2.2](#).



**Table 2.2** Dimensionless parameters for Case 2

Parameter	Real values	Nominal values	Definition
$k$	$1 + 0.7/(y + 1)$	1	Diffusion coefficient
$\nu$	10	10	
$\beta_T$	$12(\cos(x) + 1)$	---	Heat of reaction
$\beta_u$	20	20	Heat transfer coefficient
$\gamma$	2	---	Activation energy

## 2.2 White-Box Modeling: Model Reduction for Known DPS

Rigorous mathematical models could be derived from the first-principle knowledge under simplified conditions, but they may involve unknown parameters. We will review the parameter estimation problem in [Section 2.3](#). Here, we assume that the PDE description of the DPS is completely known. Then the simulation and control of the DPS are usually accomplished by transforming the PDE and boundary conditions into a finite-dimensional system, such as ordinary differential equation or difference equation ([DE](#)). These lumping (i.e., model reduction) methods include: eigenfunction method, Green's function method, finite difference method, and a class of weighted residual method (e.g., Galerkin, collocation, finite element, spectral and Karhunen-Loève method).

### 2.2.1 Eigenfunction Method

The analytical solution of linear partial differential equations could be obtained using the method of [separation of variables](#) ([Powers, 1999](#)). First, assume the solution can be expressed by the following form of separation of variables

$$y(x, t) = \sum_{i=1}^{\infty} \phi_i(x) y_i(t) = \bar{\phi}^T(x) \bar{y}(t), \quad (2.11)$$

where  $\bar{\phi}(x)$  and  $\bar{y}(t)$  are the corresponding spatial and temporal vectors, respectively. Substituting it into the original linear PDE will yield the eigenvalues and [eigenfunctions](#). For  $\mathcal{A}$ , the standard eigenvalue and eigenfunction problem is of the form

$$\mathcal{A}\phi_j = \lambda_j\phi_j, j = 1, \dots, \infty, \quad (2.12)$$

where  $\lambda_j$  denotes an eigenvalue and  $\phi_j$  denotes an eigenfunction. For many typical operator  $\mathcal{A}$  and boundary conditions, the eigenvalue and eigenfunction can be found from the book ([Butkovskiy, 1982](#)). It is an infinite-dimensional eigenfunction solution. By truncation, a finite-dimensional approximation solution will be obtained.

A low-order model may be possible only if the system is **self-adjoint**. Otherwise, a high-order solution should be used for a satisfactory accuracy. High-order models always result in a difficult control realization. This is primarily attributed to the lack of measurement for characterizing the distributed nature and the lack of actuators for control implementation.

Moreover, the condition of separation of variables is very rigor. Whether or not the method of separation of variables can be applied to a particular problem depends on not only the differential equation but also on the shape of the domain and the form of the boundary conditions.

In particular, for a nonlinear PDE, it is difficult to separate the variables and find the set of analytical eigenfunctions. One approach is to linearize the nonlinear system at a nominal state using the Taylor series expansion. The resulting system is a linear system plus nonlinear terms. The eigenfunctions of linear part can be used to transfer the PDE to an ODE. Rigorously speaking, this method is different from the original method of separation of variables, and in fact it belongs to a new method, i.e., weighted residual method, which will be discussed in [Section 2.2.4](#).

### 2.2.2 Green's Function Method

The characteristic of linear DPS can be completely represented by the *Green's function* as below (also called the impulse response function or kernel).

$$y(z,t) = \int_0^t \int_0^\pi g(z,\zeta,t-\tau)u(\zeta,\tau)d\zeta d\tau. \quad (2.13)$$

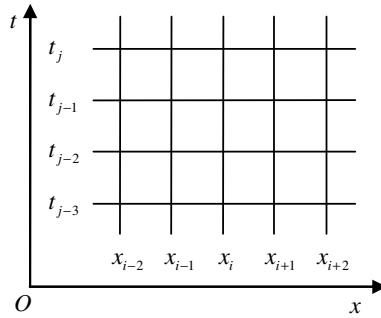
If the eigenvalue and eigenfunction can be solved analytically, the Green's function can be expressed by an infinite-dimensional eigenfunction expansion analytically. By truncation, a finite-dimensional approximation can be obtained. The Green's functions of many typical linear differential operators have been given in ([Butkovskiy, 1982](#)). This approach assumes the PDE is linear, though most of DPS are essentially nonlinear. Furthermore, a low-order eigenfunction representation of Green's function may be possible only if the system is self-adjoint. However, there are no assurances that they are self-adjoint. Fortunately, for the non-self-adjoint system, the singular function representation of Green's function could be low-order, and can be estimated from the input-output data. More details are introduced in [Section 2.4.1](#).

### 2.2.3 Finite Difference Method

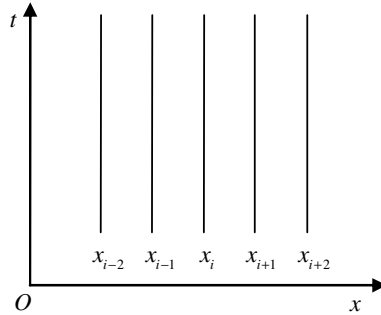
*Finite difference method* (FDM) is a popular method to provide the numerical solution of the PDE ([Mitchell & Griffiths, 1980](#)). The spatio-temporal variables are discretized within the time-space domain as illustrated in [Figure 2.1a](#). Derivatives at each discretization node are approximated by the difference over a small interval, which can be forward, backward and central difference derived often from Taylor expansion. Then the PDE system is transformed into a set of difference equations, whose order is proportional to the number of spatial discretization nodes. The most attractive feature of FDM is that it can work for all kinds of DPS with various

boundary conditions and regular domain. However, it usually requires a high-order model for an accurate solution, and has the disadvantages of heavy computational burden.

The *method of lines* (MOL) (Schiesser, 1991) is a special case of the FDM, with only partial derivatives in the spatial direction replaced by finite difference approximations, as illustrated in Figure 2.1b. This results in a system of ODE because of the spatial discretization. It has the similar strength and weakness as FDM.



(a) Finite difference method



(b) Method of lines

**Fig. 2.1** Geometric interpretations of finite difference and method of lines

## 2.2.4 Weighted Residual Method

The *weighted residual method* (WRM) (Ray, 1981; Fletcher, 1984) is the most often used and most efficient lumping method for DPS. It is well known that a continuous function can be approximated using *Fourier series* (Zill & Cullen, 2001). Based on this principle, the spatio-temporal variable  $y(x, t)$  of the DPS can be expanded by a set of *spatial basis functions* (BFs)  $\{\phi_i(x)\}_{i=1}^{\infty}$  as follows

$$y(x, t) = \sum_{i=1}^{\infty} \phi_i(x) y_i(t) = \bar{\phi}^T(x) \bar{y}(t), \quad (2.14)$$

where  $\bar{\phi}(x)$  and  $\bar{y}(t)$  are the corresponding vectors. Similar to Fourier series, the spatial BFs are often ordered from slow to fast in the spatial frequency domain. Because the fast modes contribute little to the whole system, only the first  $n$  slow modes in the expansion will be retained in practice (Fletcher, 1984)

$$y_n(x, t) = \sum_{i=1}^n \phi_i(x) y_i(t) = \bar{\phi}_n^T(x) \bar{y}_n(t), \quad (2.15)$$

where  $\bar{\phi}_n(x)$  and  $\bar{y}_n(t)$  are the corresponding vectors. Thus, the spatio-temporal variable is separated into a set of spatial BFs and the temporal variables, as depicted in Figure 2.2. The key is to select proper spatial BFs, and construct the finite-order (low-order) temporal model as explained in Figure 2.3. Finally, through the time-space synthesis, the spatio-temporal system will be recovered.

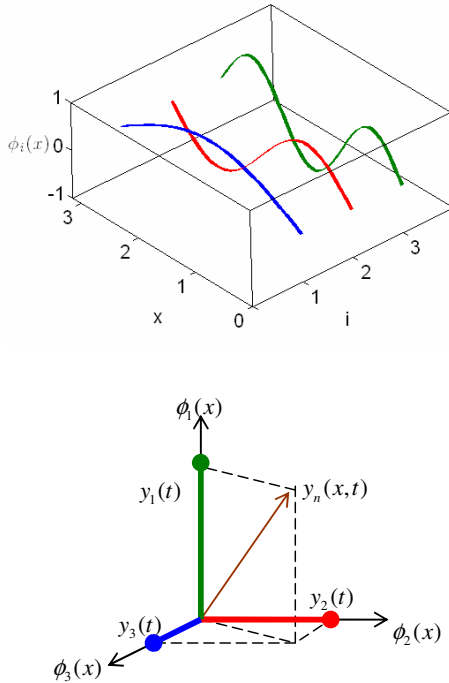
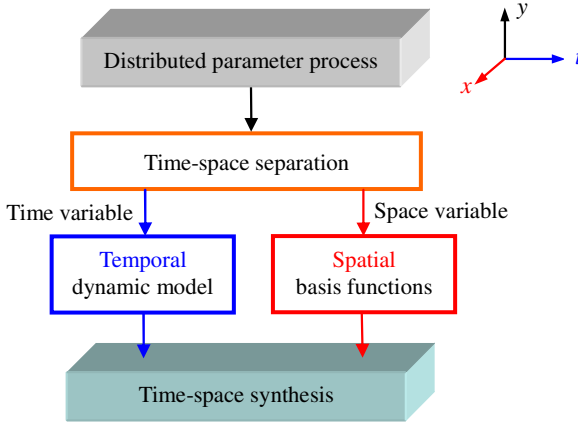


Fig. 2.2 Geometric interpretation of time-space separation for  $n=3$



**Fig. 2.3** Framework of weighted residual method

In the WRM, the equation residual of the model (2.1) generated from the truncated expansion can be expressed as

$$R(x,t) = \dot{y}_n - \left( \alpha \frac{\partial^2 y_n}{\partial x^2} + \beta \frac{\partial y_n}{\partial x} + f(y_n) + wbu \right), \quad (2.16)$$

which is made small in the sense that

$$(R, \varphi_i) = 0, i = 1, \dots, n, \quad (2.17)$$

where  $\{\varphi_i(x)\}_{i=1}^n$  are a set of **weighting functions** to be chosen. As shown in **Figure 2.4**, the minimization of the residual  $R$  actually turns to minimize its projections onto weighting functions. This is an easy way to obtain a  $n$ -order ODE model for  $\{y_i(t)\}_{i=1}^n$ .

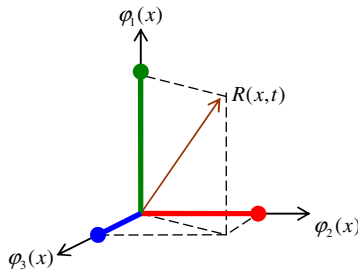


**Fig. 2.4** Geometric interpretation of weighted residual method

Notice that WRM is an extension of the eigenfunction method with the difference that WRM may use any of basis functions, while the eigenfunction method uses the eigenfunctions of the linear operator. It is possible to apply WRM to both linear and nonlinear PDE systems.

The accuracy and efficiency of WRM is very dependent on the basis and weighting functions chosen (Fletcher, 1984). Thus, in the following sections, WRM will be further classified into different methods according to the type of weighting and basis functions used. Of course, all these methods are the combination of temporal model construction and spatial BFs selection.

### 2.2.4.1 Classification Based on Weighting Functions

Many methods have been proposed based on the selection of weighting functions. The most popular approach appears to be *Galerkin method* and *collocation method*.

#### 2.2.4.1.1 Galerkin Method

If the weighting functions  $\{\phi_i(x)\}_{i=1}^n$  are chosen to be the BFs  $\{\phi_i(x)\}_{i=1}^n$ , then the method is called the *Galerkin method* (Ray, 1981; Fletcher, 1984). It has the advantage that the residual is made orthogonal to each BF and is, therefore, the best solution possible in the space made up of the  $n$  functions  $\phi_i(x)$ . Because it does not need to find other weighting functions, this method is relatively simple and most often used.

Consider the PDE system described by (2.1)-(2.3), define the first finite modes  $\bar{y}_n(t) = [y_1(t), y_2(t), \dots, y_n(t)]^T$  as slow modes and the last infinite modes  $\bar{y}_r(t) = [y_{n+1}(t), y_{n+2}(t), \dots, y_\infty(t)]^T$  as fast modes, using the Galerkin method yields

$$\frac{d\bar{y}_n}{dt} = A_r \bar{y}_n + A_{nr} \bar{y}_r + F_n(\bar{y}_n, \bar{y}_r) + B_n u, \quad (2.18)$$

$$\frac{d\bar{y}_r}{dt} = A_m \bar{y}_n + A_r \bar{y}_r + F_r(\bar{y}_n, \bar{y}_r) + B_r u, \quad (2.19)$$

$$y = C_n \bar{y}_n + C_r \bar{y}_r, \quad \bar{y}_n(0) = 0, \quad \bar{y}_r(0) = 0, \quad (2.20)$$

where  $A_n$ ,  $A_r$ ,  $A_{nr}$ ,  $A_m$ ,  $F_n$ ,  $F_r$ ,  $B_n$ ,  $B_r$ ,  $C_n$  and  $C_r$  are proper dimensional matrix (see Balas, 1983; Christofides, 2001b). Even though the basis functions are orthonormal, the terms  $A_{nr}$  and  $A_m$  may be nonzero because of *spill-over effects* (Balas, 1986). The spill-over means that those residual modes have effects on the dominant modes (modes coupling). It is true that  $(\phi_i, \phi_j) = \delta_{ij}$ , but it is typically not true that  $(\phi_i, A\phi_j) = \delta_{ij}$ . That means  $A_{nr} \neq 0$  and  $A_m \neq 0$ .

Because the fast modes contribute very little to the whole system, after neglecting the residual modes the following finite-dimensional nonlinear system is obtained

$$\frac{d\bar{y}_n}{dt} = A_r \bar{y}_n + F_n(\bar{y}_n, 0) + B_n u, \quad (2.21)$$

$$y = C_n \bar{y}_n, \quad \bar{y}_n(0) = 0, \quad (2.22)$$

This approach is referred to the linear Galerkin method because the residual modes are completely ignored.

### 2.2.4.1.2 Collocation Method

The weighting functions of the *collocation method* (Ray, 1981) are chosen to be *Dirac delta functions*  $\delta(x - x_i)$ ,  $i = 1, \dots, n$ . The residuals vanish at collocation nodes  $\{x_i\}_{i=1}^n$ , i.e.  $R(x_i) = 0$ , so the collocation nodes are very critical for the modeling performance. Fortunately, some mathematical theories show that they can be specified automatically in an optimal way. For example, they can be chosen as the roots of the *orthogonal polynomials* (e.g. Lefèvre *et al.*, 2000; Dochain *et al.*, 1992). If the orthogonal functions are used as the BFs, it is so called the *orthogonal collocation method* (Ray, 1981).

Both Galerkin and collocation methods are linear reduction methods that work fine for the linear DPS. Since the fast modes  $\{y_i(t)\}_{i=n+1}^\infty$  are completely ignored, some information of the slow modes may also get lost for the nonlinear DPS because of the coupling between the slow and fast modes. To improve the model accuracy and avoid a high-order model at the same time, *nonlinear reduction methods* are often used for the nonlinear DPS modeling, where some fast modes  $\{y_i(t)\}_{i=n+1}^{n+m}$  are compensated as a function of the slow modes  $\{y_i(t)\}_{i=1}^n$ . One form of *nonlinear reduction method* is based on *inertial manifold (IM)* (Temam, 1988), where the fast modes are accurately described by the slow modes, and then the DPS can be exactly transformed into a finite-dimensional system. However, for many nonlinear DPS, IM may not exist or may be difficult to find.

#### *Remark 2.1: Approximated Inertial Manifold Method*

To overcome the above problems, the *approximated inertial manifold (AIM)* is used to approximately compensate the fast modes with the slow modes (Foias, Jolly *et al.*, 1988; Shvartsman & Kevrikidis, 1998; Christofides & Daoutidis, 1997). Even for the systems with unknown existence of IM, the AIM method can often achieve a better performance than the linear Galerkin or collocation methods.

A general expression of fast modes  $\hat{y}_r$  is given by

$$\hat{y}_r = G(\bar{y}_n(t), u), \quad (2.23)$$

With substitution of (2.23) into (2.18), a finite-dimensional model is given by

$$\frac{d\bar{y}_n}{dt} = A_r \bar{y}_n + A_{nr} \hat{y}_r + F_n(\bar{y}_n, \hat{y}_r) + B_n u. \quad (2.24)$$

An application of the AIM method can increase the accuracy of the reduced-order system without increasing the order of the basis functions.

The key problem is to obtain an approximation of  $G$ . There are several approaches to obtain the AIM.

- To assume that the fast modes are at pseudo-steady state, then the so-called *steady manifold* (Foias & Temam, 1988) can approximate IM easily, by ignoring the dynamic information of the fast modes.
- To consider the dynamic information, another AIM is used by integrating the fast modes for a short time using an *implicit Euler method* (Foias, Jolly *et al.*, 1988).
- To further improve the approximation accuracy, a novel procedure based on *singular perturbations method* can be used to construct the AIM with an arbitrary accuracy under certain conditions (Christofides & Daoutidis, 1997; Christofides, 2001b).

All the above AIM can be implemented in either the Galerkin or the collocation approach, which leads to *Galerkin AIM* and *collocation AIM* methods. There are other means of obtaining the AIM, such as, finite difference, which is not discussed here.

**Remark 2.2: Other Weighting Functions**

Note that the weighting functions are not limited to previous choices. For example, in method of subdomains, the weighting functions are chosen to be a set of Heaviside functions breaking the region into subdomain; in method of moments, the weighting functions are chosen to be powers of  $x$ .

**2.2.4.2 Classification Based on Basis Functions**

Selection of spatial BFs is critical to the WRM. It will have a great impact to the modeling performance. As shown in Table 2.3, the spatial BFs can be classified into *local*, and *global* types, and further into *analytical* and *data-based* functions. In general, there are three major approaches, the *finite element method* (FEM), the *spectral method* and the *Karhunen-Loève* (KL) method.

**Table 2.3** Classification of spatial basis functions

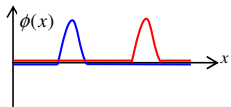
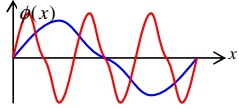
Type of BF	Analytical	Data-based
Local	FEM	
	<ul style="list-style-type: none"> <li>• Low-order piecewise polynomials</li> <li>• Splines</li> <li>• Wavelets, ..., etc.</li> </ul>	



Table 2.3 (continued)

Global	Spectral method	KL method
	<ul style="list-style-type: none"> <li>● Fourier series</li> <li>● Eigenfunctions</li> <li>● Orthogonal polynomials, ..., etc.</li> </ul>	

The data-based *KL* BFs are often global; and no data-based local BFs have been reported so far. Thus, rigorously speaking, *KL* method can also be considered as a kind of basis functions in spectral method. However, it is convenient to discuss them separately because they have some important differences. Different model reduction approach will be generated when different spatial BFs work with the Galerkin, collocation and AIM method.

### 2.2.4.2.1 Finite Element Method

The spatial BFs of the *FEM* are local. The spatial domain is first discretized into sub-domains. Then the *low-order piecewise polynomials* (Brenner & Ridgway Scott, 1994), *splines* (Höllig, 2003), and *wavelets* (Ko, Kurdila & Pilant, 1995; Mahadevan & Hoo, 2000) are often used as local BFs in subdomains. The number of basis functions is determined by the number of discretization points. Figure 2.5 shows an example of piecewise linear polynomials in one dimension.

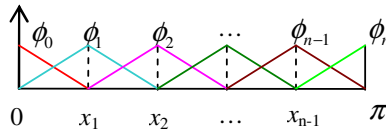


Fig. 2.5 Piecewise linear polynomials in one dimension

Further combined with temporal model construction methods, different applications are reported.

- Examples include, the *spline-Galerkin method* for the order reduction of the controller (Balas, 1986), the *wavelet-Galerkin method* and the *wavelet-Galerkin-AIM method* (Mahadevan & Hoo, 2000) for the reduced-order modeling.
- Other examples include, the *piecewise polynomials-Galerkin method* for an AIM implementation (Marion & Temam, 1990), the *wavelet-collocation method* for numerical simulation (Cruz *et al.*, 2001), and the *wavelet-collocation-AIM method* for the reduced-order modeling (Adrover *et al.*, 2000 & 2002).

The most attractive feature of the FEM is its flexible ability to handle complex geometries and boundaries because of the local BFs used. Due to its flexibility, many FEM software products are developed for the DPS simulation. Because of the local BFs, the FEM often requires a high-order model for a good approximation. The higher the order is, the larger the computational burden will be. Other disadvantages of a high-order solution include stability analysis and synthesis of implemental controllers. For the purpose of control synthesis for the DPS, it is reasonable to seek a methodology that yields a finite-order and accurate enough approximation model.

Both FDM and MOL can fall into the framework of FEM, if their spatial BFs and weighting functions are both chosen as Dirac delta functions. Thus, the FDM and MOL can be viewed as a subset of the FEM approach. The differences between FEM and FDM are:

- (1) The FDM is an approximation to the differential equation; the FEM is an approximation to its solution.
- (2) The FEM is easy to handle complex geometries (and boundaries) with relative ease, and FDM in its basic form is restricted to handle rectangular shapes and simple alterations.
- (3) The most attractive feature of FDM is its ease in implementation.
- (4) The quality of a FEM approximation is often higher than that of the corresponding FDM approach, because the quality of the approximation between grid points is poor in FDM.

#### 2.2.4.2.2 Spectral Method

The spatial BFs of the *spectral method* are global and orthogonal in the whole spatial domain (Canuto *et al.*, 1988; Boyd, 2000). Due to the global nature of BFs, the spectral method can achieve a lower order model than the FEM. However, for the same reason, an efficient spectral method often requires that the system has a regular space domain and smooth output. In particular, most of parabolic systems have the spectral gap between the slow and fast modes, thus it is possible to derive an accurate low-order model using the spectral method. To obtain a satisfactory model, the BFs should be carefully designed according to some practical situations such as boundary condition and space domain. Some typical BFs are discussed as follows.

##### *Fourier Series*

*Fourier series* has some good properties such as approximation capability, infinite differential and periodic functions. So it is often used for the processes with periodic boundary conditions and a finite domain (Boyd, 2000; Canuto *et al.*, 1988).

##### *Eigenfunctions*

The *eigenfunctions* (EF) of the linear or linearized spatial operator can be selected as basis functions. For a spatial operator  $\mathcal{A}$  in (2.4), the eigenvalue and eigenfunction problem is of the form

$$\mathcal{A}\phi_i = \lambda_i\phi_i, i = 1, \dots, \infty, \quad (2.25)$$

where  $\lambda_i$  denotes the  $i$ th eigenvalue and  $\phi_i$  denotes the  $i$ th eigenfunction. Figure 2.6 shows the first four eigenfunctions of Case 1:  $\phi_i = \sqrt{2/\pi} \sin(iz)$ , ( $i = 1, \dots, 4$ ). Eigenfunctions are suitable for most of parabolic PDE systems (Christofides, 1998; Christofides & Baker, 1999) because their eigenspectrum display a separation of the eigenvalues, i.e. slow and fast modes as shown in Figure 2.7. In this situation, an accurate model with a finite number of eigenfunctions is possible.

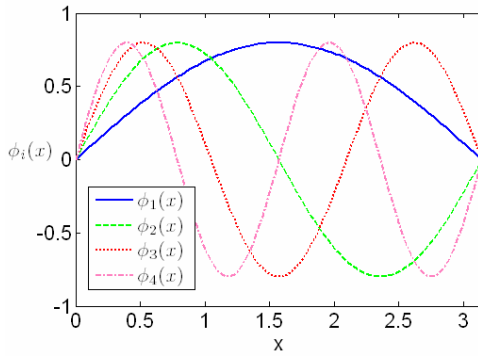


Fig. 2.6 Eigenfunctions of Case 1

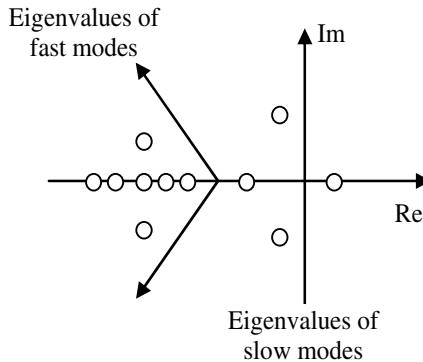


Fig. 2.7 Separation of eigenspectrum

Many control applications are based on the finite-order ODE models derived from the *EF-Galerkin method*, especially for quasi-linear parabolic systems. For example, control of a class of quasi-linear parabolic diffusion-reaction processes (Dubljevic, Christofides & Kevrekidis, 2004), and control of more complex

distributed systems, which include the cases of parameter uncertainties (Armaou & Christofides, 2001b; Christofides & Baker, 1999) and input constraints (El-Farra, Armaou & Christofides, 2003; El-Farra & Christofides, 2004). To further improve the modeling performance, the *EF-Galerkin-AIM method* is reported to control quasi-linear parabolic processes (Christofides & Daoutidis, 1997), the process in time-dependent spatial domains (Armaou & Christofides, 1999), and the process with parameter uncertainties (Christofides, 1998).

Except the above successful applications, the EF method also has its limitations.

- When the spatial operator is self-adjoint (Gay & Ray, 1995), the model may be low-order. However, for the non-self-adjoint system, the resulting model is of higher order or even unstable because of the slow convergence of the EF solution (Gay & Ray, 1995; Mahadevan & Hoo, 2000; Hoo & Zheng, 2001).
- For many typical operators and regular boundary conditions, the eigenvalue and EF can be easily derived (Butkovskiy, 1982). However, for the system with nonlinear spatial operators, spatially varying parameters, complex boundary conditions and irregular domain, it will be very difficult and even impossible to get analytical EF.
- EF may be hardly applied to hyperbolic systems, because they do not show the clear separated eigenspectrum. Thus, the *method of characteristics* (Ray, 1981) might be a good choice, where the system is transformed into a set of ODEs, which describe the original DPS along with their characteristic lines.

### *Orthogonal Polynomials*

*Orthogonal polynomials* are also popular in model reduction of the DPS. For example, the *polynomial-collocation method* is used to derive a low-order DPS model for the purpose of simulation and control (Lefèvre *et al.*, 2000), and for the adaptive control (Dochain *et al.*, 1992). In general, *Chebyshev polynomials* (Boyd, 2000; Canuto *et al.*, 1988) and *Legendre polynomials* (Canuto *et al.*, 1988) are suitable for non-periodic problem defined on a finite domain. *Laguerre polynomials* work well on the semi-infinite domain. *Hermite polynomials* (Boyd, 2000) are useful for the problems with an infinite domain. These functions are very flexible and can be applicable to a broad class of systems. However, they may not be optimal since these general polynomials do not utilize any specific knowledge about the system.

#### **2.2.4.2.3 Karhunen-Loève Method**

The **KL** method, also known as **proper orthogonal decomposition (POD)** or **principal component analysis (PCA)**, is a statistical analysis technique of obtaining the so called **empirical eigenfunctions (EEFs)** from the numerical or experimental data (Sirovich, 1987; Holmes *et al.*, 1996; Newman, 1996a). The basic idea of the KL expansion is to find those modes which represent the dominant character of the system.

The spatio-temporal dynamics can be separated into orthonormal spatial and temporal modes using the **singular value decomposition (SVD)**

$$y(x, t) = \sum_{i=1}^{\infty} \sigma_i \phi_i(x) \psi_i(t), \sigma_1 \geq \sigma_2 \geq \dots \geq \sigma_{\infty}, \quad (2.26)$$

where singular values  $\sigma_i$  denote the importance of the modes, **left singular functions**  $\phi_i(x)$  represent spatial modes, and **right singular functions**  $\psi_i(t)$  are temporal modes. The KL method is actually implemented in different ways. Using the spatio-temporal data (snapshots), the KL method is transformed into an eigenfunction/eigenvalue problem of a **spatial two-point correlation function** (Sirovich, 1987)

$$\int_0^{\pi} C_x(x, \zeta) \phi_i(\zeta) d\zeta = \lambda_i \phi_i(x), \quad (2.27)$$

where  $C_x(x, \zeta) = \frac{1}{T} \int_0^T y(x, t) y(\zeta, t) dt$ . This method is computationally efficient when the relevant number of snapshots is significantly larger than the dimension of the discretization. On the contrary, assuming that  $\phi_i(x) = \sum_{t=1}^T \gamma_{it} y(x, t)$ , then a smaller eigenvector/eigenvalue problem of a **temporal two-point correlation function** is used instead (Sirovich, 1987)

$$C_t \gamma_i = \lambda_i \gamma_i, \quad (2.28)$$

where  $C_t(t, \tau) = \frac{1}{T} \int_0^{\pi} y(x, t) y(x, \tau) dx$ .

The EEFs are found in an ordered manner based on the values of  $\sigma_i$  or  $\lambda_i$  ( $\lambda_i = \sigma_i^2$ ), with the first EEF as the most dominant behavior, the second as the next dominant and so on. Usually, only the first few modes can capture the most important dynamics of the system, thus a small number of EEFs can be selected to yield a low-order model. **Figure 2.8** shows the empirical eigenfunctions of **Case 1**.

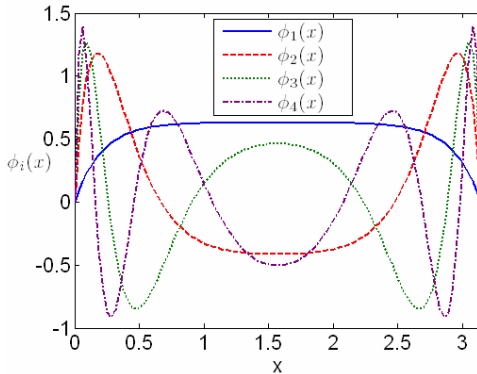


**Fig. 2.8** Empirical eigenfunctions of Case 1

The *KL-Galerkin method* could be one of the most commonly used DPS modeling methods. It has been applied to system analysis, model reduction, numerical simulation of many complex distributed systems, e.g., *fluid flow* (Holmes *et al.*, 1996; Deane *et al.*, 1991; Park & Cho, 1996a), *thermal process* (Park & Cho, 1996b; Newman, 1996b; Banerjee, Cole & Jensen, 1998; Adomaitis, 2003), and *diffusion-convection-reaction process* (Armaou & Christofides, 2001c), etc. Many control applications can be carried out, e.g., control of the growth of thin films in a *chemical vapor deposition reactor* (Banks, Beeler, Kepler & Tran, 2002), control of a diffusion-reaction process (Armaou & Christofides, 2001a), control of a thin shell system (Banks, del Rosario & Smith, 2000), and optimization of diffusion-convection-reaction processes (Bendersky & Christofides, 2000).

The applications of *KL-Galerkin-AIM method* (Baker & Christofides, 2000; Aing *et al.*, 1997) and the *KL-collocation method* (Adomaitis, 1995; Baker & Christofides, 1999; Theodoropoulou *et al.*, 1998) are also studied for simulation, control and optimization of thermal processes.

### **Remark 2.3: Spectral Method and KL Method**

Compared with the spectral method, the KL method is applicable to a wider range of complex distributed systems, including those with irregular domain, nonlinear spatial operator and nonlinear boundary conditions. Because BFs of the KL method can provide an optimal linear representation of spatio-temporal data themselves (Holmes *et al.*, 1996; Dür, 1998), it may generate a lower-order and more accurate model than the FEM and the spectral method. However, its major drawback is that the KL method depends on cases and lacks a systematic solution for one class of systems. Thus, experiment settings such as the input signal, the time interval, the number of snapshots, the values of system parameters (Park & Cho, 1996b), and the initial conditions (Graham & Kevrekidis, 1996) have to be carefully chosen for an efficient application.

## **2.2.5 Comparison Studies of Spectral and KL Method**

Spectral method stems from Fourier series expansion while Karhunen-Loève method comes from the idea of principle component analysis. There are some differences in the applications. Spectral method does not require any sensor, while KL method requires some sensors for learning basis functions. The number of basis functions resulting from KL method is fewer than or equal to the number of sensors used. Therefore the number of sensors determines the order of the model in KL method, while the number of eigenfunctions is equal to the model order in spectral method.

In order to compare the eigenfunctions and KL basis functions from a view of sensor number or model order, a modeling performance index is defined as *mean of absolute relative error* (MARE):  $\frac{1}{NL} \sum_{i=1}^N \sum_{t=1}^L \left| \frac{y(x_i, t) - \hat{y}(x_i, t)}{y(x_i, t)} \right|$ , where  $y(x_i, t)$  and  $\hat{y}(x_i, t)$  are true and estimated output at location  $x_i$  and time  $t$ ,  $N$  and  $L$  are the number of spatial locations and the time length.

As shown in [Figure 2.9](#), both spectral and KL methods are applicable for this quasi-linear parabolic system, where the horizontal axis is the model order for spectral method and the sensor number for KL method. The model order of KL method is fixed as 3. As the model order of spectral method or the sensor number of KL method increases, the modeling error becomes smaller. When the sensor number is too small, KL method will perform worse than spectral method. However, when the sensor number is large enough, KL method will be better than spectral method.

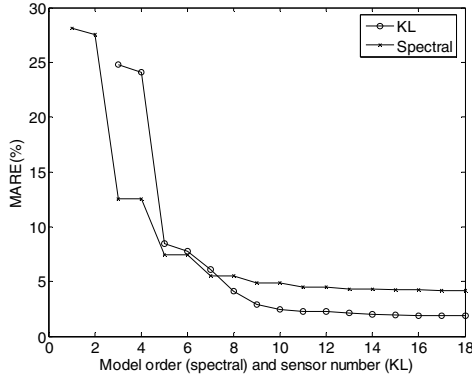


**Fig. 2.9** KL and spectral method for Case 1

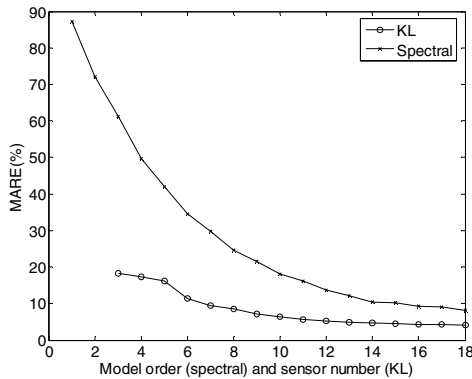


**Fig. 2.10** KL and spectral method for Case 2

As shown in [Figure 2.10](#), KL method is also efficient for this nonlinear parabolic system, while spectral method fails. This is because this system is very close to hyperbolic PDE, which does not show clearly separated eigenspectrum. In order to obtain the comparative accuracy, the number of sensors required in KL method is less than the model order in spectral method. In other words, KL basis functions

may be more efficient than the eigenfunctions under some conditions, and that is obvious in the case of the non-separated eigenspectrum.

The limitation of spectral and KL method is that a PDE description of the process must be known. If there is uncertainty in the process, the derived model will have a poorly approximation capability. In this case, the data-based modeling is often used to obtain an accurate model, which will be discussed in [Section 2.4.4 - 2.4.6](#).

## 2.3 Grey-Box Modeling: Parameter Estimation for Partly Known DPS

All the previous model reduction methods require that the PDE description of the system is known. However, in many cases it is difficult to obtain an exact PDE description of the process from the physical and chemical laws only, so the data-based modeling must be employed to find the unknown DPS. In general, problems can be classified in two different cases: *parameter estimation* for known structure and *system identification* for unknown structure. In either case the model reduction methods introduced in [Section 2.2](#) will play an important role.

This section will discuss parameter estimation problem for grey-box DPS modeling. When the PDE structure of the system is known and only some parameters are unknown, these parameters can be estimated from the experimental data ([Banks & Kunisch, 1989](#)). Once the parameters are determined, the PDE model reduction can be used for real applications, such as simulation, control, and optimization. Some earlier survey papers are given by [Kubrusly \(1977\)](#) and [Polis & Goodson \(1976\)](#).

### 2.3.1 FDM Based Estimation

After computing all the derivative terms in the PDE with the finite difference method, the unknown parameters can be estimated by minimizing the [equation error](#) ([Coca & Billings, 2000](#); [Müller & Timmer, 2004](#)). It will lead to linear or nonlinear regression problem according to the type of PDE. Because it does not need to solve the PDE, this method is relatively simple. However, some data smoothing or de-noise techniques may be needed to reduce noise sensitivity. More sensors are usually used to obtain accurate parameter estimation if the parameters are temporally or spatially varying.

Since the predicted output can be computed from the dynamical PDE model using the finite difference method, and thus the system parameters can be found by minimizing the [output error](#) between the measurement and the prediction ([Banks & Kunisch, 1989](#)). For example, [Kubrusly & Curtain, \(1977\)](#) proposed a stochastic approximation algorithm for the spatially varying parameter estimation of the second-order linear parabolic PDE with the random input and noisy measurement. [Uciński & Korbicz \(1990\)](#) presented a recursive least-squares method to estimate spatially varying parameters of the parabolic DPS with noisy outputs. In



addition, based on the ODE model derived from the *method of lines*, Vande Wouwer *et al.*, (2006) used a Levenberg-Marquardt algorithm to estimate constant parameters.

The comparison studies of the equation error and output error approaches are provided by Müller & Timmer (2004).

- The equation error approach is to first construct the left and right sides of the PDE in (2.1) from data, then to estimate the model by minimizing the equation residual given in (2.16).
- In the output error approach, the model is figured out by minimizing the error between the measured output and the predicted output as shown in Figure 2.11.

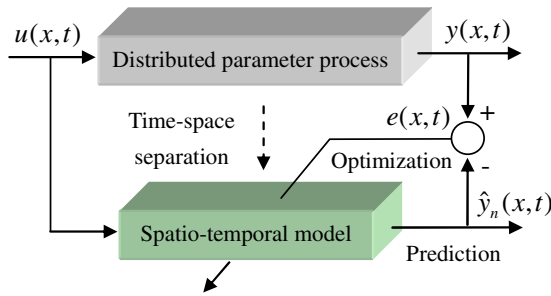


Fig. 2.11 Output error approach

Because the output error method needs to solve the PDE, its optimization computation may be complex. However, it does not need to estimate the derivative from the noisy data. The equation error and output error approaches can also be performed using *FEM*, *spectral* and *KL* methods.

### 2.3.2 FEM Based Estimation

Based on the *FEM-Galerkin* approximation, Rannacher & Vexler (2005) estimated the constant parameters for the elliptic PDE. With the finite spatial BF expansion of the parameters, Fernandez-Berdaguer, Santos & Sheen (1996) estimated the spatially varying parameters by minimizing the output error and regularization error with a quasi-linearization algorithm. The regularization error is formed from the output error by adding a penalty for model complexity which will help to solve an ill-posed problem or to prevent the overfitting. Based on the finite element parameterization of the parameters, Carotenuto & Raiconi (1980) estimated the spatially varying parameters of the linear parabolic DPS using nonlinear optimization techniques. Uciński & Korbicz (1990) proposed a recursive least-squares method to estimate spatially varying parameters of the parabolic DPS under noisy outputs.

Based on the *FEM-spline-Galerkin* approximation, Banks, Crowley & Kunisch (1983) studied the parameters estimation for the linear and nonlinear second-order parabolic and hyperbolic PDE systems. With the piecewise linear splines approximation of the parameters, Banks & Daniel Lamm (1985) presented the spatially and temporally varying parameters estimation for the linear parabolic system. With the Legendre polynomial or splines function approximation of the parameters, Banks, Reich & Rosen, (1991) estimated unknown spatially and/or temporally varying parameters of the linear or nonlinear DPS. With the finite-dimensional parameterization, Demetriou & Rosen (1994) proposed an adaptive parameter estimation algorithm for a class of second-order linear distributed systems with spatially varying parameters.

### 2.3.3 Spectral Based Estimation

Each term in the PDE is reconstructed from the data using the finite-dimensional expansion onto a set of spatial and temporal orthogonal functions, and then double integrating the PDE with respect to time and space will convert the equation error minimization problem to the problem of the algebraic equation (AE), which can be easily solved using linear regression method. This method is simple but requires the PDE to be a linear or a special nonlinear form for the AE conversion. Furthermore, many sensors may be needed due to its spatial integration. Under this approach, various orthogonal functions, e.g., Fourier series (Mohan & Datta, 1989), Chebyshev series (Horng, Chou & Tsai, 1986), Walsh-functions (Paraskevopoulos & Bounas, 1978), Laguerre polynomials (Ranganathan, Jha & Rajamani, 1984, 1986), Taylor series (Chung & Sun, 1988), general orthogonal polynomials (Lee & Chang, 1986) and block-pulse functions (Mohan & Datta, 1991), have been used for the parameter estimation.

Based on the *EF-Galerkin* method, an identification algorithm is performed using a Newton-like method for unknown constant diffusivities in the diffusion equation described by the parabolic PDE (Omatu & Matumoto, 1991). Using Lagrange interpolation polynomials as BF's of the *collocation* method, Ding, Gustafsson & Johansson (2007) studied the constant parameters estimation of a continuous paper pulp digester described by two linear hyperbolic PDE systems.

### 2.3.4 KL Based Estimation

Based on the *KL-Galerkin* approximation, Park, Kim & Cho (1998) presented the constant parameters estimation of flow reactors described by Navier-Stokes equation. Ghosh, Ravi Kumar & Kulkarni (2001) proposed a multiple shooting algorithm to estimate unknown initial conditions and constant parameters for a coupled map lattice (CML) system and a reaction-diffusion system.

## 2.4 Black-Box Modeling: System Identification for Unknown DPS

For the DPS with unknown structure which widely exist in real life applications, the black-box identification has to be used. More sensors are often required in spatial

locations to collect enough information. Modeling becomes extremely difficult because both the structure and parameters need to be figured out. There are many system identification methods for LPS. Only a few studies discuss system identification of DPS.

### 2.4.1 Green's Function Based Identification

If the analytical Green's function is not available, it can be estimated from the input-output data. For example, based on the singular function expansion of Green's function, a time-invariant Green's function model can be estimated using SVD method (Gay & Ray, 1995). This approach yielded accurate low-order solutions for linear invariant non-self-adjoint systems. A disadvantage of this approach is the time-invariance assumption. Obviously for time-varying systems, this approach is limited. To avoid the assumption, a time-varying Green's function identification method is proposed by combining the characteristics of singular value decomposition and the Karhunen-Loève expansion (SVD-KL) (Zheng, Hoo & Piovoso, 2002; Zheng & Hoo, 2002; Zheng & Hoo, 2004). The Green's function can also be estimated using other methods (Doumanidis & Fourligkas, 2001). Because the Green's function model uses one single kernel, it may only be able to approximate the linear DPS or the nonlinear DPS at the given working condition. Therefore how to extend the kernel idea to the nonlinear DPS is an important problem, which will be discussed in Chapter 6.

### 2.4.2 FDM Based Identification

A basic idea is that after a candidate set of spatial and temporal derivatives are estimated from the data using finite difference, the functions representing the model can be determined by minimizing an equation error criterion using the optimization techniques. Voss, Büchner & Abel (1998) presented alternating conditional expectation algorithm for parameter estimation under a pre-selected model structure. Bär, Hegger & Kantz (1999) used singular value decomposition or backward elimination method for the model selection.

To avoid computing temporal derivatives with finite difference for noisy data, the PDE system turns to unknown algebraic equations using implicit Adams integration over time (Guo & Billings, 2006). Then the system structure and parameters can be estimated by an orthogonal least-squares algorithm, in which the PDE operators are expanded using polynomials as BFs, and the spatial derivatives are estimated by finite difference methods. To further reduce noise sensitivity, the spatial derivatives can be estimated using a B-spline functions-based multi-resolution analysis instead of finite difference methods (Guo, Billings & Wei, 2006).

The above method can obtain an ODE or PDE model from the data. However, the ODE model will be high-order. When the PDE model is obtained, model reduction is still needed for the practical applications. Moreover, it may lead to a complicated PDE model, whose reduced model may not be suitable for practical process control.

The time-space discretization of the PDE using *FDM* can lead to the **difference equation (DE)**, which can be considered as so called **lattice dynamical system (LDS)**, thus a class of DE model identification methods are based on the identification of lattice dynamical system (Parlitz & Merkwirth, 2000; Mandelj, Grabec & Govekar, 2001; Guo & Billings, 2007). The key feature is that the model of the system is usually unchanged at different spatial locations (except the boundary) in Figure 2.12, and the dynamics of the node (**black node**) is only determined by its neighbor regions (**white nodes**). For example, Mandelj, Grabec & Govekar (2001, 2004) and Abel (2004) used nonparametric statistical identification method, and Coca & Billings (2001), Billings & Coca (2002) and Guo & Billings (2007) estimated the parametric **nonlinear autoregressive with exogenous input (NARX) model** using **orthogonal forward regression (OFR) algorithm**.

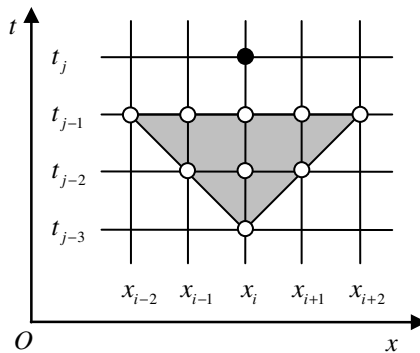


**Fig. 2.12** Geometric interpretation of FDM based identification

A good model can be obtained if the small regions are properly determined. Thus one task is to determine the proper neighborhood. The heuristic or pre-specified approaches (Parlitz & Merkwirth, 2000; Mandelj, Grabec & Govekar, 2001) as well as the theoretical analysis (Guo & Billings, 2007) have been proposed. Each local model at the node represents a state of the system, thus the model may be of a high-dimension since its dimension is determined by the number of spatial discretization points.

If the *method of lines* is used with only spatial discretization, the resulting ODE model can be estimated using traditional ODE identification techniques such as neural networks (Gonzalez-Garcia, Rico-Martinez & Kevredidis, 1998). It has similar weakness as the LDS modeling, i.e., the dimension will be high-order and the model has complex nonlinear structure.

### 2.4.3 FEM Based Identification

After choosing the proper BFs, the corresponding unknown temporal model can be estimated using traditional system identification techniques. The methodology is

similar to that shown in [Figure 2.3](#), where the temporal model is identified from the data instead of derivation from the PDE description.

The basic procedure can be expressed as follows. Suppose we have a set of sampled process input  $u(x_i, t)$  ( $i = 1, \dots, M$ ) and output  $y(x_i, t)$  ( $i = 1, \dots, N$ ). Firstly the basis function expansion

$$u(x, t) \approx \sum_{i=1}^m u_i(t) \phi_i(x), \quad (2.29)$$

$$y(x, t) \approx \sum_{i=1}^n y_i(t) \phi_i(x), \quad (2.30)$$

is used for the time/space separation and dimension reduction. Secondly the modeling problem is to estimate a finite order temporal model

$$y(t+1) = F(y(t), u(t)), \quad (2.31)$$

from  $u(t) = [u_1(t), \dots, u_m(t)]^T \in \mathbb{R}^m$  and  $y(t) = [y_1(t), \dots, y_n(t)]^T \in \mathbb{R}^n$ , where  $F: \mathbb{R}^n \times \mathbb{R}^m \rightarrow \mathbb{R}^n$  is a nonlinear function. Finally the output equation

$$y_n(z, t) = \sum_{i=1}^n y_i(t) \phi_i(z), \quad (2.32)$$

is used for the time/space synthesis.

Various lumped system identification techniques can be used to identify the unknown function  $F$ , and the neural network is often used among them. By working with different selections of BFs, FEM, spectral and KL based identification can be formulated.

[Coca & Billings \(2002\)](#) proposed a FEM based identification method. With local basis functions chosen as B-spline functions, the NARX model is identified to recover the system dynamics using the OFR algorithm for model selection and parameter estimation, with applications to a linear diffusion system and a nonlinear reaction-diffusion system. However, the model may be high-order for a satisfactory modeling accuracy because of local basis functions. In order to obtain a low-order model, the spectral and KL based identification may be two good approaches.

#### 2.4.4 Spectral Based Identification

Based on the eigenfunctions expansion and artificial neural network approximation, a neural spectral method is proposed as shown in [Figure 2.13](#). Of course, other global basis functions can also be used though they may not be optimal in sense that the model order could be high. To obtain the eigenfunctions, the nominal linear model of the system should be known. Neural spectral method usually needs more sensors, and the number of sensors at least equals or exceeds the number of eigenfunctions required for modeling.

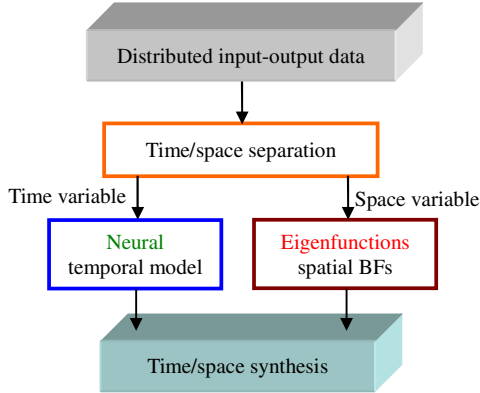


**Fig. 2.13** Neural spectral method

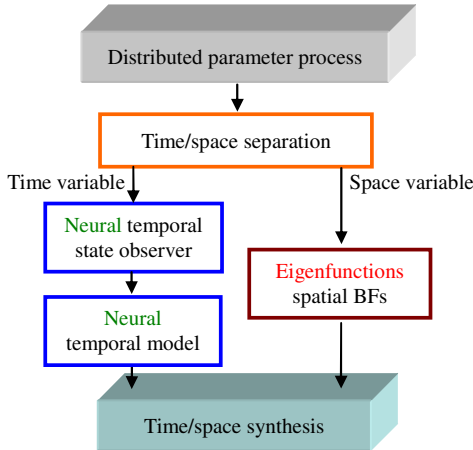


**Fig. 2.14** Neural observer spectral method

A neural observer spectral method is proposed as shown in [Figure 2.14](#) ([Deng, Li & Chen, 2005](#)), which usually needs a smaller number of sensors. The basic idea is that by utilizing a priori knowledge about the nominal model, a neural observer can be developed to estimate the higher-dimensional states from a few sensors. Therefore, a better modeling performance is obtained with fewer sensors. This method is useful for a class of partly known PDE considered with unknown parameters and nonlinearities. A simple model-based control is further developed for a class of curing thermal processes ([Li, Deng & Zhong, 2004](#)). However, as mentioned in [Section 1.2](#), neural observer spectral method has some limitations: (1) The model order is relatively high. (2) The model has a complex nonlinear structure

which is not easy for control design. (3) It is not easy to apply to other industrial processes because the intelligent observer design is very dependent on a priori knowledge of the process. This motivates us to develop simple low-order nonlinear models with less process knowledge required.

### 2.4.5 *KL Based Identification*

The neural networks are popularly integrated with the KL method to identify unknown DPS (Zhou, Liu, Dai & Yuan, 1996), as shown in Figure 2.15.

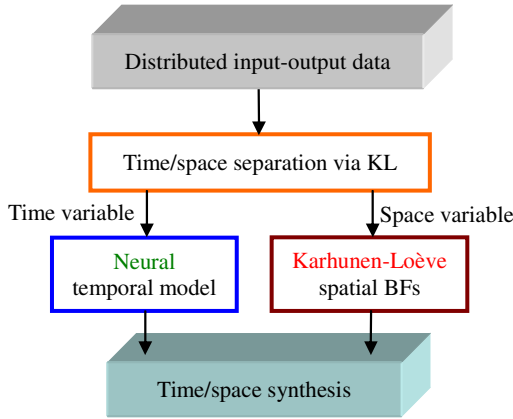


**Fig. 2.15** Neural KL method

Applications include: analysis of Kuramoto-Sivashinsky and Navier-Stokes equations (Smaoui & Al-Enezi, 2004), modeling and intelligent control of transitional flows (Sahan *et al.*, 1997), modeling of a heat convection-conduction process with the known mechanistic part and unknown nonlinearity (Romijn *et al.*, 2008). In all these work, the neural network is used for learning the nonlinearity. However, design of the neural system is not very systematic. Recently, the modeling and predictive control with applications to a tubular reactor is studied by using a fuzzy partition method for network design (Aggelogiannaki & Sarimveis, 2008). Though neural KL method may achieve a low-order model, most neural models are very complex which are actually not suitable for practical control. The approach using KL method and subspace identification is also reported for bilinear model identification and receding horizon control of a thin-film growth process (Varshney & Armaou, 2008).

### 2.4.6 *Comparison Studies of Neural Spectral and Neural KL Method*

For the neural KL method, more efficient KL basis functions are used as spatial basis function instead of the eigenfunctions in the neural spectral method. A fact is

that the eigenfunction is calculated from the system, and therefore the neural spectral method requires the linear nominal model to be known, while the neural KL method does not require any a priori knowledge of the system.

As shown in **Figure 2.16**, both neural spectral and neural KL models can give a better performance than the nominal spectral model for **Case 1** when enough sensors are used, because the nonlinear uncertainties in the system can be compensated by neural network learning using the sensor measurements. The horizontal axis is the model order for the nominal spectral method and the sensor number for neural spectral and neural KL method. The model order of neural KL method is fixed at three, where the model order of the neural spectral is set to be the number of sensors used. It also shows that the neural KL model even with smaller number of basis functions is better than the neural spectral method because of the more efficient Karhunen-Loève method.

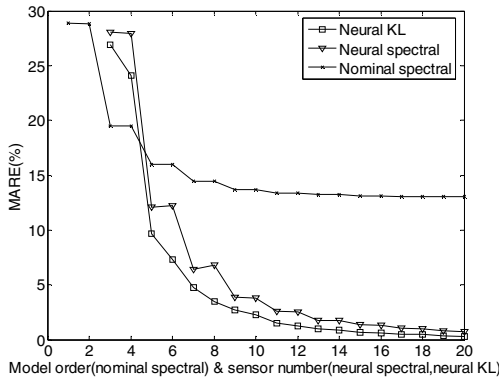


**Fig. 2.16** Neural spectral and neural KL methods for Case 1

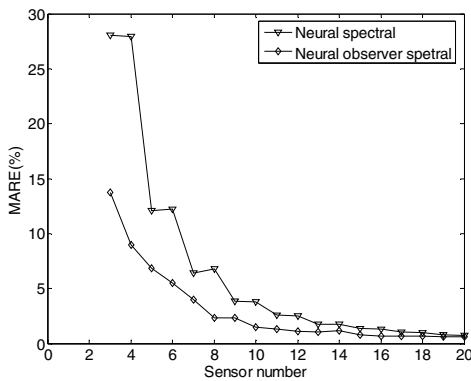


**Fig. 2.17** Neural spectral and neural observer spectral methods for Case 1



Both the neural spectral and the neural KL method need enough sensors for a good performance. As shown in Figure 2.17, for the neural observer spectral method, the required sensors are less than those of the neural spectral method.

As shown in Figure 2.18 and Figure 2.19, the neural spectral model performs much worse than the neural KL model for Case 2, where the model order of the neural spectral is equal to the sensor number while the model order of the neural KL is set to be four. It can be said the neural spectral method does not work. The neural observer spectral method also fails in this case. This is because the neural spectral and the neural observer spectral method are only suitable for the case that has significant separation of eigenspectrum. Alternately, the neural KL model is applicable to a wider range of systems.

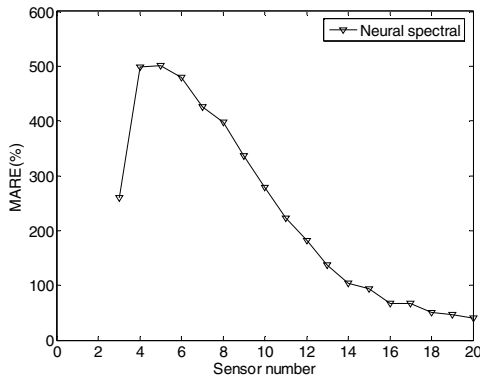


Fig. 2.18 Neural spectral method for Case 2

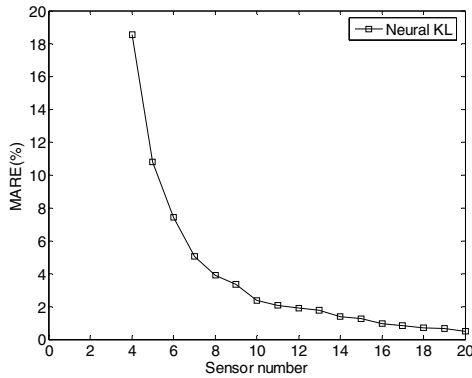


Fig. 2.19 Neural KL method for Case 2

The neural network models developed above can approximate many nonlinear systems. However, it is not easy to be used for control design because of their

inherent nonlinear property. In practice, a model with simple or special nonlinear structure is often needed. Because the KL method can achieve a lower-order model than the spectral method and is suitable for a wider range of DPS, so it will be used in the data-based modeling development.

## 2.5 Concluding Remarks

This chapter presents an overview on advances in the DPS modeling. The DPS modeling problem can be classified into three issues: *model reduction* for known DPS, *parameter estimation* for DPS with unknown parameters and *system identification* for DPS with unknown structure. Different methods have been classified into several categories according to their methodology. The underlying fundamental ideas and their strength and weakness are also presented. For numerical implementation and applications, the infinite-dimensional problem must be transformed to a finite-dimensional one, where the *model reduction* is fundamental.

The model reduction and parameter estimation of DPS are relatively mature. However, there are some problems in the system identification of DPS, which will be studied in this book.

- For the DPS system identification in [Section 2.4.2 - 2.4.5](#), most of models use neural network methods. They have complex and general nonlinear structure, which may be difficult for control design. In the LPS modeling, the block-oriented nonlinear model (e.g., Hammerstein and Wiener model) has been widely used because of their simple structures, abilities to approximate a large class of nonlinear processes and efficient control schemes (e.g., [Narendra & Gallman, 1966](#); [Stoica & Söderström, 1982](#); [Bai, 1998](#); [Zhu, 2000](#); [Gómez & Baeyens, 2004](#); [Westwick & Verhaegen, 1996](#); [Hagenblad & Ljung, 2000](#)). They consist of the interconnection of linear time invariant (LTI) systems and static nonlinearities. To best of our knowledge, the **block-oriented nonlinear models** are only studied for LPS. The extension of blocked-oriented nonlinear models to the spatio-temporal system is very useful for modeling the nonlinear DPS. Thus in [Chapter 3](#) we study the spatio-temporal modeling for the Wiener distributed parameter system. In [Chapters 4 and 5](#), the spatio-temporal modeling will be studied for the Hammerstein distributed parameter system.
- Though the Green's function model in [Section 2.4.1](#) is very suitable for control design because of its linear structure, however, it is only a linear approximation for a nonlinear DPS. How to identify a nonlinear DPS using the kernel is an important problem. Thus, the kernel based spatio-temporal modeling is presented for the nonlinear Hammerstein distributed parameter system in [Chapter 5](#). Volterra model is widely used for modeling nonlinear LPS ([Boyd & Chua, 1985](#); [Schetzen, 1980](#); [Rugh, 1981](#); [Doyle III et al., 1995](#); [Maner et al., 1996](#); [Parker et al., 2001](#)). However, it consists of a series of temporal kernels, the extension to the spatio-temporal system is very necessary for modeling the nonlinear DPS. Thus Volterra kernel based spatio-temporal modeling is presented in [Chapter 6](#).

- For the KL based neural modeling in [Section 2.4.5](#), the use of KL for dimension reduction is only a linear approximation for a nonlinear DPS. In the field of machine learning, the nonlinear principal component analysis (NL-PCA) has been widely used for nonlinear dimension reduction of high-dimensional data or known systems (e.g., [Dong & McAvoy, 1996](#); [Kramer, 1991](#); [Hsieh, 2001](#); [Kirby & Miranda, 1994](#); [Smaoui, 2004](#); [Webb, 1996](#); [Wilson, Irwin & Lightbody, 1999](#)). The application of nonlinear dimension reduction methods to the nonlinear DPS will improve the KL based modeling performance. Thus in [Chapter 7](#), the nonlinear dimension reduction based neural modeling will be discussed for the nonlinear DPS.

## References

1. Abel, M.: Nonparametric modeling and spatiotemporal dynamical systems. *International Journal of Bifurcation and Chaos* 14(6), 2027–2039 (2004)
2. Adomaitis, R.A.: RTCVD model reduction: A collocation on empirical eigenfunctions approach. Technical Report T.R.95-64, University of Maryland, College Park, Maryland (1995)
3. Adomaitis, R.A.: A reduced-basis discretization method for chemical vapor deposition reactor simulation. *Mathematical and Computer Modeling* 38(1-2), 59–175 (2003)
4. Adrover, A., Continillo, G., Crescitelli, S., Giona, M., Russo, L.: Construction of approximate inertial manifold by decimation of collocation equations of distributed parameter systems. *Computers and Chemical Engineering* 26(1), 113–123 (2002)
5. Adrover, A., Continillo, G., Crescitelli, S., Giona, M., Russo, L.: Wavelet-like collocation method for finite-dimensional reduction of distributed systems. *Computers and Chemical Engineering* 24(12), 2687–2703 (2000)
6. Aggelogiannaki, E., Sarimveis, H.: Nonlinear model predictive control for distributed parameter systems using data driven artificial neural network models. *Computers and Chemical Engineering* 32(6), 1225–1237 (2008)
7. Aling, H., Banerjee, S., Bangia, A.K., Cole, V., Ebert, J., Emani-Naeini, A., Jensen, K.F., Kevrekidis, I.G., Shvartsman, S.: Nonlinear model reduction for simulation and control of rapid thermal processing. In: *Proceedings of the 1977 American Control Conference*, Albuquerque, New Mexico, pp. 2233–2238 (1977)
8. Armaou, A., Christofides, P.D.: Nonlinear feedback control of parabolic partial differential equation systems with time-dependent spatial domains. *Journal of Mathematical Analysis & Applications* 239(1), 124–157 (1999)
9. Armaou, A., Christofides, P.D.: Finite-dimensional control of nonlinear parabolic PDE systems with time-dependent spatial domains using empirical eigenfunctions. *International Journal of Applied Mathematics and Computer Science* 11(2), 287–317 (2001a)
10. Armaou, A., Christofides, P.D.: Robust control of parabolic PDE systems with time-dependent spatial domains. *Automatica* 37(1), 61–69 (2001b)
11. Armaou, A., Christofides, P.D.: Computation of empirical eigenfunctions and order reduction for nonlinear parabolic PDE systems with time-dependent spatial domains. *Nonlinear Analysis* 47(4), 2869–2874 (2001c)
12. Bai, E.W.: An optimal two-stage identification algorithm for Hammerstein-Wiener nonlinear systems. *Automatica* 34(3), 333–338 (1998)

13. Baker, J., Christofides, P.D.: Output feedback control of parabolic PDE systems with nonlinear spatial differential operators. *Industrial & Engineering Chemistry Research* 38(11), 4372–4380 (1999)
14. Baker, J., Christofides, P.D.: Finite-dimensional approximation and control of non-linear parabolic PDE systems. *International Journal of Control* 73(5), 439–456 (2000)
15. Balas, M.J.: The Galerkin method and feedback control of linear distributed parameter systems. *Journal of Mathematical Analysis and Applications* 91(2), 527–546 (1983)
16. Balas, M.J.: Finite dimensional control of distributed parameter systems by Galerkin approximation of infinite dimensional controller. *Journal of Mathematical Analysis and Application* 114, 17–36 (1986)
17. Banerjee, S., Cole, J.V., Jensen, K.F.: Nonlinear model reduction strategies for rapid thermal processing systems. *IEEE Transactions on Semiconductor Manufacturing* 11(2), 266–275 (1998)
18. Banks, H.T., Daniel Lamm, P.K.: Estimation of variable coefficients in parabolic distributed systems. *IEEE Transactions of Automatic Control* 30(4), 386–398 (1985)
19. Banks, H.T., Kunisch, K.: Estimation techniques for distributed parameter systems. Birkhauser, Boston (1989)
20. Banks, H.T., Beeler, R.C., Kepler, G.M., Tran, H.T.: Reduced-order model modeling and control of thin film growth in a HPCVD reactor. *SIAM Journal on Applied Mathematics* 62(4), 1251–1280 (2002)
21. Banks, H.T., Crowley, J.M., Kunisch, K.: Cubic spline approximation techniques for parameter estimation in distributed systems. *IEEE Transactions on Automatic Control* 28(7), 773–786 (1983)
22. Banks, H.T., del Rosario, R.C.H., Smith, R.C.: Reduced-order model feedback control design: Numerical implementation in a thin shell model. *IEEE transactions on Automatic Control* 45(7), 1312–1324 (2000)
23. Banks, H.T., Reich, S., Rosen, I.G.: Galerkin approximation for inverse problems for nonautonomous nonlinear distributed systems. *Applied Mathematics and Optimization* 24(3), 233–256 (1991)
24. Bär, M., Hegger, R., Kantz, H.: Fitting partial differential equations to space-time dynamics. *Physical Review E* 59(1), 337–342 (1999)
25. Bendersky, E., Christofides, P.D.: Optimization of transport-reaction processes using nonlinear model reduction. *Chemical Engineering Science* 55(19), 4349–4366 (2000)
26. Billings, S.A., Coca, D.: Identification of coupled map lattice models of deterministic distributed parameter systems. *International Journal of Systems Science* 33(8), 623–634 (2002)
27. Boyd, J.P.: Chebyshev and Fourier spectral methods, 2nd edn. Dover Publications, New York (2000)
28. Boyd, S., Chua, L.O.: Fading memory and the problem of approximating nonlinear operators with Volterra series. *IEEE Transactions on Circuits and Systems* 32(11), 1150–1161 (1985)
29. Brenner, S.C., Ridgway Scott, L.: The mathematical theory of finite element methods. Springer, New York (1994)
30. Butkovskiy, A.G.: Green's functions and transfer functions handbook, 1st edn. Ellis Horwood, Chichester (1982)
31. Canuto, C., et al.: Spectral methods in fluid dynamics. Springer, New York (1988)

32. Carotenuto, L., Raiconi, G.: Identifiability and identification of a Galerkin approximation for a class of distributed parameter-systems. *International Journal of Systems Science* 11(9), 1035–1049 (1980)
33. Christofides, P.D.: Robust control of parabolic PDE systems. *Chemical Engineering Science* 53(16), 2949–2965 (1998)
34. Christofides, P.D.: Nonlinear and robust control of PDE systems: Methods and applications to transport-reaction processes. Birkhäuser, Boston (2001b)
35. Christofides, P.D., Baker, J.: Robust output feedback control of quasi-linear parabolic PDE systems. *Systems & Control Letters* 36(5), 307–316 (1999)
36. Christofides, P.D., Daoutidis, P.: Finite-dimensional control of parabolic PDE systems using approximate inertial manifolds. *Journal of Mathematical Analysis and Applications* 216(2), 398–420 (1997)
37. Chung, H.Y., Sun, Y.Y.: Parameter identification of linear distributed systems via Taylor operational matrix. *IEEE Transactions on Industrial Electronics* 35(3), 413–416 (1988)
38. Coca, D., Billings, S.A.: Direct parameter identification of distributed parameter systems. *International Journal of Systems Science* 31(1), 11–17 (2000)
39. Coca, D., Billings, S.A.: Identification of coupled map lattice models of complex spatio-temporal patterns. *Physics Letters A* 287(1-2), 65–73 (2001)
40. Coca, D., Billings, S.A.: Identification of finite dimensional models of infinite dimensional dynamical systems. *Automatica* 38(11), 1851–1865 (2002)
41. Cruz, P., Mendes, A., Magalhaes, F.D.: Using wavelets for solving PDEs: an adaptive collocation method. *Chemical Engineering Science* 56(10), 3305–3309 (2001)
42. Deane, A.E., Kevrekidis, I.G., Karniadakis, G.E., Orszag, S.A.: Low dimensional models for complex geometry flows: Application to grooved channels and circular cylinders. *Fluids Physics A* 3(10), 2337–2354 (1991)
43. Demetriou, M.A., Rosen, I.G.: Adaptive identification of second-order distributed parameter systems. *Inverse Problems* 10(2), 261–294 (1994)
44. Deng, H., Li, H.-X., Chen, G.: Spectral-approximation-based intelligent modeling for distributed thermal processes. *IEEE Transactions on Control Systems Technology* 13(5), 686–700 (2005)
45. Ding, L., Gustafsson, T., Johansson, A.: Model parameter estimation of simplified linear models for a continuous paper pulp digester. *Journal of Process Control* 17(2), 115–127 (2007)
46. Dochain, D., Babary, J.P., Tali-Maamar, N.: Modelling and adaptive control of nonlinear distributed parameter bioreactors via orthogonal collocation. *Automatica* 28(5), 873–883 (1992)
47. Dong, D., McAvoy, T.J.: Nonlinear principal component analysis-based on principal curves and neural networks. *Computers and Chemical Engineering* 20(1), 65–78 (1996)
48. Doumanidis, C.C., Fourligkas, N.: Temperature distribution control in scanned thermal processing of thin circular parts. *IEEE Transactions on Control Systems Technology* 9(5), 708–717 (2001)
49. Doyle III, F.J., Ogunnaike, B.A., Pearson, R.K.: Nonlinear model-based control using second-order Volterra Models. *Automatica* 31(5), 697–714 (1995)
50. Dubljevic, S., Christofides, P.D., Kevrekidis, I.G.: Distributed nonlinear control of diffusion-reaction processes. *International Journal of Robust and Nonlinear Control* 14(2), 133–156 (2004)

51. Dür, A.: On the optimality of the discrete Karhunen-Loève expansion. *SIAM Journal on Control and Optimization* 36(6), 1937–1939 (1998)
52. El-Farra, N.H., Christofides, P.D.: Coordinating feedback and switching for control of spatially distributed processes. *Computers and Chemical Engineering* 28(1-2), 111–128 (2004)
53. El-Farra, N.H., Armaou, A., Christofides, P.D.: Analysis and control of parabolic PDE systems with input constraints. *Automatica* 39(4), 715–725 (2003)
54. Fernandez-Berdaguer, E.M., Santos, J.E., Sheen, D.: An iterative procedure for estimation of variable coefficients in a hyperbolic system. *Applied Mathematics and Computation* 76(2-3), 213–250 (1996)
55. Fletcher, C.A.J.: *Computational Galerkin methods*, 1st edn. Springer, New York (1984)
56. Foias, C., Temam, R.: Algebraic approximation of attractors: The finite dimensional case. *Physica D* 32(2), 163–182 (1988)
57. Foias, C., Jolly, M.S., Kevrikidis, I.G., Sell, G.R., Titi, E.S.: On the computation of inertial manifolds. *Physics Letters A* 131(7-8), 433–436 (1988)
58. Gay, D.H., Ray, W.H.: Identification and control of distributed parameter systems by means of the singular value decomposition. *Chemical Engineering Science* 50(10), 1519–1539 (1995)
59. Ghosh, A., Ravi Kumar, V., Kulkarni, B.D.: Parameter estimation in spatially extended systems: The Karhunen-Loève and Galerkin multiple shooting approach. *Physical Review E* 64(5), 56222 (2001)
60. Gómez, J.C., Baeyens, E.: Identification of block-oriented nonlinear systems using orthonormal bases. *Journal of Process Control* 14(6), 685–697 (2004)
61. Gonzalez-Garcia, R., Rico-Martinez, R., Kevredidis, I.G.: Identification of distributed parameter systems: A neural net based approach. *Computers and Chemical Engineering* 22, S965–S968 (1998)
62. Graham, M.D., Kevrekidis, I.G.: Alternative approaches to the Karhunen-Loève decomposition for model reduction and data analysis. *Computers and Chemical Engineering* 20(5), 495–506 (1996)
63. Guo, L.Z., Billings, S.A.: Identification of partial differential equation models for continuous spatio-temporal dynamical systems. *IEEE Transactions on Circuits and Systems - II: Express Briefs* 53(8), 657–661 (2006)
64. Guo, L.Z., Billings, S.A.: State-space reconstruction and spatio-temporal prediction of lattice dynamical systems. *IEEE Transactions on Automatic Control* 52(4), 622–632 (2007)
65. Guo, L.Z., Billings, S.A., Wei, H.L.: Estimation of spatial derivatives and identification of continuous spatio-temporal dynamical systems. *International Journal of Control* 79(9), 1118–1135 (2006)
66. Hagenblad, A., Ljung, L.: Maximum likelihood identification of Wiener models with a linear regression initialization. In: *Proceedings of the 37th IEEE Conference Decision & Control, Tampa, Florida, USA*, pp. 712–713 (1998)
67. Höllig, K.: *Finite element methods with B-splines*. Society Industrial and Applied Mathematics, Philadelphia (2003)
68. Holmes, P., Lumley, J.L., Berkooz, G.: *Turbulence, coherent structures, dynamical systems, and symmetry*. Cambridge University Press, New York (1996)
69. Hoo, K.A., Zheng, D.: Low-order control-relevant models for a class of distributed parameter systems. *Chemical Engineering Science* 56(23), 6683–6710 (2001)

70. Horng, I.-R., Chou, J.-H., Tsai, C.-H.: Analysis and identification of linear distributed systems via Chebyshev series. *International Journal of Systems Science* 17(7), 1089–1095 (1986)
71. Hsieh, W.W.: Nonlinear principal component analysis by neural networks. *Tellus Series A - Dynamic Meteorology and Oceanography* 53(5), 599–615 (2001)
72. Kirby, M., Miranda, R.: The nonlinear reduction of high-dimensional dynamical systems via neural networks. *Physical Review Letter* 72(12), 1822–1825 (1994)
73. Ko, J., Kurdila, A.J., Pilant, M.S.: A class of finite element methods based on orthonormal compactly supported wavelets. *Computational Mechanics* 16(4), 235–244 (1995)
74. Kramer, M.A.: Nonlinear principal component analysis using autoassociative neural networks. *AIChE Journal* 37(2), 233–243 (1991)
75. Kubrusly, C.S.: Distributed parameter system identification - a survey. *International Journal of Control* 26(4), 509–535 (1977)
76. Kubrusly, C.S., Curtain, R.F.: Identification of noisy distributed parameter systems using stochastic approximation. *International Journal of Control* 25(3), 441–455 (1977)
77. Lee, T.-T., Chang, Y.-F.: Analysis and identification of linear distributed systems via double general orthogonal polynomials. *International Journal of Control* 44(2), 395–405 (1986)
78. Lefèvre, L., Dochain, D., Feye de Azevedo, S., Magnus, A.: Optimal selection of orthogonal polynomials applied to the integration of chemical reactor equations by collocation methods. *Computers and Chemical Engineering* 24(12), 2571–2588 (2000)
79. Li, H.-X., Deng, H., Zhong, J.: Model-based integration of control and supervision for one kind of curing process. *IEEE Transactions on Electronics Packaging Manufacturing* 27(3), 177–186 (2004)
80. Mahadevan, N., Hoo, K.A.: Wavelet-based model reduction of distributed parameter systems. *Chemical Engineering Science* 55(19), 4271–4290 (2000)
81. Mandelj, S., Grabec, I., Govekar, E.: Statistical approach to modeling of spatiotemporal dynamics. *International Journal of Bifurcation and Chaos* 11(11), 2731–2738 (2001)
82. Mandelj, S., Grabec, I., Govekar, E.: Nonparametric statistical modeling approach of spatiotemporal dynamics based on recorded data. *International Journal of Bifurcation and Chaos* 14(6), 2011–2025 (2004)
83. Maner, B.R., Doyle III, F.J., Ogunnaike, B.A., Pearson, R.K.: Nonlinear model predictive control of a simulated multivariable polymerization reactor using second-order Volterra models. *Automatica* 32(9), 1285–1301 (1996)
84. Marion, M., Temam, R.: Nonlinear Galerkin methods: The finite elements case. *Numerische Mathematik* 57(1), 205–226 (1990)
85. Mitchell, A.R., Griffiths, D.F.: *The finite difference method in partial differential equations*. Wiley, Chichester (1980)
86. Mohan, B.M., Datta, K.B.: Identification via Fourier series for a class of lumped and distributed parameter systems. *IEEE Transactions on Circuits and Systems* 36(11), 1454–1458 (1989)
87. Mohan, B.M., Datta, K.B.: Linear time-invariant distributed parameter system identification via orthogonal functions. *Automatica* 27(2), 409–412 (1991)
88. Müller, T.G., Timmer, J.: Parameter identification techniques for partial differential equations. *International Journal of Bifurcation and Chaos* 14(6), 2053–2060 (2004)

89. Narendra, K., Gallman, P.: An iterative method for the identification of nonlinear systems using a Hammerstein model. *IEEE Transactions on Automatic Control* 11(3), 546–550 (1966)
90. Newman, A.J.: Model reduction via the Karhunen-Loève expansion part I: An exposition. Technical Report T.R.96-32, University of Maryland, College Park, Maryland (1996a)
91. Newman, A.J.: Model reduction via the Karhunen-Loève expansion part II: Some elementary examples. Technical Report T.R.96-33, University of Maryland, College Park, Maryland (1996b)
92. Omatu, S., Matumoto, K.: Parameter identification for distributed systems and its application to air pollution estimation. *International Journal of Systems Science* 22(10), 1993–2000 (1991)
93. Paraskevopoulos, P.N., Bounas, A.C.: Distributed parameter system identification via Walsh-functions. *International Journal of Systems Science* 9(1), 75–83 (1978)
94. Park, H.M., Cho, D.H.: Low dimensional modeling of flow reactors. *International Journal of Heat and Mass Transfer* 39(16), 3311–3323 (1996a)
95. Park, H.M., Cho, D.H.: The use of the Karhunen-Loève decomposition for the modeling of distributed parameter systems. *Chemical Engineering Science* 51(1), 81–98 (1996b)
96. Park, H.M., Kim, T.H., Cho, D.H.: Estimation of parameters in flow reactors using the Karhunen-Loève decomposition. *Computers and Chemical Engineering* 23(1), 109–123 (1998)
97. Parker, R.S., Hemstra, D., Doyle III, F.J., Pearson, R.K., Ogunnaike, B.A.: The identification of nonlinear models for process control using tailored “plant-friendly” input sequences. *Journal of Process Control* 11(2), 237–250 (2001)
98. Parlitz, U., Merkwirth, C.: Prediction of spatiotemporal time series based on reconstructed local states. *Physical Review Letters* 84(9), 1890–1893 (2000)
99. Polis, M.P., Goodson, R.E.: Parameter identification in distributed systems: A synthesizing overview. *Proceedings of the IEEE* 64(1), 45–61 (1976)
100. Powers, D.L.: *Boundary value problems*, 4th edn. Academic Press, San Diego (1999)
101. Ranganathan, V., Jha, A.N., Rajamani, V.S.: Identification of linear distributed systems via Laguerre-polynomials. *International Journal of Systems Science* 15(10), 1101–1106 (1984)
102. Ranganathan, V., Jha, A.N., Rajamani, V.S.: Identification of non-linear distributed systems via a Laguerre-polynomial approach. *International Journal of Systems Science* 17(2), 241–249 (1986)
103. Rannacher, R., Vexler, B.: A priori error estimates for the finite element discretization of elliptic parameter identification problems with pointwise measurements. *SIAM Journal on Control and Optimization* 44(5), 1844–1863 (2005)
104. Ray, W.H.: *Advanced process control*. McGraw-Hill, New York (1981)
105. Romijn, R., Özkan, L., Weiland, S., Ludlage, J., Marquardt, W.: A grey-box modeling approach for the reduction of nonlinear systems. *Journal of Process Control* 18(9), 906–914 (2008)
106. Rugh, W.: *Nonlinear system theory: The Volterra/Wiener approach*. Johns Hopkins University Press, Baltimore (1981)
107. Sahan, R.A., Koc-Sahan, N., Albin, D.C., Liakopoulos, A.: Artificial neural network-based modeling and intelligent control of transitional flows. In: *Proceeding of the 1997 IEEE International Conference on Control Applications*, Hartford, CT, pp. 359–364 (1997)



108. Schetzen, M.: The Volterra and Wiener theories of nonlinear systems. Wiley, New York (1980)
109. Schiesser, W.E.: The numerical method of lines: Integration of partial differential equations. Academic Press, San Diego (1991)
110. Shvartsman, S.Y., Kevrikidis, I.G.: Nonlinear model reduction for control of distributed systems: A computer-assisted study. *AIChE Journal* 44(7), 1579–1594 (1998)
111. Sirovich, L.: Turbulence and the dynamics of coherent structures parts I-III. *Quarterly of Applied Mathematics* 45(3), 561–590 (1987)
112. Smaoui, N.: Linear versus nonlinear dimensionality reduction of high-dimensional dynamical systems. *SIAM Journal on Scientific Computing* 25(6), 2107–2125 (2004)
113. Smaoui, N., Al-Enezi, S.: Modelling the dynamics of nonlinear partial differential equations using neural networks. *Journal of Computational and Applied Mathematics* 170(1), 27–58 (2004)
114. Stoica, P., Söderström, T.: Instrumental-variable methods for identification of Hammerstein systems. *International Journal of Control* 35(3), 459–476 (1982)
115. Temam, R.: Infinite-dimensional dynamical systems in mechanics and physics. Springer, New York (1988)
116. Theodoropoulou, A., Adomaitis, R.A., Zafiriou, E.: Model reduction for optimization of rapid thermal chemical vapor deposition systems. *IEEE Transactions on Semiconductor Manufacturing* 11(1), 85–98 (1998)
117. Uciński, D., Korbicz, J.: Parameter identification of two-dimensional distributed systems. *International Journal of Systems Science* 21(12), 2441–2456 (1990)
118. Uciński, D., Korbicz, J.: Parameter identification of two-dimensional distributed systems. *International Journal of Systems Science* 21(12), 2441–2456 (1990)
119. Vande Wouwer, A., Renotte, C., Queinnec, I., Bogaerts, P.H.: Transient analysis of a wastewater treatment biofilter - Distributed parameter modelling and state estimation. *Mathematical and Computer Modelling of Dynamical Systems* 12(5), 423–440 (2006)
120. Varshney, A., Armaou, A.: Low-order ODE approximations and receding horizon control of surface roughness during thin-film growth. *Chemical Engineering Science* 63(5), 1246–1260 (2008)
121. Voss, H., Büchner, M.J., Abel, M.: Identification of continuous, spatiotemporal systems. *Physical Review E* 57(3), 2820–2823 (1998)
122. Webb, A.R.: An approach to non-linear principal components analysis using radially symmetric kernel functions. *Journal Statistics and Computing* 6(2), 159–168 (1996)
123. Westwick, D., Verhaegen, M.: Identifying MIMO Wiener systems using subspace model identification methods. *Signal Processing* 52(2), 235–258 (1996)
124. Wilson, D.J.H., Irwin, G.W., Lightbody, G.: RBF principal manifolds for process monitoring. *IEEE Transactions on Neural Networks* 10(6), 1424–1434 (1999)
125. Zheng, D., Hoo, K.A.: Low-order model identification for implementable control solutions of distributed parameter system. *Computers and Chemical Engineering* 26(7-8), 1049–1076 (2002)
126. Zheng, D., Hoo, K.A.: System identification and model-based control for distributed parameter systems. *Computers and Chemical Engineering* 28(8), 1361–1375 (2004)
127. Zheng, D., Hoo, K.A., Piovoso, M.J.: Low-order model identification of distributed parameter systems by a combination of singular value decomposition and the Karhunen-Loève expansion. *Industrial & Engineering Chemistry Research* 41(6), 1545–1556 (2002)

128. Zhou, X.G., Liu, L.H., Dai, Y.C., Yuan, W.K., Hudson, J.L.: Modeling of a fixed-bed reactor using the KL expansion and neural networks. *Chemical Engineering Science* 51(10), 2179–2188 (1996)
129. Zhu, Y.C.: Identification of Hammerstein models for control using ASYM. *International Journal of Control* 73(18), 1692–1702 (2000)
130. Zill, D.G., Cullen, M.R.: *Differential equations with boundary-value problems*, 5th edn. Brooks/Cole Thomson Learning, Pacific Grove, CA, Australia (2001)

# 3 Spatio-Temporal Modeling for Wiener Distributed Parameter Systems

**Abstract.** For Wiener distributed parameter systems (DPS), a spatio-temporal Wiener model (a linear DPS followed by a static nonlinearity) is constructed in this chapter. After the time/space separation, it can be represented by the traditional Wiener system with a set of spatial basis functions. To achieve a low-order model, the Karhunen-Loève (KL) method is used for the time/space separation and dimension reduction. Finally, unknown parameters of the Wiener system are estimated with the least-squares estimation and the instrumental variables method to achieve consistent estimation under noisy measurements. The simulation on the catalytic rod and the experiment on snap curing oven are presented to illustrate the effectiveness of this modeling method.

## 3.1 Introduction

In the identification of traditional lumped parameter systems (LPS), the **block-oriented nonlinear models** have been widely used because of their simple structures, abilities to approximate a large class of nonlinear processes and many efficient control schemes. They consist of an interconnection of linear time invariant (LTI) systems and static nonlinearities. Within this class, two common model structures are: the **Hammerstein model**, which consists of the cascade connection of a static nonlinearity followed by a LTI system, and the **Wiener model**, in which the order of linear and nonlinear blocks is reversed. This chapter will extend the Wiener system to DPS.

Wiener models are widely used in engineering practice. Modeling the pH neutralization process, the continuous stirred tank reactor and distillation columns are a few examples of their applications. Because a linear structure model can be derived from the block-oriented nonlinear model, the control design and optimization problem of the Wiener model can be easier than that of general nonlinear models (Christofides, 1997; Baker & Christofides, 2000; Armaou & Christofides, 2002; Coca & Billings, 2002; Sahan *et al.*, 1997; Deng, Li & Chen, 2005). The successful examples have been reported in the traditional ordinary differential equation (ODE) processes (Bloemen *et al.*, 2001; Jeong, Yoo & Rhee, 2001; Gerksic *et al.*, 2000; Cervantes, Agamennoni & Figueroa, 2003).

Several approaches to the identification of Wiener models can be found in the literature (Westwick & Verhaegen, 1996; Raich, Zhou & Viberg, 2005; Greblicki, 1994). There are two classes of model parameterization approaches, i.e., nonparametric (Pawlak, Hasiewicz & Wachel, 2007) and parametric approaches (Hagenblad & Ljung, 1998). The parameter identification algorithms can be

classified into the prediction error method (Wigren, 1993), the subspace method (Gómez, Jutan & Baeyens, 2004), the least-squares (LS) method (Gómez & Baeyens, 2004), the maximum likelihood method (Hagenblad & Ljung, 2000), and the instrumental variables (IV) method (Janczak, 2007), etc. Despite the existence of several well-established Wiener model identification techniques, they are only studied for lumped parameter systems.

In this chapter, a Karhunen-Loève decomposition (KL) based Wiener modeling approach is developed for nonlinear distributed parameter processes. A Wiener distributed parameter system is presented with a distributed linear DPS followed by a static nonlinearity. After the time/space separation, the Wiener distributed parameter system can be represented by a traditional Wiener system with a set of spatial basis functions. To obtain a low-order model, the time/space separation and the dimension reduction are implemented through the Karhunen-Loève decomposition. To identify a Wiener model from temporal coefficients, the least-squares estimation combined with the instrumental variables method is used. This spatio-temporal modeling method can provide consistent parameter estimates under proper conditions. The spatio-temporal Wiener model should have significant approximation capability to nonlinear distributed parameter systems. With the spatio-temporal Wiener model, many control and optimization algorithms (Bloemen *et al.*, 2001; Jeong, Yoo & Rhee, 2001; Gerksic *et al.*, 2000; Cervantes, Agamennoni & Figueroa, 2003; Gómez, Jutan & Baeyens, 2004) developed for the traditional Wiener model can be easily extended to nonlinear distributed parameter processes under unknown circumstances.

This chapter is organized as follows. The Wiener distributed parameter system is given in Section 3.2. The spatio-temporal Wiener modeling problem is described in Section 3.3. In Section 3.4, the Karhunen-Loève decomposition is introduced. The parameterization of the Wiener model is presented in Section 3.5.1. The parameter identification algorithm is given in Section 3.5.2. The numerical simulation and the experiment on snap curing oven are demonstrated in Section 3.6. Finally, a few conclusions are presented in Section 3.7.

## 3.2 Wiener Distributed Parameter System

A Wiener distributed parameter system is shown in Figure 3.1. The system consists of a distributed linear time-invariant system

$$v(x, t) = G(x, q)u(t) + d(x, t), \quad (3.1)$$

followed by a static nonlinear element  $N(\cdot): \mathbb{R} \rightarrow \mathbb{R}$ , where  $G(x, q)$  ( $1 \times m$ ) is a transfer function,  $t$  is time variable,  $x$  is spatial variable defined on the domain  $\Omega$ , and  $q$  stands for the forward shift operator. The input-output relationship of the system is then given by

$$y(x, t) = N(G(x, q)u(t) + d(x, t)), \quad (3.2)$$

where  $u(t) \in \mathbb{R}^m$  is the temporal input,  $y(x, t) \in \mathbb{R}$  and  $d(x, t) \in \mathbb{R}$  are the spatio-temporal output and process noise respectively.

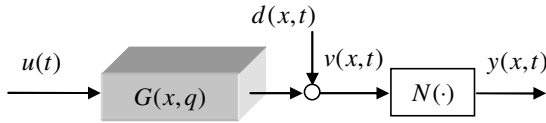


**Fig. 3.1** Wiener distributed parameter system

Suppose the transfer function  $G(x, q)$  can be expanded onto an infinite number of orthonormal spatial basis functions  $\{\varphi_i(x)\}_{i=1}^{\infty}$

$$G(x, q) = \sum_{i=1}^{\infty} \varphi_i(x) G_i(q), \tag{3.3}$$

where  $G_i(q)$  ( $1 \times m$ ) is the traditional transfer function. Thus the Wiener distributed parameter system can be represented in **Figure 3.2(a)** via a time-space separation. Suppose there exists a static nonlinearity  $F(\cdot)$  such that

$$N(\varphi(x)v(t)) = \varphi(x)F(v(t)), \tag{3.4}$$

then the Wiener distributed parameter system can be represented by a traditional Wiener system as shown in **Figure 3.2(b)**. This assumption is suitable for a wide range of systems because the nonlinear function  $F$  can be different from the function  $N$ .

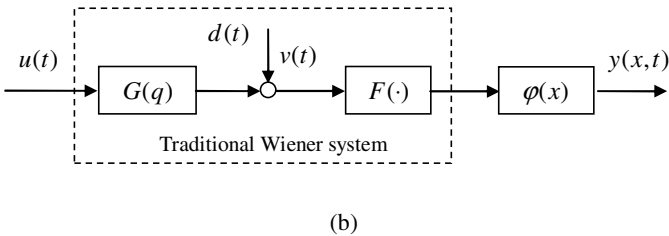
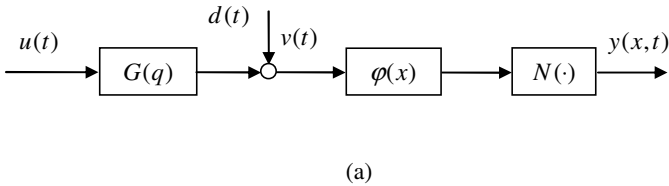


**Fig. 3.2** Time/space separation of Wiener distributed parameter system

### 3.3 Spatio-Temporal Wiener Modeling Methodology

Consider the distributed parameter system in [Figure 3.1](#). Here suppose the system is controlled by the  $m$  actuators with implemental temporal signal  $u(t)$  and certain spatial distribution. The output is measured at the  $N$  spatial locations  $x_1, \dots, x_N$ . It should be mentioned that because of the infinite dimensionality of the distributed parameter system, it may require an infinite number of actuators and sensors over the whole space to implement the perfect modeling and control. Due to some practical limitations such as hardware and cost, a limited number of actuators and sensors should be used. The minimal number of actuators and sensors may depend on the process complexity as well as the required accuracy of modeling and control. In this study, we also suppose that the output can be measured without noise, while the system is disturbed by the process noise  $d(x, t)$ . This assumption is realistic since the influence of (unmeasured) process disturbance is, in general, much greater than that of the measurement noise due to the advances in sensor technologies ([Zhu, 2002](#)).

The modeling problem is to identify a proper nonlinear spatio-temporal model from the input  $\{u(t)\}_{t=1}^L$  and the output  $\{y(x_i, t)\}_{i=1, t=1}^{N, L}$ , where  $L$  is the time length.

As shown in [Figure 3.3](#), the modeling methodology includes two stages. The first stage is the Karhunen-Loève decomposition for the time/space separation. The second stage is the traditional Wiener model identification. Using the time/space synthesis, this model can reconstruct the spatio-temporal dynamics of the system.

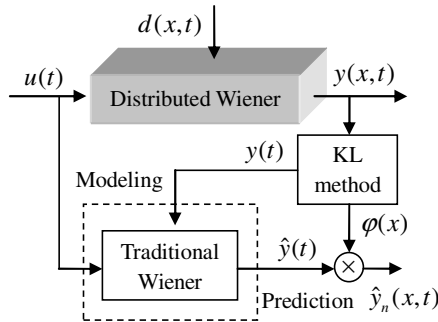


**Fig. 3.3** KL based modeling methodology for Wiener distributed parameter system

### 3.4 Karhunen-Loève Decomposition

Karhunen-Loève expansion (also known as principal component analysis) is to find an optimal basis from a representative set of process data. Suppose we have a set of observations about the process output  $\{y(x_i, t)\}_{i=1, t=1}^{N, L}$  (called snapshots) which is assumed to be uniformly sampled in the time and space for simplicity. Here the ensemble average, the norm, and the inner product are defined as

$\langle f(x,t) \rangle = \frac{1}{L} \sum_{t=1}^L f(x,t)$  ,  $\|f(x)\| = (f(x), f(x))^{1/2}$  , and  $(f(x), g(x)) = \int_{\Omega} f(x)g(x)dx$  respectively.

Motivated by Fourier series, the spatio-temporal variable  $y(x,t)$  can be expanded onto an infinite number of orthonormal spatial basis functions  $\{\varphi_i(x)\}_{i=1}^{\infty}$

$$y(x,t) = \sum_{i=1}^{\infty} \varphi_i(x) y_i(t) , \quad (3.5)$$

where the temporal coefficients can be computed from

$$y_i(t) = (\varphi_i(x), y(x,t)), i = 1, \dots, n . \quad (3.6)$$

In practice, it has to be truncated to a finite dimension

$$y_n(x,t) = \sum_{i=1}^n \varphi_i(x) y_i(t) , \quad (3.7)$$

where  $y_n(x,t)$  denotes the  $n$ th-order approximation.

The problem is how to compute the most characteristic structure  $\{\varphi_i(x)\}_{i=1}^n$  among these snapshots  $\{y(x_i,t)\}_{i=1,t=1}^{N,L}$ .

### ***Spatial Correlation Method***

Actually this problem can be formulated as the one of obtaining a set of functions  $\{\varphi_i(x)\}_{i=1}^n$  that minimizes the following objective function (Christofides, 2001b):

$$\begin{aligned} \min_{\varphi_i(x)} \quad & \langle \|y(x,t) - y_n(x,t)\|^2 \rangle \\ \text{subject to} \quad & (\varphi_i, \varphi_i) = 1, \varphi_i \in L^2(\Omega), i = 1, \dots, n. \end{aligned} \quad (3.8)$$

The constraint  $(\varphi_i, \varphi_i) = 1$  is imposed to ensure that the function  $\varphi_i(x)$  is unique. The Lagrangian functional corresponding to this constrained optimization problem is

$$J = \langle \|y(x,t) - y_n(x,t)\|^2 \rangle + \sum_{i=1}^n \lambda_i ((\varphi_i, \varphi_i) - 1) , \quad (3.9)$$

and the necessary condition of the solution can be obtained as below (Holmes, Lumley & Berkooz, 1996)

$$\int_{\Omega} R(x, \zeta) \varphi_i(\zeta) d\zeta = \lambda_i \varphi_i(x), (\varphi_i, \varphi_i) = 1, i = 1, \dots, n , \quad (3.10)$$

where  $R(x, \zeta) = \langle y(x,t) y(\zeta, t) \rangle$  is the spatial two-point correlation function,  $\varphi_i(x)$  is the  $i$ th eigenfunction,  $\lambda_i$  is the corresponding eigenvalue.

Since the data are always discrete in space, one must solve numerically the integral equation (3.10). Discretizing the integral equation gives a  $N \times N$  matrix eigenvalue problem. Thus, at most  $N$  eigenfunctions at  $N$  sampled spatial

locations can be obtained. Then one can use the curve/surface fitting method (Lancaster & Salkauskas, 1986; Dierckx, 1993) interpolate the eigenfunctions to locations where the data are not available.

### Temporal Correlation Method

When  $L$  is less than  $N$ , a computationally efficient way to obtain the solution of (3.10) is provided by the method of snapshots (Sirovich, 1991; Newman, 1996a, 1996b). The eigenfunction  $\varphi_i(x)$  is assumed to be expressed as a linear combination of the snapshots as follows

$$\varphi_i(x) = \sum_{t=1}^L \gamma_{it} y(x, t). \quad (3.11)$$

Substituting (3.11) into (3.10) gives the following eigenvalue problem:

$$\int_{\Omega} \frac{1}{L} \sum_{t=1}^L y(x, t) y(\zeta, t) \sum_{k=1}^L \gamma_{ik} y(\zeta, k) d\zeta = \lambda_i \sum_{t=1}^L \gamma_{it} y(x, t). \quad (3.12)$$

Define the temporal two-point correlation matrix as  $C$  where the element at the  $t$ th row and  $k$ th column is

$$C_{ik} = \frac{1}{L} \int_{\Omega} y(\zeta, t) y(\zeta, k) d\zeta. \quad (3.13)$$

Therefore, the  $N \times N$  eigenvalue problem (3.10) can be reduced to a  $L \times L$  problem as follows

$$C \gamma_i = \lambda_i \gamma_i. \quad (3.14)$$

where  $\gamma_i = [\gamma_{i1}, \dots, \gamma_{iL}]^T$  is the  $i$ th eigenvector. The solution of the above eigenvalue problem yields the eigenvectors  $\gamma_1, \dots, \gamma_L$ , which can be used in (3.11) to construct the eigenfunctions  $\varphi_1(x), \dots, \varphi_L(x)$ . Since the matrix  $C$  is symmetric and positive semidefinite, its eigenvalues  $\lambda_i$  are real and non-negative. Furthermore, the computed eigenfunctions are orthogonal.

### Selection of Dimension $n$

The maximum number of nonzero eigenvalues is  $K \leq \min(N, L)$ . Let the eigenvalues  $\lambda_1 > \lambda_2 > \dots > \lambda_K$  and the corresponding eigenfunctions  $\varphi_1(x), \varphi_2(x), \dots, \varphi_K(x)$  in the order of the magnitude of the eigenvalues. It can be proved that (Holmes, Lumley & Berkooz, 1996)

$$\lambda_i = \langle (y(x, t), \varphi_i(x))^2 \rangle.$$

The eigenfunction that corresponds to the first eigenvalue is considered to be the most “energetic”. The total “energy” is defined as being the sum of the eigenvalues.



To each eigenfunction, assign an “energy” percentage based on the associated eigenvalue:

$$E_i = \lambda_i / \sum_{j=1}^K \lambda_j .$$

Usually, the sufficient number of eigenfunctions that capture 99% of the system “energy” is used to determine the value of  $n$ . Experiences show that only the first few basis functions expansion can represent the dominant dynamics of many parabolic spatio-temporal systems. It can be shown (Holmes, Lumley & Berkooz, 1996) that for some arbitrary set of basis functions  $\{\phi_i(x)\}_{i=1}^n$ ,

$$\sum_{i=1}^n \langle (y(\cdot, t), \phi_i)^2 \rangle = \sum_{i=1}^n \lambda_i^2 \geq \sum_{i=1}^n \langle (y(\cdot, t), \phi_i)^2 \rangle .$$

It means that the Karhunen-Loève expansion is optimal on average in the class of representations by linear combination. That is why Karhunen-Loève expansion can give the lowest dimension  $n$ .

### 3.5 Wiener Model Identification

In order to obtain the temporal coefficients of the spatio-temporal output, define the orthogonal projection operator  $P_w$  as

$$y_w(t) = P_w y(\cdot, t) = (\varphi_w, \sum_{i=1}^{\infty} \varphi_i(\cdot) y_i(t)) = \sum_{i=1}^{\infty} (\varphi_w, \varphi_i(\cdot)) y_i(t) , \tag{3.15}$$

where  $\varphi_w = [\varphi_1, \varphi_2, \dots, \varphi_n]^T$ . Since the basis functions  $\varphi_i$ , ( $i = 1, \dots, \infty$ ) are orthonormal, the result of this projection is such that  $y_w(t) = [y_1(t), \dots, y_n(t)]^T$ . In practical case  $y_w$  can be computed from the pointwise data using spline integration. Similarly, we can define the temporal coefficients of the spatio-temporal noise as  $d_w(t) = P_w d(\cdot, t) = [d_1(t), \dots, d_n(t)]^T$ .

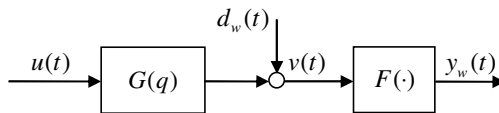


Fig. 3.4 Wiener model

Suppose that the dynamics between  $u(t)$  and  $y_w(t)$  can be described by a Wiener model. As shown in Figure 3.4, the Wiener model consists of the cascade of a linear time-invariant dynamical system with a  $n \times m$  transfer function matrix  $G(q)$  ( $q$  is the time-shift operator ( $qu(t) = u(t + \Delta t)$ ), followed by a nonlinear static

element  $F(\cdot): \mathbb{R}^n \rightarrow \mathbb{R}^n$ . The input-output relationship of the Wiener model is then given by

$$y_w(t) = F(v(t)) = F(G(q)u(t) + d_w(t)), \quad (3.16)$$

where  $u(t) \in \mathbb{R}^m$ ,  $y_w(t) \in \mathbb{R}^n$ ,  $v(t) \in \mathbb{R}^n$ , and  $d_w(t) \in \mathbb{R}^n$ , represent the temporal input, output, intermediate variable and process noise at time  $t$ , respectively.

Now the identification problem is to estimate the Wiener model from the data set  $\{u(t), y_w(t)\}_{t=1}^L$ .

### 3.5.1 Model Parameterization

It will be assumed that the transfer function matrix of the linear subsystem is represented as an orthonormal basis expansion of the following form

$$G(q) = \sum_{i=1}^{n_\alpha} \alpha_i g_i(q), \quad (3.17)$$

where  $g_i(q)$  ( $i=1, \dots, n_\alpha$ ) are known scalar basis functions,  $\alpha_i \in \mathbb{R}^{n_\alpha \times m}$  ( $i=1, \dots, n_\alpha$ ) are unknown matrix parameters.  $g_i(q)$  can be selected as finite impulse response, Laguerre (Wahlberg, 1991) and Kautz functions (Wahlberg, 1994) and generalized orthonormal basis functions (Heuberger, Van den Hof & Bosgra, 1995). Here, Laguerre functions are chosen for the development because of their simplicity, that is they are completely determined by a single parameter. The transfer functions of Laguerre functions are given by

$$g_i(q) = \frac{\sqrt{1-\xi^2}}{q-\xi} \left( \frac{1-\xi q}{q-\xi} \right)^{i-1}, i=1, 2, \dots, \infty, \quad (3.18)$$

where  $\xi$  ( $|\xi| < 1$ ) is a stable pole. It can be shown (Wahlberg, 1991) that if this pole is set close to the dominant dynamics of the system to be modeled, a significant reduction in the number of functions and parameters needed to approximate the system with arbitrary accuracy can be achieved.

The intermediate variable  $v(t)$  can be written as

$$v(t) = G(q)u(t) + d_w(t) = \sum_{i=1}^{n_\alpha} \alpha_i g_i(q)u(t) + d_w(t). \quad (3.19)$$

On the other hand, the nonlinear function  $F(\cdot)$  will be assumed to be invertible, and its inverse  $F^{-1}(\cdot)$  can be described as

$$v(t) = F^{-1}(y_w(t)) = \sum_{j=1}^{n_\beta} \beta_j f_j(y_w(t)), \quad (3.20)$$

where  $f_j(\cdot): \mathbb{R}^n \rightarrow \mathbb{R}^n$  ( $j=1, \dots, n_\beta$ ) are nonlinear basis functions such as polynomials, splines, radial basis functions and wavelets (Sjöberg *et al.*, 1995), and  $\beta_j \in \mathbb{R}^{n_\alpha \times n}$

( $j=1, \dots, n_\beta$ ) are unknown matrix parameters. Typically, the polynomial representation is chosen because it is simple to implement and analyze. The assumption of invertible nonlinearities is common in most existing Wiener identification algorithms (Hagenblad, 1999) because it is particularly convenient for control system design, whereas others (Wigren, 1994; Lacy & Bernstein, 2003) allow noninvertible nonlinearities. The orders  $n_\alpha$  and  $n_\beta$  are assumed to be known.

Under these assumptions, the identification problem is to estimate the unknown parameter matrices  $\alpha_i$  ( $i=1, \dots, n_\alpha$ ) and  $\beta_j$  ( $j=1, \dots, n_\beta$ ) from the data set  $\{u(t), y_w(t)\}_{t=1}^L$ . Once  $\beta_j$  ( $j=1, \dots, n_\beta$ ) are obtained,  $F^{-1}(\cdot)$  is known, and thus  $F(\cdot)$  can be directly obtained from  $F^{-1}(\cdot)$ .

### 3.5.2 Parameter Estimation

In order to obtain the uniqueness of the parameterization, without loss of generality, it will also be assumed that  $\beta_1 = I_n$ , with  $I_n$  standing for a  $n \times n$  identity matrix.

Combining (3.19) and (3.20), the following equation is obtained

$$f_1(y_w(t)) = \sum_{i=1}^{n_\alpha} \alpha_i g_i(q)u(t) - \sum_{j=2}^{n_\beta} \beta_j f_j(y_w(t)) + d_w(t), \quad (3.21)$$

which is a linear regression.

Defining

$$\theta = [\alpha_1, \dots, \alpha_{n_\alpha}, \beta_2, \dots, \beta_{n_\beta}]^T \in \mathbb{R}^{(mn_\alpha + mn_\beta - n) \times n}, \quad (3.22)$$

$$\phi(t) = [(g_1(q)u(t))^T, \dots, (g_{n_\alpha}(q)u(t))^T, -f_2^T(y_w(t)), \dots, -f_{n_\beta}^T(y_w(t))]^T \in \mathbb{R}^{mn_\alpha + mn_\beta - n}, \quad (3.23)$$

then (3.21) can be written as

$$f_1(y_w(t)) = \theta^T \phi(t) + d_w(t). \quad (3.24)$$

Now, an estimate  $\hat{\theta}$  of  $\theta$  can be computed by minimizing a quadratic criterion on the prediction errors

$$\hat{\theta} = \arg \min_{\theta} \left\{ \frac{1}{L} \sum_{t=1}^L \|f_1(y_w(t)) - \theta^T \phi(t)\|^2 \right\}. \quad (3.25)$$

It is well known that the **least-squares estimate** is given by

$$\hat{\theta}_{LS} = \left( \frac{1}{L} \sum_{t=1}^L \phi(t) \phi^T(t) \right)^{-1} \left( \frac{1}{L} \sum_{t=1}^L \phi(t) f_1^T(y_w(t)) \right), \quad (3.26)$$

provided that the indicated inverse exists.

The consistency of the estimate  $\hat{\theta}_{LS}$  in (3.26), can only be guaranteed in the noise free case, since the regressor  $\phi(t)$  at time  $t$  will be correlated with the disturbance  $d_w(t)$  at the same instant, even if the disturbance is a white noise process.

The **instrumental variables method** is a simple and effective tool to obtain the consistency estimation (Janczak, 2007; Hagenblad, 1999). The idea of the IV method is to project (3.24) onto the so called instrumental variables vector  $\psi(t)$  which is designed properly. Then we have

$$\hat{\theta}_{IV} = \left( \frac{1}{L} \sum_{t=1}^L \psi(t) \phi^T(t) \right)^{-1} \left( \frac{1}{L} \sum_{t=1}^L \psi(t) f_1^T(y_w(t)) \right). \quad (3.27)$$

Thus the following conditions

$$E[\psi(t) \phi^T(t)] \text{ be nonsingular,} \quad (3.28)$$

$$E[\psi(t) d^T(t)] = 0, \quad (3.29)$$

are necessary to obtain the consistent parameter estimates. That means the instrumental variables should be chosen such that they are correlated with regression variables  $\phi(t)$  but uncorrelated with the disturbance  $d_w(t)$ . The variance of the IV parameter estimate depends on the choice of instrumental variables. A higher correlation between  $\psi(t)$  and  $\phi(t)$  results in a smaller variance error. Clearly, the good instrumental variables would contain the undisturbed system outputs but these are not available for measurement. Instead, the outputs of the model, calculated with the least-squares method, can construct the required instrumental variables as below

$$\psi(t) = [(g_1(q)u(t))^T, \dots, (g_{n_\alpha}(q)u(t))^T, -f_2^T(\hat{y}_w(t)), \dots, -f_{n_\beta}^T(\hat{y}_w(t))]^T \in \mathbb{R}^{m_{n_\alpha} + m_{n_\beta} - n}. \quad (3.30)$$

Now, estimates of the parameters  $\alpha_i$  ( $i=1, \dots, n_\alpha$ ) and  $\beta_j$  ( $j=2, \dots, n_\beta$ ) can be computed by partitioning the estimate  $\hat{\theta}_{IV}$ , according to the definition of  $\theta$  in (3.22).

The identification algorithm can then be summarized as follows.

### Algorithm 3.1:

*Step 1:* Use the measured output  $\{y(x_i, t)\}_{i=1, t=1}^{N, L}$  as snapshots, find the spatial basis functions  $\{\varphi_i(x)\}_{i=1}^n$  via Karhunen-Loève decomposition using (3.10) or (3.14), calculate the temporal coefficients  $\{y_w(t)\}_{t=1}^L$  using (3.15).

*Step 2:* Select the proper Laguerre pole  $\xi$  and nonlinear basis functions  $f_j(\cdot)$ , set the system orders  $n_\alpha$  and  $n_\beta$ .

*Step 3:* Compute the least-squares estimate  $\hat{\theta}_{LS}$  of  $\theta$  as in (3.26), then obtain the parameters  $\alpha_i^{LS}$  ( $i=1, \dots, n_\alpha$ ) and  $\beta_j^{LS}$  ( $j=2, \dots, n_\beta$ ) by partitioning the estimate  $\hat{\theta}_{LS}$ , according to the definition of  $\theta$  in (3.22).

*Step 4:* Simulate the model (3.16) with  $\alpha_i^{LS}$  ( $i=1, \dots, n_\alpha$ ) and  $\beta_j^{LS}$  ( $j=2, \dots, n_\beta$ ) to construct the instrumental variables vector  $\psi(t)$  in (3.30).

*Step 5:* Estimate the parameter  $\hat{\theta}_N$  with the IV method using (3.27), then compute the parameters  $\alpha_i^{IV}$  ( $i=1,\dots,n_\alpha$ ) and  $\beta_j^{IV}$  ( $j=2,\dots,n_\beta$ ) by partitioning the estimate  $\hat{\theta}_N$ , according to the definition of  $\theta$  in (3.22).

**Remark 3.1: Unknown System Orders**

In the practical situation, the orders  $n_\alpha$  and  $n_\beta$  are not known. Also, it may only obtain suboptimal results if the model orders are less than system orders. However, if the upper bounds on the orders are known, then the bounds can be used in (3.17) and (3.20) at the expense of the increasing computational complexity. Alternatively, the performance of  $F$  and  $G$  can be improved as increasing the system orders until the satisfactory performance is achieved, at the expense of the increasing computational load at each increment.

**Remark 3.2: Determination of Laguerre Pole**

In order to obtain the significant performance, the parameter  $\xi$  is usually obtained from trials. The systematic approach for optimal selection of the Laguerre pole was proposed for the linear system (Fu & Dumont, 1993) and the nonlinear Volterra system (Campello, Favier & Amaral, 2004). For the Wiener system, one approach is the iterative optimization of  $\hat{\theta}_N$  and  $\xi$ . However, it will turn into a complex nonlinear optimization problem which will not be studied here.

**Remark 3.3: State-space Realization**

Usually a state-space realization of the identified model is required for control purpose. It can be constructed using existing results on the state-space realizations for orthonormal basis systems (Gómez, 1998).

## 3.6 Simulation and Experiment

In order to evaluate the presented modeling method, the simulation on a typical distributed process: a catalytic rod is studied first, and then the experiment and modeling for the snap curing oven are presented.

The two models to be compared are stated as follows:

- Spline functions based Wiener (SP-Wiener) model,
- Karhunen-Loève based Wiener (KL-Wiener) model.

The SP-Wiener model is constructed by replacing Karhunen-Loève basis functions  $\varphi$  in (3.15) with spline functions during the modeling procedure. See the reference (Coca & Billings, 2002; Shikin & Plis, 1995) for details on the construction of spline functions.

Define  $y(x,t)$  and  $\hat{y}_n(x,t)$  as the measured output and the prediction output respectively. Some performance indexes are set up for an easy comparison as follows:

- Spatio-temporal error  $e(x,t) = y(x,t) - \hat{y}_n(x,t)$ ,
- Spatial normalized absolute error  $SNAE(t) = \frac{1}{N} \sum_{i=1}^N |e(x_i,t)|$ ,
- Temporal normalized absolute error  $TNAE(x) = \sum |e(x,t)| / \sum \Delta t$ ,
- Root of mean squared error  $RMSE = \left( \frac{1}{NL} \sum_{i=1}^N \sum_{t=1}^L e(x_i,t)^2 \right)^{1/2}$ .

### 3.6.1 Catalytic Rod

Consider the catalytic rod given in Section 1.1.2. The mathematical model which describes the spatio-temporal evolution of the dimensionless rod temperature consists of the following parabolic PDE (Christofides, 2001b):

$$\frac{\partial y(x,t)}{\partial t} = \frac{\partial^2 y(x,t)}{\partial x^2} + \beta_r (e^{-\frac{\gamma}{1+y}} - e^{-\gamma}) + \beta_u (b(x)^T u(t) - y(x,t)) + d(x,t), \quad (3.31)$$

subject to the boundary and initial conditions:

$$y(0,t) = 0, \quad y(\pi,t) = 0, \quad y(x,0) = y_0(x),$$

where  $y(x,t)$ ,  $u(t)$ ,  $b(x)$ ,  $\beta_r$ ,  $\beta_u$  and  $\gamma$  denote the temperature in the reactor, the manipulated input (temperature of the cooling medium), the actuator distribution, the heat of reaction, the heat transfer coefficient, and the activation energy.  $d(x,t)$  is the random process noise. The process parameters are often set as

$$\beta_r = 50, \quad \beta_u = 2, \quad \gamma = 4.$$

There are available four control actuators  $u(t) = [u_1(t), \dots, u_4(t)]^T$  with the spatial distribution function  $b(x) = [b_1(x), \dots, b_4(x)]^T$ ,  $b_i(x) = H(x - (i-1)\pi/4) - H(x - i\pi/4)$ , ( $i=1, \dots, 4$ ) and  $H(\cdot)$  is the standard Heaviside function. There is no unique method to design the input signals for the nonlinear system modeling. In this case, the temporal input  $u_i(t) = 1.1 + 5 \sin(t/10 + i/10)$  ( $i=1, \dots, 4$ ) are used for exciting the system. This periodic signal which depends on the spatial location and time instant can excite the nonlinear spatio-temporal dynamics. Unlike the traditional system modeling, due to the infinite-dimensional feature, sufficient sensors should be used to measure the representative spatial features of the distributed parameter system. It depends on the complexity of the spatial dynamics as well as the required modeling accuracy. In general, the number of output measurements is larger than the number of actuators. In this case, twenty sensors uniformly distributed in the space are used for measurements. The random process noise  $d(x,t)$  is bounded by 0.01 with zero mean. The PDE system (3.31) is solved using a high-order finite difference method. This solution is used to represent the real system response. See the reference

(Strikwerda, 1989) for details on the finite difference method. The sampling interval  $\Delta t$  is 0.01 and the simulation time is 6. Totally a set of 600 data is collected. The first 500 data is used as the training data with the first 400 data as the estimation data and the next 100 data as the validation data. The validation data is used to monitor the training process and determine some design parameters in the modeling. The remaining 100 data is the testing data.

The process output  $y(x,t)$  is shown in Figure 3.5, while the first five Karhunen-Loève basis functions as shown in Figure 3.6 are used for the KL-Wiener model identification. Using the cross-validation method, the temporal bases  $g_i(q)$ , ( $i=1,\dots,8$ ) are chosen as Laguerre series with a stable pole  $\xi=0.9896$ . The nonlinear bases  $f_i(y_w)$ , ( $i=1,\dots,4$ ) are designed as the standard polynomials  $f_i(y_w)=y_w^i$ .

The prediction output  $\hat{y}_n(x,t)$  of KL-Wiener model over the whole data set is shown in Figure 3.7, with the prediction error  $e(x,t)$  presented in Figure 3.8. It is obvious that KL-Wiener model can reproduce the spatio-temporal dynamics of the original system very well. Now we compare the performance of KL-Wiener model and SP-Wiener model. The SP-Wiener model is established using thirteen third-order splines as shown in Figure 3.9 which are generated using Spline Toolbox of MATLAB. Figure 3.10 displays  $SNAE(t)$  of these two models over the whole data set, where the solid line corresponds to KL-Wiener model and the dashed line to SP-Wiener model. The  $RMSE$  of SP-Wiener and KL-Wiener models are about 0.0042402 and 0.0009848 respectively. It is apparent that KL-Wiener model performs much better than SP-Wiener model even if SP-Wiener model allows the use of more number of basis functions. This is owing to the optimal feature of the Karhunen-Loève decomposition. The spatio-temporal KL-Wiener model is very efficient which is suitable for the nonlinear distributed parameter process.

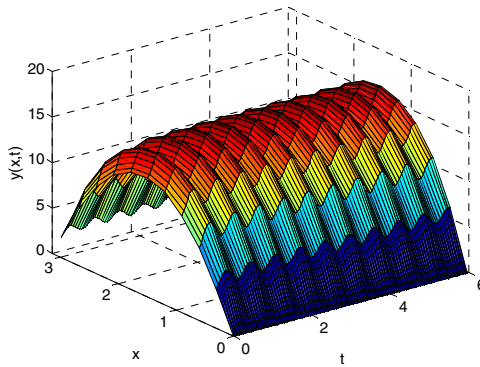


**Fig. 3.5** Catalytic rod: Measured output for Wiener modeling

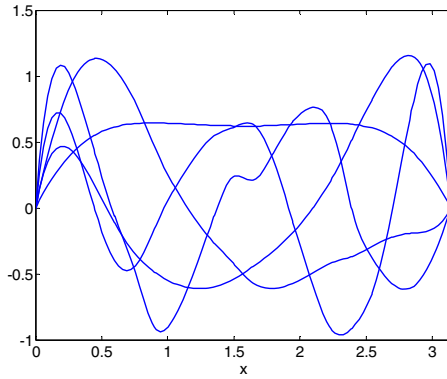


**Fig. 3.6** Catalytic rod: KL basis functions for KL-Wiener modeling

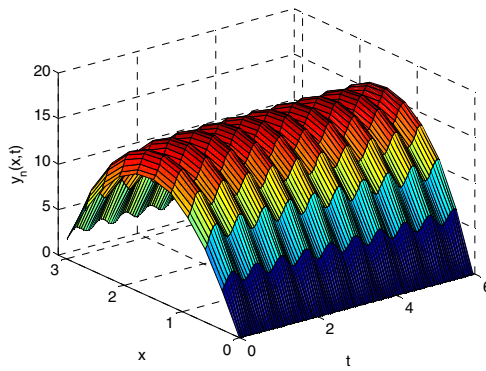


**Fig. 3.7** Catalytic rod: KL-Wiener model output

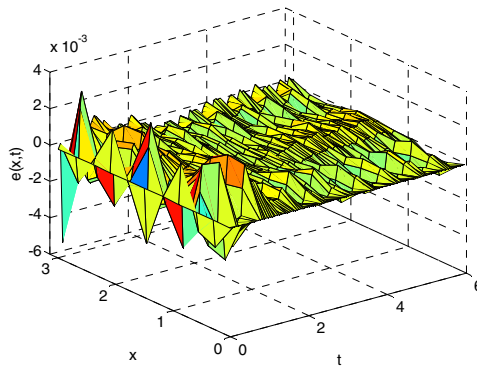


**Fig. 3.8** Catalytic rod: Prediction error of KL-Wiener model



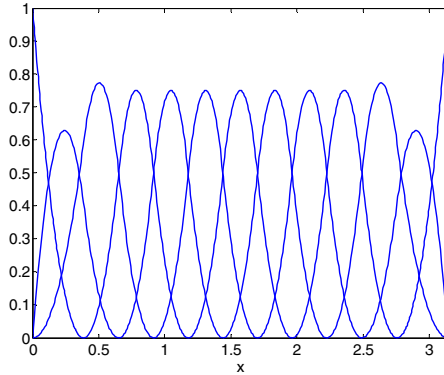


**Fig. 3.9** Catalytic rod: Spline basis functions for SP-Wiener modeling

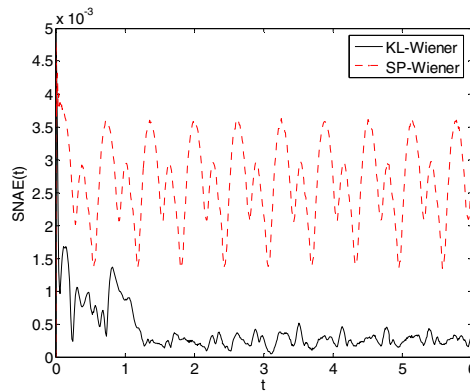


**Fig. 3.10** Catalytic rod:  $SNAE(t)$  of SP-Wiener and KL-Wiener models

### 3.6.2 Snap Curing Oven

Consider the **snap curing oven** in semiconductor back-end packaging industry provided in [Section 1.1.1](#). As shown in [Figure 1.1](#), it can provide the required curing temperature distribution ([Deng, Li & Chen, 2005](#)). The problem is to develop a model to estimate the temperature distribution inside the chamber. As shown in [Figure 3.11](#), it is equipped with four heaters (h1-h4) and sixteen temperature sensors (s1-s16) for modeling. Note that more sensors are added for collecting enough spatio-temporal dynamics information about the temperature field. Though the modeling experiment may need more sensors, once the model has been established, a few sensors will be enough for the prediction and control of the temperature distribution.

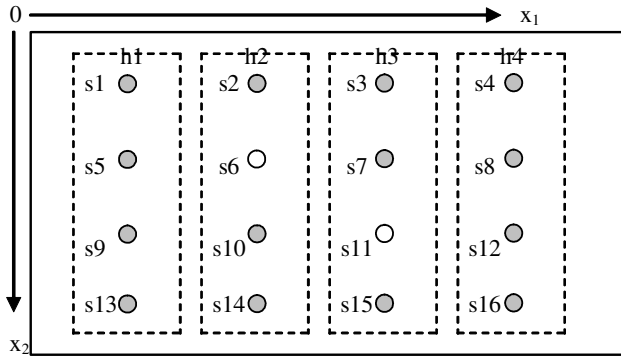


**Fig. 3.11** Sensors placement for modeling of snap curing oven

In the experiment, the random input signals are used to excite the thermal process and the first 500 samples for heater 1 are shown in [Figure 3.12](#). A total of 2100 measurements are collected with a sampling interval  $\Delta t = 10$  seconds. One thousand and four hundred of measurements from sensors (s1-s5, s7-s10, and s12-s16) are used to estimate the model. The last 700 measurements from sensors (s1-s5, s7-s10, and s12-s16) are chosen to validate the model. All 2100 measurements from the rest sensors (s6, s11), which are not used for training, will be used for testing model performance.

In the spatio-temporal Wiener modeling, five two-dimensional Karhunen-Loève basis functions are used as spatial bases and the first two of them are shown in [Figure 3.13](#) and [Figure 3.14](#). The temporal bases  $\phi_i(t)$  are chosen as Laguerre series with the time-scaling factor  $p = 0.001$  and the truncation length  $q = 3$  using the cross-validation method.

The *KL-Wiener model* is used to model the thermal process. After the training with the first 1400 data from the sensors (s1-s5, s7-s10, and s12-s16), a process model can be obtained with the performance of sensor s1 selected as the example shown in [Figure 3.15](#). Then the model will be tested using the untrained data from sensor s6 and s11. As shown in [Figure 3.16](#), the trained model can perform very well for the untrained data. The predicted temperature distribution of the oven at  $t = 10000$ s is provided in [Figure 3.17](#).

In order to provide a comparison, a *SP-Wiener model* is also constructed using twelve third-order splines as spatial basis functions. The first two of them are shown in [Figure 3.18](#) and [Figure 3.19](#). The predicted temperature distribution of the oven at  $t = 10000$ s is provided in [Figure 3.20](#). The performance index  $TNAE(x)$  over the whole data set in [Table 3.1](#) shows that *KL-Wiener model* works much better than *SP-Wiener model*. The *SP-Wiener model* is not suitable for this thermal process because of local spline basis functions used. The effectiveness of the presented modeling method is clearly demonstrated in this real application.

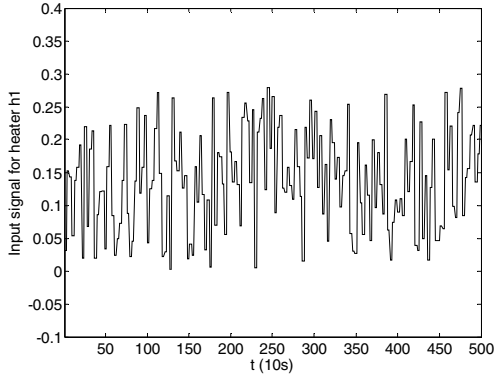


**Fig. 3.12** Snap curing oven: Input signals of heater 1 in the experiment

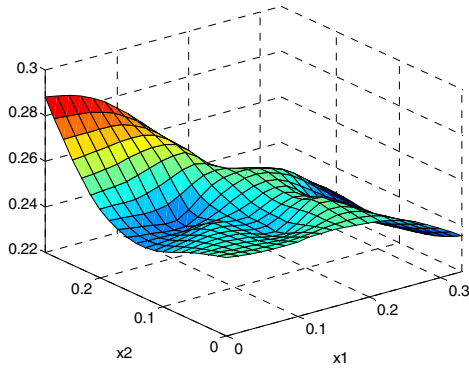


**Fig. 3.13** Snap curing oven: KL basis functions ( $i=1$ ) for KL-Wiener modeling

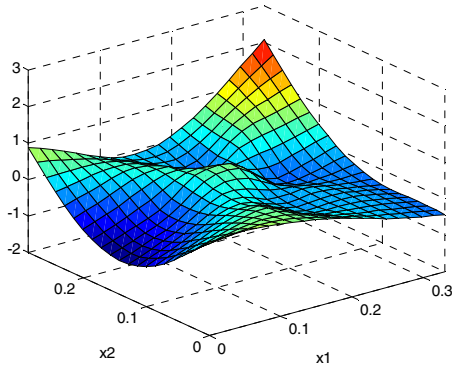


**Fig. 3.14** Snap curing oven: KL basis functions ( $i=2$ ) for KL-Wiener modeling

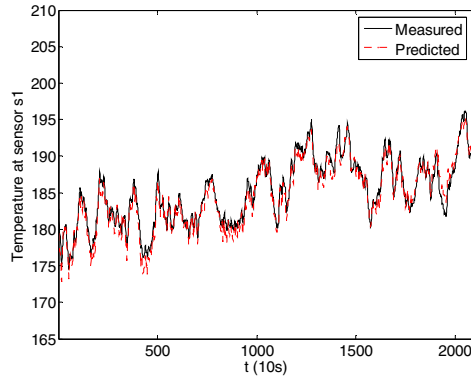


**Fig. 3.15** Snap curing oven: Performance of KL-Wiener model at sensor s1

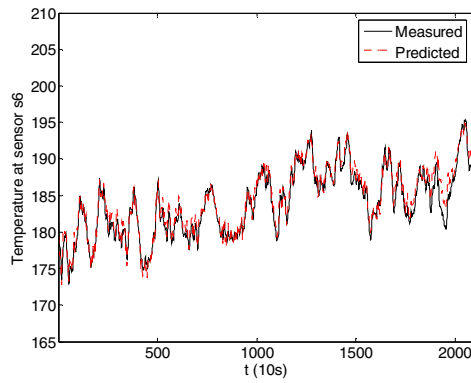


**Fig. 3.16** Snap curing oven: Performance of KL-Wiener model at sensor s6

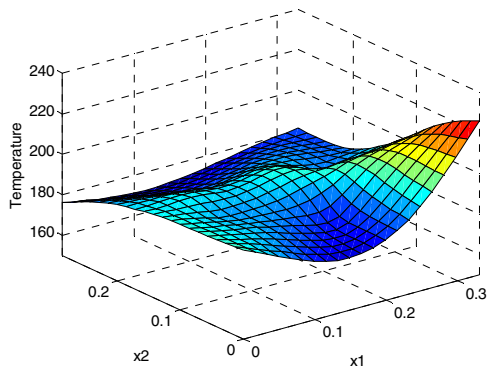


**Fig. 3.17** Snap curing oven: Predicted temperature distribution of KL-Wiener model at  $t=10000s$

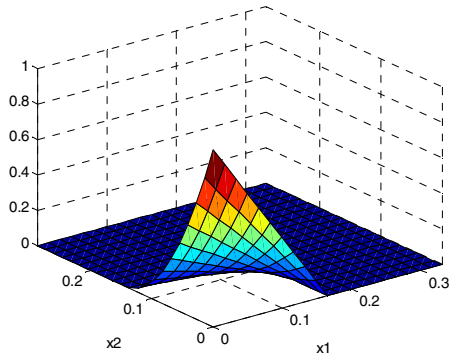


**Fig. 3.18** Snap curing oven: Spline basis functions ( $i=1$ ) for SP-Wiener modeling

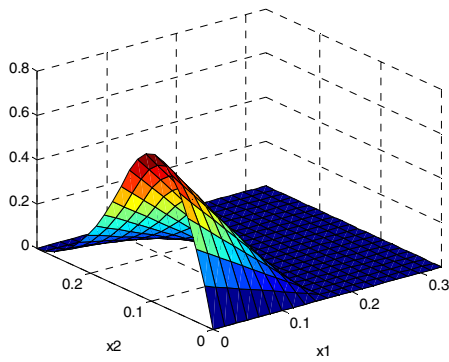


**Fig. 3.19** Snap curing oven: Spline basis functions ( $i=2$ ) for SP-Wiener modeling

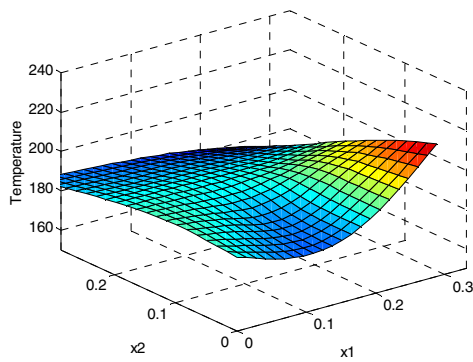


**Fig. 3.20** Snap curing oven: Predicted temperature distribution of SP-Wiener model at  $t=10000s$

**Table 3.1** Snap curing oven:  $TNAE(x)$  of KL-Wiener and SP-Wiener models

	s1	s2	s3	s4	s5	s6	s7	s8
KL-Wiener model	0.84	0.88	1.21	0.74	1.81	0.74	0.81	1.21
SP-Wiener model	13.12	14.44	13.01	13.64	12.58	13.82	13.07	15.59
	s9	s10	s11	s12	s13	s14	s15	s16
KL-Wiener model	0.94	0.84	1.05	1.35	0.75	1.04	0.86	0.79
SP-Wiener model	16.39	13.68	13.78	12.82	14.71	13.78	14.51	12.96

### 3.7 Summary

Traditional Wiener system is extended to DPS. A Wiener distributed parameter system is presented with a distributed linear DPS followed by a static nonlinearity. After the time/space separation, the Wiener distributed parameter system can be represented by traditional Wiener system with a set of spatial basis functions. A KL based spatio-temporal Wiener modeling approach has been presented. The system is assumed to have a finite-dimensional temporal input, as well as a finite-dimensional output measurement at a finite number of spatial locations. The measured output is used to construct a finite-dimensional approximation of the system output which is expanded in terms of Karhunen-Loève spatial basis functions. Using the least-squares estimation and the instrumental variables method, a Wiener model is identified to establish the dynamic relationship between the temporal coefficients and the input. The simulation on the catalytic rod and the experiment on snap curing oven have been presented to illustrate the effectiveness of this modeling method.

### References

1. Armaou, A., Christofides, P.D.: Dynamic optimization of dissipative PDE systems using nonlinear order reduction. *Chemical Engineering Science* 57(24), 5083–5114 (2002)
2. Baker, J., Christofides, P.D.: Finite-dimensional approximation and control of non-linear parabolic PDE systems. *International Journal of Control* 73(5), 439–456 (2000)
3. Bloemen, H.H.J., Chou, C.T., van den Boom, T.J.J., Verdult, V., Verhaegen, M., Backx, T.C.: Wiener model identification and predictive control for dual composition control of a distillation column. *Journal of Process Control* 11(6), 601–620 (2001)
4. Campello, R.J.G.B., Favier, G., Amaral, W.C.: Optimal expansions of discrete-time Volterra models using Laguerre functions. *Automatica* 40(5), 815–822 (2004)
5. Cervantes, A.L., Agamennoni, O.E., Figueroa, J.L.: A nonlinear model predictive control system based on Wiener piecewise linear models. *Journal of Process Control* 13(7), 655–666 (2003)
6. Christofides, P.D.: *Nonlinear and robust control of PDE systems: Methods and applications to transport-reaction processes*. Birkhäuser, Boston (2001b)

7. Christofides, P.D., Daoutidis, P.: Finite-dimensional control of parabolic PDE systems using approximate inertial manifolds. *Journal of Mathematical Analysis and Applications* 216(2), 398–420 (1997)
8. Coca, D., Billings, S.A.: Identification of finite dimensional models of infinite dimensional dynamical systems. *Automatica* 38(11), 1851–1865 (2002)
9. Deng, H., Li, H.-X., Chen, G.: Spectral-approximation-based intelligent modeling for distributed thermal processes. *IEEE Transactions on Control Systems Technology* 13(5), 686–700 (2005)
10. Dierckx, P.: *Curve and surface fitting with splines*. Clarendon, Oxford (1993)
11. Fu, Y., Dumont, G.A.: An optimum time scale for discrete Laguerre network. *IEEE Transactions on Automatic Control* 38(6), 934–938 (1993)
12. Gerksic, S., Juricic, D., Strmcnik, S., Matko, D.: Wiener model based nonlinear predictive control. *International Journal of Systems Science* 31(2), 189–202 (2000)
13. Gómez, J.C.: *Analysis of dynamic system identification using rational orthonormal bases*. PhD Thesis, The University of Newcastle, Australia (1998)
14. Gómez, J.C., Baeyens, E.: Identification of block-oriented nonlinear systems using orthonormal bases. *Journal of Process Control* 14(6), 685–697 (2004)
15. Gómez, J.C., Jutan, A., Baeyens, E.: Wiener model identification and predictive control of a pH neutralisation process. *IEE Proceedings-Control Theory and Applications* 151(3), 329–338 (2004)
16. Greblicki, W.: Nonparametric identification of Wiener systems by orthogonal series. *IEEE Transactions on Automatic Control* 39(10), 2077–2086 (1994)
17. Hagenblad, A.: *Aspects of the identification of Wiener models*. Thesis No.793, Linköping University, Sweden (1999)
18. Hagenblad, A., Ljung, L.: Maximum likelihood identification of Wiener models with a linear regression initialization. In: *Proceedings of the 37th IEEE Conference Decision & Control*, Tampa, Florida, USA, pp. 712–713 (1998)
19. Hagenblad, A., Ljung, L.: Maximum likelihood estimation of Wiener models. Report no.: LiTH-ISY-R-2308, Linköping University, Sweden (2000)
20. Heuberger, P.S.C., Van den Hof, P.M.J., Bosgra, O.H.: A generalized orthonormal basis for linear dynamical systems. *IEEE Transactions on Automatic Control* 40(3), 451–465 (1995)
21. Holmes, P., Lumley, J.L., Berkooz, G.: *Turbulence, coherent structures, dynamical systems, and symmetry*. Cambridge University Press, New York (1996)
22. Janczak, A.: Instrumental variables approach to identification of a class of MIMO Wiener systems. *Nonlinear Dynamics* 48(3), 275–284 (2007)
23. Jeong, B.-G., Yoo, K.-Y., Rhee, H.-K.: Nonlinear model predictive control using a Wiener model of a continuous methyl methacrylate polymerization reactor. *Industrial and Engineering Chemistry Research* 40(25), 5968–5977 (2001)
24. Lacy, S.L., Bernstein, D.S.: Identification of FIR Wiener systems with unknown, non-invertible, polynomial non-linearities. *International Journal of Control* 76(15), 1500–1507 (2003)
25. Lancaster, P., Salkauskas, K.: *Curve and surface fitting: An introduction*. Academic Press, London (1986)
26. Newman, A.J.: *Model reduction via the Karhunen-Loève expansion part I: An exposition*. Technical Report T.R.96-32, University of Maryland, College Park, Maryland (1996a)

27. Newman, A.J.: Model reduction via the Karhunen-Loève expansion part II: Some elementary examples. Technical Report T.R.96-33, University of Maryland, College Park, Maryland (1996b)
28. Pawlak, M., Hasiewicz, Z., Wachel, P.: On nonparametric identification of Wiener systems. *IEEE Transactions on Signal Processing* 55(2), 482–492 (2007)
29. Raich, R., Zhou, G.T., Viberg, M.: Subspace based approaches for Wiener system identification. *IEEE Transactions on Automatic Control* 50(10), 1629–1634 (2005)
30. Sahan, R.A., Koc-Sahan, N., Albin, D.C., Liakopoulos, A.: Artificial neural network-based modeling and intelligent control of transitional flows. In: *Proceeding of the 1997 IEEE International Conference on Control Applications*, Hartford, CT, pp. 359–364 (1997)
31. Shikin, E.V., Plis, A.I.: *Handbook on splines for the user*. CRC Press, Boca Raton (1995)
32. Sirovich, L.: *New perspectives in turbulence*, 1st edn. Springer, New York (1991)
33. Sjöberg, J., Zhang, Q., Ljung, L., Benveniste, A., Delyon, B., Glorennec, P., Hjalmarsson, H., Juditsky, A.: Nonlinear black-box modeling in system identification: A unified approach. *Automatica* 31(12), 1691–1724 (1995)
34. Strikwerda, J.C.: *Finite difference schemes and partial differential equations*. Wads. & Brooks/Cole Adv. Bks. & S.W., Pacific Grove (1989)
35. Wahlberg, B.: System identification using Laguerre models. *IEEE Transactions on Automatic Control* 36(5), 551–562 (1991)
36. Wahlberg, B.: System identification using Kautz models. *IEEE Transactions on Automatic Control* 39(6), 1276–1282 (1994)
37. Westwick, D., Verhaegen, M.: Identifying MIMO Wiener systems using subspace model identification methods. *Signal Processing* 52(2), 235–258 (1996)
38. Wigren, T.: Recursive prediction error identification using the nonlinear Wiener model. *Automatica* 29(4), 1011–1025 (1993)
39. Wigren, T.: Convergence analysis of recursive identification algorithms based on the nonlinear Wiener model. *IEEE Transactions on Automatic Control* 39(11), 2191–2206 (1994)
40. Zhu, Y.C.: Estimation of an N-L-N Hammerstein-Wiener model. *Automatica* 38(9), 1607–1614 (2002)



# 4 Spatio-Temporal Modeling for Hammerstein Distributed Parameter Systems

**Abstract.** A spatio-temporal Hammerstein modeling approach is presented in this chapter. To model the nonlinear distributed parameter system (DPS), a spatio-temporal Hammerstein model (a static nonlinearity followed by a linear DPS) is constructed. After the time/space separation, it can be represented by the traditional Hammerstein system with a set of spatial basis functions. To achieve a low-order model, the Karhunen-Loève (KL) method is used for the time/space separation and dimension reduction. Then a compact Hammerstein model structure is determined by the orthogonal forward regression, and their unknown parameters are estimated with the least-squares method and the singular value decomposition. The simulation and experiment are presented to show the effectiveness of this spatio-temporal modeling method.

## 4.1 Introduction

Hammerstein models are widely used in engineering practice due to their capability of approximating many nonlinear industrial processes and simple block-oriented nonlinear structure (i.e., a nonlinear static block in series with a linear dynamic system). Examples include modeling of the pH neutralization process, the continuous stirred tank reactor and distillation columns. Because a linear structure model can be derived from the block-oriented nonlinear structure, the linear control design can be easily extended to Hammerstein models. Successful control applications have been reported for traditional ordinary differential equation (ODE) processes (Fruzzetti, Palazoglu & McDonald, 1997; Samuelsson, Norlander & Carlsson, 2005). However, because the traditional Hammerstein model does not have inherent capability to process spatio-temporal information, few studies have been found in its application in the distributed parameter system (DPS).

Many approaches can be found in the identification of Hammerstein models (e.g., Narendra & Gallman, 1966; Stoica & Söderström, 1982; Bai, 1998; Chen, 2004; Zhu, 2000; Greblicki, 2006; Vörös, 2003; Gómez & Baeyens, 2004). It is notable that an algorithm based on the least-squares estimation and the singular value decomposition (LSE-SVD) is proposed for Hammerstein-Wiener systems (Bai, 1998) and extensively studied for Hammerstein systems (Gómez & Baeyens, 2004). This algorithm can avoid the local minima since it does not require any nonlinear optimization. However, the model structure is assumed to be known in advance and only unknown parameters need to be estimated (Bai 1998). In many cases, the structure is often unknown and the model terms and orders have to be determined carefully. If the structure is inappropriate, it is very difficult to

guarantee the modeling performance. In [Gómez & Baeyens \(2004\)](#), the order of linear part is determined using the linear subspace identification method and the order of nonlinear part is based on the cross-validation technique. This separated order selection may not provide a compact Hammerstein model since the term selection problem is not considered.

Because the number of possible model terms may be very large, it may lead to a very complex model and an ill-condition problem. In this chapter, we want to obtain a parsimonious model for control which should be as simple as possible. In fact, many terms are redundant and only a small number of important terms are necessary to describe the system with a given accuracy. The term selection problem has been extensively studied for the linear regression model (e.g., [Haber & Unbehauen, 1990](#); [Piroddi & Spinelli, 2003](#); [Lind & Ljung, 2008](#); [Billings \*et al.\*, 1988a, 1988b](#)). In particular, the [orthogonal forward regression \(OFR\)](#) ([Billings \*et al.\*, 1988a, 1988b](#)) is a fast and effective algorithm to determine significant model terms among a candidate set. Here we will extend the OFR to the Hammerstein model identification.

In this chapter, a Karhunen-Loève (KL) decomposition based Hammerstein modeling approach is developed for unknown nonlinear distributed parameter processes with the spatio-temporal output. A [Hammerstein distributed parameter system](#) is presented with a static nonlinearity followed by a linear DPS. After the time/space separation, this Hammerstein distributed parameter system can be represented by the traditional Hammerstein system with a set of spatial basis functions. Firstly, the KL decomposition is used for the time/space separation, where a few dominant spatial basis functions are estimated from the spatio-temporal data and the low-dimensional temporal coefficients are obtained simultaneously. Secondly, a low-order and parsimonious Hammerstein model is identified from the low-dimensional temporal data to establish the system dynamics, where the compact or sparse model structure is determined by the orthogonal forward regression algorithm, and the parameters are estimated using the least-squares method and the singular value decomposition. The presented time/space separated Hammerstein model has significant approximation capability to many nonlinear distributed parameter systems. With this model, many control and optimization algorithms designed for traditional Hammerstein model can be extended to nonlinear distributed parameter processes.

This chapter is organized as follows. The Hammerstein distributed parameter system is given in [Section 4.2](#). The spatio-temporal Hammerstein modeling problem and methodology are described in [Section 4.3](#). In [Section 4.4](#), the Karhunen-Loève decomposition based time/space separation is introduced. The parameterization of the Hammerstein model is presented in [Section 4.5.1](#). The model structure selection and the parameter identification algorithm are given in [Sections 4.5.2 and 4.5.3](#). [Section 4.6](#) contains the simulation example and the experiment on the snap curing oven. Finally, a few conclusions are presented in [Section 4.7](#).

## 4.2 Hammerstein Distributed Parameter System

A Hammerstein distributed parameter system is shown in [Figure 4.1](#). The system consists of a static nonlinear element  $N(\cdot): \mathbb{R}^m \rightarrow \mathbb{R}^m$  followed by a distributed linear time-invariant system

$$y(x, t) = G(x, q)v(t), \quad (4.1)$$

with a transfer function  $G(x, q)$  ( $1 \times m$ ), where  $t$  is time variable,  $x$  is spatial variable defined on the domain  $\Omega$ , and  $q$  stands for the forward shift operator. The input-output relationship of the system is then given by

$$y(x, t) = G(x, q)N(u(t)), \quad (4.2)$$

where  $u(t) \in \mathbb{R}^m$  is the temporal input and  $y(x, t) \in \mathbb{R}$  is the spatio-temporal output. In this chapter only the single-output (SO) system is considered. The extension of the results to the multi-output (MO) system is straightforward.

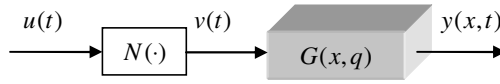


**Fig. 4.1** Hammerstein distributed parameter system

Suppose the transfer function  $G(x, q)$  can be expanded onto an infinite number of orthonormal spatial basis functions  $\{\varphi_i(x)\}_{i=1}^{\infty}$

$$G(x, q) = \sum_{i=1}^{\infty} \varphi_i(x)G_i(q), \quad (4.3)$$

where  $G_i(q)$  ( $1 \times m$ ) is the traditional transfer function. Thus actually the Hammerstein distributed parameter system can be represented by the traditional Hammerstein system via time-space separation

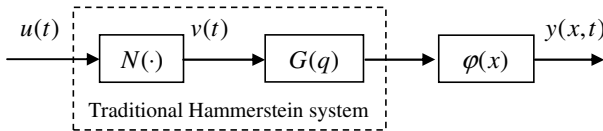


**Fig. 4.2** Time/space separation of Hammerstein distributed parameter system

### 4.3 Spatio-Temporal Hammerstein Modeling Methodology

Consider the nonlinear Hammerstein distributed parameter system in Figure 4.1. Suppose the system is controlled by the  $m$  actuators with implemental temporal signal  $u(t)$  and certain spatial distribution, and the output is measured at the  $N$  spatial locations  $x_1, \dots, x_N$ . Because of the infinite dimensionality of the distributed parameter system, it may require an infinite number of actuators and sensors over the whole space to have a perfect modeling and control. Due to practical limitations, a limited number of actuators and sensors have to be used. The number of actuators and sensors may depend on the process complexity, the desired accuracy of modeling and control, physical constraints and cost consideration etc. The modeling problem is to identify a low-order, simple nonlinear and parsimonious spatio-temporal model from the input  $\{u(t)\}_{t=1}^L$  and the output  $\{y(x_i, t)\}_{i=1, t=1}^{N, L}$ , where  $L$  is the time length.

As shown in Figure 4.3, the modeling methodology includes two stages. The first stage is the Karhunen-Loève decomposition for the time/space separation. The second stage is the traditional Hammerstein model (including the structure and parameters) identification. Using the time/space synthesis, this model can reconstruct the spatio-temporal dynamics of the system.

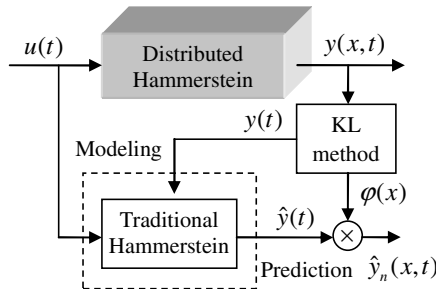


Fig. 4.3 KL based modeling methodology for Hammerstein distributed parameter system

### 4.4 Karhunen-Loève Decomposition

For simplicity, assume the process output  $\{y(x_i, t)\}_{i=1, t=1}^{N, L}$  (called snapshots) is uniformly sampled in the time and space. Here the ensemble average, the inner product and the norm are defined as  $\langle f(x, t) \rangle = \frac{1}{L} \sum_{t=1}^L f(x, t)$ ,  $(f(x), g(x)) = \int_{\Omega} f(x)g(x)dx$ , and  $\|f(x)\| = (f(x), f(x))^{1/2}$  respectively.

Motivated by Fourier series, the spatio-temporal variable  $y(x, t)$  can be expanded onto an infinite number of orthonormal spatial basis functions  $\{\varphi_i(x)\}_{i=1}^{\infty}$

$$y(x,t) = \sum_{i=1}^{\infty} \varphi_i(x) y_i(t), \quad (4.4)$$

Because the spatial basis functions are orthonormal, i.e.,  $(\varphi_i(x), \varphi_j(x)) = \int_{\Omega} \varphi_i(x) \varphi_j(x) dx = 0$  ( $i \neq j$ ), or 1 ( $i = j$ ), the temporal coefficients can be computed from

$$y_i(t) = (\varphi_i(x), y(x,t)), i = 1, \dots, n. \quad (4.5)$$

In practice, it has to be truncated to a finite dimension

$$y_n(x,t) = \sum_{i=1}^n \varphi_i(x) y_i(t), \quad (4.6)$$

where  $y_n(x,t)$  denotes the  $n$ th-order approximation. Similarly a finite order truncation of  $G(x,q)$  is given by

$$G_n(x,q) = \sum_{i=1}^n \varphi_i(x) G_i(q). \quad (4.7)$$

The main problem of using Karhunen-Loève decomposition for the time/space separation is to compute the most characteristic spatial structure  $\{\varphi_i(x)\}_{i=1}^n$  among the spatio-temporal output  $\{y(x_i,t)\}_{i=1,t=1}^{N,L}$ . The typical  $\{\varphi_i(x)\}_{i=1}^n$  can be found by minimizing the following objective function

$$\begin{aligned} \min_{\varphi_i(x)} \langle \|y(x,t) - y_n(x,t)\|^2 \rangle \\ \text{subject to } (\varphi_i, \varphi_i) = 1, \varphi_i \in L^2(\Omega), i = 1, \dots, n. \end{aligned} \quad (4.8)$$

The orthonormal constraint  $(\varphi_i, \varphi_i) = 1$  is imposed to ensure that the function  $\varphi_i(x)$  is unique.

Actually, Karhunen-Loève decomposition can be implemented in several ways, e.g., spatial correlation method and temporal correlation method. Because the Karhunen-Loève expansion is optimal on average in the class of representations by linear combination, it can give the lowest dimension  $n$  among all linear expansions. See [Section 3.4](#) for more details about the implementations and the determination of dimension  $n$ .

## 4.5 Hammerstein Model Identification

After identifying the dominant spatial basis functions  $\{\varphi_i(x)\}_{i=1}^n$ , the corresponding temporal coefficients  $\{y_i(t)\}_{i=1}^n$  of the spatial-temporal output  $y(x,t)$  can be obtained using (4.5). In practice  $\{y_i(t)\}_{i=1}^n$  can be computed from the pointwise data using the spline integration. Define  $y(t) = [y_1(t), \dots, y_n(t)]^T$ .

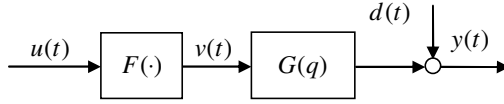


**Fig. 4.4** Hammerstein model

Suppose that the dynamics between  $u(t)$  and  $y(t)$  can be described by a Hammerstein model. As shown in [Figure 4.4](#), the Hammerstein model consists of the cascade of a nonlinear static element  $F(\cdot): \mathbb{R}^m \rightarrow \mathbb{R}^m$  followed by a linear time-invariant (LTI) dynamical system  $G(q)$  (a  $n \times m$  transfer function matrix), where  $q$  is the time-shift operator ( $qu(t) = u(t + \Delta t)$ ). The input-output relationship of the Hammerstein model is then given by

$$y(t) = G(q)v(t) + d(t) = G(q)F(u(t)) + d(t), \quad (4.9)$$

where  $u(t) \in \mathbb{R}^m$ ,  $y(t) \in \mathbb{R}^n$ ,  $v(t) \in \mathbb{R}^n$  and  $d(t) \in \mathbb{R}^n$  represent the temporal input, output, intermediate variable and modeling error at time  $t$ , respectively.

Now the identification is to estimate the Hammerstein model from the low-dimensional temporal data set  $\{u(t), y(t)\}_{t=1}^L$ .

### 4.5.1 Model Parameterization

Assume that the LTI system  $G(q)$  has the ARX form

$$y(t) = A(q^{-1})y(t) + B(q^{-1})v(t), \quad (4.10)$$

where  $A(q^{-1})$  and  $B(q^{-1})$  are  $n \times n$  and  $n \times m$  matrix polynomials

$$A(q^{-1}) = A_1 q^{-1} + \dots + A_{n_y} q^{-n_y}, \quad (4.11)$$

$$B(q^{-1}) = B_1 q^{-1} + \dots + B_{n_u} q^{-n_u}. \quad (4.12)$$

Here  $A_i \in \mathbb{R}^{n \times n}$  ( $i = 1, \dots, n_y$ ) and  $B_i \in \mathbb{R}^{n \times m}$  ( $i = 1, \dots, n_u$ ) are unknown matrix parameters,  $n_u$  and  $n_y$  are the maximum input and output lags respectively. On the other hand, assume that the nonlinear static element  $F(u)$  can be approximated by

$$v(t) = F(u) = \sum_{i=1}^{n_f} C_i f_i(u), \quad (4.13)$$

where  $f_i(\cdot): \mathbb{R}^m \rightarrow \mathbb{R}^m$  ( $i = 1, \dots, n_f$ ) are nonlinear basis functions such as polynomials, splines, radial basis functions and wavelets ([Sjöberg et al., 1995](#)),  $C_i \in \mathbb{R}^{m \times m}$

( $i=1, \dots, n_f$ ) are unknown matrix parameters, and  $n_f$  is the number of basis functions.

Many algorithms have been proposed to identify this class of models when the values of  $n_y$ ,  $n_u$  and  $n_f$  are known. However, their true values are often unknown at the beginning of the identification. Moreover, experiences show that often many terms in (4.11)-(4.13) are redundant and can be removed from the model. Therefore, there exist the values of  $n_{ys}$ ,  $n_{us}$  and  $n_{fs}$  (generally  $n_{ys} \ll n_y$ ,  $n_{us} \ll n_u$  and  $n_{fs} \ll n_f$ ), such that the model

$$y(t) = A_s(q^{-1})y(t) + B_s(q^{-1})v(t), \quad (4.14)$$

$$A_s(q^{-1}) = A_{i_1}q^{-i_1} + \dots + A_{i_{n_{ys}}}q^{-i_{n_{ys}}}, \quad (4.15)$$

$$B_s(q^{-1}) = B_{j_1}q^{-j_1} + \dots + B_{j_{n_{us}}}q^{-j_{n_{us}}}, \quad (4.16)$$

$$v = F_s(u) = C_{k_1}f_{k_1}(u) + \dots + C_{k_{n_{fs}}}f_{k_{n_{fs}}}(u), \quad (4.17)$$

can provide a satisfactory representation over the range considered for the measured input-output data, where  $i_r \in \{1, \dots, n_y\}$ ,  $j_w \in \{1, \dots, n_u\}$  and  $k_v \in \{1, \dots, n_f\}$ . Here we extend the OFR algorithm to determine the compact structure of the Hammerstein model.

### 4.5.2 Structure Selection

Substituting (4.11)-(4.13) into (4.10), the input-output relationship can be written as

$$y(t) = \sum_{i=1}^{n_y} A_i y(t-i) + \sum_{j=1}^{n_u} B_j \sum_{k=1}^{n_f} C_k f_k(u(t-j)) + e(t), \quad (4.18)$$

where  $e(t)$  is the equation error. Define  $D_{jk} = B_j C_k \in \mathbb{R}^{n \times m}$ , then (4.18) can be rewritten as

$$y(t) = \sum_{i=1}^{n_y} A_i y(t-i) + \sum_{j=1}^{n_u} \sum_{k=1}^{n_f} D_{jk} f_k(u(t-j)) + e(t). \quad (4.19)$$

For every row  $p$  in (4.19), we have the following single-output (SO) form

$$y_p(t) = \sum_{i=1}^{n_y} A_i(p, :) y(t-i) + \sum_{j=1}^{n_u} \sum_{k=1}^{n_f} D_{jk}(p, :) f_k(u(t-j)) + e_p(t), \quad (4.20)$$

and

$$y_p(t) = \sum_{i=1}^{n_y} \sum_{w=1}^n A_i(p, w) y_w(t-i) + \sum_{j=1}^{n_u} \sum_{k=1}^m \sum_{l=1}^m D_{jk}(p, l) f_{kl}(u(t-j)) + e_p(t), \quad (4.21)$$

where  $A(i, \cdot)$  symbolizes the  $i$ th row of  $A$  and  $A(i, j)$  denotes the element at the  $i$ th row and  $j$ th column of  $A$ . (4.21) can be written as a linear regression form

$$y_p(t) = \sum_{i=1}^M \phi_i(t) \theta_{pi} + e_p(t), \quad (4.22)$$

where the regressors  $\phi_i(t)$  ( $i=1, \dots, M$ ) are formed from  $y_w(t-i)$  and  $f_{kl}(u(t-j))$ ,  $\theta_{pi}$  ( $p=1, \dots, n$ ,  $i=1, \dots, M$ ) are the corresponding parameters  $A_i(p, w)$  and  $D_{jk}(p, l)$ , and  $M = nn_y + mn_p n_u$ .

### Orthogonal Forward Regression

In the OFR algorithm (Billings *et al.*, 1988a, 1988b), all the terms in (4.22) are orthogonalized as below

$$y_p(t) = \sum_{i=1}^M \psi_i(t) z_{pi} + e_p(t), \quad (4.23)$$

where  $\psi_i(t)$  and  $z_{pi}$  denote orthogonal regressors and unknown parameters respectively. Since the regressors are orthogonal, the unknown parameter and **error reduction ratio (ERR)** can be computed one by one

$$\hat{z}_{pi} = \frac{\sum_{t=1}^L \psi_i(t) y_p(t)}{\sum_{t=1}^L \psi_i^2(t)},$$

$$err_{pi} = \frac{\sum_{t=1}^L [\psi_i(t) \hat{z}_{pi}]^2}{\sum_{t=1}^L y_p^2(t)}.$$

The **ERR** values can give a measure of the significance of each candidate model term.

- *Selection of the first term*

All the terms  $\phi_i(t)$ ,  $i=1, \dots, M$  in (4.22) are considered as the possible candidates for the first significant term in (4.23)

$$\psi_1^{(i)}(t) = \phi_i(t), 1 \leq i \leq M.$$

Then the parameters and the corresponding error reduction ratios are computed



$$\hat{z}_1^{(pi)} = \frac{\sum_{t=1}^L \psi_1^{(i)}(t) y_p(t)}{\sum_{t=1}^L [\psi_1^{(i)}(t)]^2}, 1 \leq i \leq M,$$

$$err_1^{(pi)} = \frac{\sum_{t=1}^L [\psi_1^{(i)}(t) \hat{z}_1^{(pi)}]^2}{\sum_{t=1}^L y_p^2(t)}, 1 \leq i \leq M.$$

The term corresponding to the maximum error reduction ratio (e.g.,  $\psi_j(t)$ ), is selected as the first significant term  $\psi_1(t)$  in (4.23).

- *Selection of the other terms*

All other terms, except  $\psi_j(t)$ , are considered as candidates to be orthogonalized into (4.23). Compute

$$\psi_2^{(i)}(t) = \phi_i(t) - \alpha_{12}^{(i)} \psi_1(t), 1 \leq i \leq M, i \neq j,$$

where

$$\alpha_{12}^{(i)} = \frac{\sum_{t=1}^L \psi_1(t) \phi_i(t)}{\sum_{t=1}^L \psi_1^2(t)}.$$

Then estimate the parameters and compute the corresponding error reduction ratios

$$\hat{z}_2^{(pi)} = \frac{\sum_{t=1}^L \psi_2^{(i)}(t) y_p(t)}{\sum_{t=1}^L [\psi_2^{(i)}(t)]^2}, 1 \leq i \leq M, i \neq j,$$

$$err_2^{(pi)} = \frac{\sum_{t=1}^L [\psi_2^{(i)}(t) \hat{z}_2^{(pi)}]^2}{\sum_{t=1}^L y_p^2(t)}, 1 \leq i \leq M, i \neq j.$$

The term with the maximum error reduction ratio is then selected as the second term  $\psi_2(t)$ . Continue the above procedure, and stop at the  $M_{ps}$  step until

$$1 - \sum_{i=1}^{M_{ps}} err_{pi} < \rho_e,$$

where  $\rho_e$  is a desired error. Because only the most significant term is selected, the OFR algorithm will provide a parsimonious model.

- *Structure design of the Hammerstein model*

From the selected orthogonal model

$$y_p(t) = \sum_{i=1}^{M_{ps}} \psi_i(t) z_{pi} + e_p(t),$$

it is straightforward to obtain the index set of the corresponding terms  $\phi_i(t)$  in the SO model (4.22) as  $I_{ps} = \{i_1, \dots, i_{M_{ps}}\}$ ,  $p=1, \dots, n$ . Now define a combination of the selected term index as

$$I_c = I_{1s} \cup I_{2s} \cup \dots \cup I_{ns}.$$

For the multi-output (MO) Hammerstein model (4.19), the index sets of significant terms  $I_{ys} = \{i_1, \dots, i_{n_{ys}}\}$ ,  $I_{us} = \{j_1, \dots, j_{n_{us}}\}$ , and  $I_{fs} = \{k_1, \dots, k_{n_f}\}$  will be determined by  $I_c$ . The selection rule is that for each  $i \in \{1, \dots, n_y\}$ ,  $j \in \{1, \dots, n_u\}$  and  $k \in \{1, \dots, n_f\}$ , if any element of the corresponding model term vector  $y(t-i) \in \mathbb{R}^n$  and  $f_k(u(t-j)) \in \mathbb{R}^m$  belongs to  $I_c$ , then the corresponding  $i$ ,  $j$  and  $k$  are selected as the elements of  $I_{ys}$ ,  $I_{us}$  and  $I_{fs}$  respectively. For example, if the significant terms of  $y_w(t-i)$  in  $I_c$  look like those in Figure 4.5, then  $I_{ys} = \{2, 4, 6\}$ . This rule is relatively conservative because a whole column will be selected if any element in that column is significant. However, it is used here because preserving a small set of redundant terms is often better and also more reasonable than deleting some significant terms.

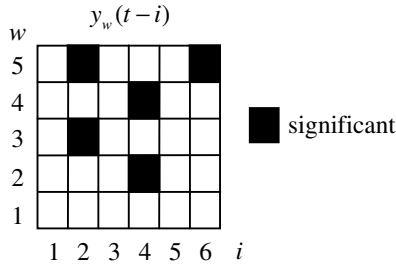


**Fig. 4.5** Structure design of Hammerstein model

As a result, the model structure of linear and nonlinear parts of the Hammerstein model can be determined as follows

$$y(t) = A_s(q^{-1})y(t) + B_s(q^{-1})v(t), \quad (4.24)$$

$$A_s(q^{-1}) = A_{i_1} q^{-i_1} + \dots + A_{i_{n_{ys}}} q^{-i_{n_{ys}}}, \quad (4.25)$$

$$B_s(q^{-1}) = B_{j_1} q^{-j_1} + \dots + B_{j_{n_{us}}} q^{-j_{n_{us}}}, \quad (4.26)$$

$$v(t) = F_s(u) = C_{k_1} f_{k_1}(u) + \dots + C_{k_{n_{fs}}} f_{k_{n_{fs}}}(u). \quad (4.27)$$

### 4.5.3 Parameter Estimation

Substituting (4.25)-(4.27) into (4.24) will have

$$y(t) = \sum_{r=1}^{n_{ys}} A_r y(t-i_r) + \sum_{w=1}^{n_{us}} B_w \sum_{v=1}^{n_{fs}} C_{k_v} f_{k_v}(u(t-j_w)) + e(t). \quad (4.28)$$

The problem is to estimate unknown parameter matrices  $A_r$  ( $r=1, \dots, n_{ys}$ ),  $B_w$  ( $w=1, \dots, n_{us}$ ) and  $C_{k_v}$  ( $v=1, \dots, n_{fs}$ ) from the data set  $\{u(t), y(t)\}_{t=1}^L$ .

#### Least-squares Estimation

Define  $D_{j_w k_v} = B_w C_{k_v} \in \mathbb{R}^{n \times m}$ , then (4.28) can be rewritten as

$$y(t) = \sum_{r=1}^{n_{ys}} A_r y(t-i_r) + \sum_{w=1}^{n_{us}} \sum_{v=1}^{n_{fs}} D_{j_w k_v} f_{k_v}(u(t-j_w)) + e(t). \quad (4.29)$$

Obviously, (4.29) can be expressed as a linear regression form

$$y(t) = \Theta \Phi(t) + e(t), \quad (4.30)$$

where

$$\Theta = [A_1, \dots, A_{n_{ys}}, D_{j_1 k_1}, \dots, D_{j_1 k_{n_{fs}}}, \dots, D_{j_{n_{us}} k_1}, \dots, D_{j_{n_{us}} k_{n_{fs}}}] \in \mathbb{R}^{n \times (m_{ys} + m_{us} n_{fs})}, \quad (4.31)$$

$$\Phi(t) = [y(t-i_1)^T, \dots, y(t-i_{n_{ys}})^T, f_{k_1}(u(t-j_1))^T, \dots, f_{k_{n_{fs}}}(u(t-j_{n_{us}}))^T]^T \in \mathbb{R}^{m_{ys} + m_{us} n_{fs}}. \quad (4.32)$$

It is well known that the estimate  $\hat{\Theta}$  can be obtained using the recursive least-squares method. Then  $\hat{A}_r$  ( $r=1, \dots, n_{ys}$ ) and  $\hat{D}_{j_w k_v}$  ( $w=1, \dots, n_{us}$ ,  $v=1, \dots, n_{fs}$ ) can be easily derived from  $\hat{\Theta}$ . Now the problem is to reconstruct  $B_w$  and  $C_{k_v}$  from  $\hat{D}_{j_w k_v}$ .

#### Singular Value Decomposition

With the following definitions for the matrices  $B$  and  $C$ ,

$$B = [B_{j_1}^T, B_{j_2}^T, \dots, B_{j_{n_{us}}}^T]^T \in \mathbb{R}^{m_{us} \times m}, \quad (4.33)$$

$$C = [C_{k_1}, C_{k_2}, \dots, C_{k_{n_{fs}}}]^T \in \mathbb{R}^{m_{fs} \times m}, \quad (4.34)$$

it is easy to see that

$$BC^T = \begin{bmatrix} B_{j_1} C_{k_1} & \cdots & B_{j_1} C_{k_{n_{fs}}} \\ B_{j_2} C_{k_1} & \cdots & B_{j_2} C_{k_{n_{fs}}} \\ \vdots & \ddots & \vdots \\ B_{j_{n_{us}}} C_{k_1} & \cdots & B_{j_{n_{us}}} C_{k_{n_{fs}}} \end{bmatrix} = D \in \mathbb{R}^{n_{us} \times mn_{fs}}. \quad (4.35)$$

An estimate  $\hat{D}$  of the matrix  $D$  can then be obtained from the estimate  $\hat{D}_{j_w k_v}$ . The problem now is how to estimate the parameter matrices  $B$  and  $C$  from the estimate  $\hat{D}$ . It is clear that the closest, in the Frobenius norm sense, estimates  $\hat{B}$  and  $\hat{C}$  are those that solve the following optimization problem

$$(\hat{B}, \hat{C}) = \arg \min_{B, C} \{ \|\hat{D} - BC^T\|_F^2 \}.$$

The solution to this optimization problem is provided by the SVD of the matrix  $\hat{D}$  (Bai, 1998; Gómez & Baeyens, 2004).

**Theorem 4.1** (Gómez & Baeyens, 2004):

Let  $\hat{D} \in \mathbb{R}^{n_{us} \times mn_{fs}}$  have rank  $\gamma \geq m$ , and let the economy-size SVD of  $\hat{D}$  be given by

$$\hat{D} = U_\gamma \Sigma_\gamma V_\gamma^T = \sum_{i=1}^{\gamma} \sigma_i \mu_i v_i^T, \quad (4.36)$$

where the singular matrix  $\Sigma_\gamma = \text{diag}\{\sigma_i\}$  such that

$$\sigma_1 \geq \cdots \geq \sigma_\gamma > 0,$$

and where the matrices  $U_\gamma = [\mu_1, \dots, \mu_\gamma] \in \mathbb{R}^{n_{us} \times \gamma}$  and  $V_\gamma = [v_1, \dots, v_\gamma] \in \mathbb{R}^{mn_{fs} \times \gamma}$  contain only the first  $\gamma$  columns of the unitary matrices  $U \in \mathbb{R}^{n_{us} \times mn_{us}}$  and  $V \in \mathbb{R}^{mn_{fs} \times mn_{fs}}$  provided by the full SVD of  $\hat{D}$ ,

$$\hat{D} = U \Sigma V^T, \quad (4.37)$$

respectively. Then the matrices  $\hat{B} \in \mathbb{R}^{n_{us} \times m}$  and  $\hat{C} \in \mathbb{R}^{mn_{fs} \times m}$  that minimize the norm  $\|\hat{D} - BC^T\|_F^2$ , are given by

$$(\hat{B}, \hat{C}) = \arg \min_{B, C} \{ \|\hat{D} - BC^T\|_F^2 \} = (U_1, V_1 \Sigma_1), \quad (4.38)$$

where  $U_1 \in \mathbb{R}^{n_{us} \times m}$ ,  $V_1 \in \mathbb{R}^{mn_{fs} \times m}$  and  $\Sigma_1 = \text{diag}\{\sigma_1, \dots, \sigma_m\}$  are given by the following partition of the economy-size SVD in (4.36)

$$\hat{D} = [U_1 \quad U_2] \begin{bmatrix} \Sigma_1 & 0 \\ 0 & \Sigma_2 \end{bmatrix} \begin{bmatrix} V_1^T \\ V_2^T \end{bmatrix}, \quad (4.39)$$

and the approximation error is given by

$$\|\hat{D} - \hat{B}\hat{C}^T\|_F^2 = \sum_{i=m+1}^{\gamma} \sigma_i^2. \quad (4.40)$$

The identification algorithm can then be summarized as follows. ■

**Algorithm 4.1:**

*Step 1:* Use the measured output  $\{y(x_i, t)\}_{i=1, t=1}^{N, L}$  as snapshots, find the spatial basis functions  $\{\varphi_i(x)\}_{i=1}^n$  via Karhunen-Loève decomposition, and calculate the temporal coefficients  $\{y(t)\}_{t=1}^L$  using (4.5).

*Step 2:* Determine the significant terms of the Hammerstein model as in (4.24) and (4.27) using the orthogonal forward regression in [Section 4.5.2](#).

*Step 3:* Compute the least-squares estimate  $\hat{\Theta}$  in (4.30), and then obtain  $\hat{A}_r$  ( $r=1, \dots, n_{ys}$ ) and  $\hat{D}_{j_w k_v}$  ( $w=1, \dots, n_{us}, v=1, \dots, n_{fs}$ ) from  $\hat{\Theta}$  as in (4.31).

*Step 4:* Construct the matrix  $\hat{D}$  using  $\hat{D}_{j_w k_v}$  as in (4.35), and then compute the economy-size SVD of  $\hat{D}$  as in (4.36), and the partition of this decomposition as in (4.39).

*Step 5:* Compute  $\hat{B}$  and  $\hat{C}$  as  $\hat{B} = U_1$  and  $\hat{C} = V_1 \Sigma_1$  respectively, and then obtain the estimates of the parameter matrices  $\hat{B}_{j_w}$  ( $w=1, \dots, n_{us}$ ) and  $\hat{C}_{k_v}$  ( $v=1, \dots, n_{fs}$ ) from  $\hat{B}$  and  $\hat{C}$  as in (4.33) and (4.34). ■

Finally, the estimated Hammerstein model can be used in the simulation mode for the spatio-temporal dynamics prediction as below

$$\hat{y}(t) = \sum_{r=1}^{n_{ys}} \hat{A}_r \hat{y}(t - i_r) + \sum_{w=1}^{n_{us}} \hat{B}_{j_w} \sum_{v=1}^{n_{fs}} \hat{C}_{k_v} f_{k_v}(u(t - j_w)),$$

$$\hat{y}_n(x, t) = \sum_{i=1}^n \varphi_i(x) \hat{y}_i(t).$$

## 4.6 Simulation and Experiment

In order to evaluate the presented modeling method, firstly the simulation on a typical distributed processes: the catalytic rod is given. Then we apply it to the snap curing oven.

The two models to be compared are stated as follows:

- Karhunen-Loève based Hammerstein ([KL-Hammerstein](#)) model,
- Spline functions based Hammerstein ([SP-Hammerstein](#)) model.

The SP-Hammerstein model is constructed by replacing Karhunen-Loève basis functions  $\varphi$  in (4.5) with spline functions during the modeling procedure. See the reference (Shikin & Plis, 1995; Coca & Billings, 2002) for details on the construction of spline functions.

Define  $y(x,t)$  and  $\hat{y}_n(x,t)$  as the measured output and the prediction output respectively. Some performance indexes are set up for an easy comparison as follows:

- Spatio-temporal error,  $e(x,t) = y(x,t) - \hat{y}_n(x,t)$ ,
- Spatial normalized absolute error,  $SNAE(t) = \frac{1}{N} \sum_{i=1}^N |e(x_i,t)|$ ,
- Temporal normalized absolute error,  $TNAE(x) = \sum |e(x,t)| / \sum \Delta t$ .

### 4.6.1 Catalytic Rod

Consider the catalytic rod given in Sections 1.1.2 and 3.6.1. In the simulation, assume the process noise  $d(x,t)$  in (3.31) is zero. The inputs are  $u_i(t) = 1.1 + 5 \sin(t/10 + i/10)$  ( $i=1, \dots, 4$ ). Nineteen sensors uniformly distributed in the space are used for measurements. The sampling interval  $\Delta t$  is 0.01 and the simulation time is 5. Totally the 500 data are collected, where the first 300 data are used for model estimation, the next 100 data for validation, and the remaining 100 data for model testing.

The measured output  $y(x,t)$  of the system is shown in Figure 4.6. As shown in Figure 4.7, the first five Karhunen-Loève basis functions are used for the KL-Hammerstein modeling. Using the cross-validation, the parameters for the linear part of the Hammerstein model are set to  $n_y = 3$  and  $n_u = 9$ . The radial basis functions  $f_k(u) = \exp\{-\|u - c_k\|_2^2 / 2\sigma^2\}$  ( $k=1, \dots, n_f$ ,  $n_f = 10$ ) with the centers  $c_k$  uniformly distributed in the  $(-3.9, 6.1)$  and the width  $\sigma = 1$  are selected as the basis functions of the nonlinear part. Starting with this initial model, the OFR algorithm in Section 4.5.2 leads to the following compact Hammerstein model

$$y(t) = A_s(q^{-1})y(t) + B_s(q^{-1})v(t),$$

$$A_s(q^{-1}) = A_1q^{-1} + A_2q^{-2} + A_3q^{-3},$$

$$B_s(q^{-1}) = B_1q^{-1} + B_2q^{-2} + B_4q^{-4} + B_9q^{-9},$$

$$v = F_s(u) = C_1f_1(u) + C_2f_2(u) + C_4f_4(u) + C_5f_5(u) + C_6f_6(u) + C_7f_7(u),$$

where the unknown parameters are estimated using the LSE-SVD algorithm.

The predicted output  $\hat{y}_n(x,t)$  and prediction error  $e(x,t)$  over the whole data set of KL-Hammerstein model are presented in Figure 4.8 and Figure 4.9 respectively. Obviously the KL-Hammerstein model can approximate the spatio-temporal dynamics of original system very well. Now the performance of KL-Hammerstein model is compared with SP-Hammerstein model. As shown in Figure 4.10, eleven

third-order splines are used as spatial basis functions in the SP-Hammerstein modeling. Figure 4.11 displays  $SNAE(t)$  of these two models over the whole data set, where the solid line corresponds to KL-Hammerstein model and the dashed line to SP-Hammerstein model. It can be found that the performance of KL-Hammerstein model is much better than SP-Hammerstein model even if SP-Hammerstein model uses more number of basis functions. This is owing to the optimal Karhunen-Loève basis functions. The KL-Hammerstein model is very efficient for this nonlinear distributed parameter process. For the KL-Hammerstein modeling, two algorithms: OFR-LSE-SVD and LSE-SVD (i.e., without the structure selection using the OFR algorithm) are also compared. The OFR algorithm can make the KL-Hammerstein model compact. In fact, the simulation in Figure 4.12 shows that it can also obtain a more accurate model because a suitable model structure can be selected.

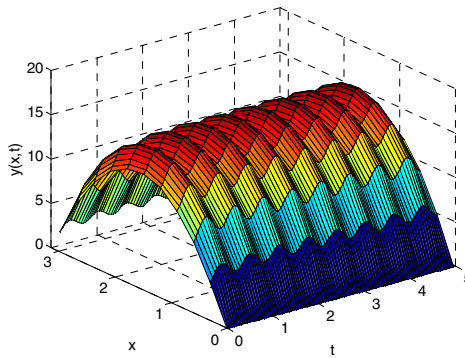


**Fig. 4.6** Catalytic rod: Measured output for Hammerstein modeling

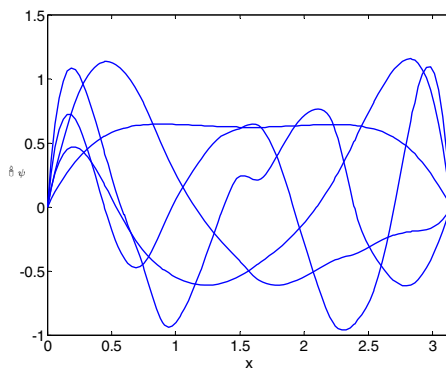


**Fig. 4.7** Catalytic rod: KL basis functions for KL-Hammerstein modeling

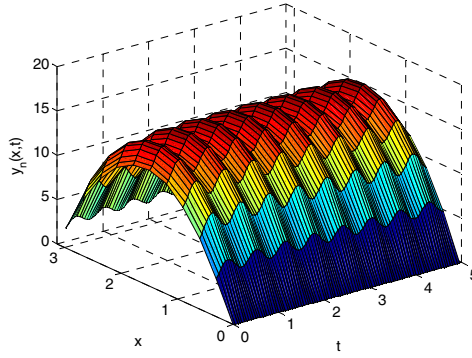


**Fig. 4.8** Catalytic rod: KL-Hammerstein model output

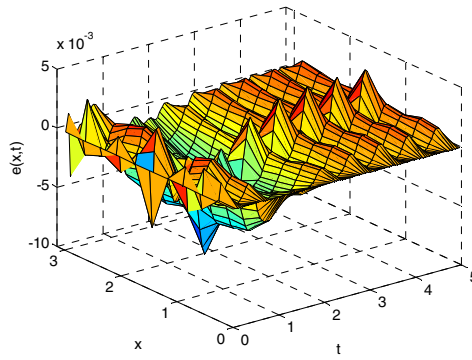


**Fig. 4.9** Catalytic rod: Prediction error of KL-Hammerstein model

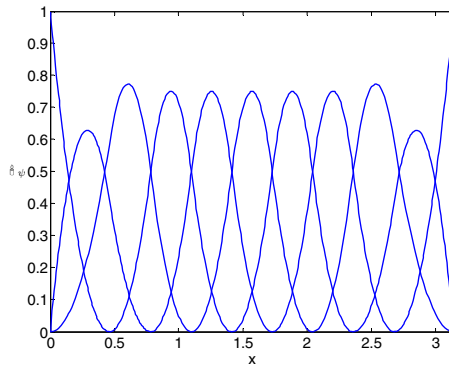


**Fig. 4.10** Catalytic rod: Spline basis functions for SP-Hammerstein modeling



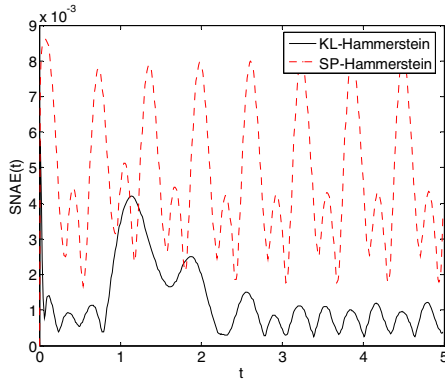


**Fig. 4.11** Catalytic rod: Comparison of SP- and KL-Hammerstein models

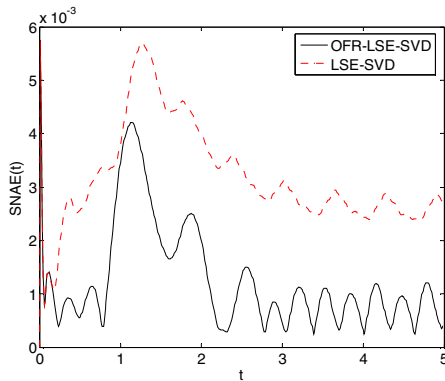


**Fig. 4.12** Catalytic rod: Comparison of OFR-LSE-SVD and LSE-SVD algorithms for KL-Hammerstein model

### 4.6.2 Snap Curing Oven

Consider the **snap curing oven** (Figure 1.1 and Figure 3.11) provided in Sections 1.1.1 and 3.6.2. In the experiment, a total of 2100 measurements are collected with a sampling interval  $\Delta t = 10$  seconds. One thousand and four hundred of measurements from sensors (s1-s5, s7-s10, and s12-s16) are used to estimate the model. The last 700 measurements from the sensors (s1-s5, s7-s10, and s12-s16) are chosen to validate the model during the training. All 2100 measurements from the rest sensors (s6, s11) are used for model testing.

In the *KL-Hammerstein model* modeling, five two-dimensional Karhunen-Loève basis functions are used as spatial bases and the first two of them are shown in Figure 4.13 and Figure 4.14. The parameters for the linear part of the model are  $n_y = 6$  and  $n_u = 1$ . The basis functions  $f_k(u)$  of the nonlinear part are designed as standard polynomials  $f_k(u) = u^k$  ( $k = 1, \dots, n_f$ ,  $n_f = 2$ ). From this initial model

structure, the significant term selection procedure using the OFR algorithm leads to the following parsimonious model

$$y(t) = A_s(q^{-1})y(t) + B_s(q^{-1})v(t),$$

$$A_s(q^{-1}) = A_1q^{-1} + A_2q^{-2} + A_3q^{-3} + A_5q^{-5},$$

$$B_s(q^{-1}) = B_1q^{-1},$$

$$v = F_s(u) = C_1f_1(u) + C_2f_2(u).$$

After the parameters are estimated using the first 1400 data from the sensors (s1-s5, s7-s10, and s12-s16), the Hammerstein model can be obtained with the significant performance such as the sensor s1 in Figure 4.15. It also performs very well for the untrained locations such as the sensor s6 in Figure 4.16. The predicted temperature distribution of the oven at  $t=10000$ s is provided in Figure 4.17.

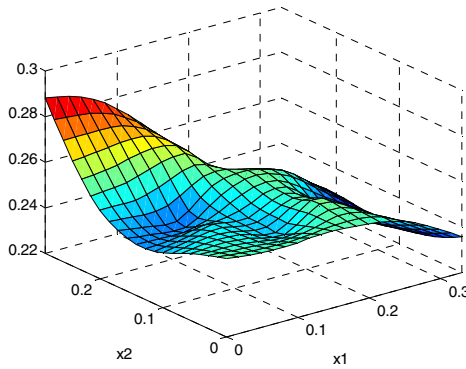


**Fig. 4.13** Snap curing oven: KL basis functions ( $i=1$ ) for KL-Hammerstein modeling

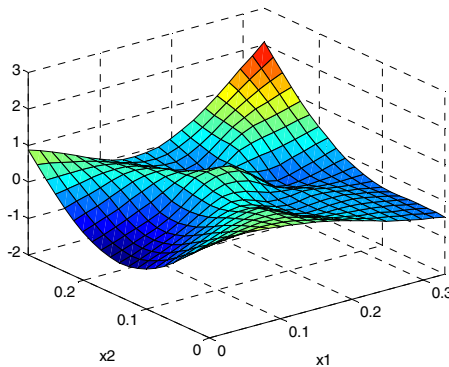


**Fig. 4.14** Snap curing oven: KL basis functions ( $i=2$ ) for KL-Hammerstein modeling

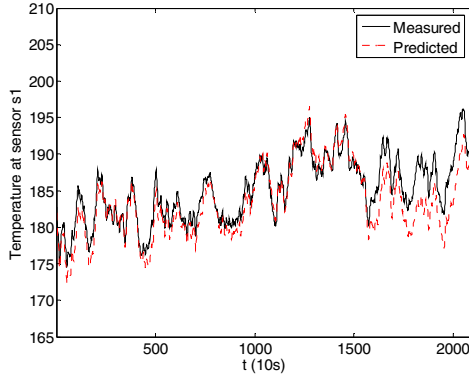


**Fig. 4.15** Snap curing oven: Performance of KL-Hammerstein model at sensor s1

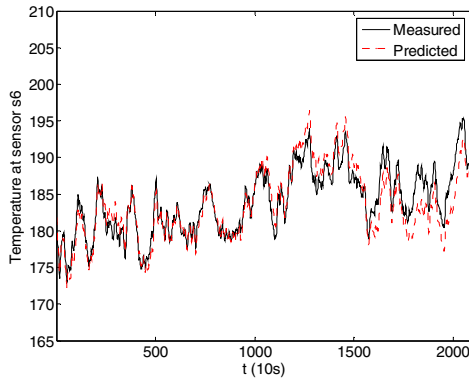


**Fig. 4.16** Snap curing oven: Performance of KL-Hammerstein model at sensor s6

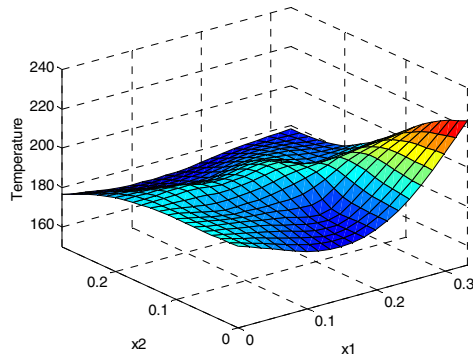


**Fig. 4.17** Snap curing oven: Predicted temperature distribution of KL-Hammerstein model at  $t=10000s$

In order to provide a comparison, a SP-Hammerstein model is also constructed using nine third-order splines as spatial basis functions. The first two of them are shown in [Figure 4.18](#) and [Figure 4.19](#). The performance index  $TNAE(x)$  over the whole data set in [Table 4.1](#) shows that the KL-Hammerstein model works much better than the SP-Hammerstein model because of local spline basis functions used in the SP-Hammerstein model. As shown in [Table 4.2](#), the OFR-LSE-SVD algorithm can produce a more accurate KL-Hammerstein model than the LSE-SVD algorithm. The effectiveness of the presented modeling method is clearly demonstrated in this real application.

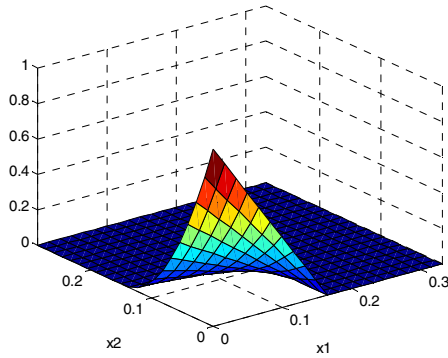


**Fig. 4.18** Snap curing oven: Spline basis functions ( $i=1$ ) for SP-Hammerstein modeling

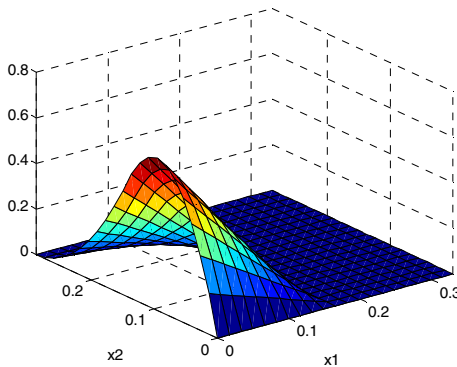


**Fig. 4.19** Snap curing oven: Spline basis functions ( $i=2$ ) for SP-Hammerstein modeling

**Table 4.1** Snap curing oven:  $TNAE(x)$  of KL-Hammerstein and SP-Hammerstein models

	s1	s2	s3	s4	s5	s6	s7	s8
KL-Hammerstein	1.88	1.63	2	1.52	2.4	1.52	1.62	1.64
SP-Hammerstein	1.5	3.46	4.1	1.77	2.7	2.86	1.85	2.03
	s9	s10	s11	s12	s13	s14	s15	s16
KL-Hammerstein	1.45	1.83	2.08	1.94	1.57	2.15	1.47	1.54
SP-Hammerstein	4.32	2.81	3.14	4.85	2.4	3.84	3.34	1.2

**Table 4.2** Snap curing oven:  $TNAE(x)$  of OFR-LSE-SVD and LSE-SVD algorithms for KL-Hammerstein model

	s1	s2	s3	s4	s5	s6	s7	s8
OFR-LSE-SVD	1.88	1.63	2	1.52	2.4	1.52	1.62	1.64
LSE-SVD	2.33	1.76	2.54	1.69	3.09	1.68	1.97	1.43
	s9	s10	s11	s12	s13	s14	s15	s16
OFR-LSE-SVD	1.45	1.83	2.08	1.94	1.57	2.15	1.47	1.54
LSE-SVD	1.46	2.16	2.54	2.52	1.82	2.67	1.67	1.71

## 4.7 Summary

In this chapter, a KL based Hammerstein modeling approach is presented for unknown nonlinear distributed parameter processes with the spatio-temporal output. A Hammerstein distributed parameter system is presented with a static nonlinearity followed by a linear DPS. After the time/space separation, this Hammerstein distributed parameter system can be represented by the traditional Hammerstein system with a set of spatial basis functions. The time/space separation is implemented using the Karhunen-Loève method, where the spatio-temporal output is expanded onto a small number of dominant spatial basis functions with temporal coefficients. Then a low-order compact Hammerstein model is estimated from the low-dimensional temporal data, where the compact model structure is selected based on the orthogonal forward regression, and the parameters are estimated using the least-squares estimation and the singular value decomposition. The algorithm does not require any nonlinear optimization and is numerically robust. The simulation and experiment are presented to show the effectiveness of this spatio-temporal modeling method.

## References

1. Bai, E.W.: An optimal two-stage identification algorithm for Hammerstein-Wiener nonlinear systems. *Automatica* 34(3), 333–338 (1998)
2. Billings, S.A., Korenberg, M.J., Chen, S.: Identification of output-affine systems using an orthogonal least squares algorithm. *International Journal of Systems Science* 19(8), 1559–1568 (1988a)

3. Billings, S.A., Korenberg, M.J., Chen, S.: Identification of MIMO non-linear systems using a forward-regression orthogonal estimator. *International Journal of Control* 49(6), 2157–2189 (1988b)
4. Chen, H.F.: Pathwise convergence of recursive identification algorithms for Hammerstein systems. *IEEE Transactions on Automatic Control* 49(10), 1641–1649 (2004)
5. Coca, D., Billings, S.A.: Identification of finite dimensional models of infinite dimensional dynamical systems. *Automatica* 38(11), 1851–1865 (2002)
6. Fruzzetti, K.P., Palazoglu, A., McDonald, K.A.: Nonlinear model predictive control using Hammerstein models. *Journal of Process Control* 7(1), 31–41 (1997)
7. Gómez, J.C., Baeyens, E.: Identification of block-oriented nonlinear systems using orthonormal bases. *Journal of Process Control* 14(6), 685–697 (2004)
8. Greblicki, W.: Continuous-time Hammerstein system identification from sampled data. *IEEE Transactions on Automatic Control* 51(7), 1195–1200 (2006)
9. Haber, R., Unbehauen, H.: Structure identification of nonlinear dynamic systems - A survey on input/output approaches. *Automatica* 26(4), 651–677 (1990)
10. Lind, I., Ljung, L.: Regressor and structure selection in NARX models using a structured ANOVA approach. *Automatica* 44(2), 383–395 (2008)
11. Narendra, K., Gallman, P.: An iterative method for the identification of nonlinear systems using a Hammerstein model. *IEEE Transactions on Automatic Control* 11(3), 546–550 (1966)
12. Piroddi, L., Spinelli, W.: An identification algorithm for polynomial NARX models based on simulation error minimization. *International Journal of Control* 76(17), 1767–1781 (2003)
13. Samuelsson, P., Norlander, H., Carlsson, B.: An integrating linearization method for Hammerstein models. *Automatica* 41(10), 1825–1828 (2005)
14. Shikin, E.V., Plis, A.I.: *Handbook on splines for the user*. CRC Press, Boca Raton (1995)
15. Sjöberg, J., Zhang, Q., Ljung, L., Benveniste, A., Delyon, B., Glorennec, P., Hjalmarsson, H., Juditsky, A.: Nonlinear black-box modeling in system identification: A unified approach. *Automatica* 31(12), 1691–1724 (1995)
16. Stoica, P., Söderström, T.: Instrumental-variable methods for identification of Hammerstein systems. *International Journal of Control* 35(3), 459–476 (1982)
17. Vörös, J.: Recursive identification of Hammerstein systems with discontinuous nonlinearities containing dead-zones. *IEEE Transactions on Automatic Control* 48(12), 2203–2206 (2003)
18. Zhu, Y.C.: Identification of Hammerstein models for control using ASYM. *International Journal of Control* 73(18), 1692–1702 (2000)

# 5 Multi-channel Spatio-Temporal Modeling for Hammerstein Distributed Parameter Systems

**Abstract.** A multi-channel spatio-temporal Hammerstein modeling approach is presented in this chapter. As a special case of the model described in [Chapter 4](#), a spatio-temporal Hammerstein model is constructed with a static nonlinearity followed by a linear spatio-temporal kernel. When the model structure is matched with the system, a basic single-channel identification algorithm with the algorithm used in the [Chapter 4](#) can work well. When there is unmodeled dynamics, a multi-channel modeling framework can provide a better performance, because more channels used can attract more information from the process. The modeling convergence can be guaranteed under noisy measurements. The simulation example and the experiment on snap curing oven are presented to show the effectiveness of this modeling method.

## 5.1 Introduction

In the process control, Hammerstein models have been successfully used to represent many practical nonlinear ODE processes ([Eskinat, Johnson & Luyben, 1991](#); [Fruzzetti, Palazoglu & McDonald, 1997](#)). However, Hammerstein models are only studied for lumped parameter systems (LPS) because they are only temporal models and can not model spatial dynamics. This chapter will extend the traditional Hammerstein modeling into nonlinear distributed parameter systems (DPS) via the spatio-temporal kernel idea.

For the traditional Hammerstein modeling, several methods have been proposed in the literature ([Narendra & Gallman, 1966](#); [Stoica, 1981](#); [Bai, 1998](#); [Bai & Li, 2004](#); [Chen, 2004](#); [Zhu, 2000](#); [Greblicki, 2006](#); [Vörös, 2003](#); [Gómez & Baeyens, 2004](#)). It is notable that an algorithm based on the least-squares estimation and the singular value decomposition (LSE-SVD) is proposed for Hammerstein-Wiener systems ([Bai, 1998](#)) and extensively studied for Hammerstein systems ([Gómez & Baeyens, 2004](#)). The algorithm is derived from the use of basis functions for the representation of the linear and the nonlinear parts. In the case of model matching, the consistency of the estimates can be guaranteed under certain conditions. However, in the presence of unmodeled dynamics, further studies are required.

In this chapter, in order to model the nonlinear distributed parameter system, a spatio-temporal Hammerstein model is presented by adding the space variables into the traditional Hammerstein model, which consists of the cascade connection of a static nonlinearity followed by a distributed dynamical linear time-invariant system.

The linear time-invariant DPS is represented by a spatio-temporal kernel, i.e., Green's function in [Section 2.5.1](#). This spatio-temporal kernel makes the Hammerstein model have spatio-temporal modeling capability.

A basic identification algorithm based on LSE-SVD is designed as follows. Firstly, the nonlinear and the distributed linear parts are expanded onto spatial and temporal basis functions with unknown coefficients. In order to reduce the parametric complexity, the Karhunen-Loève (KL) decomposition is used to find the dominant spatial basis functions and Laguerre polynomials are selected as the temporal basis functions. Then, using the Galerkin method, the spatio-temporal modeling will turn into a traditional modeling problem in the time domain. Subsequently, the least-squares techniques can be used to identify a parameter matrix charactering the product of parameters of the linear and the nonlinear parts. Finally, by using SVD, optimal estimates of the parameters of each part can be obtained. This basic identification algorithm can provide consistent estimates under some assumptions in the case of model matching.

In the presence of unmodeled dynamics, a multi-channel identification algorithm is presented to compensate the residuals of the single-channel model and further reduce the modeling error. This algorithm is noniterative and numerically robust since it is based only on the least-squares estimation and the singular value decomposition. The convergent estimates can be guaranteed under proper assumptions. The spatio-temporal Hammerstein model can be easily used for many applications such as model predictive control due to its simple nonlinear structure. The simulation and experiment demonstrate the effectiveness of the presented modeling method.

The difference with [Chapter 4](#) is described as follows:

- Different Hammerstein models are used. In this chapter, a new Hammerstein model is constructed with a Green's function (time/space nature) and a static nonlinear function. This new constructed Hammerstein model has time/space nature and is used to directly model DPS. It can be considered as a kernel-based scheme. In [Chapter 4](#), the Hammerstein distributed parameter system is constructed from a lumped Hammerstein system via the time/space synthesis based on the Karhunen-Loève method.
- Different identification algorithms are used. In this chapter, the kernel structure of the multi-channel Hammerstein system is given, so the identification mainly focuses on the parameter estimation with the LSE-SVD algorithm. In [Chapter 4](#), the modeling is a single-channel Hammerstein modeling, and the identification needs to consider both model structure design and parameter estimation with the OFR and the LSE-SVD algorithm.

This chapter is organized as follows. In [Section 5.2](#), the Hammerstein distributed parameter system is presented via the spatio-temporal kernel. The single-channel identification algorithm is derived in [Section 5.3](#). The multi-channel modeling approach and analysis are provided in [Section 5.4](#). Simulation example and experiment are presented to illustrate the performance of the presented modeling approach in [Section 5.5](#), and finally, some conclusions are provided in [Section 5.6](#).



## 5.2 Hammerstein Distributed Parameter System

A **Hammerstein distributed parameter system** is shown in **Figure 5.1**. The system consists of a static nonlinear element  $N(\cdot): \mathbb{R} \rightarrow \mathbb{R}$  followed by a distributed linear time-invariant system

$$y(x, t) = \sum_{\tau=0}^t \int_{\Omega} g(x, \zeta, \tau) v(\zeta, t - \tau) d\zeta, \quad (5.1)$$

Here a spatio-temporal kernel model, i.e., Green's function  $\theta^*$  is used to represent the linear DPS with a transfer function  $G(x, \zeta, q)$  ( $1 \times 1$ ), where  $x$  and  $\zeta$  are spatial variables defined on the domain  $\Omega$ , and  $q$  stands for the forward shift operator. The input-output relationship of the system is then given by

$$y(x, t) = \sum_{\tau=0}^t \int_{\Omega} g(x, \zeta, \tau) N(u(\zeta, t - \tau)) d\zeta + d(x, t), \quad (5.2)$$

where  $u(x, t) \in \mathbb{R}$  and  $y(x, t) \in \mathbb{R}$  are the input and output at time  $t$ , and  $d(x, t) \in \mathbb{R}$  includes the unmodeled dynamics and the stochastic disturbance. For easy understanding, the integral operator is used for spatial operation and sum operator for temporal operation. In this study, only the single-input-single-output (**SISO**) system is considered. The extension of the results to the multi-input-multi-output (**MIMO**) system is straightforward.

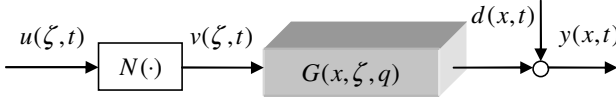


**Fig. 5.1** Hammerstein distributed parameter system

The problem is to estimate  $N$  and  $G$  from the input-output data  $\{u(\zeta_i, t), y(x_j, t)\}$ , ( $i = 1, \dots, n_u$ ,  $j = 1, \dots, n_y$ ,  $t = 1, \dots, n_t$ ), where  $\zeta_i, x_j \in \Omega$ ,  $n_u$  and  $n_y$  are the number of sampled spatial points of the input and output, and  $n_t$  is the time length. For simplicity, assume that the spatial points  $\zeta_i$  and  $x_j$  are uniformly distributed over the spatial domain.

## 5.3 Basic Identification Approach

### 5.3.1 Basis Function Expansion

In general, the input  $u(x, t)$  has finite degrees of freedom since only a finite number of actuators are available in practice. Thus assume that the input  $u(x, t)$  can be

formulated in terms of a finite number of spatial input basis functions  $\{\psi_i(x)\}_{i=1}^m$  as follows

$$u(x,t) = \sum_{i=1}^m \psi_i(x) a_i(t), \quad (5.3)$$

where  $a_i(t) = \int_{\Omega} u(x,t) \psi_i(x) dx$  is the time coefficient (implemental input signal),  $\psi_i(x)$  describes how the control action  $a_i(t)$  is distributed in the spatial domain  $\Omega$ , and  $m$  is the number of actuators, which can be determined by physical knowledge.

Ideally, the output  $y(x,t)$  and the error  $d(x,t)$  can be expressed by an infinite set of orthonormal spatial output basis functions  $\{\varphi_i(x)\}_{i=1}^{\infty}$  as follows

$$y(x,t) = \sum_{i=1}^{\infty} \varphi_i(x) b_i(t), \quad (5.4)$$

$$d(x,t) = \sum_{i=1}^{\infty} \varphi_i(x) d_i(t), \quad (5.5)$$

where  $b_i(t) = \int_{\Omega} y(x,t) \varphi_i(x) dx$  and  $d_i(t) = \int_{\Omega} d(x,t) \varphi_i(x) dx$  are the time coefficients respectively. This is because of inherently infinite-dimensional characteristic of distributed parameter system. Practically, both  $y(x,t)$  and  $d(x,t)$  can be truncated into  $n$  dimensions as below

$$y_n(x,t) = \sum_{i=1}^n \varphi_i(x) b_i(t), \quad (5.6)$$

$$d_n(x,t) = \sum_{i=1}^n \varphi_i(x) d_i(t). \quad (5.7)$$

$\varphi_i(x)$  are usually selected as standard orthonormal functions such as Fourier series, Legendre polynomials, Jacobi polynomials and Chebyshev polynomials (Datta & Mohan, 1995). In this study, the KL decomposition (Park & Cho, 1996a, 1996b) is used to identify the empirical dominant basis functions from the process data. Among all linear expansions, the KL expansion is the most efficient in the sense that for a given approximation error, the number of KL bases required is minimal. Owing to this, the KL decomposition can help to reduce the number of estimated parameters.

Assume that the intermediate output  $v(x,t) \in \mathbb{R}$  can be described as

$$v(x,t) = N(u(x,t)) = \sum_{i=1}^m \sum_{j=1}^v \psi_i(x) \beta_j h_j(a_i(t)), \quad (5.8)$$

where  $h_j(\cdot): \mathbb{R} \rightarrow \mathbb{R}$  ( $j=1, \dots, v$ ) are nonlinear basis functions and  $\beta_j \in \mathbb{R}$  ( $j=1, \dots, v$ ) are coefficients. Typically, the nonlinear functions  $h_j(\cdot)$  can be chosen as polynomials, radial basis functions, wavelets (Sjöberg *et al.*, 1995) and so on.

Assuming that the kernel  $g(x, \zeta, \tau)$  in (5.2) is absolutely integrable on time domain  $[0, \infty)$  at any spatial point  $x$  and  $\zeta$ , which means that the corresponding model is stable, then it can be represented by means of orthonormal temporal basis functions. Theoretically, the kernel is supposed to be expanded onto spatial output bases  $\{\varphi_i(x)\}_{i=1}^{\infty}$ , spatial input bases  $\{\psi_j(\zeta)\}_{j=1}^m$  and temporal bases  $\{\phi_k(t)\}_{k=1}^{\infty}$  as follows

$$g(x, \zeta, \tau) = \sum_{i=1}^{\infty} \sum_{j=1}^m \sum_{k=1}^{\infty} \alpha_{i,j,k} \varphi_i(x) \psi_j(\zeta) \phi_k(\tau), \quad (5.9)$$

where  $\alpha_{i,j,k} \in \mathbb{R}$  ( $i=1, \dots, \infty, j=1, \dots, m, k=1, \dots, \infty$ ) are constant coefficients of basis functions  $\varphi_i(x) \psi_j(\zeta) \phi_k(\tau)$ . Practically, a finite-dimensional truncation

$$g_{n,l}(x, \zeta, \tau) = \sum_{i=1}^n \sum_{j=1}^m \sum_{k=1}^l \alpha_{i,j,k} \varphi_i(x) \psi_j(\zeta) \phi_k(\tau), \quad (5.10)$$

is often good enough for a realistic approximation, where  $n$  and  $l$  are the dimension of output bases and temporal bases respectively.  $\phi_k(t)$  can be selected as Laguerre functions (Wahlberg, 1991), Kautz functions (Wahlberg, 1994) and generalized orthonormal basis functions (Heuberger, Van den Hof, & Bosgra, 1995). Here, Laguerre functions are chosen for the development, due to their simplicity and robustness to the choice of sampling period and model order (Wahlberg, 1991). Laguerre function is defined as a functional series (Zervos & Dumont, 1988)

$$\phi_i(t) \triangleq \sqrt{2\xi} \frac{e^{-\xi t}}{(i-1)!} \cdot \frac{d^{i-1}}{dt^{i-1}} [t^{i-1} \cdot e^{-2\xi t}], i = 1, 2, \dots, \infty, \xi > 0, \quad (5.11)$$

where  $\xi$  is the time-scaling factor and  $t \in [0, \infty)$  is time variable. The Laplace transform of the  $i^{\text{th}}$  Laguerre function is given by (5.12)

$$\phi_i(s) = \sqrt{2\xi} \frac{(s - \xi)^{i-1}}{(s + \xi)^i}, i = 1, 2, \dots, \infty, \xi > 0. \quad (5.12)$$

Laguerre functions (5.11) and (5.12) form a complete orthonormal basis in the function space  $L_2(\mathbb{R}_+)$  and  $H_2(C_+)$  respectively.

Substitution of (5.4), (5.5), (5.8) and (5.9) into (5.2) with a  $n$ -dimensional truncation of output bases will have

$$y_n(x, t) = \sum_{\tau=0}^t \int_{\Omega} \sum_{i=1}^n \sum_{j=1}^m \sum_{k=1}^{\infty} \alpha_{i,j,k} \varphi_i(x) \psi_j(\zeta) \phi_k(\tau) \sum_{r=1}^m \sum_{s=1}^v \psi_r(\zeta) \beta_s h_s(a_r(t - \tau)) d\zeta + d_n(x, t), \quad (5.13)$$

To make the kernel  $g_{n,l}(x, \zeta, \tau)$  explicit, (5.13) can be rewritten as

$$y_n(x, t) = \sum_{\tau=0}^t \int_{\Omega} \sum_{i=1}^n \sum_{j=1}^m \sum_{k=1}^l \alpha_{i,j,k} \varphi_i(x) \psi_j(\zeta) \phi_k(\tau) \sum_{r=1}^m \sum_{s=1}^v \psi_r(\zeta) \beta_s h_s(a_r(t - \tau)) d\zeta + \tilde{d}_n(x, t), \quad (5.14)$$

where

$$\begin{aligned}\tilde{d}_n(x, t) &= \sum_{i=1}^n \varphi_i(x) \tilde{d}_i(t), \\ \tilde{d}_i(t) &= \sum_{\tau=0}^t \int_{\Omega} \sum_{j=1}^m \sum_{k=l+1}^{\infty} \alpha_{i,j,k} \psi_j(\zeta) \phi_k(\tau) \sum_{r=1}^m \sum_{s=1}^v \psi_r(\zeta) \beta_s h_s(a_r(t-\tau)) d\zeta + d_i(t).\end{aligned}$$

### 5.3.2 Temporal Modeling Problem

Equation (5.14) can be further simplified into

$$\sum_{i=1}^n \varphi_i(x) b_i(t) = \sum_{i=1}^n \varphi_i(x) \sum_{j=1}^m \sum_{k=1}^l \alpha_{i,j,k} \sum_{r=1}^m \sum_{s=1}^v \beta_s \psi_{j,r} \ell_{k,s,r}(t) + \sum_{i=1}^n \varphi_i(x) \tilde{d}_i(t), \quad (5.15)$$

where

$$\psi_{j,r} = \int_{\Omega} \psi_j(\zeta) \psi_r(\zeta) d\zeta, \quad (5.16)$$

$$\ell_{k,s,r}(t) = \sum_{\tau=0}^t \phi_k(\tau) h_s(a_r(t-\tau)), \quad (5.17)$$

Using the Galerkin method (Christofides, 2001b), the projection of (5.15) onto the output basis functions  $\varphi_h(x)$  ( $h=1, \dots, n$ ) will lead to the following  $n$  equations

$$\begin{aligned}\sum_{i=1}^n \int_{\Omega} \varphi_h(x) \varphi_i(x) dx b_i(t) &= \sum_{i=1}^n \int_{\Omega} \varphi_h(x) \varphi_i(x) dx \sum_{j=1}^m \sum_{k=1}^l \alpha_{i,j,k} \sum_{r=1}^m \sum_{s=1}^v \beta_s \psi_{j,r} \ell_{k,s,r}(t) \\ &+ \sum_{i=1}^n \int_{\Omega} \varphi_h(x) \varphi_i(x) dx \tilde{d}_i(t).\end{aligned}$$

Since  $\{\varphi_i(x)\}_{i=1}^n$  are orthonormal, we have

$$b(t) = \sum_{j=1}^m \sum_{k=1}^l \sum_{s=1}^v \alpha_{j,k} \beta_s L_{j,k,s}(t) + \tilde{d}(t), \quad (5.18)$$

where

$$b(t) = [b_1(t), \dots, b_n(t)]^T \in \mathbb{R}^n, \quad (5.19)$$

$$\tilde{d}(t) = [\tilde{d}_1(t), \dots, \tilde{d}_n(t)]^T \in \mathbb{R}^n. \quad (5.20)$$

$$\alpha_{j,k} = [\alpha_{1,j,k}, \dots, \alpha_{n,j,k}]^T \in \mathbb{R}^n, \quad (5.21)$$

$$L_{j,k,s}(t) = \sum_{r=1}^m \psi_{j,r} \ell_{k,s,r}(t) \in \mathbb{R}, \quad (5.22)$$

### 5.3.3 Least-Squares Estimation

Equation (5.18) can be expressed in a linear regression form

$$b(t) = \Theta^T \Phi(t) + \tilde{d}(t), \quad (5.23)$$

where

$$\Theta = [\alpha_{1,1}\beta_1, \dots, \alpha_{1,1}\beta_v, \dots, \alpha_{m,l}\beta_1, \dots, \alpha_{m,l}\beta_v]^T \in \mathbb{R}^{n \times mlv}, \quad (5.24)$$

$$\Phi(t) = [L_{1,1,1}(t), \dots, L_{1,1,v}(t), \dots, L_{m,l,1}(t), \dots, L_{m,l,v}(t)]^T \in \mathbb{R}^{mlv}. \quad (5.25)$$

In practice,  $u$  and  $y$  are uniformly sampled over the spatial domain. In this case,  $b(t)$  can be computed from the pointwise data  $y(x,t)$  using spline interpolation in the spatial domain. The accurate  $a(t) = [a_1(t), \dots, a_m(t)]^T$  can be obtained from  $u(x,t)$  using the inversion operation of a matrix formed by the basis functions provided that  $n_u \geq m$ . Then,  $\Phi(t)$  can be constructed from  $a(t)$ .

Considering  $n_t$  set of temporal data  $\{\Phi(t), b(t)\}_{t=1}^{n_t}$ , it is well known from (Ljung, 1999) that by minimizing a quadratic criterion on the prediction errors

$$\hat{\Theta} = \arg \min_{\Theta} \left\{ \frac{1}{n_t} \sum_{t=1}^{n_t} \|b(t) - \Theta^T \Phi(t)\|^2 \right\}, \quad (5.26)$$

$\Theta$  can be estimated using the least-squares method as follows

$$\hat{\Theta} = \left( \frac{1}{n_t} \sum_{t=1}^{n_t} \Phi(t) \Phi^T(t) \right)^{-1} \left( \frac{1}{n_t} \sum_{t=1}^{n_t} \Phi(t) b^T(t) \right), \quad (5.27)$$

provided that the indicated inverse exists.

The next problem is how to estimate the parameters  $\alpha_{j,k}$  ( $j=1, \dots, m, k=1, \dots, l$ ) and  $\beta_s$  ( $s=1, \dots, v$ ) from the estimate  $\hat{\Theta}$  in (5.27).

### 5.3.4 Singular Value Decomposition

For convenience, we define  $\alpha = [\alpha_{1,1}^T, \dots, \alpha_{m,l}^T]^T \in \mathbb{R}^{mml}$  and  $\beta = [\beta_1, \dots, \beta_v]^T \in \mathbb{R}^v$ . It is clear that the parameterization (5.8) and (5.9) is not unique, since any parameter vectors  $\alpha\sigma$  and  $\beta\sigma^{-1}$ , under nonzero constant  $\sigma$ , can provide the same input/output equation (5.14). A technique that can be used to obtain uniqueness is to normalize the parameter vectors  $\alpha$  (or  $\beta$ ), for instance assuming that  $\|\beta\|_2 = 1$ . Under this assumption, the parameterization in (5.8) and (5.9) is unique.

From the definition of the parameter matrix  $\Theta$  in (5.24), it is easy to see that

$$\Theta = \text{blockvec}(\Theta_{\alpha\beta}),$$

where  $\text{blockvec}(\Theta_{\alpha\beta})$  is the block column matrix obtained by stacking the block columns of  $\Theta_{\alpha\beta}$  on the top of each other, and  $\Theta_{\alpha\beta} \in \mathbb{R}^{v \times nml}$  has been defined as

$$\Theta_{\alpha\beta} \triangleq \begin{bmatrix} \beta_1 \alpha_{1,1}^T & \cdots & \beta_1 \alpha_{m,1}^T \\ \beta_2 \alpha_{1,1}^T & \cdots & \beta_2 \alpha_{m,1}^T \\ \vdots & \ddots & \vdots \\ \beta_v \alpha_{1,1}^T & \cdots & \beta_v \alpha_{m,1}^T \end{bmatrix} = \beta \alpha^T. \quad (5.28)$$

Thus an estimate  $\hat{\Theta}_{\alpha\beta}$  of the matrix  $\Theta_{\alpha\beta}$  can be obtained from the estimate  $\hat{\Theta}$  in (5.27). The problem now is to estimate the parameter matrices  $\alpha$  and  $\beta$  from  $\hat{\Theta}_{\alpha\beta}$ .

In order to solve this problem, an important fact should be pointed out. It is clear that the closest, in the Frobenius norm sense, approximation of  $\hat{\Theta}_{\alpha\beta}$  is not just a single pair of  $\hat{\alpha}$  and  $\hat{\beta}$  but a series of pairs  $(\hat{\beta}^c, \hat{\alpha}^c)$ , ( $c=1, \dots, p$ ) that solve the following optimization problem

$$(\hat{\beta}^c, \hat{\alpha}^c) = \arg \min_{\alpha^c, \beta^c} \{ \|\hat{\Theta}_{\alpha\beta} - \sum_{c=1}^p \beta^c (\alpha^c)^T\|_F^2 \}, \quad (5.29)$$

where the Frobenius norm of a matrix  $A \in \mathbb{R}^{m \times n}$  is defined as  $\|A\|_F = (\sum_{i=1}^m \sum_{j=1}^n A_{ij}^2)^{1/2}$ .

To illustrate this fact, a lemma (Golub & Van Loan, 1989) should be introduced.

**Lemma 5.1:**

Let  $\hat{\Theta}_{\alpha\beta} \in \mathbb{R}^{v \times nml}$  have rank  $\gamma \geq 1$ , and let the economy-size SVD of  $\hat{\Theta}_{\alpha\beta}$  be given by

$$\hat{\Theta}_{\alpha\beta} = U_\gamma \Sigma_\gamma V_\gamma^T = \sum_{i=1}^{\gamma} \sigma_i \mu_i v_i^T, \quad (5.30)$$

where the singular matrix  $\Sigma_\gamma = \text{diag}\{\sigma_i\}$  such that

$$\sigma_1 \geq \cdots \geq \sigma_\gamma > 0,$$

and where the matrices  $U_\gamma = [\mu_1, \dots, \mu_\gamma] \in \mathbb{R}^{v \times \gamma}$  and  $V_\gamma = [v_1, \dots, v_\gamma] \in \mathbb{R}^{nml \times \gamma}$  contain only the first  $\gamma$  columns of the unitary matrices  $U \in \mathbb{R}^{v \times v}$  and  $V \in \mathbb{R}^{nml \times nml}$  provided by the full SVD of  $\hat{\Theta}_{\alpha\beta}$ ,

$$\hat{\Theta}_{\alpha\beta} = U \Sigma V^T,$$

respectively. Then  $\forall p \leq \gamma$ , the following equation holds

$$(\hat{\beta}^c, \hat{\alpha}^c) = \arg \min_{\alpha^c, \beta^c} \{ \|\hat{\Theta}_{\alpha\beta} - \sum_{c=1}^p \beta^c (\alpha^c)^T\|_F^2 \} = (\mu_c, \nu_c \sigma_c), (c = 1, \dots, p), \quad (5.31)$$

where  $(\hat{\beta}^c, \hat{\alpha}^c)$  is defined as the  $c^{\text{th}}$  channel, and  $p$  is the number of channels. The parameter approximation error is given by

$$\mathcal{E}^p = \|\hat{\Theta}_{\alpha\beta} - \sum_{c=1}^p \beta^c (\alpha^c)^T\|_F^2 = \sum_{c=p+1}^{\gamma} \sigma_c^2. \quad (5.32)$$

Based on [Lemma 5.1](#), the estimated parameters  $\hat{\alpha}$  and  $\hat{\beta}$  can be obtained by

$$(\hat{\beta}, \hat{\alpha}) = \arg \min_{\alpha, \beta} \{ \|\hat{\Theta}_{\alpha\beta} - \beta(\alpha)^T\|_F^2 \} = (\mu_1, \nu_1 \sigma_1). \quad (5.33)$$

The consistency in the previous work ([Bai, 1998](#); [Gómez & Baeyens, 2004](#)) can be extended to this basic identification approach under certain conditions (e.g., model matching and zero-mean disturbance). However, if such conditions are not satisfied, it would be difficult to obtain a solution. In the following section, a novel multi-channel identification approach will be presented to provide a better solution.

## 5.4 Multi-channel Identification Approach

### 5.4.1 Motivation

#### *Definition 5.1:*

The system (5.2) is named as a **single-channel Hammerstein system**. The **multi-channel Hammerstein system** is formed by the parallel connection of  $p$  single-channel Hammerstein systems. ■

For a single-channel Hammerstein model, we can see from (5.28) that  $\text{rank}(\Theta_{\alpha\beta}) = 1$ , since  $\Theta_{\alpha\beta}$  is the product of a column vector  $\beta$  and a row vector  $\alpha^T$ . However, generally speaking, its estimate  $\hat{\Theta}_{\alpha\beta}$  from process data can not be exactly expressed as the product of a column vector and a row vector due to unmodeled dynamics and disturbance. That is  $\text{rank}(\hat{\Theta}_{\alpha\beta}) > 1$ . The unmodeled dynamics refer to the error between the single-channel model and the system, which may be too large. In addition,  $\sigma_2/\sigma_1$  (see (5.30)) can not always be small enough to make the parameter approximation error (5.32) acceptable. Thus, it is very necessary to add more channels to compensate the modeling residuals.

### 5.4.2 Multi-channel Identification

The presented multi-channel identification methodology is shown in [Figure 5.2](#).

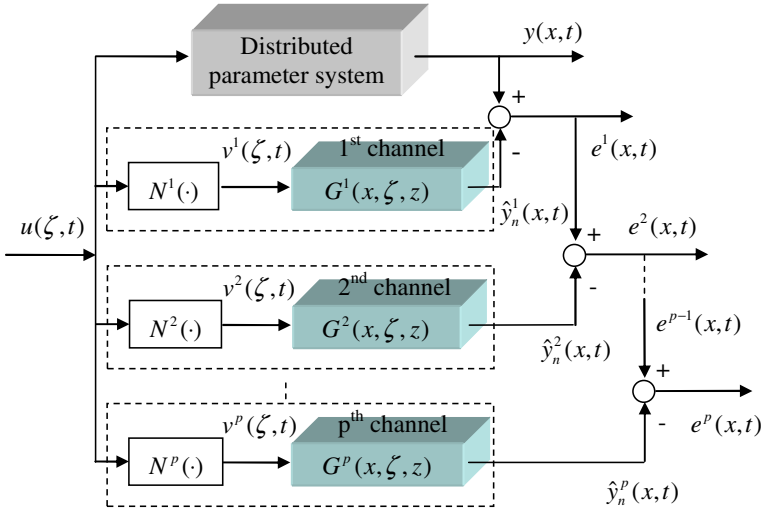


**Fig. 5.2** Multi-channel identification of spatio-temporal Hammerstein model

A sequential identification algorithm is designed as follows. Firstly, the 1<sup>st</sup> channel model is estimated using the basic identification algorithm from the input-output data  $\{u(x, t), y(x, t)\}_{t=1}^{n_t}$ . Secondly, the 1<sup>st</sup> channel model error  $e^1(x, t) = y(x, t) - \hat{y}_n^1(x, t)$  is regarded as the new output, and then the 2<sup>nd</sup> channel model is identified. Similarly,  $e^2(x, t), \dots, e^{p-1}(x, t)$  can determine the 3<sup>rd}, \dots, p^{\text{th}} channel models, and so on.</sup>

However, the sequential identification algorithm for each channel may lead to a computational burden problem. According to [Lemma 5.1](#), the multi-channel identification algorithm can be easily implemented simultaneously as below.

**Algorithm 5.1:**

*Step 1:* Determine the input basis functions  $\{\psi_i(x)\}_{i=1}^m$ , find the output basis functions  $\{\varphi_i(x)\}_{i=1}^n$  using the KL method, choose the Laguerre polynomials  $\{\phi_i(t)\}_{i=1}^l$ , then obtain the corresponding temporal coefficients  $\{a(t)\}_{t=1}^{n_t}$  and  $\{b(t)\}_{t=1}^{n_o}$  of the input  $\{u(x_i, t)\}_{i=1, t=1}^{n_u, n_t}$  and output  $\{y(x_j, t)\}_{j=1, t=1}^{n_y, n_t}$  respectively.

*Step 2:* Compute the linear regressors  $\Phi(t)$  according to (5.17) and (5.25) using  $\{a(t)\}_{t=1}^{n_t}$ , then compute the least-squares estimate  $\hat{\Theta}$  as in (5.27), and construct the matrix  $\hat{\Theta}_{\alpha\beta}$  such that  $\hat{\Theta} = \text{blockvec}(\hat{\Theta}_{\alpha\beta})$ .

*Step 3:* Compute the economy-size SVD of  $\hat{\Theta}_{\alpha\beta}$  as in [Lemma 5.1](#), and the partition of this decomposition as in (5.30).



Step 4: Compute the estimates of the parameter vectors  $\hat{\alpha}^c$  and  $\hat{\beta}^c$  as  $\hat{\beta}^c = \mu_c$  and  $\hat{\alpha}^c = v_c \sigma_c$  ( $c = 1, \dots, p$ ), respectively.

**Remark 5.1:**

It is important to note that the algorithm intrinsically delivers estimates that satisfy the uniqueness condition  $\|\hat{\beta}^c\|_2 = 1$ , since the matrix  $\mu_c$  in the SVD of  $\hat{\Theta}_{\alpha\beta}^c$  is a unitary matrix.

**Multi-channel Hammerstein model**

Based on Algorithm 5.1, a multi-channel spatio-temporal Hammerstein model consisting of  $p$  channels

$$\hat{y}_n(x, t) = \sum_{c=1}^p \sum_{r=0}^l \int_{\Omega} \sum_{i=1}^n \sum_{j=1}^m \sum_{k=1}^l \hat{\alpha}_{i,j,k}^c \varphi_i(x) \psi_j(\zeta) \phi_k(\tau) \sum_{r=1}^m \sum_{s=1}^v \psi_r(\zeta) \hat{\beta}_s^c h_s(a_r(t-\tau)) d\zeta, \quad (5.34)$$

is constructed to approximate the nonlinear DPS as shown in Figure 5.3. Each channel consists of the cascade connection of a static nonlinear block represented by basis functions, followed by a dynamic linear block represented by spatio-temporal Laguerre model as shown in Figure 5.4. The transfer functions in Figure 5.4 can be derived from (5.12) as follows

$$\kappa_1(s) = \frac{\sqrt{2\xi}}{s + \xi}, \kappa_2(s) = \dots = \kappa_l(s) = \frac{s - \xi}{s + \xi},$$

where  $\xi$  is the time-scaling factor.

Note that in Figure 5.3 and Figure 5.4,  $\hat{y}_n(x, t) = \sum_{c=1}^p \hat{y}_n^c(x, t)$ ,

$$\hat{v}^c(\zeta, t) = \sum_{r=1}^m \sum_{s=1}^v \psi_r(\zeta) \hat{\beta}_s^c h_s(a_r(t)) \quad , \quad \hat{D}_{j,k}^c(x) = \sum_{i=1}^n \hat{\alpha}_{i,j,k}^c \varphi_i(x) \quad \text{and}$$

$$L_{j,k}^c(t) = \sum_{r=1}^m \sum_{s=1}^v \psi_{j,r} \hat{\beta}_s^c \ell_{k,s,r}(t).$$

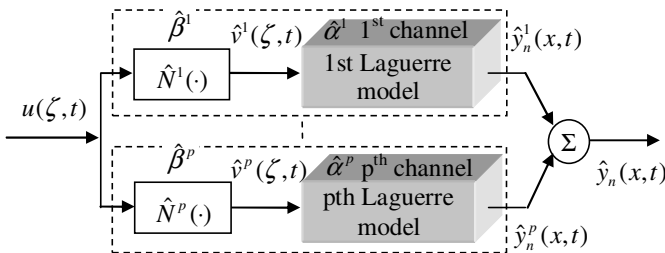
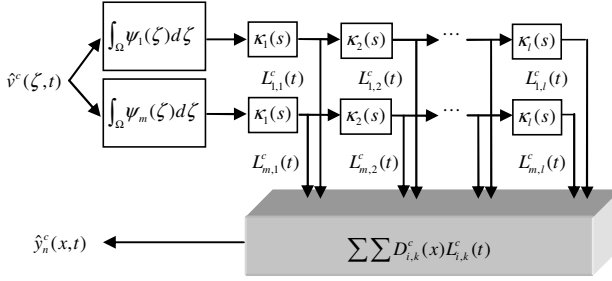


Fig. 5.3 Multi-channel spatio-temporal Hammerstein model



**Fig. 5.4** Spatio-temporal Laguerre model of the  $c^{\text{th}}$  channel

**Remark 5.2:**

If the time scale  $\xi$  is chosen suitably, then the Laguerre series can efficiently model any stable linear plant (Wang & Culett, 1995). Usually, the parameter  $\xi$  which gives a good performance is obtained from trials. Many studies have dealt with the time scale selection problem using such as offline optimization (Campello *et al.*, 2004) and online adaptation (Tanguy *et al.*, 2000) methods. For another parameter  $l$ , there are no theoretical methods but only some empirical ones so far. ■

Based on Lemma 5.1, we can give the following theorem to show the advantage of multi-channel mechanism.

**Theorem 5.1:**

For a spatio-temporal Hammerstein system (5.2), if the estimated matrix  $\hat{\Theta}_{\alpha\beta}$  has rank  $\gamma \geq 1$  and the parameters of the  $c^{\text{th}}$  channel  $(\hat{\beta}^c, \hat{\alpha}^c)$  ( $c = 1, \dots, p, p \leq \gamma$ ) are obtained by (5.31), then the parameter approximation error (5.32) will satisfy

$$\varepsilon^1 > \varepsilon^2 > \dots > \varepsilon^p > \dots > \varepsilon^\gamma = 0 .$$

**Proof:** This can be easily drawn from Lemma 5.1. ■

Theorem 5.1 means that the parameter approximation error will be reduced by increasing the channel number  $p$ . Moreover, the model complexity can also be controlled by the number of channels. There is a tradeoff between the complexity and accuracy. Due to the property of the SVD, the parameter of the  $c^{\text{th}}$  channel is the  $c^{\text{th}}$  principal component of the whole parameter space. Therefore, only the first few dominant channels can construct a good model.

**5.4.3 Convergence Analysis**

An important issue is the convergence of the estimated parameters as the number of data points  $n$ , tends to infinity. Now, we will give a convergence theorem to support the presented algorithm.

For simplicity, let  $y_n(x, t) = H(x, t, \Theta, \{u(\zeta, \tau)\})$  denote a multi-channel Hammerstein model with  $n, l, v < \infty$

$$y_n(x, t) = \sum_{c=1}^p \sum_{\tau=0}^t \int_{\Omega} \sum_{i=1}^n \sum_{j=1}^m \sum_{k=1}^l \alpha_{i,j,k}^c \varphi_i(x) \psi_j(\zeta) \phi_k(\tau) \sum_{r=1}^m \sum_{s=1}^v \psi_r(\zeta) \beta_s^c h_s(a_r(t-\tau)) d\zeta, \quad (5.35)$$

where  $\Theta = \sum_{c=1}^p [\alpha_{1,1}^c \beta_1^c, \dots, \alpha_{1,l}^c \beta_l^c, \dots, \alpha_{m,1}^c \beta_1^c, \dots, \alpha_{m,l}^c \beta_l^c]^T \in \mathbb{R}^{p \times nml}$ ,  $\alpha_{j,k}^c$  ( $j=1, \dots, m$ ,  $k=1, \dots, l$ ) are defined by (5.21), and  $\{u(\zeta, \tau)\} = \{u(\zeta, \tau) \mid \zeta \in \Omega, \tau = 1, \dots, t\}$ .

We always assume that there is an optimal model

$$y_n^*(x, t) = H(x, t, \Theta^*, \{u(\zeta, \tau)\}), \quad (5.36)$$

with an optimal parameter matrix  $\Theta^*$  such that

$$\Theta^* = \arg \min_{\Theta \in D_{\Theta}} \{ \bar{E}(y(x, t) - H(x, t, \Theta, \{u(\zeta, \tau)\}))^2 \}, \quad (5.37)$$

where  $\bar{E}f(x, t)^2 = \lim_{n_t \rightarrow \infty} \frac{1}{n_t} \sum_{t=1}^{n_t} \frac{1}{A} \int_{\Omega} E f(x, t)^2 dx$ ,  $A = \int_{\Omega} dx$  and  $E$  is expectation operator.

Let  $D_{\Theta}$  be compact. Define  $\Theta_{\alpha\beta}^* \in \mathbb{R}^{p \times nml}$  such that  $\Theta^* = \text{blockvec}(\Theta_{\alpha\beta}^*)$ .

Under the uniform spatial discretization,  $\frac{1}{A} \sum_{i=1}^{\infty} b_i(t)^2 = \frac{1}{A} \int_{\Omega} y(x, t)^2 dx$  can be replaced by  $\frac{1}{n_y} \sum_{j=1}^{n_y} y(x_j, t)^2$ . However, the accurate  $a(t)$  can be obtained provided that  $n_u \geq m$ . Therefore, according to the details of the developed identification algorithm, the minimization problem (5.26) is indeed equivalent to the following problem

$$\hat{\Theta} = \arg \min_{\Theta \in D_{\Theta}} \left\{ \frac{1}{n_t} \frac{1}{n_y} \sum_{t=1}^{n_t} \sum_{j=1}^{n_y} (y(x_j, t) - H(x_j, t, \Theta, \{u(\zeta, \tau)\}))^2 \right\}. \quad (5.38)$$

It should be mentioned that, (5.26) can be considered as a practical implementation of (5.38) in order to reduce the involved spatial complexity. However, the theoretical analysis should be performed in the spatio-temporal domain.

### Assumption 5.1:

Let  $W(x, t)$  be the  $\sigma$ -algebra generated by  $(d(x, t), \dots, d(x, 0))$ . For each  $t, \tau$  ( $t \geq \tau$ ) and any  $x, \zeta \in \Omega$ , there exist random variables  $y_{\tau}^0(x, t)$  ( $y_{\tau}^0(x, t) = 0$ ),  $u_{\tau}^0(\zeta, t)$  ( $u_{\tau}^0(\zeta, t) = 0$ ), that belong to  $W(x, t)$ , but are independent of  $W(x, \tau)$ , such that

$$E | y(x, t) - y_{\tau}^0(x, t) |^4 < M \lambda^{t-\tau},$$

$$E | u(\zeta, t) - u_{\tau}^0(\zeta, t) |^4 < M \lambda^{t-\tau},$$

for some  $M < \infty$ ,  $\lambda < 1$ .

**Assumption 5.2:**

Assume that the model  $y_n(x, t) = H(x, t, \Theta, \{u(\zeta, \tau)\})$  is differentiable with respect to  $\Theta$  for all  $\Theta \in D_\Theta$ . Assume that

$$|H(x, t, \Theta, \{u_1(\zeta, \tau)\}) - H(x, t, \Theta, \{u_2(\zeta, \tau)\})| \leq M \sum_{\tau=0}^t \lambda^{t-\tau} \sup_{\zeta \in \Omega} |u_1(\zeta, \tau) - u_2(\zeta, \tau)|,$$

and  $|H(x, t, \Theta, \{0(\zeta, \tau)\})| \leq M$ , where  $\Theta$  belongs to an open neighborhood of  $D_\Theta$ ,  $M < \infty$  and  $\lambda < 1$ .

**Assumption 5.3:**

Define  $\varepsilon(x, t, \Theta) = y(x, t) - H(x, t, \Theta, \{u(\zeta, \tau)\})$  and there exists

$$\left| \frac{\partial \varepsilon(x, t, \Theta)^2}{\partial \Theta} \right| \leq M \varepsilon(x, t, \Theta)^2, \quad \Theta \in D_\Theta, \quad \forall x \in \Omega, \quad \forall t.$$

**Remark 5.3:**

**Assumption 5.1** means that the system to be identified is exponentially stable, i.e., the remote past of the process is “forgotten” at an exponential rate. **Assumption 5.2** has three meanings. First, the model is differential with respect to the parameters. Second, the model may not increase faster than the linear one. Third, the model is also exponentially stable. Regarding **Assumption 5.3**, the derivative of the modeling error with respect to the parameters is bounded by the modeling error. Such conditions are required to make the parameter optimization procedure feasible, and guarantee the following convergence.

**Theorem 5.2:**

For a spatio-temporal Hammerstein system (5.2), the multi-channel model (5.34) is estimated using **Algorithm 5.1**. If **Assumption 5.1**, **Assumption 5.2** and **Assumption 5.3** are satisfied, then  $\sum_{c=1}^p \hat{\beta}^c (\hat{\alpha}^c)^T \rightarrow \Theta_{\alpha\beta}^*$  and  $\hat{y}_n(x, t) \rightarrow y_n^*(x, t)$  w. p. 1 as  $n_t \rightarrow \infty$ ,  $n_y \rightarrow \infty$ , and  $p \rightarrow \gamma$ , where  $\gamma = \text{rank}(\Theta_{\alpha\beta}^*)$ .

**Proof:**

In order to obtain the convergence with probability 1, the following lemma, which is the direct extension of the previous work (**Cramér & Leadbetter, 1967; Ljung, 1978**), is needed in the proof of **Theorem 5.2**.

**Lemma 5.2:**

Let  $\xi(x, t)$  be a random variable with zero-mean value and with

$$|E(\xi(x, t)\xi(x, \tau))| \leq M \frac{t^\alpha + \tau^\beta}{1 + |t - \tau|^\beta}, \quad x \in \Omega, M < \infty, 0 \leq 2\alpha < \beta < 1. \quad (5.39)$$

Then

$$\frac{1}{n_t} \sum_{t=1}^{n_t} \zeta(x, t) \rightarrow 0, \text{ w. p. 1 as } n_t \rightarrow \infty. \quad (5.40)$$

where ‘w. p. 1’ means ‘with probability 1’.

■

We now turn to the proof of **Theorem 5.2**. The convergence of the estimation  $\hat{\Theta}$

$$\hat{\Theta} \rightarrow \Theta^*, \text{ w. p. 1 as } n_t \rightarrow \infty, n_y \rightarrow \infty, \quad (5.41)$$

implies that

$$\hat{\Theta}_{\alpha\beta} \rightarrow \Theta_{\alpha\beta}^*, \text{ w. p. 1 as } n_t \rightarrow \infty, n_y \rightarrow \infty. \quad (5.42)$$

By **Lemma 5.1**, we have

$$\sum_{c=1}^p \hat{\beta}^c (\hat{\alpha}^c)^T \rightarrow \hat{\Theta}_{\alpha\beta}, \text{ as } p \rightarrow \gamma,$$

where  $\gamma = \text{rank}(\hat{\Theta}_{\alpha\beta})$ . Therefore

$$\sum_{c=1}^p \hat{\beta}^c (\hat{\alpha}^c)^T \rightarrow \Theta_{\alpha\beta}^*, \text{ w. p. 1 as } n_t \rightarrow \infty, n_y \rightarrow \infty, p \rightarrow \gamma. \quad (5.43)$$

Since  $H(x, t, \Theta, \{u(\zeta, \tau)\})$  is continuous with respect to  $\Theta$ , the convergence of parameters as in (5.43) naturally leads to the convergence of the model to its optimum

$$\hat{y}_n(x, t) \rightarrow y_n^*(x, t), \text{ w. p. 1 as } n_t \rightarrow \infty, n_y \rightarrow \infty, p \rightarrow \gamma. \quad (5.44)$$

Define

$$Q_{n_y, n_t}(\Theta) = \frac{1}{n_y} \sum_{j=1}^{n_y} \left\{ \frac{1}{n_t} \sum_{t=1}^{n_t} \mathcal{E}(x_j, t, \Theta)^2 \right\}.$$

As define in (5.37),  $\Theta^*$  minimizes

$$\bar{E}(y(x, t) - H(x, t, \Theta, \{u(\zeta, \tau)\}))^2 = \lim_{n_y \rightarrow \infty} \{ \lim_{n_t \rightarrow \infty} EQ_{n_y, n_t}(\Theta) \},$$

and the estimate  $\hat{\Theta}$  minimizes  $Q_{n_y, n_t}$  as defined in (5.38).

In order to prove (5.41), we should prove the convergence as follows

$$\sup_{\Theta \in D_\Theta} |Q_{n_y, n_t}(\Theta) - EQ_{n_y, n_t}(\Theta)| \rightarrow 0, \text{ w. p. 1 as } n_t \rightarrow \infty, n_y \rightarrow \infty. \quad (5.45)$$

One feasible solution is to achieve the following convergence at any fixed spatial variable  $x$  before working at the spatio-temporal space.

$$\sup_{\Theta \in D_\Theta} \frac{1}{n_t} \sum_{t=1}^{n_t} |\mathcal{E}(x, t, \Theta)^2 - E\mathcal{E}(x, t, \Theta)^2| \rightarrow 0, \text{ w. p. 1 as } n_t \rightarrow \infty. \quad (5.46)$$

To achieve the convergence of (5.46), we have to obtain the convergence first at the pre-defined small open sphere, and then extend it to the global domain  $D_\Theta$  using Heine-Borel's theorem.

***Convergence of modeling error  $\varepsilon$  to its optimum over  $B$  :***

Define the supremum between the model error and its optimum as a random variable

$$\eta(x, t) = \eta(x, t, \Theta^0, \rho) = \sup_{\Theta \in B} [\varepsilon(x, t, \Theta)^2 - E\varepsilon(x, t, \Theta)^2].$$

Let  $D$  be the open neighborhood of  $D_\Theta$  and choose  $\Theta^0 \in D_\Theta$ . We can define a small open sphere centered at  $\Theta^0$  as

$$B(\Theta^0, \rho) = \{\Theta \mid \|\Theta - \Theta^0\| < \rho\}.$$

Let  $B = B(\Theta^0, \rho) \cap D$ , then

$$\sup_{\Theta \in B} \frac{1}{n_t} \sum_{t=1}^{n_t} [\varepsilon(x, t, \Theta)^2 - E\varepsilon(x, t, \Theta)^2] \leq \frac{1}{n_t} \sum_{t=1}^{n_t} \eta(x, t). \quad (5.47)$$

Define  $\xi(x, t) = \eta(x, t) - E\eta(x, t)$ . If we can prove

- $\xi(x, t)$  satisfies [Lemma 5.2](#) and
  - the mean of  $\eta(x, t)$  is infinitesimal,
- then  $\eta(x, t)$  is also infinitesimal.

Firstly, we consider

$$|E(\xi(x, t)\xi(x, \tau))| = \text{Cov}[\eta(x, t), \eta(x, \tau)].$$

Define  $\eta_\tau^0(x, t) = \sup_{\Theta \in B} [\varepsilon_\tau^0(x, t, \Theta)^2 - E\varepsilon(x, t, \Theta)^2]$ , with

$$\varepsilon_\tau^0(x, t, \Theta) = y_\tau^0(x, t) - H(x, t, \Theta, \{u_\tau^0(\zeta, j)\}), \quad t > \tau,$$

where  $\{u_\tau^0(\zeta, j)\}$  denotes the input set  $(u_\tau^0(\zeta, t), \dots, u_\tau^0(\zeta, \tau+1), 0, \dots, 0)$  for all  $\zeta \in \Omega$ ,  $y_\tau^0(x, t)$  and  $u_\tau^0(\zeta, j)$  are the variables introduced in [Assumption 5.1](#). For convenience, let  $u_\tau^0(\zeta, j) = 0$  and  $y_\tau^0(x, j) = 0$  for  $j < \tau$ . Obviously  $\eta_\tau^0(x, t)$  is independent of  $\eta(x, \tau)$  from [Assumption 5.1](#).

Hence

$$\text{Cov}[\eta(x, t), \eta(x, \tau)] = \text{Cov}[\eta(x, t) - \eta_\tau^0(x, t), \eta(x, \tau)].$$

Then using Schwarz's inequality, we have

$$|E(\xi(x, t)\xi(x, \tau))| \leq [E\eta(x, \tau)^2 E(\eta(x, t) - \eta_\tau^0(x, t))^2]^{1/2}. \quad (5.48)$$

Since

$$\begin{aligned} |\eta(x, t) - \eta_r^0(x, t)| &\leq \sup_{\Theta \in B} |\mathcal{E}(x, t, \Theta)^2 - \varepsilon_r^0(x, t, \Theta)^2| \\ &\leq \sup_{\Theta \in B} \{|\mathcal{E}(x, t, \Theta)| + |\varepsilon_r^0(x, t, \Theta)|\} \times \sup_{\Theta \in B} |\mathcal{E}(x, t, \Theta) - \varepsilon_r^0(x, t, \Theta)|, \end{aligned}$$

using [Assumption 5.2](#), we can further have

$$\begin{aligned} |\eta(x, t) - \eta_r^0(x, t)| &\leq M \left[ \sum_{j=0}^t \lambda^{t-j} \{ |y(x, j)| + |y_r^0(x, j)| + \sup_{\zeta \in \Omega} |u(\zeta, j)| + \sup_{\zeta \in \Omega} |u_r^0(\zeta, j)| \} \right] \times \\ &\quad \left[ \sum_{j=0}^t \lambda^{t-j} \{ |y(x, j) - y_r^0(x, j)| + \sup_{\zeta \in \Omega} |u(\zeta, j) - u_r^0(\zeta, j)| \} \right]. \end{aligned}$$

Using [Assumption 5.1](#) and Schwarz's inequality, we can finally derive

$$E |\eta(x, t) - \eta_r^0(x, t)|^2 \leq M \lambda^{t-\tau}. \quad (5.49)$$

Following the similar derivation above and using [Assumption 5.2](#) and [Assumption 5.1](#), we can also derive

$$E \eta(x, \tau)^2 \leq M. \quad (5.50)$$

Placing (5.49) and (5.50) into (5.48), we can easily derive that  $\xi(x, t)$  satisfies [Lemma 5.2](#), that is

$$\frac{1}{n_t} \sum_{t=1}^{n_t} \xi(x, t) = \frac{1}{n_t} \sum_{t=1}^{n_t} (\eta(x, t) - E\eta(x, t)) \rightarrow 0, \text{ w. p. 1 as } n_t \rightarrow \infty. \quad (5.51)$$

Secondly, we derive the mean value of  $\eta$

$$E\eta(x, t) = E \sup_{\Theta \in B} [\mathcal{E}(x, t, \Theta)^2 - E\mathcal{E}(x, t, \Theta)^2].$$

Since the right-hand side is continuous with respect to  $\Theta$ ,  $E\eta(x, t)$  should be small if  $B$  is small. Furthermore, by [Assumption 5.3](#),

$$\left| \frac{\partial \mathcal{E}(x, t, \Theta)^2}{\partial \Theta} \right| \leq M |\mathcal{E}(x, t, \Theta)|^2 \leq M \left[ \sum_{j=0}^t \lambda^{t-j} \{ |y(x, j)| + \sup_{\zeta \in \Omega} |u(\zeta, j)| \} \right]^2,$$

where we again have used the uniform bounds in [Assumption 5.2](#). Consequently, by [Assumption 5.1](#),

$$E \sup_{\Theta \in B} \left| \frac{\partial \mathcal{E}(x, t, \Theta)^2}{\partial \Theta} \right|^2 \leq M.$$

Now

$$\begin{aligned}
E\eta(x,t) &= E \sup_{\Theta \in B} [\varepsilon(x,t,\Theta)^2 - E\varepsilon(x,t,\Theta)^2] \\
&\leq E \sup_{\Theta \in B} [\varepsilon(x,t,\Theta)^2 - \varepsilon(x,t,\Theta^0)^2] + \sup_{\Theta \in B} E[\varepsilon(x,t,\Theta^0)^2 - \varepsilon(x,t,\Theta)^2] \\
&\leq [E \sup_{\Theta \in B} \left| \frac{\partial \varepsilon(x,t,\Theta)^2}{\partial \Theta} \right| + \sup_{\Theta \in B} E \left| \frac{\partial \varepsilon(x,t,\Theta)^2}{\partial \Theta} \right|] \times \sup_{\Theta \in B} |\Theta - \Theta^0| \\
&\leq M^0 \rho.
\end{aligned} \tag{5.52}$$

Finally, from (5.52), (5.47) becomes

$$\sup_{\Theta \in B} \frac{1}{n_t} \sum_{t=1}^{n_t} [\varepsilon(x,t,\Theta)^2 - E\varepsilon(x,t,\Theta)^2] \leq \frac{1}{n_t} \sum_{t=1}^{n_t} (\eta(x,t) - E\eta(x,t)) + M^0 \rho. \tag{5.53}$$

It is clear to see from (5.51) that the first term of the right-hand side is arbitrarily small for sufficiently large  $n_t$ . Since  $\rho$  can also be arbitrarily small, therefore

$$\sup_{\Theta \in B} \frac{1}{n_t} \sum_{t=1}^{n_t} |\varepsilon(x,t,\Theta)^2 - E\varepsilon(x,t,\Theta)^2| \rightarrow 0, \text{ w. p. 1 as } n_t \rightarrow \infty. \tag{5.54}$$

**Convergence extension to global  $D_\Theta$ :**

Since  $D_\Theta$  is compact, by applying Heine-Borel's theorem, from (5.54) the following result is easily concluded

$$\sup_{\Theta \in D_\Theta} \frac{1}{n_t} \sum_{t=1}^{n_t} |\varepsilon(x,t,\Theta)^2 - E\varepsilon(x,t,\Theta)^2| \rightarrow 0, \text{ w. p. 1 as } n_t \rightarrow \infty. \tag{5.55}$$

**Extension to spatio-temporal domain:**

Obviously

$$\sup_{\Theta \in D_\Theta} |Q_{n_y, n_t}(\Theta) - EQ_{n_y, n_t}(\Theta)| \leq \frac{1}{n_y} \sum_{j=1}^{n_y} \sup_{\Theta \in D_\Theta} \frac{1}{n_t} \sum_{t=1}^{n_t} |\varepsilon(x_j, t, \Theta)^2 - E\varepsilon(x_j, t, \Theta)^2|,$$

therefore

$$\sup_{\Theta \in D_\Theta} |Q_{n_y, n_t}(\Theta) - EQ_{n_y, n_t}(\Theta)| \rightarrow 0, \text{ w. p. 1 as } n_t \rightarrow \infty, n_y \rightarrow \infty. \tag{5.56}$$

■

## 5.5 Simulation and Experiment

In order to evaluate the presented modeling method, we first present the simulation on a typical distributed process, and then apply it to the snap curing oven.



For an easy comparison, some performance indexes are set up as follows:

- Spatio-temporal error  $e(x,t) = y(x,t) - \hat{y}_n(x,t)$ ,
- **Spatial normalized absolute error**,  $SNAE(t) = \int |e(x,t)| dx / \int dx$ ,
- **Temporal normalized absolute error**,  $TNAE(x) = \sum |e(x,t)| / \sum \Delta t$ ,
- **Root of mean squared error**,  $RMSE = (\int \sum e(x,t)^2 dx / \int dx \sum \Delta t)^{1/2}$ .

### 5.5.1 Packed-Bed Reactor

Consider the **packed-bed reactor** given in [Section 1.1.2](#). A dimensionless model that describes temperature distribution in the reactor is provided as follows ([Christofides, 1998](#))

$$\begin{aligned} \varepsilon_p \frac{\partial y_g}{\partial t} &= -\frac{\partial y_g}{\partial x} + \alpha_c (y - y_g) - \alpha_g (y_g - \psi(x)a(t)), \\ \frac{\partial y}{\partial t} &= \frac{\partial^2 y}{\partial x^2} + \beta_0 e^{\frac{\gamma y}{1+y}} - \beta_c (y - y_g) - \beta_p (y - \psi(x)a(t)), \end{aligned} \quad (5.57)$$

subject to the boundary conditions

$$\begin{aligned} x=0, y_g &= 0, \frac{\partial y}{\partial x} = 0, \\ x=1, \frac{\partial y}{\partial x} &= 0, \end{aligned} \quad (5.58)$$

where  $y_g$ ,  $y$  and  $a$  denote the dimensionless temperature of the gas, the catalyst and jacket, respectively. A small positive value  $\varepsilon_p$  denotes the ratio of the heat capacitance of the gas phase vs the heat capacitance of the catalytic phase.  $\alpha_c$ ,  $\alpha_g$ ,  $\beta_0$ ,  $\gamma$ ,  $\beta_c$ , and  $\beta_p$  are other system parameters. See [Christofides \(1998\)](#) for more details. It is assumed that only catalyst temperature measurements are available. The problem is to model the dynamics for the catalyst temperature.

The values of the process parameters are given below

$$\varepsilon_p = 0.01, \gamma = 21.14, \beta_c = 1.0, \beta_p = 15.62, \beta_0 = -0.003, \alpha_c = 0.5 \text{ and } \alpha_g = 0.5.$$

A heater is used with the spatial distribution  $\psi(x) = \sin(\pi x)$ ,  $0 \leq x \leq 1$ . In the numerical calculation, we set the input  $a(t) = 1.1 + 1.5 \sin(t/20)$ . In the simulation, sixteen sensors are used in order to capture the sufficient spatial information. The random process noise is bounded by 0.003 with zero mean so that the noisy data for the modeling have a **signal-to-noise ratio (SNR)** of around 21dB. The sampling period  $\Delta t$  is 0.0001 and the simulation time is 0.13. A noisy data set of 1300 data is collected. The first 1100 data is used as the training data with the first 900 data as the estimation data and the next 200 data as the validation data. The validation data

is used to monitor the training process and determine some design parameters using the cross-validation method. The remaining 200 data is the testing data.

The process output  $y(x,t)$  is shown in Figure 5.5, while the obtained KL basis functions are shown in Figure 5.6 with  $n=3$ . Using the cross-validation the temporal bases  $\phi_i(t)$ , ( $i=1,\dots,10$ ) are chosen as Laguerre series with time-scaling factor  $\xi = 20.5$ . The nonlinear bases are polynomials as  $h_i(a) = a^i$  ( $i=1,\dots,4$ ).

The prediction output  $\hat{y}_n(x,t)$  of the 3-channel Hammerstein model is shown in Figure 5.7, with the prediction error  $e(x,t)$  presented in Figure 5.8. It is obvious that the 3-channel Hammerstein model can approximate the original spatio-temporal dynamics very well. As shown in Figure 5.9 and Figure 5.10, as the channel number increases, the prediction error  $SNAE(t)$  and  $TNAE(x)$  over the whole data set will decrease, which is consistent with the theoretical analysis. As illustrated in Figure 5.11, the 3-channel Hammerstein modeling error  $RMSE$  will become smaller when using more sensors. Numbers of sensors used should be determined by the complexity of spatial dynamics to be modeled.

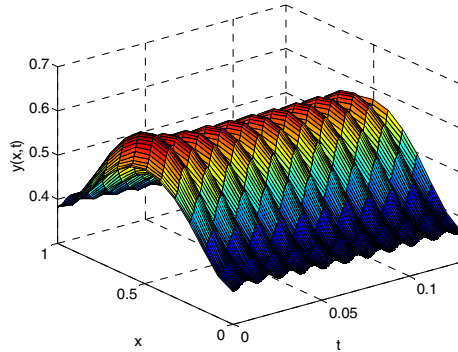


Fig. 5.5 Packed-bed reactor: Process output for multi-channel Hammerstein modeling

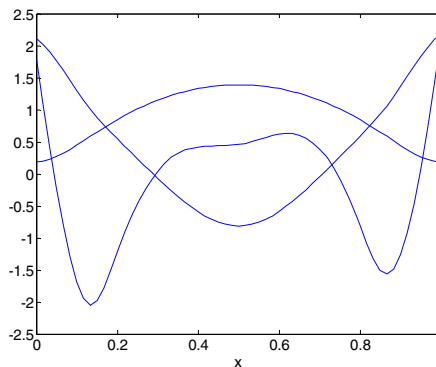
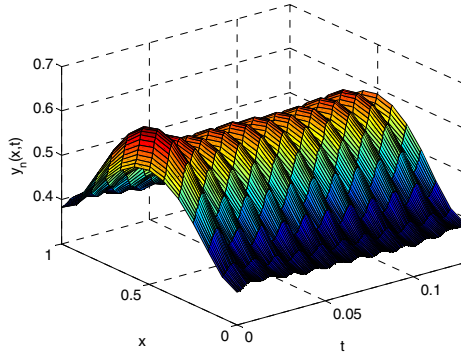
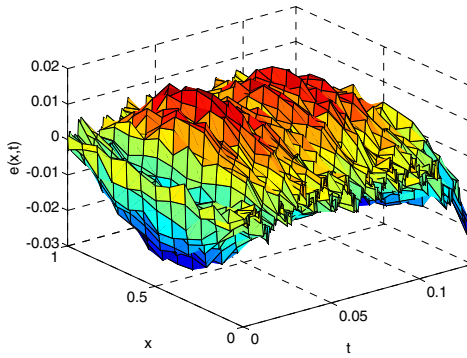


Fig. 5.6 Packed-bed reactor: KL basis functions for multi-channel Hammerstein modeling



**Fig. 5.7** Packed-bed reactor: Prediction output of 3-channel Hammerstein model



**Fig. 5.8** Packed-bed reactor: Prediction error of 3-channel Hammerstein model

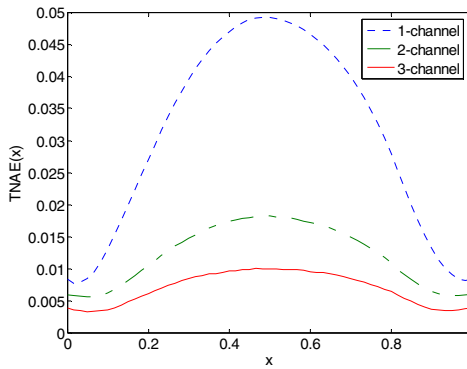


**Fig. 5.9** Packed-bed reactor:  $TNAE(x)$  of Hammerstein models

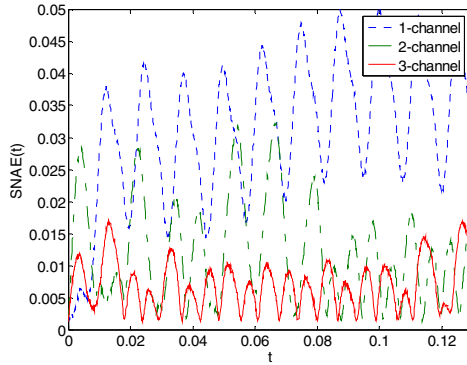


**Fig. 5.10** Packed-bed reactor:  $SNAE(t)$  of Hammerstein models

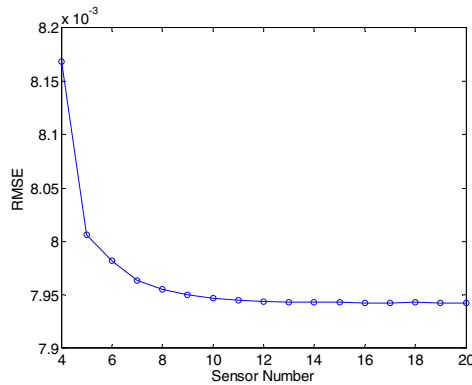


**Fig. 5.11** Packed-bed reactor:  $RMSE$  of 3-channel Hammerstein model

### 5.5.2 Snap Curing Oven

Consider the **snap curing oven** (Figure 1.1 and Figure 3.11) provided in Sections 1.1.1 and 3.6.2. In the experiment, a total of 2400 measurements are collected with a sampling interval  $\Delta t = 10$  seconds. One thousand and six hundred of measurements from sensors (s1-s5, s7-s10, and s12-s16) are used to estimate the model. The last 800 measurements from sensors (s1-s5, s7-s10, and s12-s16) are chosen to validate the model during the training. All 2400 measurements from the rest sensors (s6, s11) are used for modeling performance testing.

In the spatio-temporal Hammerstein modeling, five two-dimensional Karhunen-Loève basis functions are used as spatial bases and the first two of them are shown in Figure 5.12 and Figure 5.13. The temporal bases  $\phi_i(t)$  are chosen as Laguerre series with the time-scaling factor  $p = 0.001$  and the truncation length  $q = 3$  using the cross-validation method.

The *3-channel Hammerstein model* is used to model the thermal process. After the training using the first 1600 data from the sensors (s1-s5, s7-s10, and s12-s16), a process model can be obtained with the significant performance such as the sensor s1 in [Figure 5.14](#). The model also performs very well for the untrained locations such as the sensor s6 in [Figure 5.15](#). The predicted temperature distribution of the oven at  $t=10000\text{s}$  is provided in [Figure 5.16](#). The performance comparisons over the whole data set in [Table 5.1](#) further show that the *3-channel Hammerstein model* has a much better performance than the *1- and 2-channel Hammerstein model*. The effectiveness of the presented modeling method is clearly demonstrated in this real application.

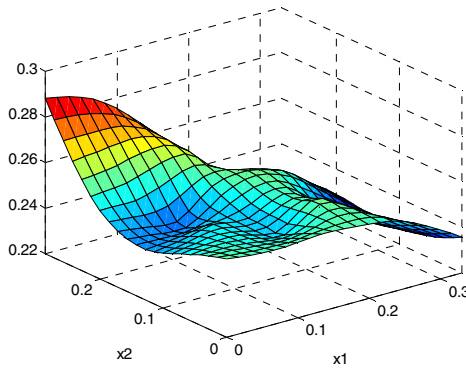


**Fig. 5.12** Snap curing oven: KL basis functions ( $i=1$ ) for multi-channel Hammerstein modeling

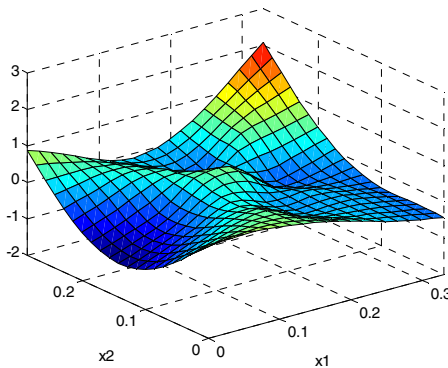


**Fig. 5.13** Snap curing oven: KL basis functions ( $i=2$ ) for multi-channel Hammerstein modeling

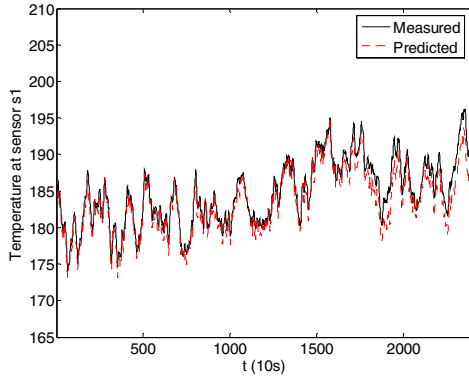


**Fig. 5.14** Snap curing oven: Performance of 3-channel Hammerstein model at sensor s1

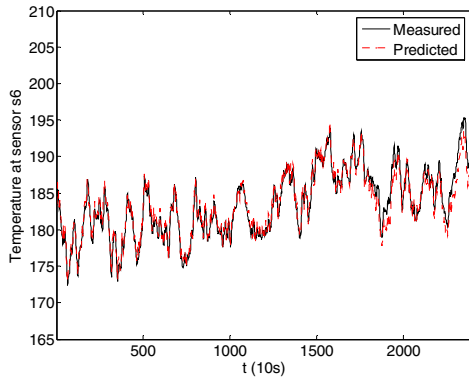


**Fig. 5.15** Snap curing oven: Performance of 3-channel Hammerstein model at sensor s6

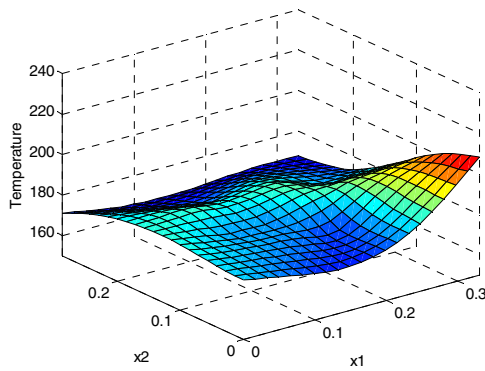


**Fig. 5.16** Snap curing oven: Predicted temperature distribution of 3-channel Hammerstein model at  $t=10000s$

**Table 5.1** Snap curing oven:  $TNAE(x)$  of Hammerstein models

	s1	s2	s3	s4	s5	s6	s7	s8
1-channel model	2.24	1.91	2.31	1.74	2.6	1.87	1.96	1.8
2-channel model	1.39	1.26	1.64	1.21	2.03	0.94	1.26	1.63
3-channel model	1.17	1.05	1.32	0.86	1.91	0.73	0.95	1.37
	s9	s10	s11	s12	s13	s14	s15	s16
1-channel model	1.51	2.26	2.6	2.16	2.08	2.59	1.62	1.97
2-channel model	1.11	1.54	1.94	1.54	0.9	1.71	1.1	1.19
3-channel model	1.01	1.35	1.75	1.43	0.75	1.5	0.94	1.05

## 5.6 Summary

A novel multi-channel spatio-temporal Hammerstein modeling approach is presented for nonlinear distributed parameter systems. The Hammerstein distributed parameter model consists of the static nonlinear and the distributed dynamical linear parts. The distributed linear part is represented by a spatio-temporal kernel, i.e., Green's function. In the single-channel Hammerstein modeling, using the Galerkin method with the expansion onto KL spatial bases and Laguerre temporal bases, the spatio-temporal modeling is reduced to a traditional temporal modeling problem. The unknown parameters can be easily estimated using the least-squares estimation and the singular value decomposition. In the presence of unmodeled dynamics, a multi-channel Hammerstein modeling approach is used which can improve the modeling performance since the single-channel Hammerstein will lead to a relatively large modeling error. This modeling method provides convergent estimates under some conditions. The simulation example and the experiment on snap curing oven are presented to show the effectiveness of this modeling method and its potential to industrial applications.

## References

- [1] Bai, E.W.: An optimal two-stage identification algorithm for Hammerstein-Wiener nonlinear systems. *Automatica* 34(3), 333–338 (1998)
- [2] Bai, E.W., Li, D.: Convergence of the iterative Hammerstein system identification algorithm. *IEEE Transactions on Automatic Control* 49(11), 1929–1940 (2004)
- [3] Campello, R.J.G.B., Favier, G., Amaral, W.C.: Optimal expansions of discrete-time Volterra models using Laguerre functions. *Automatica* 40(5), 815–822 (2004)
- [4] Chen, H.F.: Pathwise convergence of recursive identification algorithms for Hammerstein systems. *IEEE Transactions on Automatic Control* 49(10), 1641–1649 (2004)
- [5] Christofides, P.D.: Robust control of parabolic PDE systems. *Chemical Engineering Science* 53(16), 2949–2965 (1998)

- [6] Christofides, P.D.: Nonlinear and robust control of PDE systems: Methods and applications to transport-reaction processes. Birkhäuser, Boston (2001b)
- [7] Cramér, H., Leadbetter, M.R.: Stationary and related stochastic processes. Wiley, New York (1967)
- [8] Datta, K.B., Mohan, B.M.: Orthogonal functions in systems and control. World Scientific, Singapore (1995)
- [9] Eskinat, E., Johnson, S., Luyben, W.: Use of Hammerstein models in identification of nonlinear systems. *AIChE Journal* 37(2), 255–268 (1991)
- [10] Fruzzetti, K.P., Palazoglu, A., McDonald, K.A.: Nonlinear model predictive control using Hammerstein models. *Journal of Process Control* 7(1), 31–41 (1997)
- [11] Golub, G., Van Loan, C.: Matrix computations, 3rd edn. Johns Hopkins University Press, Baltimore (1996)
- [12] Gómez, J.C., Baeyens, E.: Identification of block-oriented nonlinear systems using orthonormal bases. *Journal of Process Control* 14(6), 685–697 (2004)
- [13] Greblicki, W.: Continuous-time Hammerstein system identification from sampled data. *IEEE Transactions on Automatic Control* 51(7), 1195–1200 (2006)
- [14] Heuberger, P.S.C., Van den Hof, P.M.J., Bosgra, O.H.: A generalized orthonormal basis for linear dynamical systems. *IEEE Transactions on Automatic Control* 40(3), 451–465 (1995)
- [15] Ljung, L.: Convergence analysis of parametric identification methods. *IEEE Transactions on Automatic Control* 23(5), 770–783 (1978)
- [16] Ljung, L.: System identification: Theory for the user, 2nd edn. Prentice-Hall, Englewood Cliffs (1999)
- [17] Narendra, K., Gallman, P.: An iterative method for the identification of nonlinear systems using a Hammerstein model. *IEEE Transactions on Automatic Control* 11(3), 546–550 (1966)
- [18] Park, H.M., Cho, D.H.: Low dimensional modeling of flow reactors. *International Journal of Heat and Mass Transfer* 39(16), 3311–3323 (1996a)
- [19] Park, H.M., Cho, D.H.: The use of the Karhunen-Loève decomposition for the modeling of distributed parameter systems. *Chemical Engineering Science* 51(1), 81–98 (1996b)
- [20] Sjöberg, J., Zhang, Q., Ljung, L., Benveniste, A., Delyon, B., Glorennec, P., Hjalmarsson, H., Juditsky, A.: Nonlinear black-box modeling in system identification: A unified approach. *Automatica* 31(12), 1691–1724 (1995)
- [21] Stoica, P.: On the convergence of an iterative algorithm used for Hammerstein system identification. *IEEE Transactions on Automatic Control* 26(4), 967–969 (1981)
- [22] Tanguy, N., Morvan, R., Vilbé, P., Calvez, L.C.: Online optimization of the time scale in adaptive Laguerre-based filters. *IEEE Transactions on Signal Processing* 48(4), 1184–1187 (2000)
- [23] Wahlberg, B.: System identification using Laguerre models. *IEEE Transactions on Automatic Control* 36(5), 551–562 (1991)
- [24] Wahlberg, B.: System identification using Kautz models. *IEEE Transactions on Automatic Control* 39(6), 1276–1282 (1994)
- [25] Wang, L., Cluett, W.R.: Optimal choice of time-scaling factor for linear system approximation using Laguerre models. *IEEE Transactions on Automatic Control* 39(7), 1463–1467 (1995)



- [26] Vörös, J.: Recursive identification of Hammerstein systems with discontinuous nonlinearities containing dead-zones. *IEEE Transactions on Automatic Control* 48(12), 2203–2206 (2003)
- [27] Zervos, C.C., Dumont, G.A.: Deterministic adaptive control based on Laguerre series representation. *International Journal of Control* 48(6), 2333–2359 (1988)
- [28] Zhu, Y.C.: Identification of Hammerstein models for control using ASYM. *International Journal of Control* 73(18), 1692–1702 (2000)

# 6 Spatio-Temporal Volterra Modeling for a Class of Nonlinear DPS

**Abstract.** To model the nonlinear distributed parameter system (DPS), a spatio-temporal Volterra model is presented with a series of spatio-temporal kernels. It can be considered as a nonlinear generalization of Green's function or a spatial extension of the traditional Volterra model. To obtain a low-order model, the Karhunen-Loève (KL) method is used for the time/space separation and dimension reduction. Then the model can be estimated with a least-squares algorithm with the convergence guaranteed under noisy measurements. The simulation and experiment are conducted to demonstrate the effectiveness of the presented modeling method.

## 6.1 Introduction

In general, the linear distributed parameter system (DPS) can be represented using the impulse response function (i.e., Green's function and kernel). In some cases, the Green's function can be derived from the first-principle knowledge (Butkovskiy, 1982). On the other hand, when the analytical Green's function is not available, it can be estimated from the input-output data (Gay & Ray, 1995; Zheng, Hoo & Piovoso, 2002; Zheng & Hoo, 2002, 2004; Doumanidis & Fourligkas, 2001). However, the Green's function model uses one single kernel, which can only approximate the nonlinear system around the given working condition.

In the modeling of traditional lumped parameter systems (LPS), the fading memory nonlinear system (FMNS) (Boyd & Chua, 1985) has been proposed to cover a wide range of industrial processes, whose dependence on past inputs decreases rapidly with time in large-scale range around the working point. The dynamics of the FMNS can be modeled by the Volterra series to any desired accuracy (Boyd & Chua, 1985) because Volterra series are constructed by a series of kernels, from the 1<sup>st</sup>-order, the 2<sup>nd</sup>-order, and up to the high-order kernels. Extensive research has been reported for lumped system identification and control design using the Volterra model (Schetzen, 1980; Rugh, 1981; Doyle III *et al.*, 1995; Maner *et al.*, 1996; Parker *et al.*, 2001). However, the Volterra model is only studied in LPS, because the traditional Volterra series do not have spatio-temporal nature.

Similarly, many distributed parameter processes may have the features of FMNS. In order to model unknown nonlinear distributed parameter systems, the spatio-temporal kernel-based idea from the Green's function will be expanded into the Volterra series. A spatio-temporal Volterra model can be constructed by adding the space variables into the traditional Volterra model. Thus, this kind of

spatio-temporal Volterra model should be capable to model a wide range of nonlinear DPS with stable dynamics and fading memory features. Since no feedback is involved, the Volterra model is guaranteed to be stable.

The spatio-temporal Volterra modeling approach is designed as follows. Firstly, the unknown nonlinear DPS to be estimated is expressed by a spatio-temporal Volterra model with a set of spatio-temporal kernels. In order to estimate the spatio-temporal kernels from the input-output data, each kernel is expanded onto spatial and temporal basis functions with unknown coefficients. To reduce the parametric complexity, the Karhunen-Loève (KL) method is used to find the dominant spatial basis functions and the Laguerre polynomials are selected as the temporal basis functions. Secondly, using the Galerkin method, this spatio-temporal modeling problem will turn into a temporal modeling problem. Thirdly, unknown parameters can be easily estimated using the least-squares method in the time domain. After the time/space synthesis of kernels, the spatio-temporal Volterra model can be constructed. Moreover, the state space representation of spatio-temporal Volterra model can be easily obtained. The convergent estimation can be guaranteed under certain conditions. The simulation and the experiment demonstrate the effectiveness of the presented modeling method.

This chapter is organized as follows. The spatio-temporal Volterra model is presented in Section 6.2. Section 6.3 presents the spatio-temporal Volterra modeling approach. The state space realization is provided in Section 6.4. Section 6.5 gives the convergence analysis. The simulation and the experiment are demonstrated in Section 6.6.

## 6.2 Spatio-Temporal Volterra Model

It is well known that a linear continuous DPS can be represented as a linear mapping from the input  $u(x,t)$  to the output  $y(x,t)$ , where  $x \in \Omega$  denotes space variable,  $\Omega$  is the spatial domain, and  $t$  is time. This mapping can be expressed in a Fredholm integral equation of the first kind containing a square-integrable kernel  $g$  (i.e., impulse response function or Green's function) (Butkovskiy, 1982; Gay & Ray, 1995)

$$y(x,t) = \int_{\Omega} \int_0^t g(x,\zeta,t,\tau) u(\zeta,\tau) d\tau d\zeta. \quad (6.1)$$

On the other hand, a lumped parameter system

$$y(t) = N(\{u(\tau)\}) + d(t),$$

where  $\{u(\tau)\} = \{u(\tau) | \tau = 1, \dots, t\}$  is the input,  $t$  is the discretized time instant,  $y$  and  $d$  are the output and the stochastic disturbance, and  $N$  is an operator with the fading memory feature, can be approximated by a discrete-time Volterra model (Boyd & Chua, 1985)

$$y(t) = \sum_{r=1}^{\infty} \sum_{\tau_1=0}^t \cdots \sum_{\tau_r=0}^t g_r(t, \tau_1, \dots, \tau_r) \prod_{v=1}^r u(\tau_v), \quad (6.2)$$

where  $g_r$  is the  $r^{\text{th}}$ -order temporal kernel.

Motivated by (6.1) and (6.2), for a distributed parameter system

$$y(x, t) = N(\{u(\zeta, \tau)\}) + d(x, t), \quad (6.3)$$

where  $\{u(\zeta, \tau)\} = \{u(\zeta, \tau) \mid \zeta \in \Omega, \tau = 1, \dots, t\}$  is the input, a **spatio-temporal Volterra model** is constructed by adding the space variables into the traditional Volterra model

$$y(x, t) = \sum_{r=1}^{\infty} \int_{\Omega} \cdots \int_{\Omega} \sum_{\tau_1=0}^t \cdots \sum_{\tau_r=0}^t g_r(x, \zeta_1, \dots, \zeta_r, t, \tau_1, \dots, \tau_r) \prod_{v=1}^r u(\zeta_v, \tau_v) d\zeta_v, \quad (6.4)$$

where  $g_r$  is the  $r$ th-order spatio-temporal Volterra kernel, which denotes the influence of the input at the location  $\zeta_1, \dots, \zeta_r$  and the time  $\tau_1, \dots, \tau_r$  on the output at the location  $x$  and the time  $t$ . For easy understanding, the integral operator is used for the spatial operation and the sum operator for the temporal operation. Similar to (6.1), it is reasonable that the time/space variables in (6.4) are symmetrical. Obviously, the Green's function model is a first-order spatio-temporal Volterra model, and the kernels of the spatio-temporal Volterra model can be seen as the high-dimensional generalizations of the Green's function. Actually, the form of spatio-temporal Volterra model (6.4) can be derived for the DPS using Taylor expansion as traditional Volterra series derivation (Rugh, 1981), which is not included here for simplicity.

The model (6.4) can work for both the time-varying and the time-invariant systems. For the time-invariant system, the kernel will be invariant and represented as follows

$$g_r(x, \zeta_1, \dots, \zeta_r, t, \tau_1, \dots, \tau_r) = g_r(x, \zeta_1, \dots, \zeta_r, t - \tau_1, \dots, t - \tau_r). \quad (6.5)$$

Similarly the model (6.4) can also work for the space-varying or space-invariant system. When the model is homogeneous in the space domain, there exists

$$g_r(x, \zeta_1, \dots, \zeta_r, t, \tau_1, \dots, \tau_r) = g_r(x - \zeta_1, \dots, x - \zeta_r, t, \tau_1, \dots, \tau_r). \quad (6.6)$$

In this study, we only consider the time-invariant and space-varying case (6.5) since it is very common in the real applications. Substituting (6.5) into (6.4) will have the following expression

$$y(x, t) = \sum_{r=1}^{\infty} \int_{\Omega} \cdots \int_{\Omega} \sum_{\tau_1=0}^t \cdots \sum_{\tau_r=0}^t g_r(x, \zeta_1, \dots, \zeta_r, \tau_1, \dots, \tau_r) \prod_{v=1}^r u(\zeta_v, t - \tau_v) d\zeta_v. \quad (6.7)$$

The model (6.7) is still not applicable because of its infinite-order. In practice, the higher order terms can be neglected and only the first  $R$  kernels need to be taken into account as below

$$y(x, t) = \sum_{r=1}^R \int_{\Omega} \cdots \int_{\Omega} \sum_{\tau_1=0}^t \cdots \sum_{\tau_r=0}^t g_r(x, \zeta_1, \dots, \zeta_r, \tau_1, \dots, \tau_r) \prod_{v=1}^r u(\zeta_v, t - \tau_v) d\zeta_v + v(x, t), \quad (6.8)$$

where the error term  $v(x, t)$  includes unmodeled dynamics and external noise. The modeling accuracy and the model complexity can be controlled by the order  $R$ .

### 6.3 Spatio-Temporal Modeling Approach

Now the problem is to estimate a spatio-temporal Volterra model (6.8) from a set of spatio-temporal input-output data  $\{u(x,t) \mid x \in \Omega, t = 1, \dots, n_t\}$ ,  $\{y(x_j, t) \mid x_j \in \Omega, j = 1, \dots, n_y, t = 1, \dots, n_t\}$ , where  $n_t$  denotes the time length and  $n_y$  is the number of sampled spatial points of the output. For simplicity, it is assumed that the spatial information of the input is known from some physical knowledge and the locations  $x_j$  ( $j = 1, \dots, n_y$ ) are uniformly distributed over the spatial domain. In order to achieve a good modeling performance, the order  $R$  can be determined in an incremental way using the cross-validation technique or some optimization methods. Once the order is determined, the next problem is to estimate the kernels. The main difficulty comes from the time/space coupling of kernels.

Using a simple time/space discretization for kernels  $g_r(x, \zeta_1, \dots, \zeta_r, \tau_1, \dots, \tau_r)$ , ( $r = 1, \dots, R$ ) will lead to a large amount of parameters to be estimated. However, it is important to reduce the parametric complexity, improve the numerical condition and decrease the variance of the estimated parameters. This can be done using the time/space method, i.e., expanding the kernels in terms of a relatively small number of orthonormal basis functions such as KL spatial bases and Laguerre temporal bases. After the time/space separation, the original spatio-temporal problem will turn to the traditional temporal modeling problem. Thus, the unknown parameters can be easily estimated in the temporal domain. Finally, the spatio-temporal Volterra model can be reconstructed using the time/space synthesis. The modeling idea is shown in Figure 6.1. The time/space separation and synthesis are very critical for this identification approach, which are the key differences from the traditional Volterra modeling.

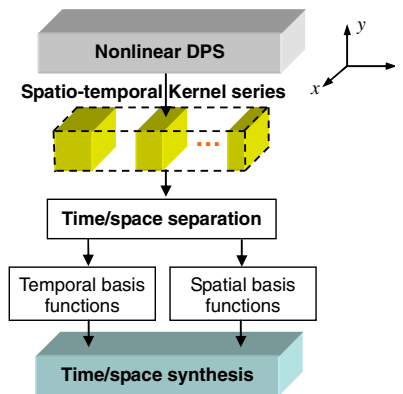


Fig. 6.1 Spatio-temporal Volterra modeling approach

### 6.3.1 Time/Space Separation

For simplicity, the input  $u(x,t)$  is assumed to have a finite-dimensional freedom since only a finite number of actuators are available in practice. Therefore the input  $u(x,t)$  can be formulated in terms of a finite number of spatial input basis functions  $\{\psi_i(x)\}_{i=1}^m$

$$u(x,t) = \sum_{i=1}^m \psi_i(x) a_i(t), \quad (6.9)$$

where  $a_i(t) = \int_{\Omega} u(x,t) \psi_i(x) dx$  is the time coefficient (input signal) and  $m$  is the number of actuators. Ideally, the output  $y(x,t)$  and the error  $v(x,t)$  can be expressed by an infinite set of orthonormal spatial output basis functions  $\{\varphi_i(x)\}_{i=1}^{\infty}$

$$y(x,t) = \sum_{i=1}^{\infty} \varphi_i(x) b_i(t), \quad (6.10)$$

$$v(x,t) = \sum_{i=1}^{\infty} \varphi_i(x) v_i(t), \quad (6.11)$$

where  $b_i(t) = \int_{\Omega} y(x,t) \varphi_i(x) dx$  and  $v_i(t) = \int_{\Omega} v(x,t) \varphi_i(x) dx$  are the time coefficients of the output and error respectively. This is because of the inherently infinite-dimensional characteristic of the DPS. Practically, for most of parabolic systems, both output  $y(x,t)$  and error  $v(x,t)$  can be truncated into  $n$  dimensions as below

$$y_n(x,t) = \sum_{i=1}^n \varphi_i(x) b_i(t), \quad (6.12)$$

$$v_n(x,t) = \sum_{i=1}^n \varphi_i(x) v_i(t). \quad (6.13)$$

The dimension  $n$  will be dependent on how the eigenspectrum of the DPS is separated into slow and fast modes, the type of spatial basis functions and the required modeling accuracy. For convenience, define  $\mathbf{a}(t) = [a_1(t), \dots, a_m(t)]^T \in \mathbb{R}^m$ ,  $\mathbf{b}(t) = [b_1(t), \dots, b_n(t)]^T \in \mathbb{R}^n$  and  $\mathbf{v}(t) = [v_1(t), \dots, v_n(t)]^T \in \mathbb{R}^n$ .

Assuming that the kernels in (6.8) are absolutely integrable on the time domain  $[0, \infty)$  at any spatial point  $x$  and  $\zeta$ , which means that the corresponding spatio-temporal Volterra model is stable, then they can be represented by means of orthonormal temporal basis functions. The kernels are supposed to be expanded onto input bases  $\{\psi_i(x)\}_{i=1}^m$ , output bases  $\{\varphi_i(x)\}_{i=1}^n$  and temporal bases  $\{\phi_i(t)\}_{i=1}^q$

$$g_r(\cdot) = \sum_{i=1}^n \sum_{j_1=1}^m \cdots \sum_{j_r=1}^m \sum_{k_1=1}^q \cdots \sum_{k_r=1}^q \theta_{ij_1 \dots j_r k_1 \dots k_r}^{(r)}(\varphi_i(x) \prod_{v=1}^r \psi_{j_v}(\zeta_v) \phi_{k_v}(\tau_v)), \quad (6.14)$$

where  $\theta_{j_1 \dots j_r, k_1 \dots k_r}^{(r)}$  is the corresponding constant coefficient of the  $r^{\text{th}}$ -order kernel onto output bases  $\varphi_i(x)$ , input bases  $\psi_{j_1}(\zeta_1), \dots, \psi_{j_r}(\zeta_r)$  and temporal bases  $\phi_{k_1}(\tau_1), \dots, \phi_{k_r}(\tau_r)$ ,  $n$  is the dimension of output bases and  $q$  is the dimension of temporal bases. Theoretically, both  $n$  and  $q$  should be infinite for the DPS. Practically, for most of parabolic systems, finite  $n$  and  $q$  are often enough for a realistic approximation. Obviously they are affected by the required modeling accuracy. On the other hand,  $n$  is also dependent on the slow/fast eigenspectrum of the DPS and the type of spatial basis functions; and  $q$  is also related to the complexity of the system dynamics.

### *Selection of basis functions*

The choice of basis functions will have a significant effect on the modeling performance, and the selections are summarized as follows.

(1)  $\varphi_i(x)$  is usually selected as standard orthonormal functions such as Fourier series, Legendre polynomials, Jacobi polynomials and Chebyshev polynomials (Datta & Mohan, 1995). In this study, the KL method (Park & Cho, 1996a, 1996b) is chosen to identify the empirical spatial basis functions from the representative process data because fewer parameters need to be estimated in the Volterra modeling. Usually, the “energy method” is used to determine the small value of  $n$ . See Section 3.4 for more details.

(2)  $\psi_i(x)$  is often determined from some physical knowledge, which describes the distribution of the control action  $a_i(t)$  in the spatial domain  $\Omega$ .

(3)  $\phi_i(t)$  is often chosen as Laguerre function, Kautz function (Wahlberg, 1991; Wahlberg, 1994; Wahlberg & Mäkilä, 1996) or generalized orthonormal basis function (Heuberger, Van den Hof, & Bosgra, 1995). Here, Laguerre function is chosen for the development, because of its simplicity, and robustness to the sampling interval and the model dimension (Wahlberg, 1991). Laguerre functions are defined as a functional series (Zervos & Dumont, 1988)

$$\phi_i(t) \triangleq \sqrt{2p} \frac{e^{pt}}{(i-1)!} \cdot \frac{d^{i-1}}{dt^{i-1}} [t^{i-1} \cdot e^{-2pt}], \quad i=1, 2, \dots, \infty, \quad p > 0, \quad (6.15)$$

where  $p$  is the time-scaling factor, and  $t \in [0, \infty)$  is a time variable. The Laplace transform of the  $i^{\text{th}}$  Laguerre function is given by

$$\phi_i(s) = \sqrt{2p} \frac{(s-p)^{i-1}}{(s+p)^i}, \quad i=1, 2, \dots, \infty, \quad p > 0. \quad (6.16)$$

Laguerre functions (6.15) and (6.16) form a complete orthonormal basis in the function space  $L_2(0, \infty)$  and  $H_2(C_+)$  respectively.

### 6.3.2 Temporal Modeling Problem

Substitution of (6.9) and (6.12)-(6.14) into (6.8) will have

$$\begin{aligned} \sum_{h=1}^n \varphi_h(x) b_h(t) &= \sum_{r=1}^R \int_{\Omega} \cdots \int_{\Omega} \sum_{\tau_1=0}^t \cdots \sum_{\tau_r=0}^t \sum_{i=1}^n \sum_{j_1=1}^m \cdots \sum_{j_r=1}^m \sum_{k_1=1}^q \cdots \sum_{k_r=1}^q \theta_{ij_1 \dots j_r k_1 \dots k_r}^{(r)} \\ &\quad \times \varphi_i(x) \prod_{v=1}^r \psi_{j_v}(\zeta_v) \phi_{k_v}(\tau_v) \sum_{w_v=1}^m \psi_{w_v}(\zeta_v) a_{w_v}(t - \tau_v) d\zeta_v + \sum_{h=1}^n \varphi_h(x) v_h(t). \end{aligned} \quad (6.17)$$

Equation (6.17) can be further simplified into

$$\begin{aligned} \sum_{h=1}^n \varphi_h(x) b_h(t) &= \sum_{r=1}^R \sum_{i=1}^n \varphi_i(x) \sum_{j_1=1}^m \cdots \sum_{j_r=1}^m \sum_{k_1=1}^q \cdots \sum_{k_r=1}^q \theta_{ij_1 \dots j_r k_1 \dots k_r}^{(r)} \prod_{v=1}^r \sum_{w_v=1}^m \psi_{j_v w_v} l_{k_v w_v}(t) \\ &\quad + \sum_{h=1}^n \varphi_h(x) v_h(t). \end{aligned} \quad (6.18)$$

where

$$\psi_{jw} = \int_{\Omega} \psi_j(\zeta) \psi_w(\zeta) d\zeta, \quad (6.19)$$

$$l_{kw}(t) = \sum_{\tau=0}^t \phi_k(\tau) a_w(t - \tau). \quad (6.20)$$

Using the Galerkin method (Christofides, 2001b), projecting (6.18) onto the output basis functions  $\varphi_{h_1}(x)$  ( $h_1 = 1, \dots, n$ ) will lead to the following expression

$$\begin{aligned} \int_{\Omega} \varphi_{h_1}(x) \sum_{h_2=1}^n \varphi_{h_2}(x) b_{h_2}(t) dx &= \sum_{r=1}^R \sum_{i=1}^n \int_{\Omega} \varphi_{h_1}(x) \varphi_i(x) dx \sum_{j_1=1}^m \cdots \sum_{j_r=1}^m \sum_{k_1=1}^q \cdots \sum_{k_r=1}^q \theta_{ij_1 \dots j_r k_1 \dots k_r}^{(r)} \\ &\quad \times \prod_{v=1}^r \sum_{w_v=1}^m \psi_{j_v w_v} l_{k_v w_v}(t) + \sum_{i=1}^n \int_{\Omega} \varphi_{h_1}(x) \varphi_i(x) dx v_i(t). \end{aligned}$$

Re-arranging the order of integration and summation, it becomes

$$\begin{aligned} \sum_{h_2=1}^n \varphi_{h_1 h_2} b_{h_2}(t) &= \sum_{r=1}^R \sum_{i=1}^n \varphi_{h_1 i} \sum_{j_1=1}^m \cdots \sum_{j_r=1}^m \sum_{k_1=1}^q \cdots \sum_{k_r=1}^q \theta_{ij_1 \dots j_r k_1 \dots k_r}^{(r)} \prod_{v=1}^r \sum_{w_v=1}^m \psi_{j_v w_v} l_{k_v w_v}(t) \\ &\quad + \sum_{i=1}^n \varphi_{h_1 i} v_i(t). \end{aligned} \quad (6.21)$$

where  $\varphi_{h_1 h_2} = \int_{\Omega} \varphi_{h_1}(x) \varphi_{h_2}(x) dx$ .

Since the matrix  $\{\varphi_{h_1 h_2}\}$  is invertible due to the orthonormal bases, the following expression can be derived from (6.21).

$$\mathbf{b}(t) = \sum_{r=1}^R \sum_{j_1=1}^m \cdots \sum_{j_r=1}^m \sum_{k_1=1}^q \cdots \sum_{k_r=1}^q \theta_{j_1 \dots j_r k_1 \dots k_r}^{(r)} \prod_{v=1}^r \sum_{w_v=1}^m \psi_{j_v w_v} l_{k_v w_v}(t) + \mathbf{v}(t). \quad (6.22)$$

where



$$\boldsymbol{\theta}_{j_1 \dots j_r}^{(r)} = [\boldsymbol{\theta}_{1j_1 \dots j_r}^{(r)}, \dots, \boldsymbol{\theta}_{n_{j_1 \dots j_r}^{(r)}}^{(r)}]^T \in \mathbb{R}^n. \quad (6.23)$$

### 6.3.3 Parameter Estimation

Equation (6.22) can be expressed in a linear regression form

$$\mathbf{b}(t) = \boldsymbol{\Theta}^T \boldsymbol{\Phi}(t) + \mathbf{v}(t), \quad (6.24)$$

where

$$\boldsymbol{\Theta} = [\boldsymbol{\Theta}^{(1)}, \boldsymbol{\Theta}^{(2)}, \dots, \boldsymbol{\Theta}^{(R)}]^T \in \mathbb{R}^{(mq + \dots + m^R q^R) \times n}, \quad (6.25)$$

$$\boldsymbol{\Phi} = [\boldsymbol{\Phi}^{(1)}, \boldsymbol{\Phi}^{(2)}, \dots, \boldsymbol{\Phi}^{(R)}]^T \in \mathbb{R}^{mq + \dots + m^R q^R}, \quad (6.26)$$

and

$$\boldsymbol{\Theta}^{(r)} = [\boldsymbol{\theta}_{1 \dots 11 \dots 1}^{(r)} \dots \boldsymbol{\theta}_{m \dots m q \dots q}^{(r)}] \in \mathbb{R}^{n \times m^r q^r},$$

$$\boldsymbol{\Phi}^{(r)} = [I_{1 \dots 11 \dots 1}^{(r)} \dots I_{m \dots m q \dots q}^{(r)}] \in \mathbb{R}^{m^r q^r},$$

$$I_{j_1 \dots j_r}^{(r)}(t) = \prod_{v=1}^r \sum_{w_v=1}^m \psi_{j_v w_v} l_{k_v w_v}(t) \in \mathbb{R}.$$

In practice,  $u$  and  $y$  are uniformly sampled over the spatial domain. In this case,  $\mathbf{a}$  and  $\mathbf{b}$  can also be computed from the pointwise data using spline interpolation in the spatial domain. Then,  $\boldsymbol{\Phi}(t)$  can be constructed from  $\mathbf{a}$ .

Now considering the  $n_t$  set of temporal data  $\{\mathbf{a}(t) \mid t = 1, \dots, n_t\}$ ,  $\{\mathbf{b}(t) \mid t = 1, \dots, n_t\}$ , it is well known from (Ljung, 1999) that by minimizing a quadratic criterion of the prediction errors

$$\hat{\boldsymbol{\Theta}} = \arg \min_{\boldsymbol{\Theta}} \left\{ \frac{1}{n_t} \sum_{t=1}^{n_t} \|\mathbf{b}(t) - \boldsymbol{\Theta}^T \boldsymbol{\Phi}(t)\|^2 \right\}, \quad (6.27)$$

where  $\|\mathbf{f}(t)\|^2 = \mathbf{f}^T(t) \mathbf{f}(t)$ ,  $\boldsymbol{\Theta}$  can be estimated using the least-squares method as follows

$$\hat{\boldsymbol{\Theta}} = \left( \frac{1}{n_t} \sum_{t=1}^{n_t} \boldsymbol{\Phi}(t) \boldsymbol{\Phi}^T(t) \right)^{-1} \left( \frac{1}{n_t} \sum_{t=1}^{n_t} \boldsymbol{\Phi}(t) \mathbf{b}^T(t) \right), \quad (6.28)$$

provided that the indicated inverse exists. This condition can be guaranteed when using persistently exciting input.

After the kernels in (6.14) are reconstructed using the time/space synthesis from the estimated parameters  $\hat{\boldsymbol{\Theta}}$ , the spatio-temporal Volterra model can be obtained from (6.8).

## 6.4 State Space Realization

The spatio-temporal Volterra model (6.8) can also be transformed into a state space form. The Laguerre network representation of the realization procedure is shown in Figure 6.2, where the transfer functions

$$G_1(s) = \frac{\sqrt{2p}}{s+p}, G_2(s) = \dots = G_q(s) = \frac{s-p}{s+p},$$

can be derived from (6.16), and  $p$  is the time-scaling factor.

The variable  $l_{kw}(t)$  in (6.20) is defined as the state. It can be shown that the state satisfies the following difference equations (Zervos & Dumont, 1988)

$$\mathbf{L}_w(t+1) = \mathbf{K}_w \mathbf{L}_w(t) + \mathbf{H}_w a_w(t), \quad w=1, \dots, m.$$

where  $\mathbf{L}_w(t) = [l_{1w}, \dots, l_{qw}]^T \in \mathbb{R}^q$ , the matrices  $\mathbf{K}_w \in \mathbb{R}^{q \times q}$  and  $\mathbf{H}_w \in \mathbb{R}^q$  are defined in the following. If  $\Delta t$  is the sampling period and

$$\eta_1 = e^{-p\Delta t}, \eta_2 = \Delta t + \frac{2}{p}(e^{-p\Delta t} - 1), \eta_3 = -\Delta t e^{-p\Delta t} - \frac{2}{p}(e^{-p\Delta t} - 1), \eta_4 = \sqrt{2p} \frac{(1 - e^{-p\Delta t})}{p},$$

then

$$\mathbf{K}_w = \begin{bmatrix} \eta_1 & 0 & \dots & 0 \\ \frac{-\eta_1 \eta_2 - \eta_3}{\Delta t} & \eta_1 & \dots & 0 \\ \vdots & \vdots & \ddots & \vdots \\ \frac{(-1)^{q-1} \eta_2^{q-2} (\eta_1 \eta_2 + \eta_3)}{\Delta t^{q-1}} & \dots & \frac{-(\eta_1 \eta_2 + \eta_3)}{\Delta t} & \eta_1 \end{bmatrix},$$

and

$$\mathbf{H}_w^T = [\eta_4, \quad (-\eta_2 / \Delta t) \eta_4, \quad \dots, \quad (-\eta_2 / \Delta t)^{q-1} \eta_4].$$

Finally, the state equation can be written as

$$\mathbf{L}(t+1) = \mathbf{K} \mathbf{L}(t) + \mathbf{H} a(t), \quad (6.29)$$

where  $\mathbf{L}(t) = [\mathbf{L}_1^T, \dots, \mathbf{L}_m^T]^T \in \mathbb{R}^{mq}$ ,  $\mathbf{K} = \text{diag}(\mathbf{K}_w) \in \mathbb{R}^{mq \times mq}$  and  $\mathbf{H} = \text{diag}(\mathbf{H}_w) \in \mathbb{R}^{mq \times m}$ .

The output equation can be derived as follows. Using (6.18), the model output is given by

$$\begin{aligned} y_n(x, t) &= \sum_{i=1}^n \sum_{j_1=1}^m \sum_{k_1=1}^q \varphi_i(x) \theta_{ij_1 k_1}^{(1)} \sum_{w_1=1}^m \psi_{j_1 w_1} l_{k_1 w_1}(t) + \sum_{i=1}^n \sum_{j_1=1}^m \sum_{j_2=1}^m \sum_{k_1=1}^q \sum_{k_2=1}^q \varphi_i(x) \theta_{ij_1 j_2 k_1 k_2}^{(2)} \\ &\quad \times \sum_{w_1=1}^m \sum_{w_2=1}^m \psi_{j_1 w_1} \psi_{j_2 w_2} l_{k_1 w_1}(t) l_{k_2 w_2}(t) + \dots \end{aligned}$$

Define  $c_{k_1 w_1}(x) = \sum_{i=1}^n \sum_{j_1=1}^m \varphi_i(x) \theta_{ij_1 k_1}^{(1)} \psi_{j_1 w_1}$  and  $d_{k_1 k_2 w_1 w_2}(x) = \sum_{i=1}^n \sum_{j_1=1}^m \sum_{j_2=1}^m \varphi_i(x) \theta_{ij_1 j_2 k_1 k_2}^{(2)} \psi_{j_1 w_1} \psi_{j_2 w_2}$ ,

we have

$$y_n(x, t) = \sum_{w_1=1}^m \sum_{k_1=1}^q c_{k_1 w_1}(x) l_{k_1 w_1}(t) + \sum_{w_1=1}^m \sum_{w_2=1}^m \sum_{k_1=1}^q \sum_{k_2=1}^q d_{k_1 k_2 w_1 w_2}(x) l_{k_1 w_1}(t) l_{k_2 w_2}(t) + \dots$$

Define

$$C_{w_1}(x) = \begin{bmatrix} c_{1w_1} \\ \vdots \\ c_{qw_1} \end{bmatrix}, D_{w_1 w_2}(x) = \begin{bmatrix} d_{11w_1 w_2} & \dots & d_{1qw_1 w_2} \\ \vdots & \ddots & \vdots \\ d_{q1w_1 w_2} & \dots & d_{qqw_1 w_2} \end{bmatrix},$$

then we have

$$y_n(x, t) = \sum_{w_1=1}^m [C_{w_1}(x)^T L_{w_1}(t) + \sum_{w_2=1}^m L_{w_1}(t)^T D_{w_1 w_2}(x) L_{w_2}(t)] + \dots \tag{6.30}$$

Finally, the output equation (6.30) can be further written in a simpler matrix form

$$y_n(x, t) = C(x)^T L(t) + L(t)^T D(x) L(t) + \dots, \tag{6.31}$$

where the spatial matrices  $C(x)$  and  $D(x)$  are given by

$$C(x) = \begin{bmatrix} C_1 \\ \vdots \\ C_m \end{bmatrix}, D(x) = \begin{bmatrix} D_{11} & \dots & D_{1m} \\ \vdots & \ddots & \vdots \\ D_{m1} & \dots & D_{mm} \end{bmatrix}.$$

It can be seen from (6.29) and (6.31) that the spatio-temporal Volterra model can be transformed into a spatio-temporal Wiener model in a state space form. Based on the state space model or original spatio-temporal Volterra model, traditional lumped controller design approaches such as model predictive control (Wang, 2004) and adaptive control (Zervos & Dumont, 1988) can be applied to the DPS.

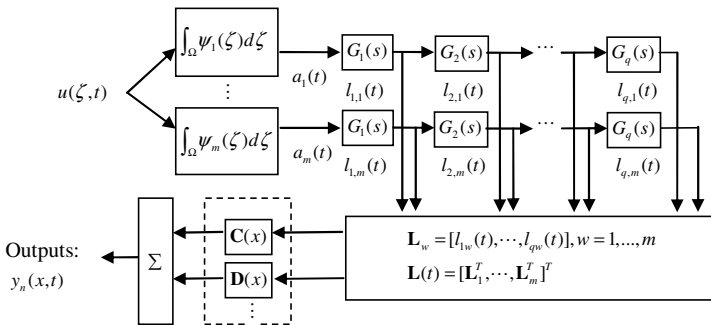


Fig. 6.2 Laguerre network for state space realization of Volterra model

## 6.5 Convergence Analysis

For simplicity, let  $y_n(x, t) = V(x, t, \boldsymbol{\theta}, \{u(\zeta, \tau)\})$  denote a finite-order spatio-temporal Volterra model with  $R, n, q < \infty$

$$y_n(x, t) = \sum_{r=1}^R \int_{\Omega} \cdots \int_{\Omega} \sum_{\tau_1=0}^t \cdots \sum_{\tau_r=0}^t \sum_{i=1}^n \sum_{j_1=1}^m \cdots \sum_{j_r=1}^m \sum_{k_1=1}^q \cdots \sum_{k_r=1}^q \boldsymbol{\theta}_{j_1 \dots j_r k_1 \dots k_r}^{(r)} \times \varphi_i(x) \prod_{v=1}^r \psi_{j_v}(\zeta_v) \phi_{k_v}(\tau_v) u(\zeta_v, \tau_v) d\zeta_v, \quad (6.32)$$

where the parameter matrix  $\boldsymbol{\theta}$  is defined by (6.25).

Because the functions  $\{\psi_i(x)\}_{i=1}^m$ ,  $\{\varphi_i(x)\}_{i=1}^n$  and  $\{\phi_i(t)\}_{i=1}^q$  are basis functions, the spatio-temporal Volterra model structure  $y_n(x, t) = V(x, t, \boldsymbol{\theta}, \{u(\zeta, \tau)\})$  is identifiable, i.e.,

$$V(x, t, \boldsymbol{\theta}_1, \{u(\zeta, \tau)\}) = V(x, t, \boldsymbol{\theta}_2, \{u(\zeta, \tau)\}) \Rightarrow \boldsymbol{\theta}_1 = \boldsymbol{\theta}_2.$$

The convergence of the parameters and the model will be discussed below.

Based on the approximation result of Volterra series (Boyd & Chua, 1985) for traditional nonlinear processes, a nonlinear time-invariant DPS with the fading memory feature can also be approximated by a finite-order spatio-temporal Volterra model.

For a nonlinear time-invariant DPS  $y(x, t) = N(\{u(\zeta, \tau)\}) + d(x, t)$  with the fading memory feature on the input set  $U$ , and a finite-order spatio-temporal Volterra model  $y_n(x, t) = V(x, t, \boldsymbol{\theta}, \{u(\zeta, \tau)\})$  with  $R, n, q < \infty, \forall \delta > 0$ , we always assume that there exists a nonempty parameter set

$$D_{\theta} = \{\boldsymbol{\theta} \mid y(x, t) - V(x, t, \boldsymbol{\theta}, \{u(\zeta, \tau)\}) \leq \delta, \forall u \in U\}.$$

Then there is an optimal model

$$y_n^*(x, t) = V(x, t, \boldsymbol{\theta}^*, \{u(\zeta, \tau)\}), \quad (6.33)$$

with an optimal parameter matrix  $\boldsymbol{\theta}^*$  such that

$$\boldsymbol{\theta}^* = \arg \min_{\boldsymbol{\theta} \in D_{\theta}} \{\bar{E}(y(x, t) - V(x, t, \boldsymbol{\theta}, \{u(\zeta, \tau)\}))^2\}, \quad (6.34)$$

where  $\bar{E}f(x, t)^2 = \lim_{n_y \rightarrow \infty} \frac{1}{n_y} \sum_{i=1}^{n_y} \frac{1}{A} \int_{\Omega} Ef(x, t)^2 dx$ ,  $A = \int_{\Omega} dx$  and  $E$  is an expectation operator.

Under the uniform spatial discretization,  $\frac{1}{A} \sum_{i=1}^{\infty} b_i(t)^2 = \frac{1}{A} \int_{\Omega} y(x, t)^2 dx$  can be replaced by  $\frac{1}{n_y} \sum_{j=1}^{n_y} y(x_j, t)^2$ . Therefore, according to the details of the identification

algorithm developed in Section 6.3, the minimization problem (6.27) is indeed equivalent to the following problem

$$\hat{\boldsymbol{\theta}} = \arg \min_{\boldsymbol{\theta} \in D_{\boldsymbol{\theta}}} \left\{ \frac{1}{n_x} \frac{1}{n_y} \sum_{t=1}^{n_t} \sum_{j=1}^{n_y} (y(x_j, t) - V(x_j, t, \boldsymbol{\theta}, \{u(\zeta, \tau)\}))^2 \right\}. \quad (6.35)$$

It should be mentioned that the algorithm (6.27) can be considered as a practical implementation of (6.35) in order to reduce the involved spatial complexity. However, the theoretical analysis should be performed in the spatio-temporal domain.

**Assumption 6.1:**

For  $y(x, t) = N(\{u(\zeta, \tau)\}) + d(x, t)$ , let  $W(x, t)$  be the  $\sigma$ -algebra generated by  $(d(x, t), \dots, d(x, 0))$ . For each  $t, \tau$  ( $t \geq \tau$ ) and any  $x, \zeta \in \Omega$ , there exist random variables  $y_{\tau}^0(x, t)$  ( $y_{\tau}^0(x, t) = 0$ ),  $u_{\tau}^0(\zeta, t)$  ( $u_{\tau}^0(\zeta, t) = 0$ ) that belong to  $W(x, t)$  but are independent of  $W(x, \tau)$ , such that

$$E |y(x, t) - y_{\tau}^0(x, t)|^4 < M \lambda^{t-\tau},$$

$$E |u(\zeta, t) - u_{\tau}^0(\zeta, t)|^4 < M \lambda^{t-\tau},$$

for some  $M < \infty$ ,  $\lambda < 1$ .

**Assumption 6.2:**

Assume that the model  $y_n(x, t) = V(x, t, \boldsymbol{\theta}, \{u(\zeta, \tau)\})$  is differentiable with respect to  $\boldsymbol{\theta}$  for all  $\boldsymbol{\theta} \in D_{\boldsymbol{\theta}}$ . Let  $D_{\boldsymbol{\theta}}$  be compact. Assume that

$$|V(x, t, \boldsymbol{\theta}, \{u_1(\zeta, \tau)\}) - V(x, t, \boldsymbol{\theta}, \{u_2(\zeta, \tau)\})| \leq M \sum_{\tau=0}^t \lambda^{t-\tau} \sup_{\zeta \in \Omega} |u_1(\zeta, \tau) - u_2(\zeta, \tau)|,$$

$$\left| \frac{\partial V(x, t, \boldsymbol{\theta}, \{u_1(\zeta, \tau)\})}{\partial \boldsymbol{\theta}} - \frac{\partial V(x, t, \boldsymbol{\theta}, \{u_2(\zeta, \tau)\})}{\partial \boldsymbol{\theta}} \right| \leq M \sum_{\tau=0}^t \lambda^{t-\tau} \sup_{\zeta \in \Omega} |u_1(\zeta, \tau) - u_2(\zeta, \tau)|,$$

and  $|V(x, t, \boldsymbol{\theta}, \{0(\zeta, \tau)\})| \leq M$ , where  $\boldsymbol{\theta}$  belongs to an open neighborhood of  $D_{\boldsymbol{\theta}}$ ,  $M < \infty$  and  $\lambda < 1$ .

**Assumption 6.3:**

Define  $\varepsilon(x, t, \boldsymbol{\theta}) = y(x, t) - V(x, t, \boldsymbol{\theta}, \{u(\zeta, \tau)\})$  and there exists

$$\left| \frac{\partial \varepsilon(x, t, \boldsymbol{\theta})^2}{\partial \boldsymbol{\theta}} \right| \leq M \varepsilon(x, t, \boldsymbol{\theta})^2, \quad \boldsymbol{\theta} \in D_{\boldsymbol{\theta}}, \quad \forall x \in \Omega, \quad \forall t.$$

**Theorem 6.1:**

For a nonlinear time-invariant DPS  $y(x, t) = N(\{u(\zeta, \tau)\}) + d(x, t)$  with the fading memory feature, let  $\hat{y}_n(x, t) = V(x, t, \hat{\boldsymbol{\theta}}, \{u(\zeta, \tau)\})$  be the spatio-temporal Volterra model where  $\hat{\boldsymbol{\theta}}$  is estimated using (6.27). If **Assumption 6.1**, **Assumption 6.2** and

**Assumption 6.3** are satisfied, then  $\hat{\boldsymbol{\theta}} \rightarrow \boldsymbol{\theta}^*$  and  $\hat{y}_n(x, t) \rightarrow y_n^*(x, t)$  w. p. 1 as  $n_t \rightarrow \infty$  and  $n_y \rightarrow \infty$ , where  $\boldsymbol{\theta}^*$  and  $y_n^*(x, t)$  are given by (6.34) and (6.33). ■

**Proof:**

In order to obtain the convergence with probability 1, the **Lemma 5.2**, which is the direct extension of the previous work (**Cramér & Leadbetter, 1967; Ljung, 1978**), is needed in the proof of **Theorem 6.1**.

We now turn to the proof of **Theorem 6.1**. Since  $V(x, t, \boldsymbol{\theta}, \{u(\zeta, \tau)\})$  is continuous with respect to  $\boldsymbol{\theta}$ , the convergence of parameters

$$\hat{\boldsymbol{\theta}} \rightarrow \boldsymbol{\theta}^*, \text{ w. p. 1 as } n_t \rightarrow \infty, n_y \rightarrow \infty, \quad (6.36)$$

naturally leads to the convergence of the model to its optimum

$$\hat{y}_n(x, t) \rightarrow y_n^*(x, t), \text{ w. p. 1 as } n_t \rightarrow \infty, n_y \rightarrow \infty.$$

Define

$$Q_{n_y, n_t}(\boldsymbol{\theta}) = \frac{1}{n_y} \sum_{j=1}^{n_y} \left\{ \frac{1}{n_t} \sum_{t=1}^{n_t} \mathcal{E}(x_j, t, \boldsymbol{\theta})^2 \right\}.$$

As defined in (6.34),  $\boldsymbol{\theta}^*$  minimizes

$$\bar{E}(y(x, t) - V(x, t, \boldsymbol{\theta}, \{u(\zeta, \tau)\}))^2 = \lim_{n_y \rightarrow \infty} \{ \lim_{n_t \rightarrow \infty} EQ_{n_y, n_t}(\boldsymbol{\theta}) \},$$

and the estimate  $\hat{\boldsymbol{\theta}}$  minimizes  $Q_{n_y, n_t}$  as defined in (6.35).

In order to prove (6.36), we should prove the following convergence

$$\sup_{\boldsymbol{\theta} \in D_{\boldsymbol{\theta}}} |Q_{n_y, n_t}(\boldsymbol{\theta}) - EQ_{n_y, n_t}(\boldsymbol{\theta})| \rightarrow 0, \text{ w. p. 1 as } n_t \rightarrow \infty, n_y \rightarrow \infty. \quad (6.37)$$

One feasible solution is to achieve the following convergence at any fixed spatial variable  $x$  before working at the spatio-temporal space.

$$\sup_{\boldsymbol{\theta} \in D_{\boldsymbol{\theta}}} \frac{1}{n_t} \sum_{t=1}^{n_t} |\mathcal{E}(x, t, \boldsymbol{\theta})^2 - E\mathcal{E}(x, t, \boldsymbol{\theta})^2| \rightarrow 0, \text{ w. p. 1 as } n_t \rightarrow \infty. \quad (6.38)$$

To achieve the convergence of (6.38), we have to obtain the convergence first at the pre-defined small open sphere, and then extend it to the global domain  $D_{\boldsymbol{\theta}}$  using Heine-Borel's theorem.

**Convergence of modeling error  $\varepsilon$  to its optimum over  $B$ :**

Define the supremum between the model error and its optimum as a random variable

$$\eta(x, t) = \eta(x, t, \boldsymbol{\theta}^0, \rho) = \sup_{\boldsymbol{\theta} \in B} [\mathcal{E}(x, t, \boldsymbol{\theta})^2 - E\mathcal{E}(x, t, \boldsymbol{\theta})^2].$$

Let  $D$  be the open neighborhood of  $D_\theta$  and choose  $\boldsymbol{\theta}^0 \in D_\theta$ . We can define a small open sphere centered at  $\boldsymbol{\theta}^0$  as

$$B(\boldsymbol{\theta}^0, \rho) = \{\boldsymbol{\theta} \mid \|\boldsymbol{\theta} - \boldsymbol{\theta}^0\| < \rho\}.$$

Let  $B = B(\boldsymbol{\theta}^0, \rho) \cap D$ , then

$$\sup_{\boldsymbol{\theta} \in B} \frac{1}{n_t} \sum_{t=1}^{n_t} [\mathcal{E}(x, t, \boldsymbol{\theta})^2 - E\mathcal{E}(x, t, \boldsymbol{\theta})^2] \leq \frac{1}{n_t} \sum_{t=1}^{n_t} \eta(x, t). \quad (6.39)$$

Define  $\xi(x, t) = \eta(x, t) - E\eta(x, t)$ . If we can prove

- $\xi(x, t)$  satisfies [Lemma 5.2](#) and
- the mean of  $\eta(x, t)$  is infinitesimal,

then  $\eta(x, t)$  is also infinitesimal.

Firstly, we consider

$$|E(\xi(x, t)\xi(x, \tau))| = \text{Cov}[\eta(x, t), \eta(x, \tau)].$$

Define  $\eta_\tau^0(x, t) = \sup_{\boldsymbol{\theta} \in B} [\mathcal{E}_\tau^0(x, t, \boldsymbol{\theta})^2 - E\mathcal{E}(x, t, \boldsymbol{\theta})^2]$ , with

$$\mathcal{E}_\tau^0(x, t, \boldsymbol{\theta}) = y_\tau^0(x, t) - V(x, t, \boldsymbol{\theta}, \{u_\tau^0(\zeta, j)\}), \quad t > \tau,$$

where  $\{u_\tau^0(\zeta, j)\}$  denotes the input set  $(u_\tau^0(\zeta, t), \dots, u_\tau^0(\zeta, \tau+1), 0, \dots, 0)$  for all  $\zeta \in \Omega$ ,  $y_\tau^0(x, t)$  and  $u_\tau^0(\zeta, j)$  are the variables introduced in [Assumption 6.1](#). For convenience, let  $u_\tau^0(\zeta, j) = 0$  and  $y_\tau^0(x, j) = 0$  for  $j < \tau$ . Obviously  $\eta_\tau^0(x, t)$  is independent of  $\eta(x, \tau)$  from [Assumption 6.1](#).

Hence

$$\text{Cov}[\eta(x, t), \eta(x, \tau)] = \text{Cov}[\eta(x, t) - \eta_\tau^0(x, t), \eta(x, \tau)].$$

Then using Schwarz's inequality, we have

$$|E(\xi(x, t)\xi(x, \tau))| \leq [E\eta(x, \tau)^2 E(\eta(x, t) - \eta_\tau^0(x, t))^2]^{1/2}. \quad (6.40)$$

Since

$$\begin{aligned} |\eta(x, t) - \eta_\tau^0(x, t)| &\leq \sup_{\boldsymbol{\theta} \in B} |\mathcal{E}(x, t, \boldsymbol{\theta})^2 - \mathcal{E}_\tau^0(x, t, \boldsymbol{\theta})^2| \\ &\leq \sup_{\boldsymbol{\theta} \in B} \{|\mathcal{E}(x, t, \boldsymbol{\theta})| + |\mathcal{E}_\tau^0(x, t, \boldsymbol{\theta})|\} \times \sup_{\boldsymbol{\theta} \in B} |\mathcal{E}(x, t, \boldsymbol{\theta}) - \mathcal{E}_\tau^0(x, t, \boldsymbol{\theta})|, \end{aligned}$$

using [Assumption 6.2](#), we can further have

$$|\eta(x,t) - \eta_\tau^0(x,t)| \leq M \left[ \sum_{j=0}^t \lambda^{t-j} \{ |y(x,j)| + |y_\tau^0(x,j)| + \sup_{\zeta \in \Omega} |u(\zeta,j)| + \sup_{\zeta \in \Omega} |u_\tau^0(\zeta,j)| \} \times \right. \\ \left. \left[ \sum_{j=0}^t \lambda^{t-j} \{ |y(x,j) - y_\tau^0(x,j)| + \sup_{\zeta \in \Omega} |u(\zeta,j) - u_\tau^0(\zeta,j)| \} \right] \right].$$

Using [Assumption 6.1](#) and Schwarz's inequality, we can finally derive

$$E |\eta(x,t) - \eta_\tau^0(x,t)|^2 \leq M \lambda^{t-\tau}. \quad (6.41)$$

Following the similar derivation above and using [Assumption 6.2](#) and [Assumption 6.1](#), we can also derive

$$E \eta(x,\tau)^2 \leq M. \quad (6.42)$$

Placing (6.41) and (6.42) into (6.40), we can easily derive that  $\xi(x,t)$  satisfies [Lemma 5.2](#), that is

$$\frac{1}{n_t} \sum_{t=1}^{n_t} \xi(x,t) = \frac{1}{n_t} \sum_{t=1}^{n_t} (\eta(x,t) - E\eta(x,t)) \rightarrow 0, \text{ w. p. 1 as } n_t \rightarrow \infty. \quad (6.43)$$

Secondly, the mean value of  $\eta$  can be expressed as,

$$E\eta(x,t) = E \sup_{\theta \in B} [\mathcal{E}(x,t,\theta)^2 - E\mathcal{E}(x,t,\theta)^2].$$

Since the right-hand side is continuous with respect to  $\theta$ ,  $E\eta(x,t)$  should be small if  $B$  is small. Furthermore, by [Assumption 6.3](#),

$$|\frac{\partial \mathcal{E}(x,t,\theta)^2}{\partial \theta}| \leq M |\mathcal{E}(x,t,\theta)|^2 \leq M \left[ \sum_{j=0}^t \lambda^{t-j} \{ |y(x,j)| + \sup_{\zeta \in \Omega} |u(\zeta,j)| \} \right]^2,$$

where we again have used the uniform bounds in [Assumption 6.2](#). Consequently, by [Assumption 6.1](#),

$$E \sup_{\theta \in B} |\frac{\partial \mathcal{E}(x,t,\theta)^2}{\partial \theta}|^2 \leq M.$$

Now

$$\begin{aligned} E\eta(x,t) &= E \sup_{\theta \in B} [\mathcal{E}(x,t,\theta)^2 - E\mathcal{E}(x,t,\theta)^2] \\ &\leq E \sup_{\theta \in B} [\mathcal{E}(x,t,\theta)^2 - \mathcal{E}(x,t,\theta^0)^2] + \sup_{\theta \in B} E[\mathcal{E}(x,t,\theta^0)^2 - \mathcal{E}(x,t,\theta)^2] \\ &\leq [E \sup_{\theta \in B} |\frac{\partial \mathcal{E}(x,t,\theta)^2}{\partial \theta}| + \sup_{\theta \in B} E |\frac{\partial \mathcal{E}(x,t,\theta)^2}{\partial \theta}|] \times \sup_{\theta \in B} |\theta - \theta^0| \\ &\leq M^0 \rho. \end{aligned} \quad (6.44)$$

Finally from (6.44), (6.39) becomes

$$\sup_{\theta \in B} \frac{1}{n_t} \sum_{t=1}^{n_t} [\mathcal{E}(x,t,\theta)^2 - E\mathcal{E}(x,t,\theta)^2] \leq \frac{1}{n_t} \sum_{t=1}^{n_t} (\eta(x,t) - E\eta(x,t)) + M^0 \rho. \quad (6.45)$$



It is clearly seen from (6.43) that the first term of the right-hand side is arbitrarily small for a sufficiently large  $n_t$ . Since  $\rho$  can be arbitrarily small, therefore

$$\sup_{\theta \in B} \frac{1}{n_t} \sum_{t=1}^{n_t} |\mathcal{E}(x, t, \theta)^2 - E\mathcal{E}(x, t, \theta)^2| \rightarrow 0, \text{ w. p. 1 as } n_t \rightarrow \infty. \quad (6.46)$$

### **Convergence extension to global $D_\theta$ :**

Since  $D_\theta$  is compact, by applying Heine-Borel's theorem, the following result is easily derived from (6.46),

$$\sup_{\theta \in D_\theta} \frac{1}{n_t} \sum_{t=1}^{n_t} |\mathcal{E}(x, t, \theta)^2 - E\mathcal{E}(x, t, \theta)^2| \rightarrow 0, \text{ w. p. 1 as } n_t \rightarrow \infty. \quad (6.47)$$

### **Extension to spatio-temporal domain:**

Obviously, we have

$$\sup_{\theta \in D_\theta} |Q_{n_y, n_t}(\theta) - EQ_{n_y, n_t}(\theta)| \leq \frac{1}{n_y} \sum_{j=1}^{n_y} \sup_{\theta \in D_\theta} \frac{1}{n_t} \sum_{t=1}^{n_t} |\mathcal{E}(x_j, t, \theta)^2 - E\mathcal{E}(x_j, t, \theta)^2|,$$

Thus, the following conclusion is derived,

$$\sup_{\theta \in D_\theta} |Q_{n_y, n_t}(\theta) - EQ_{n_y, n_t}(\theta)| \rightarrow 0, \text{ w. p. 1 as } n_t \rightarrow \infty, n_y \rightarrow \infty. \quad (6.48)$$

■

## **6.6 Simulation and Experiment**

In order to evaluate the presented modeling method, the simulation on the catalytic rod is studied first. Then the experiment and modeling for snap curing oven are presented. For an easy comparison, some performance indexes are established for the DPS as follows

- **Spatial normalized absolute error**,  $SNAE(t) = \int |e(x, t)| dx / \int dx$ ,
- **Temporal normalized absolute error**,  $TNAE(x) = \sum |e(x, t)| / \sum \Delta t$ ,
- **Root of mean squared error**,  $RMSE = (\int \sum e(x, t)^2 dx / \int dx \sum \Delta t)^{1/2}$ .

### **6.6.1 Catalytic Rod**

Consider the **catalytic rod** given in **Sections 1.1.2 and 3.6.1**. In the simulation, assume the process noise  $d(x, t)$  in (3.31) is zero. Twenty-two sensors uniformly distributed in the space are used to measure the temperature distribution. The sampling interval is  $\Delta t = 0.01$  and the simulation time is 5.

The measured process output  $y(x,t)$  is shown in Figure 6.3, where the first 250 data are used for model training, the next 150 data for validation and the remaining 100 data for model testing. As show in Figure 6.4, the first four Karhunen-Loève basis functions are used for the spatio-temporal Volterra modeling. The temporal bases  $\phi_i(t)$  are chosen as Laguerre functions with the time-scaling factor  $p=4.5$  and the truncation length  $q=4$  using the cross-validation method.

The predicted output  $\hat{y}_n(x,t)$  and the prediction error  $e(x,t) = y - \hat{y}_n$  of the 2<sup>nd</sup>-order spatio-temporal Volterra model are presented in Figure 6.5 and Figure 6.6 respectively. It is obvious that the 2<sup>nd</sup>-order spatio-temporal Volterra model can satisfactorily model the process. For many applications, the 2<sup>nd</sup>-order model is enough for a good approximation, and too high-order models may cause the over-complexity problem. As shown in Figure 6.7 and Figure 6.8, the 2<sup>nd</sup>-order spatio-temporal Volterra model performs much better than the 1<sup>st</sup>-order spatio-temporal Volterra model (i.e., Green's function model) because the 1<sup>st</sup>-order spatio-temporal Volterra model is basically a linear system.

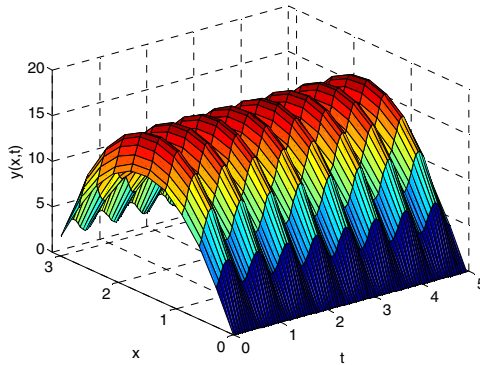


**Fig. 6.3** Catalytic rod: Measured output for Volterra modeling

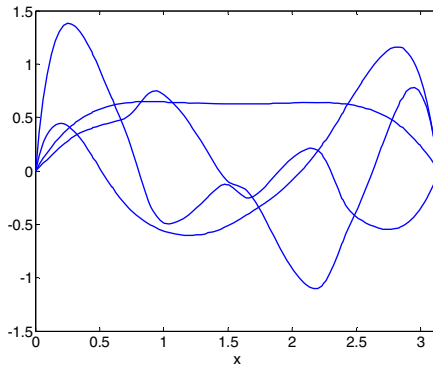


**Fig. 6.4** Catalytic rod: KL basis functions for Volterra modeling

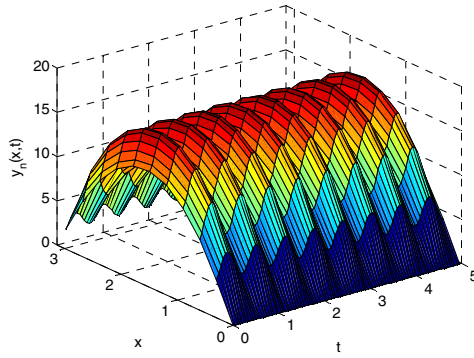


**Fig. 6.5** Catalytic rod: Predicted output of 2<sup>nd</sup>-order Volterra model

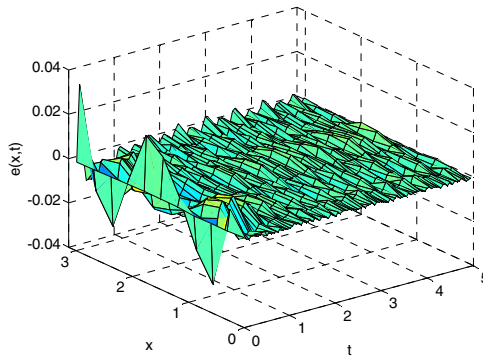


**Fig. 6.6** Catalytic rod: Prediction error of 2<sup>nd</sup>-order Volterra model

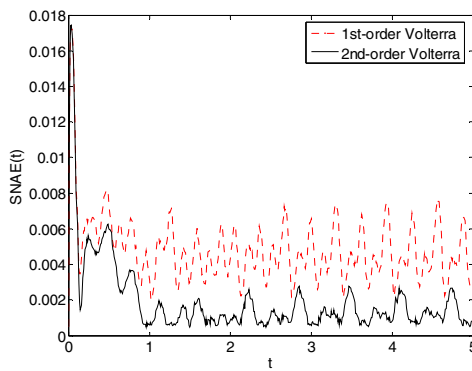


**Fig. 6.7** Catalytic rod:  $SNAE(t)$  of 1<sup>st</sup> and 2<sup>nd</sup>-order Volterra models

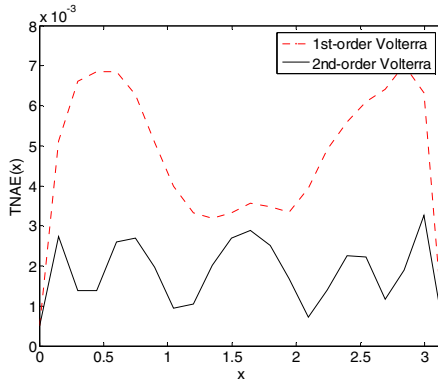


**Fig. 6.8** Catalytic rod:  $TNAE(x)$  of 1<sup>st</sup> and 2<sup>nd</sup>-order Volterra models

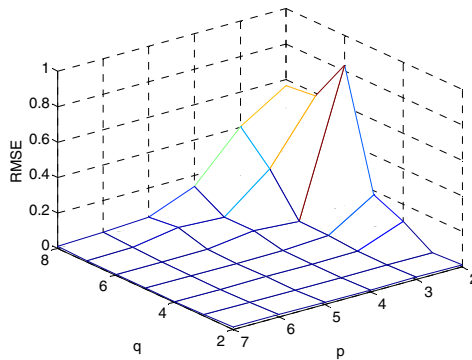


**Fig. 6.9** Catalytic rod:  $RMSE$  of 2<sup>nd</sup>-order Volterra model

The modeling performance is also affected by the number of Laguerre temporal basis functions ( $q$ ) and the time-scaling factor ( $p$ ). **Figure 6.9** displays  $RMSE$  of the 2<sup>nd</sup>-order spatio-temporal Volterra model with respect to these two parameters. It is shown that this modeling approach is robust to these parameters since there are a wide range of parameters which can be chosen to obtain a good performance.

### 6.6.2 Snap Curing Oven

Consider the **snap curing oven** (**Figure 1.1** and **Figure 3.11**) provided in **Sections 1.1.1** and **3.6.2**. In the experiment, a total of 2100 measurements are collected with a sampling interval  $\Delta t = 10$  seconds. One thousand and four hundred of measurements from sensors (s1-s5, s7-s10, and s12-s16) are used to estimate the model. The last 700 measurements from sensors (s1-s5, s7-s10, and s12-s16) are chosen to validate the model and determine the time-scaling factor and truncation length of

Laguerre series using the cross-validation method. All 2100 measurements from the rest sensors (s6, s11) are used for model testing.

In the spatio-temporal Volterra modeling, five two-dimensional Karhunen-Loève basis functions are used as spatial bases and the first two of them are shown in Figure 6.10 and Figure 6.11. The temporal bases  $\phi_i(t)$  are chosen as Laguerre series with the time-scaling factor  $p = 0.001$  and the truncation length  $q = 3$ .

The 2<sup>nd</sup>-order spatio-temporal Volterra model is used to model the thermal process. After the training using the first 1400 data from the sensors (s1-s5, s7-s10, and s12-s16), a process model can be obtained with the significant performance such as the sensor s1 in Figure 6.12. The model also performs very well for the untrained locations such as the sensor s6 in Figure 6.13. The predicted temperature distribution of the oven at  $t=10000$ s is provided in Figure 6.14. The performance

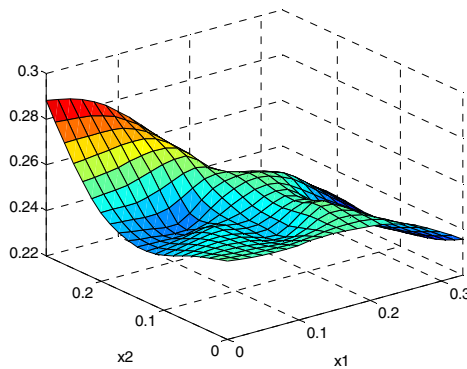


Fig. 6.10 Snap curing oven: KL basis functions ( $i=1$ ) for Volterra modeling

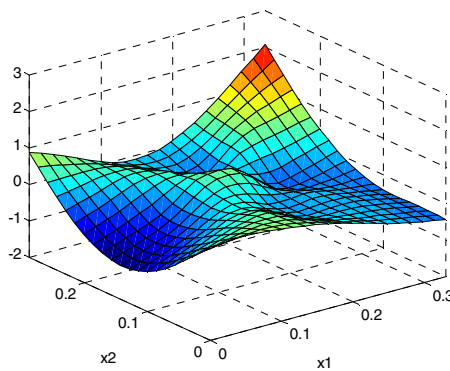
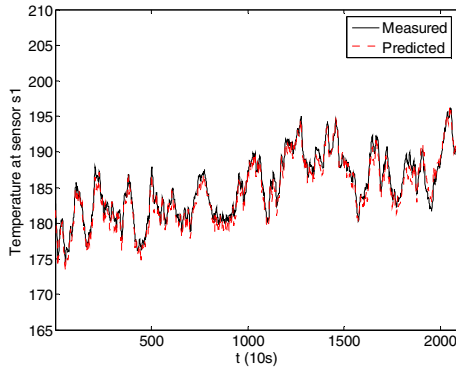
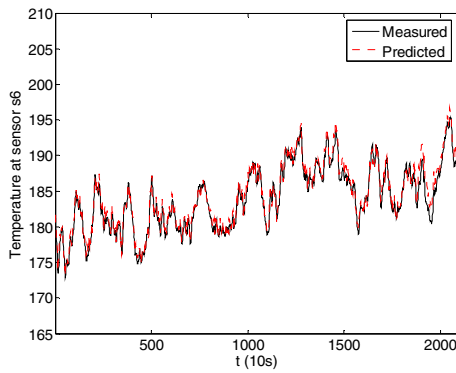


Fig. 6.11 Snap curing oven: KL basis functions ( $i=2$ ) for Volterra modeling



**Fig. 6.12** Snap curing oven: Performance of 2<sup>nd</sup>-order Volterra model at sensor s1



**Fig. 6.13** Snap curing oven: Performance of 2<sup>nd</sup>-order Volterra model at sensor s6

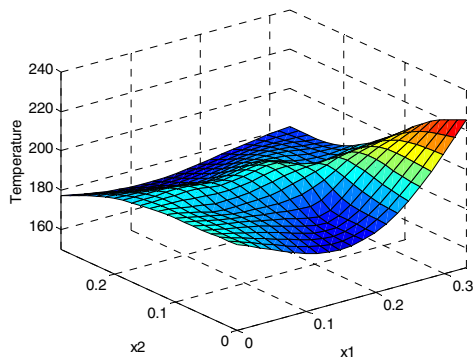


**Fig. 6.14** Snap curing oven: Predicted temperature distribution of 2<sup>nd</sup>-order Volterra model at  $t=10000s$

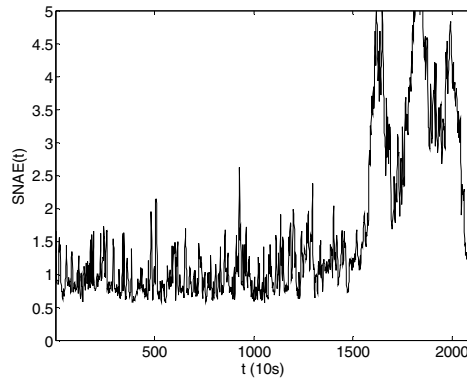


**Fig. 6.15** Snap curing oven:  $SNAE(t)$  of 1<sup>st</sup>-order Volterra model

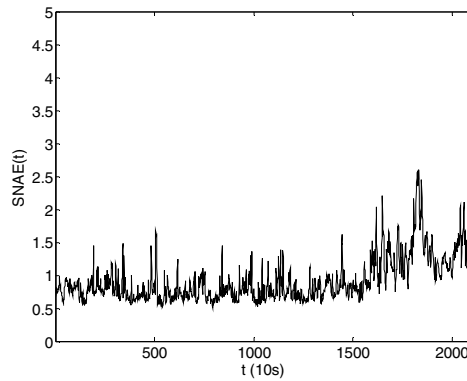


**Fig. 6.16** Snap curing oven:  $SNAE(t)$  of 2<sup>nd</sup>-order Volterra model

**Table 6.1** Snap curing oven:  $TNAE(x)$  of 1st and 2nd-order Volterra models

	s1	s2	s3	s4	s5	s6	s7	s8
1 <sup>st</sup> -order model	1.87	1.44	1.75	1.34	1.75	1.55	1.5	1.59
2 <sup>nd</sup> -order model	0.79	0.71	1.2	0.71	1.59	0.65	0.78	1.24
	s9	s10	s11	s12	s13	s14	s15	s16
1 <sup>st</sup> -order model	1.13	1.81	2.1	1.43	1.85	2.22	1.13	1.52
2 <sup>nd</sup> -order model	0.86	0.86	1.33	1.08	0.71	1	0.7	0.55

comparisons over the whole data set in [Figure 6.15](#) and [Figure 6.16](#) and [Table 6.1](#) further show that the 2<sup>nd</sup>-order spatio-temporal Volterra model has a much better performance than the 1<sup>st</sup>-order spatio-temporal Volterra model. The effectiveness of the presented modeling method is clearly demonstrated in this real application.

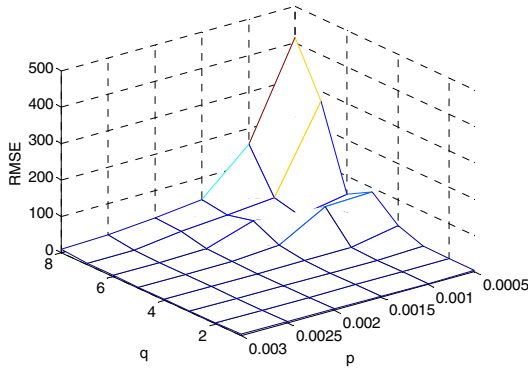


**Fig. 6.17** Snap curing oven:  $RMSE$  of 2<sup>nd</sup>-order Volterra model

As shown in [Figure 6.17](#), a good modeling performance can be maintained in a wide range of parameter space about the number of Laguerre temporal basis functions ( $q$ ) and the time-scaling factor ( $p$ ). Note that though the modeling gives some certain robustness to the selection of  $p$  and  $q$ , their selection is still very important in modeling of real systems. If they are not properly selected, the modeling algorithm may become divergent due to the process noise and disturbance.

## 6.7 Summary

A Volterra kernel based spatio-temporal modeling approach is presented for unknown nonlinear distributed parameter systems. The spatio-temporal Volterra model is constructed, where the kernels are functions of time and space variables. In order to estimate the kernels, they are expanded onto Karhunen-Loève spatial bases as well as Laguerre temporal bases with unknown coefficients. With the help of the Galerkin method, these unknown parameters can be estimated from the process data using the least-squares method in the temporal domain. This spatio-temporal Volterra model can achieve a better performance than the Green's function model. The presented modeling algorithm provides convergent and satisfactory estimates. The simulation and experiment are conducted to demonstrate the effectiveness of the presented modeling method and its potential application to a wide range of nonlinear DPS.

## References

- [1] Boyd, S., Chua, L.O.: Fading memory and the problem of approximating nonlinear operators with Volterra series. *IEEE Transactions on Circuits and Systems* 32(11), 1150–1161 (1985)
- [2] Butkovskiy, A.G.: *Green's functions and transfer functions handbook*, 1st edn. Ellis Horwood, Chichester (1982)



- [3] Christofides, P.D.: Nonlinear and robust control of PDE systems: Methods and applications to transport-reaction processes. Birkhäuser, Boston (2001b)
- [4] Cramér, H., Leadbetter, M.R.: Stationary and related stochastic processes. Wiley, New York (1967)
- [5] Datta, K.B., Mohan, B.M.: Orthogonal functions in systems and control. World Scientific, Singapore (1995)
- [6] Doumanidis, C.C., Fourligkas, N.: Temperature distribution control in scanned thermal processing of thin circular parts. *IEEE Transactions on Control Systems Technology* 9(5), 708–717 (2001)
- [7] Doyle III, F.J., Ogunnaike, B.A., Pearson, R.K.: Nonlinear model-based control using second-order Volterra Models. *Automatica* 31(5), 697–714 (1995)
- [8] Gay, D.H., Ray, W.H.: Identification and control of distributed parameter systems by means of the singular value decomposition. *Chemical Engineering Science* 50(10), 1519–1539 (1995)
- [9] Heuberger, P.S.C., Van den Hof, P.M.J., Bosgra, O.H.: A generalized orthonormal basis for linear dynamical systems. *IEEE Transactions on Automatic Control* 40(3), 451–465 (1995)
- [10] Ljung, L.: Convergence analysis of parametric identification methods. *IEEE Transactions on Automatic Control* 23(5), 770–783 (1978)
- [11] Ljung, L.: System identification: Theory for the user, 2nd edn. Prentice-Hall, Englewood Cliffs (1999)
- [12] Maner, B.R., Doyle III, F.J., Ogunnaike, B.A., Pearson, R.K.: Nonlinear model predictive control of a simulated multivariable polymerization reactor using second-order Volterra models. *Automatica* 32(9), 1285–1301 (1996)
- [13] Park, H.M., Cho, D.H.: Low dimensional modeling of flow reactors. *International Journal of Heat and Mass Transfer* 39(16), 3311–3323 (1996a)
- [14] Park, H.M., Cho, D.H.: The use of the Karhunen-Loève decomposition for the modeling of distributed parameter systems. *Chemical Engineering Science* 51(1), 81–98 (1996b)
- [15] Parker, R.S., Heemstra, D., Doyle III, F.J., Pearson, R.K., Ogunnaike, B.A.: The identification of nonlinear models for process control using tailored “plant-friendly” input sequences. *Journal of Process Control* 11(2), 237–250 (2001)
- [16] Rugh, W.: Nonlinear system theory: The Volterra/Wiener approach. Johns Hopkins University Press, Baltimore (1981)
- [17] Schetzen, M.: The Volterra and Wiener theories of nonlinear systems. Wiley, New York (1980)
- [18] Wahlberg, B.: System identification using Laguerre models. *IEEE Transactions on Automatic Control* 36(5), 551–562 (1991)
- [19] Wahlberg, B.: System identification using Kautz models. *IEEE Transactions on Automatic Control* 39(6), 1276–1282 (1994)
- [20] Wahlberg, B., Mäkilä, P.M.: Approximation of stable linear dynamical systems using Laguerre and Kautz functions. *Automatica* 32(5), 693–708 (1996)
- [21] Wang, L.: Discrete model predictive controller design using Laguerre functions. *Journal of Process Control* 14(2), 131–142 (2004)
- [22] Zervos, C.C., Dumont, G.A.: Deterministic adaptive control based on Laguerre series representation. *International Journal of Control* 48(6), 2333–2359 (1988)

- [23] Zheng, D., Hoo, K.A.: Low-order model identification for implementable control solutions of distributed parameter system. *Computers and Chemical Engineering* 26(7-8), 1049–1076 (2002)
- [24] Zheng, D., Hoo, K.A.: System identification and model-based control for distributed parameter systems. *Computers and Chemical Engineering* 28(8), 1361–1375 (2004)
- [25] Zheng, D., Hoo, K.A., Piovoso, M.J.: Low-order model identification of distributed parameter systems by a combination of singular value decomposition and the Karhunen-Loève expansion. *Industrial & Engineering Chemistry Research* 41(6), 1545–1556 (2002)

# 7 Nonlinear Dimension Reduction Based Neural Modeling for Nonlinear Complex DPS

**Abstract.** A nonlinear principal component analysis (NL-PCA) based neural modeling approach is presented for a lower-order or more accurate solution for nonlinear distributed parameter systems (DPS). One NL-PCA network is trained for the nonlinear dimension reduction and the nonlinear time/space reconstruction. The other neural model is to learn the system dynamics with a linear/nonlinear separated model structure. With the powerful capability of dimension reduction and the intelligent learning, this approach can model the nonlinear complex DPS with much more complexity. The simulation on the catalytic rod and the experiment on the snap curing oven will demonstrate the effectiveness of the presented method.

## 7.1 Introduction

Karhunen-Loève (KL) decomposition has been widely used for distributed parameter system (DPS) identification with the help of traditional system identification techniques (Sahan *et al.*, 1997; Zhou, Liu, Dai & Yuan, 1996; Aggelogiannaki & Sarimveis, 2007; Smaoui & Al-Enezi, 2004; Qi & Li, 2008a). Karhunen-Loève decomposition, also called principal component analysis (PCA) (Baker & Christofides, 2000; Armaou & Christofides, 2002; Park & Cho, 1996a, 1996b; Hoo & Zheng, 2001; Newman, 1996a, 1996b), is a popular approach to find the principal spatial structures from the data. Among all linear expansion, PCA basis functions can give a lower-dimensional model. However, the traditional PCA is a linear dimension reduction (i.e., linear projection and linear reconstruction) method, and it may not be very suitable to model the nonlinear dynamics efficiently (Malthouse, 1998). This is because PCA produces a linear approximation to the original nonlinear problem, which may not guarantee the assumption that minor components do not contain important information (Wilson, Irwin & Lightbody, 1999).

This has naturally motivated the development of nonlinear PCA (NL-PCA) for the nonlinear problem. NL-PCA is a nonlinear dimension reduction method, which can retain more information using fewer components. In the field of machine learning, NL-PCA has been used to deal with the nonlinear dimension reduction problem. Examples include principal curves/surfaces (Dong & McAvoy, 1996), multi-layer auto-associative neural networks (Kramer, 1991; Saegusa, Sakano & Hashimoto, 2004; Hsieh, 2001; Hinton & Salakhutdinov, 2006; Kirby & Miranda, 1994; Smaoui, 2004), the kernel function approach (Webb, 1996; Schölkopf, Smola & Muller, 1998), and the radial basis function (RBF) networks (Wilson, Irwin &

Lightbody, 1999). However, they mainly focus on the reduction and analysis of the high-dimensional data or the known system.

In this chapter, a nonlinear dimension reduction based spatio-temporal modeling is developed for unknown nonlinear distributed parameter systems. The approach consists of two major stages. First, a NL-PCA network is trained for the nonlinear dimension reduction. With the help of finite spatial measurement, the well-trained NL-PCA network can transform and reduce the high-dimensional spatio-temporal data into the low-dimensional time series data and reconstruct them back to the spatio-temporal data. Then, a low-order neural network can be easily established for dynamic modeling with the help of traditional identification technique. The simulation and experiment demonstrates that this nonlinear dimension reduction based modeling can achieve a better performance than the linear dimension reduction based approach when modeling the nonlinear DPS.

This chapter is organized as follows. The novel NL-PCA based spatio-temporal modeling methodology is described in Section 7.2. The presented NL-PCA based spatio-temporal modeling is implemented using neural networks in Section 7.3, with simulation and experiment conducted in Section 7.4. Finally, a few conclusions are presented in Section 7.5.

## 7.2 Nonlinear PCA Based Spatio-Temporal Modeling Framework

### 7.2.1 Modeling Methodology

Consider a nonlinear distributed parameter system,  $u(t) \in \mathbb{R}^m$  is the temporal input, and  $y(x, t) \in \mathbb{R}$  is the spatio-temporal output, where  $x \in \Omega$  is the spatial variable,  $\Omega$  is the space domain, and  $t$  is the temporal variable. Here the system is controlled by the  $m$  actuators with temporal signal  $u(t)$  and certain spatial distribution. The output is measured at the  $N$  spatial locations  $x_1, \dots, x_N$ . The modeling objective is to identify a low-order spatio-temporal model from the temporal input  $\{u(t)\}_{t=1}^L$  and the spatio-temporal output  $\{y(x_i, t)\}_{i=1, t=1}^{N, L}$ , where  $L$  is the time length.

One method, called “modeling-then-reduce”, is to identify a high-order model from the data and then perform the model reduction. For the high-dimensional model, a large number of functions and parameters need to be estimated, and a complex model reduction has to be used to derive a low-order model.

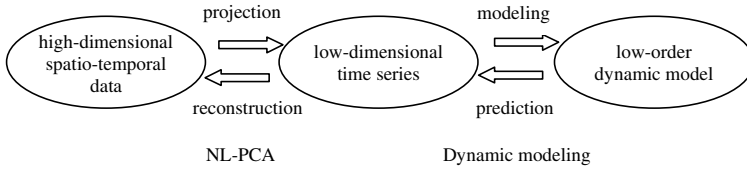
In this study, a two-stage spatio-temporal modeling methodology is used and depicted in Figure 7.1. The first stage is for the dimension reduction, where the high-dimensional spatio-temporal output data  $\{y(x_i, t)\}_{i=1, t=1}^{N, L}$  can be reduced to the low-dimensional time series data  $\{y(t)\}_{t=1}^L$ . The second stage is for the dynamic modeling, where a low-order temporal model is identified using the time series data. Using the prediction of the temporal model and the nonlinear time/space reconstruction, this modeling method can reproduce the spatio-temporal dynamics of the distributed system. This methodology can be regarded as “reduce-then-modeling”.

It can greatly reduce the computational complexity involved in the low-order modeling.

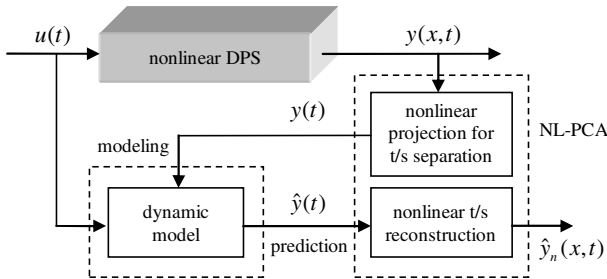
As shown in **Figure 7.1(a)**, the nonlinear dimension reduction approach should include two functions:

- Nonlinear projection for time/space separation - a nonlinear transformation from the high-dimensional time/space domain into the low-dimensional time series.
- Nonlinear time/space reconstruction - a nonlinear reverse transformation from the reduced-dimensional time series to the original time/space domain.

Obviously, the projection and the reconstruction should be invertible for a good reproduction of the original spatio-temporal dynamics. As shown in **Figure 7.1(b)**, the first step is to learn the nonlinear projection and reconstruction using NL-PCA method, and the second is to model the system dynamics using traditional nonlinear identification techniques.



(a) Modeling philosophy



(b) Modeling construction

**Fig. 7.1** NL-PCA based spatio-temporal modeling methodology

## 7.2.2 Principal Component Analysis

The main problem of using PCA for the dimension reduction is to compute the most characteristic spatial structure  $\{\varphi_i(x)\}_{i=1}^n$  among the spatio-temporal output  $\{y(x_i, t)\}_{i=1, t=1}^{N, L}$ , where  $n$  is the number of spatial basis functions (i.e., the dimension of the time domain,  $n < N$ ). For simplicity, assume the process output is uniformly sampled in time and space.

Taking  $(\varphi_i, \varphi_i) = 1$  without loss of generality, the projection and reconstruction of PCA have the following linear form

$$y_i(t) = (\varphi_i(x), y(x, t)), i = 1, \dots, n, \quad (7.1)$$

$$y_n(x, t) = \sum_{i=1}^n \varphi_i(x) y_i(t). \quad (7.2)$$

Then the reconstruction error can be defined as  $e(x, t) = y(x, t) - y_n(x, t)$ . The spatial principal axes  $\{\varphi_i(x)\}_{i=1}^n$  can be found by minimizing the following objective function

$$\min_{\varphi_i(x)} \langle \|e(x, t)\|^2 \rangle. \quad (7.3)$$

### *Spatial correlation method*

There are several implementations of PCA. The simple one is based on the spatial correlation function. The necessary condition of the solution of (7.3) can be obtained as below (Holmes, Lumley & Berkooz, 1996)

$$\int_{\Omega} R(x, \zeta) \varphi_i(\zeta) d\zeta = \lambda_i \varphi_i(x), (\varphi_i, \varphi_i) = 1, i = 1, \dots, n, \quad (7.4)$$

where  $R(x, \zeta) = \langle y(x, t) y(\zeta, t) \rangle$  is the spatial two-point correlation function. Since the matrix  $R$  is symmetric and positive semidefinite, the computed eigenfunctions are orthogonal.

Because the data are always discrete in space, one must solve numerically the integral equation (7.4). Discretizing the integral equation gives a  $N \times N$  matrix eigenvalue problem. Thus, at most  $N$  eigenfunctions at  $N$  sampled spatial locations can be obtained. Then one can interpolate the eigenfunctions to locations where the data are not available.

### *Dimension determination*

The maximum number of nonzero eigenvalues is  $K \leq N$ . Let the eigenvalues  $\lambda_1 > \lambda_2 > \dots > \lambda_K$  and the corresponding eigenfunctions  $\varphi_1(x), \varphi_2(x), \dots, \varphi_K(x)$  in the order of the magnitude of the eigenvalues. The ratio of the sum of the  $n$  largest eigenvalues to the total sum

$$\eta = \sum_{i=1}^n \lambda_i / \sum_{i=1}^K \lambda_i, \quad (7.5)$$

gives the fraction of the variance retained in the  $n$ -dimensional space defined by the eigenfunctions associated with those eigenvalues (Webb, 1996). One method of estimating the intrinsic dimension is to take the value of  $n$  for which  $\eta$  is sufficiently large. A value of more than 0.9 is often taken. In general, only the first few basis functions expansion can represent the dominant dynamics of the

spatio-temporal system. It can be shown (Holmes, Lumley & Berkooz, 1996) that for some arbitrary set of basis functions  $\{\phi_i(x)\}_{i=1}^n$ , the following result holds

$$\sum_{i=1}^n \langle (y(\cdot, t), \phi_i)^2 \rangle = \sum_{i=1}^n \lambda_i^2 \geq \sum_{i=1}^n \langle (y(\cdot, t), \phi_i)^2 \rangle .$$

It means that the PCA expansion is optimal on average in the class of linear dimension reduction methods.

### 7.2.3 Nonlinear PCA for Projection and Reconstruction

Unlike the linear PCA, the **NL-PCA** allows the projection and the reconstruction to be arbitrary nonlinear function. Finding these two functions is the first step for the spatio-temporal modeling.

The nonlinear projection is in the form

$$y_i(t) = G_i(y_x(t)), i = 1, \dots, n , \quad (7.6)$$

where  $y_x(t) = [y(x_1, t), \dots, y(x_N, t)]^T \in \mathbb{R}^N$  and  $n$  is the reduced dimension in the time domain ( $n < N$ ). A compact vector form is described in the following

$$y(t) = G(y_x(t)) , \quad (7.7)$$

where  $y(t) = [y_1(t), \dots, y_n(t)]^T \in \mathbb{R}^n$  and  $G(\cdot) = [G_1(\cdot), \dots, G_n(\cdot)]^T : \mathbb{R}^N \rightarrow \mathbb{R}^n$ . Here  $G_i(\cdot) : \mathbb{R}^N \rightarrow \mathbb{R}$  is referred to as the  $i$ th nonlinear spatial principal axis.

The reconstruction is completed by a second nonlinear function  $H(\cdot) : \mathbb{R}^{n+1} \rightarrow \mathbb{R}$  as below

$$y_n(x, t) = H(x, y(t)) . \quad (7.8)$$

Here  $y_n(x, t)$  denotes the  $n$ th-order approximation, and the function  $H$  with the spatial variable  $x$  is used to reproduce the output at sampled spatial locations as well as any other locations.

The reconstruction error is measured by  $e(x, t) = y(x, t) - y_n(x, t)$ . The functions  $G$  and  $H$  are selected to minimize the following objective function

$$\min_{G, H} \langle \|e(x, t)\|^2 \rangle . \quad (7.9)$$

where the ensemble average, norm and inner product are defined as  $\langle f(x, t) \rangle = \frac{1}{L} \sum_{t=1}^L f(x, t)$ ,  $\|f(x)\| = (f(x), f(x))^{1/2}$  and  $(f(x), g(x)) = \int_{\Omega} f(x)g(x)dx$ .

### 7.2.4 Dynamic Modeling

The second step for the spatio-temporal modeling is to establish the dynamic relationship between  $y(t)$  and  $u(t)$ . Due to the reduced dimensionality of  $y(t)$ , the

spatio-temporal modeling becomes a simple low-order temporal modeling, for which traditional nonlinear system identification techniques can be easily applied.

The time series data  $y(t)$  is often described by a deterministic nonlinear autoregressive with exogenous input (NARX) model (Leontaritis & Billings, 1985)

$$y(t) = F(y(t-1), \dots, y(t-d_y), u(t-1), \dots, u(t-d_u)) + e(t), \quad (7.10)$$

where  $d_u$  and  $d_y$  denote the maximum input and output lags respectively, and  $e(t)$  denotes the model error. The unknown function  $F$  can be estimated from the input/output data  $\{u(t), y(t)\}_{t=1}^L$  using such as polynomials, radial basis functions, wavelets and kernel functions (Sjöberg *et al.*, 1995), where the low-dimensional time series  $y(t)$  can be obtained using the nonlinear projection function of NL-PCA described in (7.7).

In summary, the estimated spatio-temporal model is composed of a low-order temporal model

$$\hat{y}(t) = \hat{F}(\hat{y}(t-1), \dots, \hat{y}(t-d_y), u(t-1), \dots, u(t-d_u)), \quad (7.11)$$

and a spatio-temporal reconstruction equation

$$\hat{y}_n(x, t) = H(x, \hat{y}(t)), \quad (7.12)$$

where  $\hat{y}(t)$  and  $\hat{y}_n(x, t)$  denote the model predictions. Given the initial conditions, the model (7.11) can generate a prediction  $\hat{y}(t)$  at any time  $t$ . Combined with (7.12), this low-order model can reproduce the spatio-temporal output over the whole time/space domain.

## 7.3 Nonlinear PCA Based Spatio-Temporal Modeling in Neural System

### 7.3.1 Neural Network for Nonlinear PCA

The optimization (7.9) can be solved using different mathematical tools, which will lead to various NL-PCA implementations. One popular approach is to use a five-layer feedforward neural network (Kramer, 1991). As shown in Figure 7.2, the first and fifth layers are the input and output layers, respectively. The three hidden layers are the projection layer for learning  $G$ , the bottleneck layer for dynamic modeling, and the reconstruction layer for learning  $H$ , respectively. The dimension of the bottleneck layer has been significantly reduced. The spatial variable  $x$  is added in the reconstruction layer to possess the capability of processing the spatial information.

Note that the nodes of projection and reconstruction layers will be nonlinear activation functions (e.g. sigmoid functions) for modeling arbitrary  $G$  and  $H$ . The nodes of input layer, output layer and bottleneck layer can be linear functions. The projection and reconstruction functions can be expressed as



$$y(t) = G(y_x(t)) = W_2 \Phi_2(W_1 y_x(t) + b_1) + b_2, \tag{7.13}$$

$$y_n(x, t) = H(x, y(t)) = W_4 \Phi_4(W_3 y(t) + V_3 x + b_3) + b_4, \tag{7.14}$$

where  $W_i$  and  $b_i$  denote the weight and bias between the  $i^{\text{th}}$ -layer to the  $(i+1)^{\text{th}}$ -layer ( $i=1, \dots, 4$ ),  $V_3$  denotes the weight of the spatial variable  $x$  between the 3<sup>th</sup>-layer and the 4<sup>th</sup>-layer, and  $\Phi_i$  denotes the activation function of the  $i^{\text{th}}$ -layer ( $i=2, 4$ ).

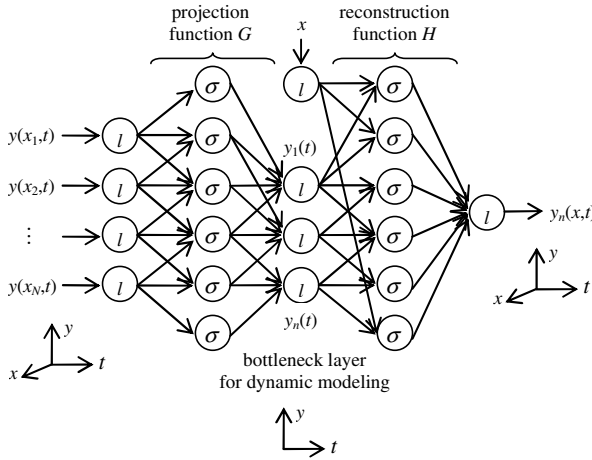


**Fig. 7.2** NL-PCA network  
 ( $\sigma$  indicates sigmoid nodes,  $l$  indicates linear nodes)

**Nonlinear PCA network design**

The network size is critical to the nonlinear dimension reduction. The number of nodes in the projection and reconstruction layers is related to the complexity of nonlinear functions  $G$  and  $H$ . The number of nodes in the bottleneck layer denotes the intrinsic dimension of the time series. Once the network structure is determined, the maximum capability of the projection and the reconstruction is fixed.

In practice, there should be large enough number of nodes for the high accuracy. However, because of finite length of training data available, too many nodes may cause the over-fitting problem. The tradeoff between the training accuracy and the risk of the overfitting can be managed using some techniques such as the cross-validation (Kramer, 1991; Wilson, Irwin & Lightbody, 1999) and regularization (Hsieh, 2001; Wilson, Irwin & Lightbody, 1999).

The intrinsic dimension of the time series can be determined by the sequential NL-PCA (Kramer, 1991) or hierarchical NL-PCA (Saegusa, Sakano & Hashimoto, 2004) in advance. The linear PCA can also give an initial guess. In this study, we

define a measure of the proportion of variance in the data explained by the reconstruction as in Webb (1996)

$$\eta = 1 - \frac{\sum_{i=1}^N \sum_{t=1}^L (y(x_i, t) - y_n(x, t))^2}{\sum_{i=1}^N \sum_{t=1}^L (y(x_i, t) - \bar{y}(x_i))^2}, \quad (7.15)$$

where  $\bar{y}(x_i) = \langle y(x_i, t) \rangle$  is the mean of the data at the location  $x_i$ . Note that the criterion (7.5) in linear PCA is a special case of (7.15), but this measure can help to determine the intrinsic dimension in nonlinear case.

### Nonlinear PCA network training

This multi-layer network can be trained by any appropriate algorithm such as backpropagation (Ham & Kostanic, 2001) to minimize the reconstruction error (7.9). The training of the multi-layer network involves a nonlinear optimization where the solution of the weights may be sensitive to the initial conditions. Recently, Hinton & Salakhutdinov (2006) have proposed an efficient approach to solve this problem.

### 7.3.2 Neural Network for Dynamic Modeling

In our studies, the model (7.10) is assumed to be the following form

$$y(t) = Ay(t-1) + \bar{F}(y(t-1)) + Bu(t-1) + e(t), \quad (7.16)$$

where the matrices  $A \in \mathbb{R}^{n \times n}$  and  $B \in \mathbb{R}^{n \times m}$  denote the linear part, and  $\bar{F}: \mathbb{R}^n \rightarrow \mathbb{R}^n$  denotes the nonlinear part. It can be easily seen from (3.31) that the system in the simulation studies can give a linear and nonlinear separated model when using linear PCA for the dimension reduction. This model can still be used in the NL-PCA based modeling since it may reduce the complexity of nonlinear function  $F$  in (7.10). Moreover it is an affine model in the input and then many nonlinear control algorithms developed for affine ODE models can be easily extended to the nonlinear DPS.

In the identification procedure,  $\bar{F}$  is approximated as a RBF network, then the model (7.16) can be rewritten as

$$y(t) = Ay(t-1) + WK(y(t-1)) + Bu(t-1) + e(t), \quad (7.17)$$

where  $W = [W_1, \dots, W_l] \in \mathbb{R}^{n \times l}$  denotes the weight,  $K(\cdot) = [K_1(\cdot), \dots, K_l(\cdot)]^T: \mathbb{R}^n \rightarrow \mathbb{R}^l$  denotes the radial basis function, and  $l$  is the number of neurons. The radial basis function is often selected as Gaussian kernel  $K_i(y) = \exp\{-(y - c_i)^T \Sigma_i^{-1} (y - c_i)/2\}$ , ( $i = 1, \dots, l$ ) with proper center vector  $c_i \in \mathbb{R}^n$  and norm matrix  $\Sigma_i \in \mathbb{R}^{n \times n}$ .

Different algorithms exist for training the hybrid RBF network. Most of them determine the parameters  $c_i$  and  $\Sigma_i$  first, and subsequently unknown parameters  $A$ ,  $B$  and  $W$  can be estimated by the recursive least-squares method (Nelles, 2001).

Note that the center  $c_i$  is often selected using clustering techniques or placed on a proper uniform grid within the relevant region of the training data. The norm matrix  $\Sigma_i$  is often chosen to be diagonal and contains the variance of the training data. The number of neurons  $l$  should be carefully determined using such as cross-validation or regularization technique to avoid the possible overfitting problem.

## 7.4 Simulation and Experiment

### 7.4.1 Catalytic Rod

Consider the **catalytic rod** given in Sections 1.1.2 and 3.6.1. In the simulation, assume the process noise  $d(x,t)$  in (3.31) is zero. The temporal input  $u_i(t)=1.1+(4+2rand) \exp(-i/5)\sin(t/14+rand)-0.4\exp(-i/20)\sin(t/2+2 rand)$  ( $i=1,\dots,4$ ) is used, where *rand* is a uniform distributed random function on  $[0, 1]$ . Twenty sensors uniformly distributed in the space are used for output measurements. The sampling interval  $\Delta t$  is 0.01 and the simulation time is 7.5. A noise-free data set of 750 data is collected from the system equation. The noise uniformly distributed on  $[-0.08(\max(y)-\min(y)), 0.08(\max(y)-\min(y))]$  is added to the noise-free data to obtain the noisy output. The measured output  $y(x,t)$  is shown in Figure 7.3. The first 500 data is used as the training data with the first 250 data as the estimation data and the next 250 data as the validation data. The validation data is used to monitor the training process and determine the NL-PCA network and RBF model size. The remaining 250 data is the testing data.

#### (1) Learning of nonlinear projection and reconstruction

A NL-PCA network is designed to project the spatio-temporal output  $\{y(x_i,t)\}_{i=1,t=1}^{N,L}$  into the low-dimensional temporal data  $\{y(t)\}_{t=1}^L$ . Using the cross-validation method the dimension of the time series is selected as  $n=2$  and the number of nodes in the projection and reconstruction layers is set to 40. The reconstruction error  $e(x,t) = y(x,t) - y_n(x,t)$  of the NL-PCA network over the estimation, validation and testing data is shown in Figure 7.4. The reduced-dimensional time series  $y_1(t)$  and  $y_2(t)$  (dashed line) are computed for training and testing the dynamic neural model as shown in Figure 7.5 and Figure 7.6, respectively.

#### (2) Nonlinear dynamic modeling of time series $y(t)$

To establish the dynamical relationship between  $y(t)$  and  $u(t)$ , a NL-PCA based RBF network (**NL-PCA-RBF**) model with five neurons is used according to the cross-validation method. The model predictions  $\hat{y}_1(t)$  and  $\hat{y}_2(t)$  (**solid line**) are

compared with  $y_1(t)$  and  $y_2(t)$  over the training and testing data as shown in [Figure 7.5](#) and [Figure 7.6](#), respectively. The comparison shows that the hybrid RBF model performs satisfactorily.

### (3) Nonlinear time/space reconstruction for $\hat{y}_n(x,t)$

Using the nonlinear time/space reconstruction, the spatio-temporal output  $\hat{y}_n(x,t)$  is reproduced from the output data of the [NL-PCA-RBF](#) model. As shown in [Figure 7.7](#) the prediction error  $e(x,t) = y(x,t) - \hat{y}_n(x,t)$  over the whole data set demonstrates that NL-PCA-RBF model can reproduce the spatio-temporal dynamics of the original system very well.

### Comparison with linear PCA based modeling

A linear PCA based RBF ([PCA-RBF](#)) model is developed for comparison, where the linear PCA is used for the dimension reduction ( $n=2$ ) and the same RBF network for the modeling according to the cross-validation method. The spatial normalized absolute error  $SNAE(t) = \int |e(x,t)| dx / \int dx$  is shown in [Figure 7.8](#). Two indexes:  $\eta$  in (7.15) and root of mean squared error  $RMSE = (\int \sum e(x,t)^2 dx / \int dx \sum \Delta t)^{1/2}$  over the estimation, validation and testing data are compared in [Table 7.1](#). It is noticed that the NL-PCA-RBF model has a better performance than the PCA-RBF model. The final modeling error consists of two parts: the dimension reduction error and the RBF model error. Obviously, NL-PCA can preserve more variance and achieve less reconstruction error than PCA. Thus, NL-PCA-RBF model can have a better performance because the RBF model is actually a universal approximator.

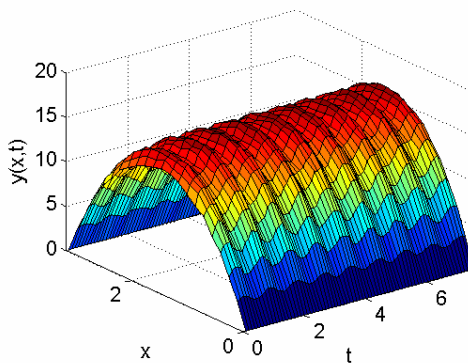


**Fig. 7.3** Catalytic rod: Measured output for neural modeling

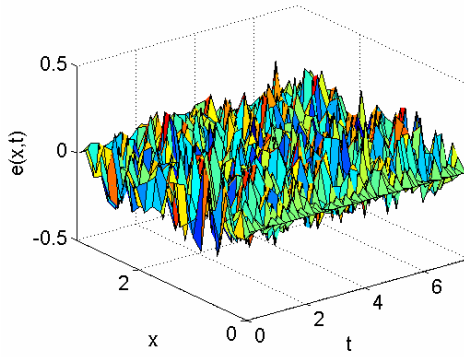


**Fig. 7.4** Catalytic rod: NL-PCA reconstruction error

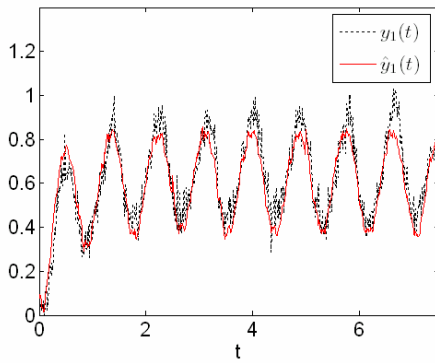


**Fig. 7.5** Catalytic rod: NL-PCA-RBF model prediction -  $\hat{y}_1(t)$

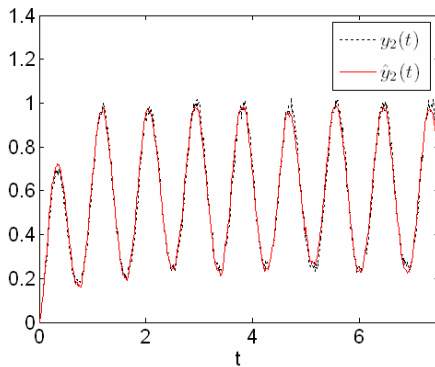


**Fig. 7.6** Catalytic rod: NL-PCA-RBF model prediction -  $\hat{y}_2(t)$

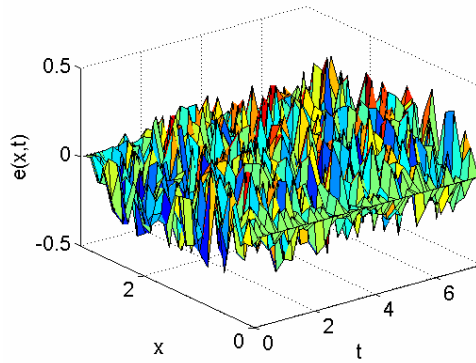


**Fig. 7.7** Catalytic rod: NL-PCA-RBF model prediction error

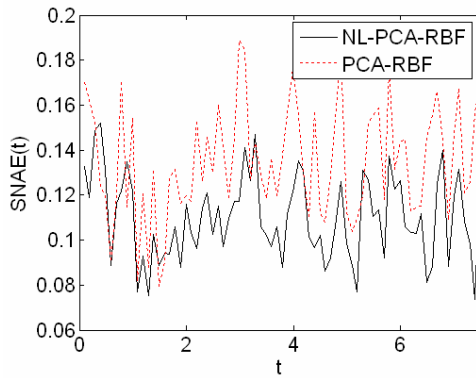


**Fig. 7.8** Catalytic rod:  $SNAE(t)$  of NL-PCA-RBF and PCA-RBF models

**Table 7.1** Catalytic rod: Comparison of PCA and NL-PCA for modeling

		PCA	NL-PCA	PCA-RBF model	NL-PCA-RBF model
$\eta$	estimation	0.9427	0.9566	0.9326	0.9462
	validation	0.9273	0.9458	0.9119	0.9334
	testing	0.9319	0.9508	0.9158	0.9377
RMSE	estimation	0.1407	0.1225	0.1527	0.1364
	validation	0.1417	0.1224	0.156	0.1357
	testing	0.1436	0.1221	0.1597	0.1374

### 7.4.2 Snap Curing Oven

Consider the **snap curing oven** (Figure 1.1 and Figure 3.11) provided in Sections 1.1.1 and 3.6.2. In the experiment, a total of 2100 measurements are collected with a sampling interval  $\Delta t = 10$  seconds. Among them, 1950 measurements

from sensors (s1-s16) are used to train the model, where the first 1800 data is the estimation data and the next 150 data is the validation data. The validation data is used to monitor the training process and determine the NL-PCA network and RBF model size. The last 150 measurements from sensors (s1-s16) are chosen to test the model.

In the NL-PCA-RBF modeling, the number of nodes in the projection, bottleneck, and reconstruction layers in NL-PCA network is 10, 2 and 15 respectively according to the cross-validation method. That means the dimension of the states will be  $n = 2$ . The model performance at the sensors s1 and s2 over the training and testing data are shown in Figure 7.9 and Figure 7.10 respectively. The predicted temperature distribution of the oven at  $t=10000$ s is provided in Figure 7.11.

For comparison, the PCA-RBF model is developed with linear PCA for the dimension reduction ( $n = 5$ ) and the same RBF network structure for the modeling. The performance index  $TNAE(x)$  (Temporal normalized absolute error,  $TNAE(x) = \sum |e(x,t)| / \sum \Delta t$ ) over the whole data set in Table 7.2 shows that NL-PCA-RBF model is better than PCA-RBF model even with more number of states.

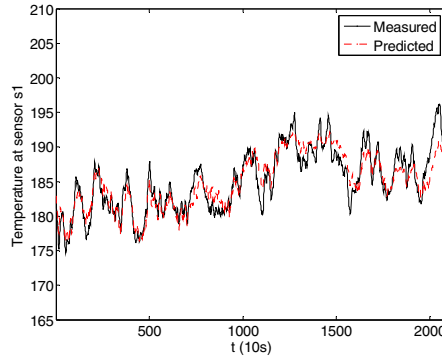


**Fig. 7.9** Snap curing oven: Performance of NL-PCA-RBF model at sensor s1

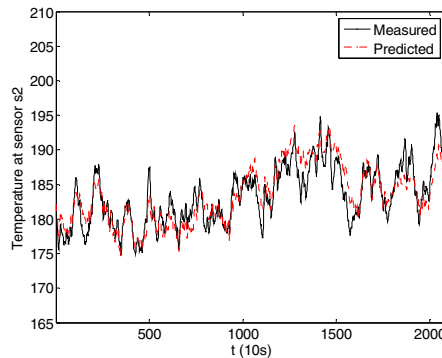


**Fig. 7.10** Snap curing oven: Performance of NL-PCA-RBF model at sensor s2

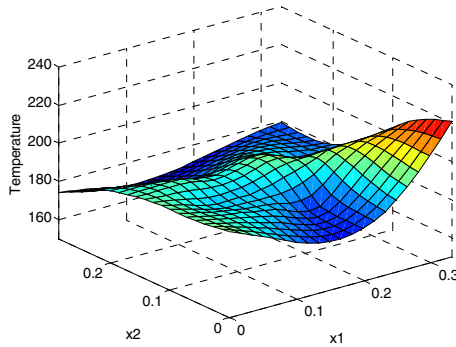


**Fig. 7.11** Snap curing oven: Predicted temperature distribution of NL-PCA-RBF model at  $t=10000s$

**Table 7.2** Snap curing oven:  $TNAE(x)$  of PCA-RBF and NL-PCA-RBF models

	s1	s2	s3	s4	s5	s6	s7	s8
PCA-RBF	1.69	1.85	1.68	1.63	1.65	1.68	1.66	1.61
NL-PCA-RBF	1.41	1.64	1.48	1.51	1.53	1.52	1.52	1.53
	s9	s10	s11	s12	s13	s14	s15	s16
PCA-RBF	1.6	1.9	1.91	1.65	1.78	1.78	1.61	1.87
NL-PCA-RBF	1.69	1.67	1.72	1.66	1.71	1.55	1.63	1.64

**Remark 7.1: Performance comparison for modeling of snap curing oven**

Different kind of model may be suitable for different system and it is usually selected by the modeling performance. The normalized absolute error  $NAE = \int \sum |e(x,t)| dx / \int dx \sum \Delta t$  over the whole data set for all models of snap curing oven (see Chapter 3 - Chapter 7) is shown in Table 7.3.

**Table 7.3** Snap curing oven: accuracy comparison for all models

Models	NAE
2 <sup>nd</sup> -order Volterra	0.9225
KL-Wiener	0.99125
3-channel Hammerstein	1.19625
NL-PCA-RBF	1.588125
KL-Hammerstein	1.765



The 2<sup>nd</sup>-order Volterra model achieves the best performance. The accuracy of KL-Wiener model is similar to 2<sup>nd</sup>-order Volterra model. Both Volterra and Wiener models are more suitable for this process than other models. The 3-channel Hammerstein model is better than KL-Hammerstein model because of more channels added. Due to the special structure of the oven, the dominant heat conduction is easier to model than the convection and radiation effect. The process is not complex enough to show the advantage of NL-PCA-RBF.

**Remark 7.2:** *Comparison of computation time for modeling of snap curing oven*

As shown in Table 7.4, the computation time is also compared for all modeling approaches. Because the time/space separation is often performed individually before the model estimation, the total modeling time can be decomposed into time/space separation time and model estimation time. For the time/space separation, the NL-PCA method for NL-PCA-RBF modeling requires the shortest time. The KL method used in other modeling will take more time than the NL-PCA because of the eigenvalue decomposition of a large matrix in (3.14). After the time/space separation, the NL-PCA-RBF model estimation requires the shortest time. The 3-channel Hammerstein modeling will take more time than KL-Hammerstein modeling because of the multi-channel model estimation. It will take almost same time to estimate other models. Overall, the NL-PCA-RBF modeling is fastest among all the methods used.

**Table 7.4** Snap curing oven: computation comparison for all modeling approaches (seconds)

Modeling approaches	T/S separation time	Model estimation time	Total time
2 <sup>nd</sup> -order Volterra	147	42	189
KL-Wiener	147	43	190
3-channel Hammerstein	147	52	199
NL-PCA-RBF	97	3	100
KL-Hammerstein	147	42	189

## 7.5 Summary

A nonlinear dimension reduction based neural modeling approach is presented for the distributed parameter system. The nonlinear PCA is used for dimension reduction and reconstruction. The traditional RBF network is used for the dynamic modeling. The nonlinear PCA has a more powerful capability of dimension reduction than the linear PCA for nonlinear systems. Thus, the presented approach can work better for nonlinear distributed parameter systems. The simulation on the catalytic rod and the experiment on the snap curing oven have demonstrated the effectiveness of the presented method.

## References

- [1] Aggelogiannaki, E., Sarimveis, H.: Nonlinear model predictive control for distributed parameter systems using data driven artificial neural network models. *Computers and Chemical Engineering* 32(6), 1225–1237 (2008)
- [2] Armaou, A., Christofides, P.D.: Dynamic optimization of dissipative PDE systems using nonlinear order reduction. *Chemical Engineering Science* 57(24), 5083–5114 (2002)
- [3] Baker, J., Christofides, P.D.: Finite-dimensional approximation and control of non-linear parabolic PDE systems. *International Journal of Control* 73(5), 439–456 (2000)
- [4] Dong, D., McAvoy, T.J.: Nonlinear principal component analysis-based on principal curves and neural networks. *Computers and Chemical Engineering* 20(1), 65–78 (1996)
- [5] Ham, F.M., Kostanic, I.: Principles of neurocomputing for science and engineering. McGraw-Hill, New York (2001)
- [6] Hinton, G.E., Salakhutdinov, R.R.: Reducing the dimensionality of data with neural networks. *Science* 313(5786), 504–507 (2006)
- [7] Holmes, P., Lumley, J.L., Berkooz, G.: Turbulence, coherent structures, dynamical systems, and symmetry. Cambridge University Press, New York (1996)
- [8] Hoo, K.A., Zheng, D.: Low-order control-relevant models for a class of distributed parameter systems. *Chemical Engineering Science* 56(23), 6683–6710 (2001)
- [9] Hsieh, W.W.: Nonlinear principal component analysis by neural networks. *Tellus Series A - Dynamic Meteorology and Oceanography* 53(5), 599–615 (2001)
- [10] Kirby, M., Miranda, R.: The nonlinear reduction of high-dimensional dynamical systems via neural networks. *Physical Review Letter* 72(12), 1822–1825 (1994)
- [11] Kramer, M.A.: Nonlinear principal component analysis using autoassociative neural networks. *AIChE Journal* 37(2), 233–243 (1991)
- [12] Leontaritis, I.J., Billings, S.A.: Input-output parametric models for non-linear systems - Part I: Deterministic non-linear systems. *International Journal of Control* 41(2), 303–328 (1985)
- [13] Malthouse, E.C.: Limitations of nonlinear PCA as performed with generic neural networks. *IEEE Transactions on Neural Networks* 9(1), 165–173 (1998)
- [14] Nelles, O.: Nonlinear system identification: From classical approaches to neural networks and fuzzy models. Springer, Berlin (2001)
- [15] Newman, A.J.: Model reduction via the Karhunen-Loève expansion part I: An exposition. Technical Report T.R.96-32, University of Maryland, College Park, Maryland (1996a)
- [16] Newman, A.J.: Model reduction via the Karhunen-Loève expansion part II: Some elementary examples. Technical Report T.R.96-33, University of Maryland, College Park, Maryland (1996b)
- [17] Park, H.M., Cho, D.H.: Low dimensional modeling of flow reactors. *International Journal of Heat and Mass Transfer* 39(16), 3311–3323 (1996a)
- [18] Park, H.M., Cho, D.H.: The use of the Karhunen-Loève decomposition for the modeling of distributed parameter systems. *Chemical Engineering Science* 51(1), 81–98 (1996b)

- [19] Qi, C.K., Li, H.-X.: Hybrid Karhunen-Loève/neural modeling for a class of distributed parameter systems. *International Journal of Intelligent Systems Technologies and Applications* 4(1-2), 141–160 (2008a)
- [20] Saegusa, R., Sakano, H., Hashimoto, S.: Nonlinear principal component analysis to preserve the order of principal components. *Neurocomputing* 61, 57–70 (2004)
- [21] Sahan, R.A., Koc-Sahan, N., Albin, D.C., Liakopoulos, A.: Artificial neural network-based modeling and intelligent control of transitional flows. In: *Proceeding of the 1997 IEEE International Conference on Control Applications*, Hartford, CT, pp. 359–364 (1997)
- [22] Schölkopf, B., Smola, A., Muller, K.-R.: Nonlinear component analysis as a kernel eigenvalue problem. *Neural Computation* 10(5), 1299–1319 (1998)
- [23] Sjöberg, J., Zhang, Q., Ljung, L., Benveniste, A., Delyon, B., Glorennec, P., Hjalmarsson, H., Juditsky, A.: Nonlinear black-box modeling in system identification: A unified approach. *Automatica* 31(12), 1691–1724 (1995)
- [24] Smaoui, N.: Linear versus nonlinear dimensionality reduction of high-dimensional dynamical systems. *SIAM Journal on Scientific Computing* 25(6), 2107–2125 (2004)
- [25] Smaoui, N., Al-Enezi, S.: Modelling the dynamics of nonlinear partial differential equations using neural networks. *Journal of Computational and Applied Mathematics* 170(1), 27–58 (2004)
- [26] Webb, A.R.: An approach to non-linear principal components analysis using radially symmetric kernel functions. *Journal Statistics and Computing* 6(2), 159–168 (1996)
- [27] Wilson, D.J.H., Irwin, G.W., Lightbody, G.: RBF principal manifolds for process monitoring. *IEEE Transactions on Neural Networks* 10(6), 1424–1434 (1999)
- [28] Zhou, X.G., Liu, L.H., Dai, Y.C., Yuan, W.K., Hudson, J.L.: Modeling of a fixed-bed reactor using the KL expansion and neural networks. *Chemical Engineering Science* 51(10), 2179–2188 (1996)

# 8 Conclusions

**Abstract.** This chapter summarizes all the methods introduced in the book, and discusses future challenges in this area.

## 8.1 Conclusions

The studies of the nonlinear DPS become more and more active and important because of advanced technological needs in the industry. The nonlinear DPS considered in this book includes, but is not limited to, a typical class of thermal process in the IC packaging and chemical industry. In general, the modeling is required for many applications such as prediction, control and optimization. However, besides the complex natures of the system including the nonlinear time-space coupling dynamics, unknown parameters and structure uncertainties will make the modeling more difficult and challenging.

After an overview of DPS modeling, the book focuses on the model identification of the unknown nonlinear DPS. The existing DPS identification methods may have some limitations for modeling the nonlinear DPS. For example, the linear kernel model can not model nonlinear dynamics, the linear dimension reduction may not be very efficient for the nonlinear system, and the very complex neural network model may result in a difficult control design. In lumped parameter processes, the popularly used simple structure models: Wiener, Hammerstein and Volterra, have only temporal nature without spatial variables. On the other hand, in the machine learning field, NL-PCA is a nonlinear dimension reduction method, which can achieve a lower order and more accurate model than the KL method for a nonlinear problem. Thus to overcome these limitations in the DPS identification, it is necessary to develop new modeling approaches with the help of different modeling and learning techniques for the nonlinear DPS.

This book is to extend the traditional Wiener/Hammerstein/Volterra/neural modeling to the nonlinear DPS with help of spatio-temporal separation. First, novel concepts of the spatio-temporal Wiener/Hammerstein/Volterra model are constructed, upon which some data-based spatio-temporal modeling approaches are developed for the nonlinear DPS, and applied on typical thermal processes in IC packaging and chemical industry. Based on the presented solutions in this book, the following conclusions can be made.

(1) A spatio-temporal Wiener modeling approach is presented in [Chapter 3](#). For modeling the nonlinear DPS, a spatio-temporal Wiener model (a linear DPS followed by a static nonlinearity) is constructed. After the time/space separation, it can be represented by the traditional Wiener system with a set of spatial basis functions.

To achieve a low-order model, the KL method is used for the time/space separation and dimension reduction. Finally, unknown parameters of the Wiener system are estimated with the least-squares estimation and the instrumental variables method to achieve consistent estimation under noisy measurements.

(2) A spatio-temporal Hammerstein modeling approach is presented in [Chapter 4](#). To model the nonlinear DPS, a spatio-temporal Hammerstein model (a static nonlinearity followed by a linear DPS) is constructed. After the time/space separation, it can be represented by the traditional Hammerstein system with a set of spatial basis functions. To achieve a low-order model, the KL method is used for the time/space separation and dimension reduction. Then a compact Hammerstein model structure is determined by the orthogonal forward regression, and their unknown parameters are estimated with the least-squares method and the singular value decomposition.

(3) A multi-channel spatio-temporal Hammerstein modeling approach is presented in [Chapter 5](#). As a special case of the model described in [Chapter 4](#), a spatio-temporal Hammerstein model is constructed with a static nonlinearity followed by a linear spatio-temporal kernel. When the model structure is matched with the system, a basic single-channel identification algorithm with the algorithm used in the [Chapter 4](#) can work well. When there is unmodeled dynamics, a multi-channel modeling framework may be needed to achieve a better performance, partially because more channels used can attract more information from the process and also increase the model complexity to match the more complicated process. The modeling convergence can be guaranteed under noisy measurements.

(4) A spatio-temporal Volterra modeling approach is presented in [Chapter 6](#). The traditional Green's function is widely used for the DPS modeling. However, it consists of a single spatio-temporal kernel and is only a linear approximation for a nonlinear system. To model the nonlinear DPS, a spatio-temporal Volterra model is presented with a series of spatio-temporal kernels. It can be considered as a nonlinear generalization of Green's function or a spatial extension of the traditional Volterra model. To obtain a low-order model, the KL method is used for the time/space separation and dimension reduction. Then the model can be estimated with a least-squares algorithm with the convergence guaranteed under noisy measurements.

(5) A NL-PCA based neural modeling approach is presented in [Chapter 7](#). The KL based neural model is widely used for modeling DPS. However, the KL method is a linear dimension reduction which is only a linear approximation for a nonlinear system. To get a lower-order or more accurate solution, a NL-PCA based neural modeling framework is proposed. One NL-PCA network is trained for the nonlinear dimension reduction and the nonlinear time/space reconstruction. The other neural model is to learn the system dynamics with a linear/nonlinear separated model structure. With the powerful capability of dimension reduction and the intelligent

learning, this approach can model the nonlinear complex DPS with much more complexity.

The effectiveness of the presented modeling approaches are verified on some typical thermal processes. Of course, they can also be applicable for other industrial distributed parameter systems.

The presented modeling approaches have the following advantages.

- Little process knowledge is required, as all these methods are data-based approaches. Thus they are more flexible because many real-world applications are in unknown environment.
- Low-dimensional states are obtained. Because of the KL method and the NL-PCA used for dimension reduction, low-dimensional models are usually obtained which are computationally fast for the real-time implementation.
- Nonlinear nature is represented in simple structures. Since the Wiener, Hammerstein, Volterra models are used, the nonlinear models developed are usually have relatively simple structures, which will help the potential applications.

Because almost no process knowledge is required in the modeling, the experiment may need many sensors for collecting sufficient spatio-temporal dynamics information. The number of sensors used should be greater than the number of necessary spatial basis functions. Otherwise, a satisfactory model may not be available. When only a few sensors can be installed, if a nominal model is known in advance and only some nonlinearities are unknown, hybrid modeling approaches, such as, the neural observer spectral method in [Section 2.5.4](#), would be applicable. Even though many sensors may be needed in the modeling, once the model is established, only a few sensors should be sufficient for real-time applications, e.g., prediction and control.

Further investigations on the control design using these models are necessary. There are some challenges which have not been well studied in system identification of the DPS.

(1) Due to the complexity of the process, different modeling methods work in different conditions. Most of the existing methods can only work in the proximity of the operating conditions due to the nonlinearity of the process. Obtaining a nonlinear model which can work very well in a wide range of the working condition is a challenging problem. The identification based on the multi-model methodology is a promising approach. Generally speaking, more input-output data persistently excited at a wide range of working conditions are needed.

(2) The placement (number and locations) of sensors and actuators are very important for the identification of DPS. The modeling accuracy may depend significantly on the choice of sensor number and locations. The actuator number and locations have an important effect on the capability of the persistent excitation in the modeling experiment. Generally, the locations and the number of actuators and sensors are not necessarily dictated by physical considerations or by intuition and, therefore, some systematic approaches should still be developed in order to reduce the cost of instrumentation and to increase the efficiency of identification.

(3) Control application is one of the major purposes for the DPS identification. A proper integration of both system identification and control for an optimal performance is very important and needs much more effort. Though there are many studies reported for LPS (e.g., Hjalmarsson, 2005; Barenthin & Hjalmarsson, 2008; Hildebrand & Solari, 2007), only a few studies have been presented for DPS (Helmicki, Jacobson, & Nett, 1990, 1992; Ding, Johansson & Gustafsson, 2009). A key problem in identification for control (e.g., robust control) is how to measure the error between the model and the unknown system from the data. This problem becomes more difficult in the DPS identification.

(4) It is noticed that current identification techniques in DPS belong to the open-loop identification. Closed-loop experiments could be advantageous in certain situations (e.g., unstable systems), which may be related to the problem of identification for control since a popular method of the iterative identification and control often needs a closed-loop operation. The extension of the closed-loop identification popularly used in LPS (Forsell & Ljung, 1999; Zhu & Butoyi, 2002) to DPS needs an intensive investigation.

(5) Optimal experiment design (e.g., selection of input-output variables, input signal design, and selection of working conditions) to obtain informative data is very important for parameter estimation and system identification of DPS. The placement (number and locations) of sensors and actuators are also critical in this topic. It is a difficult problem, particularly in nonlinear, multivariable, or hybrid case (with both continuous and discrete variables). Only a few studies are reported for parameter estimation of DPS (Qureshi, Ng & Goodwin, 1980; Rafajłowicz, 1983). The extension of the results on experiment design extensively studied in LPS identification (e.g., Forsell & Ljung, 2000; Bombois *et al.*, 2006; Pronzato, 2008) to DPS needs an intensive investigation.

## References

- [1] Barenthin, M., Hjalmarsson, H.: Identification and control: Joint input design and H-infinity state feedback with ellipsoidal parametric uncertainty via LMIs. *Automatica* 44(2), 543–551 (2008)
- [2] Bombois, X., Scorletti, G., Gevers, M., Van den Hof, P.M.J., Hildebrand, R.: Least costly identification experiment for control. *Automatica* 42(10), 1651–1662 (2006)
- [3] Ding, L., Johansson, A., Gustafsson, T.: Application of reduced models for robust control and state estimation of a distributed parameter system. *Journal of Process Control* 19(3), 539–549 (2009)
- [4] Forsell, U., Ljung, L.: Closed-loop identification revisited. *Automatica* 35(7), 1215–1241 (1999)
- [5] Forsell, U., Ljung, L.: Some results on optimal experiment design. *Automatica* 36(5), 749–756 (2000)

- [6] Helmicki, A.J., Jacobson, C.A., Nett, C.N.: Control-oriented modeling and identification of distributed parameter systems. In: Chen, G., et al. (eds.) *New Trends and Applications of Distributed Parameter Control Systems - Proceedings of the 1989 IMA Workshop on Control of Distributed Parameter Systems*, ch. 10. Marcel-Dekker, New York (1990)
- [7] Helmicki, A.J., Jacobson, C.A., Nett, C.N.: Control-oriented modeling of distributed parameter systems. *Journal of Dynamic Systems, Measurement, and Control* 144(3), 339–346 (1992)
- [8] Hildebrand, R., Solari, G.: Identification for control: Optimal input intended to identify a minimum variance controller. *Automatica* 43(5), 758–767 (2007)
- [9] Hjalmarsson, H.: From experiment design to closed-loop control. *Automatica* 41(3), 393–438 (2005)
- [10] Pronzato, L.: Optimal experimental design and some related control problems. *Automatica* 44(2), 303–325 (2008)
- [11] Qureshi, Z.H., Ng, T.S., Goodwin, G.C.: Optimum experimental design for identification of distributed parameter systems. *International Journal of Control* 31(1), 21–29 (1980)
- [12] Rafajłowicz, E.: Optimal experiment design for identification of linear distributed parameter systems: Frequency domain approach. *IEEE Transactions on Automatic Control* 28(7), 806–808 (1983)
- [13] Zhu, Y.C., Butoyi, F.: Case studies on closed-loop identification for MPC. *Control Engineering Practice* 10(4), 403–417 (2002)



# Index

## A

algebraic equation 33  
approximated inertial manifold 22

## B

black-box modeling 13  
block-oriented nonlinear model 41  
block-oriented nonlinear models 51

## C

catalytic rod 62, 86, 138, 157  
Catalytic rod 3  
Chebyshev polynomials 27  
chemical vapor deposition reactor 29  
collocation AIM 23  
collocation method 22  
coupled map lattice system 33  
curing process 1

## D

difference equation 35  
diffusion-convection-reaction  
process 29  
Dirac delta functions 22  
distributed parameter systems 1

## E

EF-Galerkin method 26  
EF-Galerkin-AIM method 27  
Eigenfunction method 16  
eigenfunctions 16, 25  
eigenspectrum 26  
empirical eigenfunctions 27  
equation error 31  
error reduction ratio 80

## F

fading memory nonlinear system 123  
finite difference method 5  
Finite difference method 17  
finite element method 5  
Finite element method 24  
first-principle modeling 13  
fluid flow 29  
Fourier series 18, 25

## G

Galerkin AIM 23  
Galerkin method 21  
Green's function 124  
Green's function method 17  
grey-box modeling 13

## H

Hammerstein distributed parameter  
system 74, 97  
Hammerstein model 6, 51  
Hermite polynomials 27

## I

implicit Euler method 23  
inertial manifold 22  
instrumental variables method 52, 60

## K

Karhunen-Loève decomposition 52, 54  
Karhunen-Loève method 5, 27  
KL-collocation method 29

KL-Galerkin method 29  
 KL-Galerkin-AIM method 29

## L

Laguerre functions 58  
 Laguerre polynomials 27  
 lattice dynamical system 35  
 least-squares estimate 59  
 least-squares estimation 52  
 Least-squares estimation 83, 101  
 left singular functions 28  
 Legendre polynomials 27  
 linear regression 33  
 linear time-invariant system 52  
 lumped parameter systems 5

## M

mean of absolute relative error 29  
 method of characteristics 27  
 method of lines 18  
 method of snapshots 56  
 model reduction 13  
 multi-channel Hammerstein system 103

## N

Navier-Stokes equation 33  
 NL-PCA 153  
 nonlinear autoregressive with exogenous input model 35  
 Nonlinear parabolic process 15  
 nonlinear principal component analysis 6

## O

ordinary differential equations 5  
 orthogonal collocation method 22  
 orthogonal forward regression 35, 74  
 Orthogonal forward regression 80  
 orthogonal least-squares 34  
 orthogonal polynomials 22  
 Orthogonal polynomials 27  
 output error 31

## P

packed-bed reactor 113  
 Packed-bed reactor 4  
 parabolic PDE 4  
 parameter estimation 13  
 partial differential equation 2  
 piecewise polynomials 24  
 piecewise polynomials-Galerkin method 24

polynomial-collocation method 27  
 principal component analysis 27  
 Principal component analysis 151  
 proper orthogonal decomposition 27

## Q

Quasi-linear parabolic process 14

## R

radial basis functions 58  
 regularization error 32  
 right singular functions 28  
 Root of mean squared error 62, 113, 138

## S

self-adjoint 17  
 separation of variables 16  
 signal-to-noise ratio 113  
 single-channel Hammerstein system 103  
 singular perturbations method 23  
 singular value decomposition 27  
 Singular value decomposition 83, 101  
 snap curing oven 1, 65, 89, 116, 141, 160  
 spatial basis functions 18  
 Spatial correlation method 55  
 Spatial normalized absolute error 62, 86, 113, 138  
 spatial two-point correlation function 28  
 spatio-temporal Hammerstein model 9  
 spatio-temporal neural model 9  
 spatio-temporal Volterra model 9, 125  
 spatio-temporal Wiener model 9  
 spectral method 5, 25  
 spill-over effects 21  
 spline-Galerkin method 24  
 splines 24  
 steady manifold 23  
 system identification 13

## T

Temporal correlation method 56  
 Temporal normalized absolute error 62, 86, 113, 138  
 temporal two-point correlation function 28  
 thermal process 29  
 thermal processes 1  
 time/space coupled 5  
 time/space separation 52  
 Time/space separation 127

**V**

Volterra model 6, 124

**W**

wavelet-collocation method 24  
wavelet-collocation-AIM method 24

wavelet-Galerkin method 24  
wavelet-Galerkin-AIM method 24  
wavelets 24  
weighted residual method 18  
weighting functions 20  
White-box modeling 16  
Wiener distributed parameter system 52  
Wiener model 6, 51